On the non-destructive quality control of tempered glass

Lena Cornelia Klara Efferz

Vollständiger Abdruck der von der Fakultät für Bauingenieurwesen und Umweltwissenschaften der Universität der Bundeswehr München zur Erlangung des akademischen Grades einer

Doktor-Ingenieurin (Dr.-Ing.)

angenommenen Dissertation.

Gutachter:

1. Univ.-Prof. Dr.-Ing. Geralt Siebert (Universität der Bundeswehr München)
2. Prof. Dr.-Ing Christian Schuler (Hochschule München)
3. Prof. dr. ir.-arch. Jan Belis (Ghent University)

Die Dissertation wurde am 03.03.2026 bei der Universität der Bundeswehr München eingereicht und durch die Fakultät für Bauingenieurwesen und Umweltwissenschaften am 22.09.2026 angenommen. Die mündliche Prüfung fand am 22.09.2026 statt.

Danksagung

Mit dem Abschluss dieser Dissertation endet ein prägender Abschnitt meines beruflichen und persönlichen Werdegangs. Die Entstehung dieser Arbeit erforderte Ausdauer, Eigeninitiative und die Bereitschaft, immer wieder neue Lösungswege zu finden. An dieser Stelle möchte ich mich bei all denjenigen bedanken, die mich während der Promotion unterstützt und motiviert haben.

Die Arbeit entstand im Rahmen meiner Tätigkeit als wissenschaftliche Mitarbeiterin an der Hochschule München. Mein außerordentlicher Dank gilt daher Prof. Dr.-Ing. Christian Schuler für die wissenschaftliche Begleitung dieser Arbeit sowie für die Unterstützung und das Vertrauen, das er mir während der gesamten Promotionszeit entgegengebracht hat. Diese Dissertation wurde als kooperative Promotion innerhalb des BayWISS Kollegs Infrastruktur, Bauen und Urbanisierung mit der Universität der Bundeswehr München angefertigt. Mein besonderer Dank gilt daher Univ.-Prof. Dr.-Ing. Geralt Siebert für die Möglichkeit, diese Promotion durchzuführen, und die Betreuung auf Seiten der Universität. Ebenso danke ich Prof. dr. ir.-arch Jan Belis für die Übernahme des Drittgutachtens sowie für das Interesse an meiner Forschung. Univ.-Prof. Dr.-Ing. Thomas Braml sei für den Promotionsvorsitz gedankt.

Mein herzlicher Dank gilt allen ehemaligen Kolleginnen und Kollegen des Labors für Stahl- und Leichtmetallbau sowie des Instituts für Material- und Bauforschung der Hochschule München. Die gegenseitige Unterstützung, das freundschaftliche Verhältnis und die angenehme Arbeitsatmosphäre haben meine Promotionszeit bereichert. Dabei möchte ich mich insbesondere bei meinen Kollegen Herrn Dr.-Ing. Paul Müller und Herrn Dr.-Ing. Steffen Dix für den fachlichen und motivierenden Austausch bedanken. Mein Dank gilt außerdem allen Projekt- und Industriepartnern, insbesondere der TU Darmstadt, für die gute Zusammenarbeit und die Bereitstellung von Probekörpern.

Mein größter Dank gilt meinen Freundinnen. Ich bin Euch so dankbar, dass Ihr mich in schwierigen Phasen ermutigt und mich mit offenen Ohren, ehrlichen Gesprächen und vielen schönen gemeinsamen Momenten begleitet habt.

Zu guter Letzt danke ich meiner Familie. Mit Euch konnte ich den Promotionsalltag immer wieder hinter mir lassen und neue Kraft schöpfen. Für die notwendige Ablenkung und die unbeschwerte Zeit abseits der Promotion bin ich Euch von Herzen dankbar.

Bodenwöhr, im Oktober 2026

Lena Efferz

Abstract

Currently, quality control of thermally toughened safety glass (TTG) and heat-strengthened glass (HSG) must be performed by destructive testing of standardized small-format specimens to verify fracture pattern and bending strength according to EN 12150-1 (2020) and EN 1863-1 (2012). These tests are costly, time-consuming, and unsuitable for comprehensive production monitoring. To reduce the need for destructive testing and enable non-destructive control of pre-stress quality, photoelastic measurements of surface stress and edge stress provide a promising alternative. The objective of this thesis is to establish generally applicable photoelastic limit values that can reliably ensure the pre-stress quality of tempered glass and thus replace destructive tests. In industrial practice, manual edge stress measurements are labor-intensive and poorly suited for inline quality control. Moreover, this work demonstrates that the evaluation procedure for edge stress specified in ASTM C1279 (2023) is not applicable to architectural glass: the edge chamfer required by European standards for tempered glass prevents direct retardation measurement at the glass edge, making extrapolation of the retardation curve unavoidable. By comparing polynomial fitting functions of different orders of photoelastic data measured by phase-shifting technique, this research identifies a 3rd degree polynomial as the most suitable extrapolation for determining edge stress. On this basis, an automated evaluation method using multiple-wavelength photoelasticity compatible with modern inline measurement systems is developed for reducing operator dependence. The experimental program comprises TTG and HSG specimens of standard format 360 mm x 1100 mm with thicknesses of 4, 6, 8, 10, and 12 mm. Photoelastic measurements of surface and edge stress are combined with fracture pattern evaluation and bending strength tests. Using quantile regression and logistic regression, statistically based photoelastic limit values for surface and edge stress are derived to fulfill the mechanical requirements of EN 12150-1 (2020) and EN 1863-1 (2012). These limits are subsequently validated on large-format specimens of 1000 mm x 3000 mm with thicknesses of 6 to 12 mm to assess their transferability from standard-size specimens to more practically relevant structural components. Performance metrics demonstrate that the current standard-based limits show poor capability to detect non-conforming glass, whereas the statistically derived limit values proposed in this work provide substantially better discrimination but also reject unnecessarily some conforming specimens. These photoelastic limits achieve an improved balance between safety and production efficiency, demonstrating the feasibility of replacing destructive tests with non-destructive photoelastic quality control for tempered glass. Finally, this work provides recommendations for non-destructive quality control methods for TTG and HSG focusing on methods for measuring and evaluating edge and surface stress.

Zusammenfassung

Derzeit muss die Qualitätskontrolle von Einscheibensicherheitsglas (ESG) und teilvorgespanntem Glas (TVG) durch zerstörende Prüfungen an genormten Kleinformatproben durchgeführt werden, um Bruchbild und Biegefestigkeit nach EN 12150-1 (2020) und EN 1863-1 (2012) zu verifizieren. Diese Tests sind kostenintensiv, zeitaufwendig und für eine umfassende Produktionsüberwachung ungeeignet. Um diese zerstörenden Prüfungen zu reduzieren und eine zerstörungsfreie Kontrolle der Vorspannqualität zu ermöglichen, stellen spannungsoptische Messungen der Oberflächendruck- und Kantenmembranspannung eine vielversprechende Alternative dar. Ziel dieser Arbeit ist es, allgemeingültige, spannungsoptische Grenzwerte zu ermitteln, mit denen die Vorspannqualität von vorgespanntem Glas zuverlässig kontrolliert und zerstörende Prüfungen ersetzt werden können. In der Praxis sind manuelle Messungen der Kantenmembranspannung arbeitsintensiv und für eine Inline-Qualitätskontrolle nur eingeschränkt geeignet. Darüber hinaus zeigt diese Arbeit, dass die in der ASTM C1279 (2023) angegebene Messmethode für Kantenmembranspannung auf Bauglas nicht anwendbar ist: Die nach europäischen Normen vorgeschriebene Fase an der Kante verhindert dort eine direkte Messung von Verzögerungen, sodass eine Extrapolation der Verzögerungskurve notwendig ist. Durch den Vergleich unterschiedlicher, Polynomfunktionen mit Daten, die mit der Phase-Shifting-Methode gemessen wurden, wird ein Polynom dritten Grades als geeignetste Extrapolationsfunktion zur Bestimmung der Kantenmembranspannung festgelegt. Darauf aufbauend wird eine Auswertemethode auf Basis der Mehrwellenlängen-Spannungsoptik entwickelt, welche als automatisiertes Inline-Messsystem eingesetzt werden kann und somit die Bedienerabhängigkeit reduziert. In experimentellen Untersuchungen werden spannungsoptische Messungen der Oberflächendruck- und Kantenmembranspannung mit Bruchbildanalysen und Biegefestigkeitsprüfungen an ESG- und TVG-Probekörpern im Standardformat 360 mm x 1100 mm mit Glasdicken von 4, 6, 8, 10 und 12 mm kombiniert. Mittels quantiler und logistischer Regressionsmodelle werden spannungsoptische Grenzwerte für die Oberflächendruck- und Kantenmembranspannung abgeleitet, welche die mechanischen Anforderungen der EN 12150-1 (2020) und EN 1863-1 (2012) erfüllen. Diese Grenzwerte werden anschließend an großformatigen ESG- und TVG-Probekörpern von 1000 mm x 3000 mm in Dicken von 6 bis 12 mm validiert, um ihre Übertragbarkeit von Standardformat auf praxisrelevantere Bauteilabmessungen zu untersuchen. Die Ergebnisse zeigen, dass sich die derzeit normbasierten Grenzwerte nicht eignen, nicht konformes Glas auszusortieren, während die in dieser Arbeit statistisch hergeleiteten Grenzwerte eine deutlich bessere Trennschärfe aufweisen. Allerdings wird auch ein Teil konformer Scheiben unnötig verworfen. Die vorgeschlagenen spannungsoptischen Grenzwerte tragen zu erhöhter Sicherheit und gesteigerter Produktionseffizienz bei und belegen die grundsätzliche Eignung, zerstörende Prüfverfahren durch eine zerstörungsfreie spannungsoptische Qualitätskontrolle für vorgespanntes Glas zu ersetzen. Abschließend werden Empfehlungen für zerstörungsfreie Qualitätskontrollmethoden für ESG und TVG gegeben, mit besonderem Fokus auf die Messung und Auswertung von Oberflächendruck- und Kantenmembranspannung.

Contents

Glossary . . . . . **xiii**

1 Introduction **1**
1.1 Motivation 1
1.2 State of the art 2
1.3 Objectives and structure 4
1.4 Own publications 6

2 Theoretical basics and analytical methods **9**
2.1 Tempered glass 9
2.1.1 Manufacturing process and glass products 9
2.1.2 Conventional quality control for tempered glass 11
2.1.2.1 Bending strength 11
2.1.2.2 Fracture pattern 14
2.2 Basics of photoelasticity 15
2.2.1 Stress-optical law and plane polariscope 17
2.2.2 Phase-shifting technique 18
2.2.3 Multiple-wavelength photoelasticity method 19
2.2.4 Scattered light method 20
2.3 Statistical approaches in experimental analysis 22
2.3.1 Types of data and level of measurement 22
2.3.2 Description of distributions 22
2.3.3 Frequency distributions 24
2.3.4 Contingency tables and metrics 26
2.3.5 Linear regression 27
2.3.5.1 Model description 27
2.3.5.2 Model interpretation 29
2.3.5.3 Model assumptions 30
2.3.6 Moderation analysis 32
2.3.6.1 Model description 32
2.3.6.2 Interpretation of the results 33
2.3.6.3 Model assumptions 33
2.3.7 Quantile regression 34
2.3.7.1 Model description 35
2.3.7.2 Model assumptions 36
2.3.8 Logistic regression 36
2.3.8.1 Model description 36
2.3.8.2 Assessment of model fit 38
2.3.8.3 Interpretation of the results 38
2.3.8.4 Model assumptions 40
2.3.9 Bootstrapping as a resample method 40

3 Residual stresses and non-destructive measurements of tempered glass 43
3.1 Distribution of residual stresses within tempered glass 43
3.2 Measuring methods for surface stress 46
3.3 Relation of surface stress to destructive tests 47
3.4 Measuring methods for edge stress 49
3.4.1 Retardation measurement at the edge 49
3.4.2 Extrapolation techniques across the chamfer 51
3.5 Relation of edge stress to destructive measurements 53
3.6 Relation between edge stress and surface stress 53
3.7 Existing photoelastic limit values 54

4 Developing a method for evaluating edge stress 57
4.1 Characterization of the chamfer issue 57
4.2 Evaluation with phase-shifting technique 59
4.2.1 Experimental setup 59
4.2.2 Interpolation of retardations 62
4.2.3 Ratio of interpolation and extrapolation width 64
4.2.4 Extrapolated edge stress values 66
4.2.5 Constraints for cubic polynomial coefficients 67
4.3 Evaluation with multiple-wavelength photoelasticity 69
4.3.1 Experimental setup 69
4.3.2 Peak detection 70
4.3.3 Combination of single cuts 71
4.3.4 Influence of 0th isochromatic order 73
4.3.5 Influence of number of peaks 75
4.3.6 Ratio of interpolation and extrapolation width 78
4.3.7 Extrapolation with constrained coefficients 79
4.4 Comparison of edge stress values measured with both photoelastic methods 80
4.5 Conclusions 81

5 Experimental investigations on standard-size specimens 83
5.1 Approach and specimens 83
5.2 Destructive testing 85
5.2.1 Bending strength 85
5.2.1.1 Test procedure 85
5.2.1.2 Results 86
5.2.2 Fracture pattern 88
5.2.2.1 Test procedure 88
5.2.2.2 Results 88
5.2.3 Evaluation of conformity for glass type 90
5.3 Photoelastic measurement of surface stress 93
5.3.1 Test procedure 93
5.3.2 Analysis of surface stress measurements 94
5.3.2.1 Results of surface stress measurements 94
5.3.2.2 Homogeneity of pre-stress at the surface 96
5.4 Photoelastic measurement of edge stress 97
5.4.1 Test procedure with phase-shifting technique 97
5.4.2 Test procedure with multiple-wavelength photoelasticity 98

5.4.3 Analysis of edge stress measurements . . . 99
5.4.3.1 Results of edge stress measurements . . . 99
5.4.3.2 Homogeneity of pre-stress at the edge . . . 103
5.4.3.3 Width of pre-stress zone of the edge . . . 104
5.4.3.4 Reproducibility of MWP measurements . . . 108
5.5 Relation between photoelastic and destructive test results . . . 110
5.5.1 Method of correlation analysis . . . 110
5.5.2 Method of moderation analysis . . . 111
5.5.3 Method of intraclass correlation . . . 111
5.5.4 Comparison of correlation analysis . . . 112
5.5.5 Influence of glass thickness and manufacturer . . . 113
5.5.5.1 Investigation of manufacturer-level clustering . . . 113
5.5.5.2 Number of fragments ~ Surface stress . . . 114
5.5.5.3 Number of fragments ~ Edge stress (MWP) . . . 116
5.5.5.4 Bending stress ~ Surface stress . . . 118
5.5.5.5 Bending stress ~ Edge stress (MWP) . . . 121
5.5.5.6 Bending stress ~ Edge stress (PST) . . . 123
5.5.5.7 Comparison of moderation analysis . . . 124
5.6 Relation between edge stress and surface stress . . . 127
5.7 Summary and conclusions . . . 130

6 Statistical definition of photoelastic stress limits . . . 133
6.1 Methodological approach . . . 133
6.2 Method of quantile regression . . . 135
6.2.1 Basics . . . 135
6.2.2 Quantifying limit values via quantile regression . . . 136
6.2.3 Thickness-specific considerations in the definition of limit values . . . 138
6.3 Method of logistic regression . . . 139
6.3.1 Basics . . . 139
6.3.2 Quantifying photoelastic stress limits via logistic regression . . . 140
6.3.3 Thickness-specific considerations in the definition of limit values . . . 143
6.4 Validation method . . . 143
6.5 Database for regression analysis . . . 144
6.6 Surface stress threshold analysis for thermally toughened glass . . . 146
6.6.1 Quantile regression . . . 147
6.6.1.1 Surface stress vs. Number of fragments . . . 147
6.6.1.2 Surface stress vs. Bending stress . . . 150
6.6.2 Logistic regression . . . 151
6.7 Edge stress threshold analysis for thermally toughened glass . . . 152
6.7.1 Quantile regression . . . 153
6.7.1.1 Edge stress (MWP) vs. Number of fragments . . . 153
6.7.1.2 Edge stress (MWP) vs. Bending stress . . . 155
6.7.1.3 Edge stress (PST) vs. Bending stress . . . 156
6.7.2 Logistic regression . . . 157
6.7.2.1 Logistic regression with edge stress (MWP) . . . 157
6.7.2.2 Logistic regression with edge stress (PST) . . . 159
6.8 Discussion of limit values for thermally toughened glass . . . 160
6.8.1 Evaluating TTG with surface stress . . . 160

6.8.2 Evaluating TTG with edge stress . . . 162
6.9 Surface stress threshold analysis for heat-strengthened glass . . . 165
6.9.1 Quantile regression for the lower limit . . . 165
6.9.2 Logistic regression for the upper limit . . . 166
6.10 Edge stress threshold analysis for heat-strengthened glass . . . 169
6.10.1 Quantile regression for the lower limit . . . 169
6.10.1.1 Edge stress (MWP) vs. Bending stress . . . 170
6.10.1.2 Edge stress (PST) vs. Bending stress . . . 171
6.10.2 Logistic regression for the upper limit . . . 172
6.10.2.1 Logistic regression with edge stress (MWP) . . . 172
6.10.2.2 Logistic regression with edge stress (PST) . . . 177
6.11 Discussion of limit values for heat-strengthened glass . . . 180
6.11.1 Evaluating HSG with surface stress . . . 180
6.11.2 Evaluating HSG with edge stress . . . 181
6.12 Conclusions . . . 185

7 Validation on large-format specimens . . . 187
7.1 Test approach and database . . . 187
7.2 Experimental investigations on large-format specimens . . . 190
7.2.1 Photoelastic and destructive results of large-format specimens . . . 191
7.2.2 Classification for large-format thermally toughened glass . . . 193
7.2.3 Classification for large-format heat-strengthened glass . . . 194
7.2.4 Homogeneity of pre-stress at the surface and edge . . . 196
7.2.5 Relations between photoelastic and destroying test results . . . 197
7.2.6 Relation between edge stress and surface stress . . . 199
7.3 Comparison between standard-format and large-format . . . 202
7.4 Summary and conclusions . . . 208

8 Recommendations for non-destructive evaluation criteria . . . 211
8.1 Measurement of surface stress . . . 211
8.2 Measurement of edge stress . . . 212
8.3 Photoelastic limit values . . . 215
8.4 Limitations . . . 216

9 Conclusion and Outlook . . . 219

Declaration on the use of Artificial Intelligence (AI) . . . 223

Bibliography . . . 225

A Appendix . . . 235
A.1 Weibull . . . 235
A.2 Correlation analysis . . . 237
A.3 Moderation analysis – contrast analysis . . . 241
A.4 Quantile regression models . . . 243
A.5 Logistic regression models . . . 245
A.6 k-fold validation . . . 247

Glossary

Symbols

General

B	width	mm
E	elastic modulus	MPa
$\text{factor}_{\text{MWP-PST}}$	discrepancy factor between MWP and PST edge stress values	–
$f_{\text{w/t}}$	factor between width of the pre-stress zone at the edge and glass thickness	–
$f_{\text{ex/int}}$	ratio between interpolation and extrapolation width	–
F_{max}	breaking force	kN
g	gravitational acceleration	m/s^2
k_e	correction factor for edge failure	–
k_s	correction factor for surface failure	–
k	correction factor for the effective bending area	–
L_{b}	distance of supporting rollers	mm
L_{s}	distance of bending rollers	mm
m	mass	kg
ν	Poisson's ratio	–
ρ	density	kg/m^3
σ_{bB}	bending stress	MPa
σ_{bG}	stress depending on dead weight	MPa

Statistics

α	significance level
α	Weibull shape parameter
β_i	predictor coefficient of the regression model
β	Weibull scale parameter
β_0	intercept of the regression model
χ^2_{LR}	likelihood-ratio chi-square statistic for logistic regression
ε	error term
$\eta(x)$	linear transformed predictor of logistic regression
L_{destr}	limit of destructive test of bending strength or fracture pattern
μ	mean of the normal distribution

n	number of samples
P	logistic probability function
p	number of predictor variables excluding the intercept
P_1, P_2, P_3	coefficients of a cubic polynomial
$\pi(x)$	logistic probability function
Q_Y	conditional quantile function of the response variable
std	sample standard deviation
τ	quantile in quantile regression
thr	probability threshold of logistic regression
σ^2	variance of the normal distribution
X	explanatory (independent) variable or predictor
$\bar{x}$	arithmetic mean
x_i	observations or observed value of predictor variable for observation i
Y	dependent variable or response
$\bar{y}$	arithmetic mean of response variable
$\hat{y}$	predicted value of the response variable
y_i	observed value of response variable for observation i

Photoelasticity

C	photoelastic material constant	TPa^{-1}
δ	relative retardation	nm
λ	wavelength	nm
m	order of the isochromatic	–
ϕ	azimuthal angle	°
ϕ_1, ϕ_2	rotation angles of the principal stresses	°
R	retardation	nm
σ	stress	MPa
σ_e	edge stress	MPa
σ_m	tensile stress in the core of the glass	MPa
σ_1, σ_2, σ_3	principal stresses on the surface	MPa
σ_s	compressive surface stress	MPa
t	thickness	mm
τ_{xy}	shear stress	MPa
U	elastic energy	$\mathrm{J/m}^2$
x_1, x_2	measuring points according to ASTM C1279 (2023)	mm
z	position in depth	mm

Abbreviations

General

A, B, C	manufacturers of the specimens
AI	Artificial Intelligence
ANSI	American National Standards Institute
ASTM	American Society for Testing and Materials
DIN	German Institute for Standardization (German: Deutsches Institut für Normung
EN	European Standard (German: Europäische Norm)
HM	Hochschule München University of Applied Sciences
ISO	International Organization for Standardization
LLM	Large Language Model
NEMA	research project: addition of photoelastic methods and analysis concepts to a standard for tempered safety glass to reduce destructive testing (German: Ergänzung einer Norm für Einscheiben-Sicherheitsglas um spannungsoptische Messmethoden und Analysekonzepte zur Reduzierung zerstörender Prüfungen)
TUDa	Technical University of Darmstadt

Material

$CaCO_3$	calcium carbonate
FTG	fully tempered glass according to ASTM C1048 (2025)
HSG	heat-strengthened glass according to EN 1863-1 (2012)
KGN	ground edge (German: Kante geschliffen)
KGS	seamed edge (German: Kante gesäumt)
Na_2CO_3	sodium carbonate
PVB	polyvinyl butyral
SiO_2	quartz sand
TTG	thermally toughened (safety) glass according to EN 12150-1 (2020)

Statistics

$adjR^2$	adjusted coefficient of determination
ANOVA	analysis of variance
AUC	area under the ROC curve
BCa	bias-corrected and accelerated
CDF	cumulative distribution function
CI	confidence interval

FN	false negatives
FP	false positives
FPR	false positive rate
HC3	heteroscedasticity-consistent standard errors (type HC3)
ICC	intraclass correlation coefficient
IQR	interquartile range
LL	log-likelihood
LogReg	logistic regression
LR	likelihood ratio
Mod	moderation
OLS	ordinary least squares
OR	odds ratio
PDF	probability density function
PR curve	precision–recall curve
Prec	precision
QQ plot	quantile–quantile plot
QuanReg	quantile regression
R^2	coefficient of determination
Rec	recall
ROC	receiver operating characteristic
SSE	sum of squares due to error
S-shaped	sigmoid curve
SSR	regression sum of squares
SST	total sum of squares
TN	true negatives
TP	true positives
TPR	true positive rate

Methods

A, A_1, A_2	vector/components of polarized light
C	conforming
CCD	charge-coupled device
GASP	grazing angle surface polarimeter
H, H_1, H_2	vector/components of light after transmitting the analyzer
LED	light-emitting diode
LUT	look-up table
MWP	multiple-wavelength photoelasticity
NC	non-conforming
PES	portable edge scanner
PPSM	pixelated phase-shifting method
PST	phase-shifting technique
RGB	red-green-blue
SCALP	scattered light polariscope

1 Introduction

1.1 Motivation

Tempered glass is an essential material in modern construction, prized for its strength and safety features. The tempering process involves heating the glass to approximately 100 °C above its glass transition temperature, followed by rapid cooling. Depending on the cooling rate, two tempered glass types with unique properties are distinguished. The requirements for these distinct glass types are outlined in the respective European standards. Thermally toughened safety glass (TTG) is required to exhibit a minimum bending strength of 120 MPa and a fine crumbly fracture pattern (EN 12150-1 2020), while heat-strengthened glass (HSG) is specified by a minimum bending strength of 70 MPa accompanied by a coarser fracture pattern (EN 1863-1 2012).

Under the factory production control regulated according to the European standards EN 12150-1 (2020) and EN 1863-1 (2012), destructive tests must be conducted on small glass samples (360 mm x 1100 mm) produced alongside full-size panes. These tests assess the fracture pattern or bending strength but are time-consuming, material-intensive, and costly: factors that are not in the interest of sustainability. Fig. 1.1a illustrates the time-consuming manual counting of fragments for TTG, and Fig. 1.1b demonstrates the destructive method of determining the bending strength by conducting a four-point bending test.

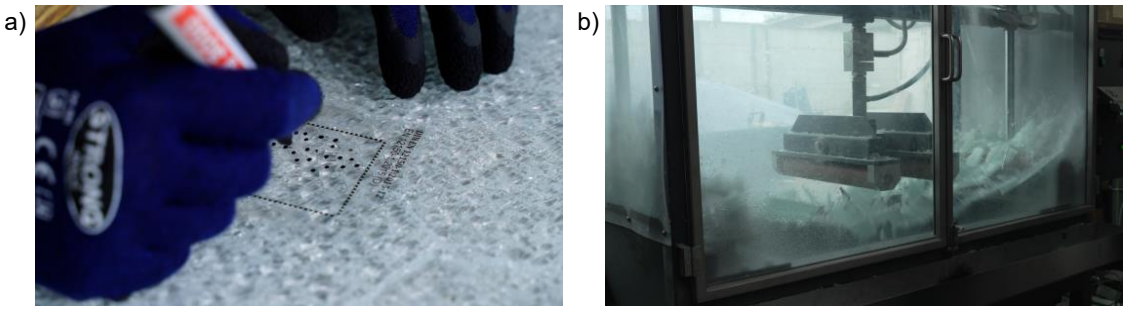

Figure 1.1: Destructive tests waste time and material, here exemplarily shown by a) manually counting the number of fragments for thermally toughened glass and b) breaking glass in a four-point bending test to determine the bending strength, by courtesy of Wolfram Schlenker

Moreover, since these destructive tests are carried out on small-format samples, it is challenging to reliably transfer the results to full-size panes, leading to uncertainties whether the required properties are truly met. Fracture pattern analysis and bending tests on full-size panes are often not included in construction projects, creating a gap in verifying the glass' performance at larger scale. During the tempering process, residual stresses are induced in the glass, resulting in compressive stresses on the surface and tensile stresses within the core of the glass. These compressive stresses suppress micro-level defects

on the surface and prevent fracture until the compressive stress is surpassed by tensile loading. This indicates a potential relationship between residual stresses and the mechanical properties of tempered glass. Therefore, non-destructive quality control of tempered glass could be achieved by assessing these residual stresses. The measurement of residual stresses can be carried out using photoelastic methods, which exploit the birefringent properties of transparent materials. Among the residual stresses, surface stress is the most widely studied and measured in both research and industry. However, surface stress measurement is operator-dependent and time-consuming, as it requires local measurements at discrete points on the glass pane. The second measurable residual stress is edge stress, which forms around the edges of the glass pane. Edge stress measurements are not yet common in the construction industry, primarily because the edge processing of tempered glass makes it challenging to measure the retardation at the outermost point of the edge. Nevertheless, given the technique of stress measurement at the edge, there is an opportunity to integrate edge stress measurement into the production process, offering a non-destructive method that could be applied automatically on each glass format, thus ensuring better control over glass quality. Currently, however, European product standards do not specify limit values for surface and edge stress that would allow for direct control over fracture patterns or bending strength.

1.2 State of the art

The tempering process induces a residual stress state characterized by a parabolic stress distribution across the glass thickness, with compressive stresses at the surfaces and tensile stresses in the core of the pane. As these stresses vary over the thickness, they are commonly referred to as thickness stresses. Simultaneously, an almost over the thickness constant compressive stress develops at the glass edge, known as edge membrane stress (Aben and Guillemet 1993). The residual stress state is stored in the glass in form of elastic energy (Pourmoghaddam and Schneider 2018b, Pourmoghaddam et al. 2019). Upon fracture, part of this stored energy is released. Depending on the magnitude of the residual stresses, this results either in the fine, crumbly fracture pattern typical for TTG or in the coarser fracture pattern characteristic of HSG. In addition, the compressive surface stresses suppress micro-defects on the surface, leading to a significant increase in bending tensile strength compared to float glass by a factor of approximately 2.7 for TTG and 1.6 for HSG. In addition to the fracture behavior (Nielsen 2017, Pour-Moghaddam 2020), residual stresses on the edge and surface can provide information on the strength behavior of glass (Aben et al. 2010, Mognato et al. 2019).

Measuring and evaluating edge stress is not a widespread practice for architectural glass. The American standard ASTM C1048 (2025) is the only normative document that stipulates a limit for edge stress. To fulfill the bending strength requirements for the glass product fully tempered glass, the minimum value required by ASTM C1048 (2025) is 67 MPa. ASTM C1279 (2023) provides the corresponding photoelastic method for measuring edge stress using a hand-held polarimeter with a wedge compensator to read the retardation at two specific measuring points. As it relies on punctual measurements, the method is complex and error-prone due to its dependence on the operator.

Furthermore, this method is subject to complications arising from the positioning of the two measuring points. According to EN 12150-1 (2020) and EN 1863-1 (2012), it is necessary

to chamfer the edges of architectural tempered glass at a 45° angle before tempering. This process of edge processing is undertaken to mitigate the risk of injury and breakage during the tempering process. However, the sloping surface of the chamfer causes reflection of the light of the measuring device, leading to errors in the data output from the retardation measurement which need a perpendicular incidence angle of light waves. Since one or both measurement points x_1 and x_2 specified by ASTM C1279 (2023) fall within or near the chamfer, their retardations cannot be evaluated. Consequently, the measurement of retardations in the area of the edge is only reliable until the start of the chamfer (Aben et al. 2015, Achintha 2021). However, to calculate the edge stress, it is necessary to consider the retardation at the furthest end of the edge. As a result, the measured data points that are available in the edge area must be interpolated and then extrapolated over the chamfer.

Nevertheless, the form of the fitting function is not consistent across research studies. Studies of Scafidi et al. (2015), Ajovalasit et al. (2014), and Ramesh and Ramakrishnan (2016) investigated and compared methods for edge stress measurement. Laufs (2000) conducted experimental and numerical investigations on edge stresses. The measurement of retardation was conducted at multiple points perpendicular to the edge, utilizing double-wedge compensation. The extrapolation of the curve of retardations towards the edge was performed using a 3rd degree polynomial function. This was verified by numerical simulation of the residual stresses on the edge. Lohr (2019) demonstrated the impact of regrinding edges on the edge stress measured by phase-shifting technique (PST), also using a 3rd degree polynomial extrapolation. Schaaf et al. (2017) developed a method for measuring retardation that involved the multiple-wavelength photoelasticity (MWP) and the fitting of the curve with a 2nd degree polynomial function.

Various automated methods were investigated for their potential to replace standard manual compensation measurement methods, such as Tardy and Sénarmont's goniometric compensation, as well as Babinet and Babinet-Soleil compensators, primarily for the purpose of car window control: Ajovalasit et al. (2014) used the center fringe method in monochromatic light and RGB (red-green-blue) photoelasticity in white light (Ajovalasit et al. 2012a and Ajovalasit et al. 2012b) and methods of PST based on Tardy and Sénarmont monochromatic light (Ajovalasit et al. 2011) to measure the retardation until the start of the chamfer. However, there were no statements about the fitting and extrapolation towards the edge. Aben et al. (2013) and Aben et al. (2015) conducted experimental measurements using the scattered light method and the tunneling effect. They extrapolated the retardation curve using a 4th degree polynomial. In their investigations, the edge stress equals the surface stress measured via scattered light.

Current manual measurement methods for edge stress are highly dependent on the operator or are not comprehensible in their measurements. The resulting variability in measurement results poses challenges in terms of reliability and consistency, which is particularly important for the safety requirements of tempered glass. Furthermore, the manual measurement of edge stress can be time-consuming and labor-intensive under production conditions, making efficient quality control difficult. The broad chamfer of architectural glass limits the availability of measurement data and prevents the use of the ASTM C1279 (2023) evaluation method. Given these limitations, there is a clear need for improved measurement techniques and evaluation methods that enable greater reproducibility and accuracy and can be integrated into existing production processes.

In comparison to edge stress measurements, surface stress measurements using the scattered

light method are a more common research practice (Pourmoghaddam et al. 2019, Mognato et al. 2019, Achintha 2021, Nielsen et al. 2021), although no explicit limit values are specified in the European standards EN 12150-1 (2020) and EN 1863-1 (2012).

For fully tempered glass, ASTM C1048 (2025) sets a minimum surface stress of 69 MPa to fulfill only the strength requirement. Research conducted by Mognato et al. (2011) indicated that this value does not align with the fracture pattern requirements of EN 12150-1 (2020) for the European glass product TTG. ISO 12540 (2017) states higher values for surface stress: minimum 80 MPa is required to fulfill the strength, and minimum 90 MPa is required to fulfill the fracture pattern. For HSG, ASTM C1048 (2025) specifies a surface stress range of 24–52 MPa which is valid for glass thicknesses $\leq$ 6 mm, whereas ISO 22509 (2020) defines a similar range of 25–55 MPa, but valid for glass thicknesses between 4 mm and 12 mm. All limit values specified in these standards are independent of format. Typical measurement instruments used to determine the surface stress are SCALP-05 (GlasStress Ltd. 2013) and the GASP system (Strainoptics. Inc. 2025). However, the corresponding single-point measurement methods are time-consuming and, consequently, inefficient for quality control during the production of architectural glass.

The relation between fracture pattern, surface compressive stress or the corresponding mid-pane tensile stress and glass thickness was studied by Mognato et al. (2011), Lee et al. (2012), and Pourmoghaddam and Schneider (2018b), Pourmoghaddam et al. (2019). Pourmoghaddam and Schneider (2018b), Pourmoghaddam et al. (2019) focused on glass panes with thicknesses of 4–12 mm and surface stresses of approx. 50–120 MPa. They found that thinner glass requires higher surface stresses for similar fragmentation. Based on the work of Kraus (2019), Nielsen et al. (2022) proposed a bilinear relationship between geometrical features of fragments and the internal strain energy. Mognato et al. (2011) analyzed panes with thickness of 4–15 mm and determined the minimum surface stresses to be 90 MPa ($t \leq 10$ mm) and 85 MPa ($t \geq 12$ mm) as limits for a safe fracture pattern specified in EN 12150-1 (2020). The correlation of the bending strength and surface stress was investigated in Mognato et al. (2017). They determined a lower boundary of 85 MPa to ensure the bending strength of clear TTG. In a later paper, Mognato et al. (2018) determined a minimum surface stress value of 90 MPa for clear TTG and the range of 35–60 MPa for clear HSG to fulfill the requirements of both strength and fracture pattern.

1.3 Objectives and structure

This dissertation addresses the research question of whether reliable limit values for edge stress and surface stress can be derived from the relationship between destructive tests and non-destructive, photoelastic measurements, and whether these values are suitable for controlling the pre-stress quality in terms of bending strength and fracture pattern of tempered glass. The main objective of this work is to reduce and eventually replace destructive testing in the quality control of European glass products of TTG (EN 12150-1 2020) and HSG (EN 1863-1 2012). Due to the lack of reliable measurement methods for European glass products, this dissertation aims to address this gap in research by proposing a suitable and reliable measurement method for edge stress. As European product standards do not specify limits for either edge stress or surface stress, the subsequent objective is to derive limit values statistically that ensure compliance with the requisite fracture pattern and bending strength of TTG according to EN 12150-1 (2020) and HSG

according to EN 1863-1 (2012). This will be accomplished through an investigation of the relationship between photoelastic stress measurements and mechanical properties, considering the influence of glass thickness.

Current quality control procedures rely on destructive testing of standard-format specimens, requiring the mechanical properties of large glass panes to be estimated indirectly. In addition, the majority of photoelastic investigations to date have been conducted on small-format glass. However, the practical and relevant formats employed in the construction field deviate from this format and have rarely been analyzed by photoelastic measurements. To address this knowledge gap concerning the strength and fracture pattern of large-format glass elements, the photoelastic limit values obtained are validated on large-format glass elements. Introducing a reliable, non-destructive quality control for full-size panes using photoelastic measurements and establishing precise limit values for edge stress and surface stress would significantly reduce material waste in the glass production and ensure the quality and safety of each glass pane.

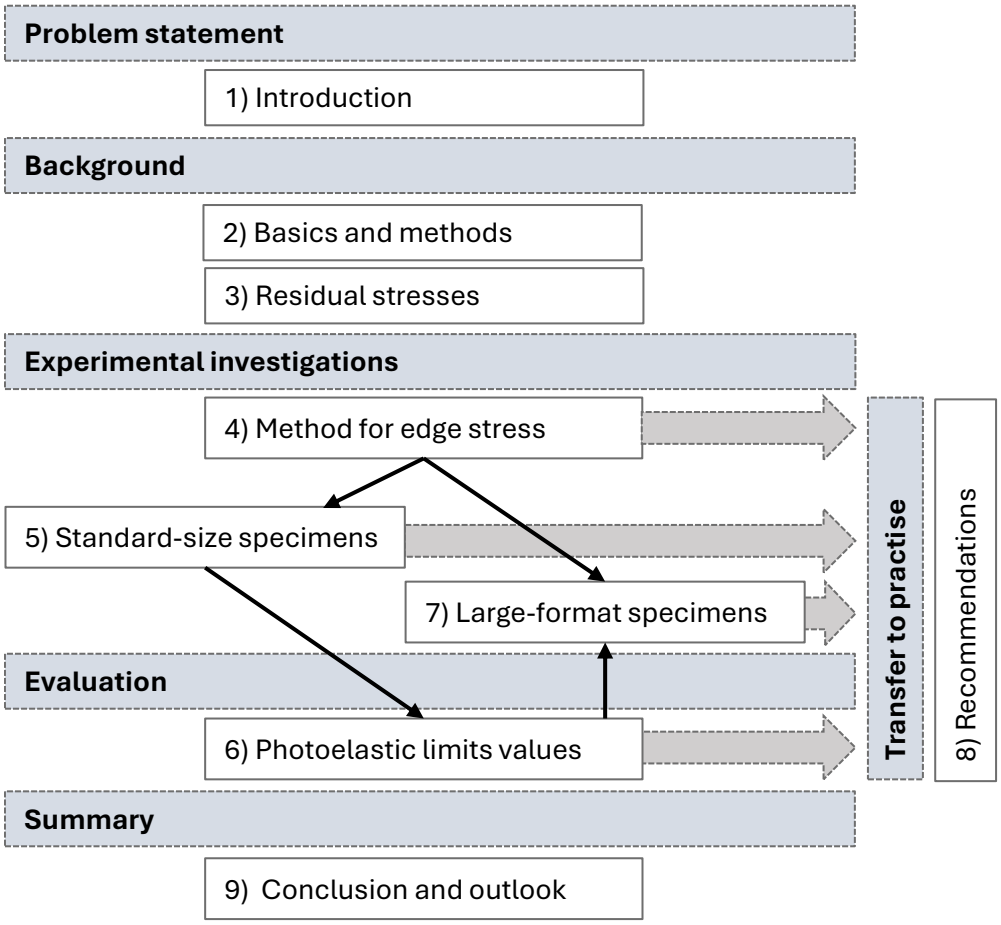

Figure 1.2: Overview over the chapter structure of this dissertation

This dissertation is organized as illustrated in Fig. 1.2. Chapters 2 and 3 provide the theoretical background on the production process and conventional quality control of tempered glass, photoelasticity, and statistical methods, along with an overview of current research on non-destructive quality control of glass using photoelastic measurements.

Chapter 4 develops two methods for measuring retardations and evaluating edge stress

using PST and MWP. The method of PST serves as a reliable basis for investigating the appropriate degree of interpolating and extrapolating the chamfer. Here, coefficients for extrapolating the retardation curve will be determined considering variations in glass thickness and pre-stress levels. Based on these parameters, the measurement method for edge stress with MWP is developed.

Chapter 5 outlines the experimental investigations on standard-format specimens, including both destructive tests for fracture pattern and bending strength as well as photoelastic measurements of surface and edge stress. First, the results from the individual tests are evaluated separately. Then, the relationships between destructive and non-destructive measurements are analyzed in correlation, linear and moderation analysis, particularly regarding the influence of manufacturer and glass thickness.

The objective of Chapter 6 is to identify suitable limit values for the photoelastic measurements of edge and surface stress using statistical methods. By conducting quantile regression and binary logistic regression analysis, the limit values for TTG and HSG are determined to ensure the safety properties required by the product standards for tempered glass in the context of quality control. Additionally, the chapter will investigate whether different limit values are necessary depending on the thickness of the glass.

Chapter 7 presents the results of the experimental investigations on large-format specimens. Here, the photoelastic limits established earlier are tested on the large-format specimens. Additionally, the transferability of photoelastic measurements from small-format to large-format specimens will be discussed. Furthermore, Chapter 8 provides recommendations and requirements for methods measuring and evaluating edge and surface stress with photoelastic limits in the context of non-destructive quality control for TTG and HSG. Chapter 9 concludes with a summary of the results, along with an outlook for future research.

1.4 Own publications

Prior to this thesis, parts of the results were pre-published by the author in peer-reviewed journal articles and conference proceedings and were presented at scientific conferences and in expert committees. The publications underlying this thesis are listed below.

Journal articles

Efferz et al. (2023)	L. Efferz, C. Schuler, and G. Siebert (2023) *Experimental determination of the strength of toughened glass in the area of near-edge holes.* Glass Structures & Engineering. doi: 10.1007/s40940-023-00245-w
Efferz et al. (2024a)	L. Efferz, C. Schuler, and G. Siebert (2024) *Photoelastic Measurements and Evaluation Methods for Edge Stress in Architectural Tempered Glass.* Glass Structures & Engineering. doi: 10.1007/s40940-024-00270-3

Efferz et al. (2024b)	L. Efferz, K. Thiele, M. Schuster, C. Schuler, G. Siebert, and J. Schneider (2024) *Relation between edge stress, bending strength, surface stress and fracture pattern of thermally toughened glass.* Glass Structures & Engineering. doi: 10.1007/s40940-024-00269-w
Efferz et al. (2025c)	L. Efferz, M. Schuster, M. A. Kraus, C. Schuler, and G. Siebert (2025) *Key parameters for the non-destructive quality control of thermally toughened safety glass.* Journal of Building Engineering. doi: 10.1016/j.jobe.2025.112613
Efferz et al. (2025b)	L. Efferz, C. Schuler, and G. Siebert (2025) *Non-destructive, photoelastic quality control for large-format, thermally toughened glass.* Glass Structures & Engineering. doi: 10.1007/s40940-025-00302-6
Efferz and Schuler (2026)	L. Efferz and C. Schuler (2026) *Oberflächendruck- und Kantenmembranspannung in thermisch vorgespanntem Glas: Zusammenhang und Bewertung spannungsoptischer Messungen.* Stahlbau 95, Sonderheft Glasbau & Fassade. doi: 10.1002/stab.70160
Efferz et al. (2026)	L. Efferz, C. Schuler, and G. Siebert (2026) *Statistical determination and evaluation of photoelastic limits for heat-strengthened glass.* Glass Structures & Engineering [accepted in publication].

Conference contributions

Efferz (2024)	L. Efferz (2024) *Determining and evaluating edge stresses.* Poster, Pecha Kucha. In: glasstec conference – glass melting pot, Düsseldorf.
Efferz (2025b)	L. Efferz (2025) *Zerstörungsfreie Qualitätskontrolle von Einscheibensicherheitsglas mit spannungsoptischen Methoden.* Labor für Stahl- und Leichtmetallbau, Hochschule München: Glas im konstruktiven Ingenieurbau 19.
Efferz (2025a)	L. Efferz (2025) *Non-Destructive Quality Control in Thermally Toughened Glass.* In: German Group of IABSE – Young Engineers Colloquium Munich 2025.

Research activities

This thesis was conducted within the scope of the author's activities as a research assistant at the Hochschule München University of Applied Sciences (HM), Munich, Germany, in the research project "NEMA - Addition of photoelastic methods and analysis concepts to a standard for tempered safety glass to reduce destructive testing". The experimental investigations presented in this work were based on specimens originating from the research project NEMA which was carried out between 1st October 2022 and 31st December 2024 in cooperation between the HM, Technical University Darmstadt (TUDa), Darmstadt, Germany and the three glass manufacturers INTERPANE Glasgesellschaft mbH, Plattling, Germany, Glas Trösch GmbH, Mengen, Germany, and Sicherheitsglastechnik Oelsnitz (Vogtl.) GmbH, Oelsnitz/Vogtl., Germany, funded by the German Federal Ministry for

Economic Affairs and Climate Action (BMWK) as part of the funding program WIPANO with funding code FKZ 03TN0037A. The corresponding final report is cited as follows:

Efferz et al. (2025a) L. Efferz, C. Schuler, M. Schuster, K. Thiele, H. Riedel, J. Schneider, A. Strobel, B. Gammenthaler, M. Siegler, M. Frank, C. Groth, T. Schuller, and P. Pfannenstill (2025)
NEMA - Addition of photoelastic methods and analysis concepts to a standard for tempered safety glass to reduce destructive testing. Final report. FKZ 03TN0037A.
Institut für Material- und Bauforschung Hochschule München, Institut für Statik und Konstruktion TU Darmstadt, INTERPANE Glasgesellschaft mbH Plattling, Glas Trösch GmbH Mengen, Sicherheitsglastechnik Oelsnitz (Vogtl.) GmbH, Softsolution GmbH. Hannover: Technische Informationsbibliothek. doi: `https://doi.org/10.34657/18731`

2 Theoretical basics and analytical methods

2.1 Tempered glass

Glass is classified as an amorphous solid that exhibits no crystalline structure below its melting point and therefore exists in a state of frozen, supercooled liquid. The material exhibits brittle failure behavior. This signifies that fracture is initiated without prior warning. The strength of glass is primarily dependent on the notch sensitivity of the surface subjected to tensile stress. Manufacturing processes inherently produce structural defects and microscopic surface flaws on glass surfaces. These defects function as stress concentrations under tensile loading, generating stress peaks at the crack tip that initiate fracture. Furthermore, strength of glass is additionally influenced by size effects, loading rate and duration, environmental medium, and temperature (Schneider et al. 2016). Notably, sustained stress exposure induces subcritical crack growth effects, which substantially reduce material strength. A further parameter influencing strength is surface pre-stress, wherein tensile stresses at surface microdefects are suppressed by compressive stresses introduced through thermal or chemical treatment.

Tempered glass is a highly used product in construction applications such as windows, façade glazing, balustrades, and interior glazing because of the increased resistance against external loadings and the specific fracture pattern. The fundamentals can be found in Griffith (1921), Beason and Morgan (1984), Nielsen (2009), Jebsen-Marwedel and Brückner (2011), Siebert and Maniatis (2012), and Schneider et al. (2016). In the construction industry, soda-lime silicate glass is predominantly used due to its favorable properties. Soda-lime silicate glass primarily consists of quartz sand (SiO_2), calcium carbonate (CaO), and sodium carbonate (Na_2O). While quartz sand functions as a network former, calcium carbonate and sodium carbonate are classified as network modifiers. Additional constituents such as potassium oxide or magnesium oxide are employed to optimize the manufacturing process. Conversely, feldspar and alumina are incorporated to enhance glass hardness and chemical resistance.

2.1.1 Manufacturing process and glass products

The basic product for many glass applications is float glass. With the development of the floating process in industrial scale in 1959, mass-produced construction glass could be manufactured industrially and on a continuous basis. Fig. 2.1 illustrates the floating process: The molten glass mass floats atop the tin bath due to its lower density compared to the tin. Due to the flat surface of the free liquids, a plane-parallel glass plate is established. To achieve the desired glass thickness, the continuous glass band is drawn upward using top rollers that grip the outer edge of the glass surface. Through this control mechanism, glass thicknesses ranging from 0.4 mm to conventionally 19 mm, and up to 28 mm, can be produced. At the beginning of the floating process, the glass mass exhibits a temperature

of 1000 °C and cools to 600 °C during the floating process, at which point the glass mass solidifies. In the annealing tunnel, the glass band is subsequently cooled in a controlled manner to room temperature, after which it can be cut and further processed.

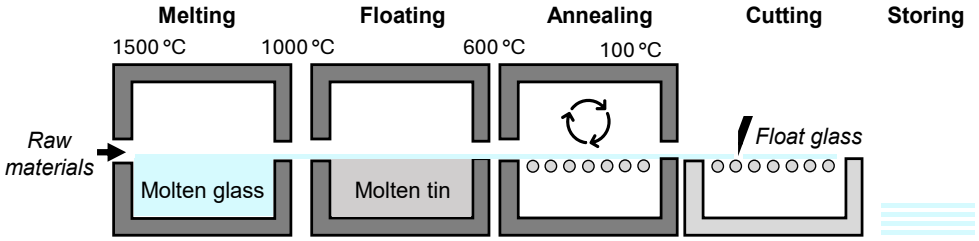

Figure 2.1: Floating process of glass adapted from Nielsen (2009) and Dix (2024)

It has been demonstrated that gradual and methodical cooling to ambient temperature results in thermally relaxed float glass, also referred to as annealed glass (EN 572-1 2016), characterized by a low bending tensile strength of approximately 45 N/mm² and modest thermal shock resistance of approximately 40 K. Float glass constitutes the fundamental base material employed in numerous mechanical processing operations.

Glass is broken and shaped to the desired format through surface scoring followed by controlled bending. Consequently, the cut glass exhibits irregular and sharp edges. For safety reasons and to prevent edge chipping, these sharp edges are subsequently chamfered through edge finishing processes. Additional edge finishing methods include ground and polished edges, wherein the edge surface is processed to the desired level of smoothness and polish (DIN 1249-11 2023).

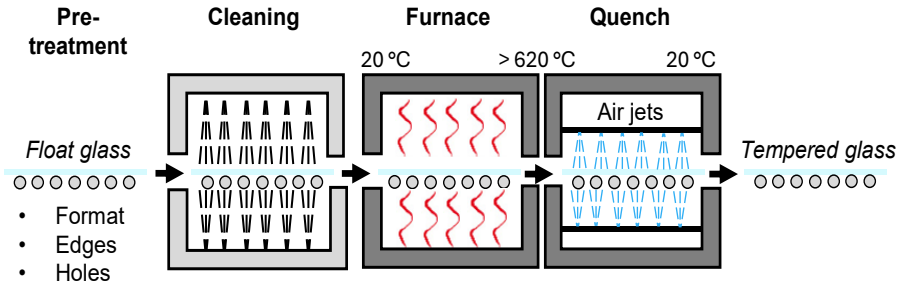

Figure 2.2: Tempering process of glass adapted from Nielsen (2009) and Dix (2024)

To increase resistance to external stresses, the base float glass can be thermally toughened. The pre-stressing can suppress the tensile stresses that initiate crack growth and subsequent fracture at surface defects. In the tempering process illustrated in Fig. 2.2, the clean and cut glass is heated homogeneously to a minimum of 620 °C, which exceeds the transformation temperature by over 100 °C. Subsequently, in the quench zone, the glass is rapidly cooled in a controlled manner through targeted air jet cooling and controlled movement of the pane. At approximately 100 °C above the transformation temperature, glass exists in a viscoelastic state, wherein the material exhibits time-dependent deformation behavior and stress relaxation can occur. Upon cooling both surfaces of the glass pane, a temperature difference develops between the surface and the glass core. This temperature gradient induces differential thermal expansion coefficients within the glass: the warmer core attempts to contract but is constrained by the cooler glass surfaces. Once returned to the elastic state of material behavior at room temperature, a residual stress state develops

across the thickness of the glass, characterized by compressive stresses at the surfaces and tensile stresses in the core. Depending on the cooling duration, two distinct glass products are formed: TTG according to EN 12150-1 (2020) or HSG according to EN 1863-1 (2012), each exhibiting different bending tensile strengths and fracture patterns.

Due to its fine fracture pattern, consisting of small, blunt fragments, TTG is classified as a safety glass. However, TTG in laminated glass with a conventional PVB (polyvinyl butyral) interlayer may exhibit limited residual load-bearing capacity after fracture, depending on the support conditions and the glass configuration. HSG exhibits a distinctly different fracture pattern. Due to the slower cooling rate, the residual stresses are substantially lower than those in TTG, which is reflected in a coarser fracture pattern similar to annealed float glass, characterized by larger, sharp fragments. Consequently, HSG is not classified as a safety glass in monolithic applications. However, when utilized as a laminated glass with PVB as the interlayer, the glass retains residual load-bearing capacity. For production reasons, the production of HSG is limited to a maximum thickness of 12 mm. Table 2.1 compares the properties of bending tensile strength, thermal shock resistance, and fracture pattern of these three glass products and their corresponding European standards.

Table 2.1: Properties of glass product of basic soda-lime silicate glass from the European standards EN 572-1 (2016), EN 1863-1 (2012), and EN 12150-1 (2020)

Glass product	European standard	Bending strength	Thermal shock resistance	Fracture pattern
Annealed float glass	EN 572-1 (2016)	45 MPa	40 K *	Large, sharp fragments
Heat-strengthened glass	EN 1863-1 (2012)	70 MPa	100 K	Large, sharp fragments with occasional island formation
Thermally toughened safety glass	EN 12150-1 (2020)	120 MPa	200 K	Fine, crumbly fragments with no residual load-bearing capacity

* Generally accepted value that is influenced by edge finishing and glass type (EN 572-1 2016)

2.1.2 Conventional quality control for tempered glass

To ensure the properties and quality of tempered glass, the European product standards EN 12150-1 (2020) and EN 1863-1 (2012) require destructive tests of small-format glass panes measuring 360 mm x 1100 mm, which must be toughened in addition to the project business. These panes must be checked for fracture pattern and bending tensile strength of the respective tempered glass type.

2.1.2.1 Bending strength

The bending strength of glass is not a material constant, but rather, as is usual with brittle materials, a measured value that depends on the quality of the surface subjected to tensile stress (Siebert and Maniatis 2012). This means that microscopic or macroscopic defects on the glass surface have a negative effect on the bending strength. Therefore, the bending

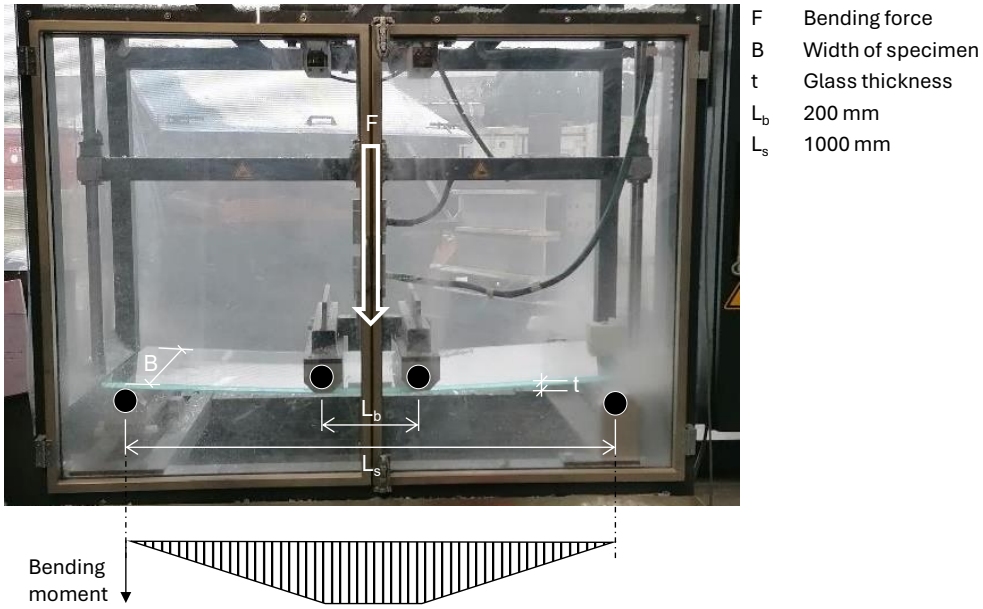

Figure 2.3: Position of specimen in four-point bending test machine with curve of bending moment based on Efferz et al. (2023)

strength of glass is a statistical value linked to the fracture probability and the load type. One method for determining the bending strength is the four-point bending test according to EN 1288-3 (2000) as illustrated in Fig. 2.3. After measuring the glass thickness t and width of the specimen B, the glass is placed in the testing machine on freely rotating rollers with a distance of $L_s = 1000$ mm. Then the specimen is loaded with two bending rollers at a distance of 200 mm (L_b) with the stress rate of 2 MPa/s, which is required in EN 1833-3, until breakage to obtain the breaking force F_{max}. The test speed depends on the thickness of the test specimens and is specified in Table 2.2.

Table 2.2: Force-controlled test speeds depending on glass thickness for stress rate of 2 MPa/s according to EN 1288-3 (2000) from Efferz et al. (2023)

Glass thickness [mm]	6	8	10	12
Force-controlled test speed [N/s]	21.6	38.4	60.1	86.4

In the area between the bending rollers L_b, there is a uniformly loaded area of the bending moment, the course of which is shown in Fig. 2.3 below. The bending stress is subsequently calculated, as outlined in Equation (2.1), by determining the breaking force F_{max}, the actual geometry of the test specimen, and the dead weight of the glass pane σ_{bG} from Equation (2.2). The latter equation is based on the gravitational acceleration g (simplified with 10 m/s^2) and the density of glass ($\rho = 2500$ kg/m^3). The factor k represents the correction factor for the effective bending area. For failure initiated at the glass edge, the correction factor $k = k_e$ ranges from 0.95 to 1.5 (Peters et al. 2023), depending on the glass thickness and the ratio of the vertical displacement of the centre of the glass plate to the glass thickness. For surface failure, the correction factor $k = k_s$ is assumed to be 1.

$$\sigma_{bB} = k \left[F_{\max} \frac{3\,(L_s - L_b)}{2Bt^2} + \sigma_{bG} \right] \tag{2.1}$$

$$\sigma_{bG} = \frac{3\varrho g L_s^2}{4t} \tag{2.2}$$

For statistical assurance, at least ten samples per batch of tempered glass must be tested and analyzed using the test setup of EN 1288-3 (2000) as required by EN 12150-1 (2020) and EN 1863-1 (2012). The characteristic bending strength must be determined as the 5% quantile with a 95% confidence level. This value represents the stress below which 95% of the specimens are expected to fail, thereby providing a conservative and safety-conscious design parameter. For tempered glass made of basic float glass, the characteristic strength should show a minimum of 120 MPa for TTG and 70 MPa for HSG. However, determining the 5% quantile from limited sample sizes involves statistical estimation, and different methodological approaches can yield different results. According to Schneider et al. (2016), the Weibull and lognormal distributions are the best approaches for estimating characteristic glass strength from bending test data.

For annealed glass, the two-parameter Weibull distribution (basics in Section 2.3.3) provides a theoretically motivated probabilistic framework based on the weakest-link concept, which is particularly suited to model the fracture behavior of brittle materials such as glass. In this framework, fracture is assumed to originate from the most critically stressed defect within the specimen, making Weibull statistics mechanistically appropriate for predicting characteristic glass strength. For tempered glass, a clear distinction must be made between the bending strength as a material and flaw-controlled property and the test bending strength obtained from mechanical testing. Due to the thermal pre-stressing, a minimum effective strength is assumed for tempered glass, which originates from the residual compressive stress. This surface compressive stress must first be overcome before tensile stresses at surface flaws become effective and fracture can occur. The test bending strength of tempered glass measured in bending tests results from the additive superposition of the externally applied stress and the residual stress present in the glass, typically the surface stress acting under bending about the weak axis. According to Equation (2.3), the bending strength σ_{bG} as material property can therefore be determined from the test bending strength σ_{test} by accounting for the residual stress $\sigma_{residual}$ as compressive stress with negative sign (Siebert and Maniatis 2012).

$$\sigma_{bB} = \sigma_{test} + \sigma_{residual} \tag{2.3}$$

According to Siebert and Maniatis (2012), the evaluation of the two-parameter Weibull distribution is only sufficient for evaluating the bending strength σ_{bG}. Therefore, when evaluating tempered glass, it is necessary to include residual stress $\sigma_{residual}$ as a location parameter, x_0, resulting in a three-parameter Weibull distribution as indicated in Equation (2.15). For Weibull distribution, parameter estimation can be performed using maximum likelihood estimation, least squares regression based on ranked data (Weibull plot methods), and the method of moments (Genschel and Meeker 2010, Teimouri et al. 2013). Comparison of the estimations methods can be found in Datsiou and Overend (2018) and Brokmann (2022).

The lognormal distribution is another distributional model applied to strength data of brittle materials, particularly when empirical data exhibit characteristics that deviate from Weibull predictions. Because the analysis presented in this work focuses exclusively on the Weibull distribution as the primary framework for strength characterization, detailed discussion of lognormal modeling is deferred to Schneider et al. (2016) and Siebert and Maniatis (2012).

2.1.2.2 Fracture pattern

The quality control of tempered glass is conducted through fracture tests, wherein the glass is examined to ascertain compliance with the prescribed fracture pattern EN 12150-1 (2020) and EN 1863-1 (2012). Five glass panes measuring 360 mm x 1100 mm without holes, perforations, or cutouts are utilized for the fracture test. Using a sharp steel tool, these panes are fractured by striking the midpoint of the long edge, 13 mm away from the edge. The panes are held without clamping at the edges by a frame to avoid scattering of glass fragments without impeding the expansion of the pane. Subsequently, the fracture pattern is evaluated with a region around the impact point having a radius of 100 mm and strips of 25 mm width at the edges excluded from the evaluation (Fig. 2.4). The evaluation of the fracture pattern must be completed within 5 min after fracture to ensure standardized assessment and to avoid changes in the fracture pattern due to further breakage of the glass fragments.

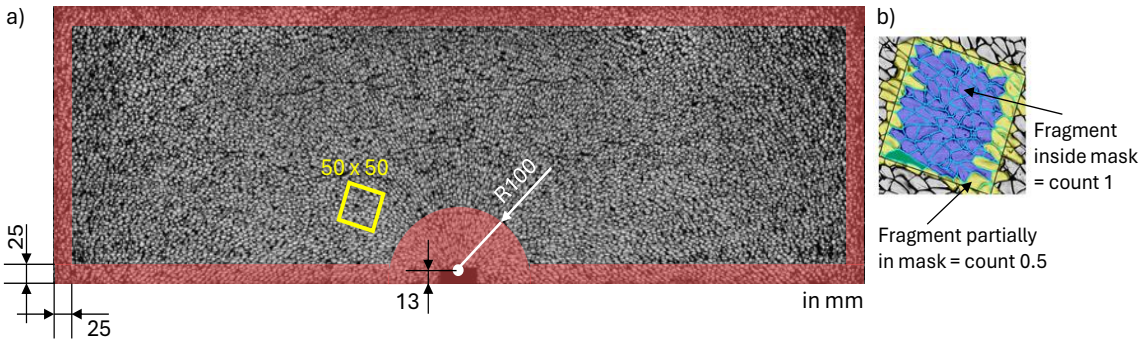

Figure 2.4: Exemplary sample of 10 mm TTG in fracture test according to EN 12150-1 (2020): a) scan of fractured glass; dimensions in mm. Red: from evaluation excluded area, center of circle: impact position (13 mm from glass edge). Yellow: 50 mm x 50 mm counting mask, b) Fragments in counting mask (yellow: fragments that are partly in the evaluation mask) and the longest fragment (green), courtesy of Miriam Schuster, based on Efferz et al. (2024b)

For TTG according to EN 12150-1 (2020), the fracture pattern test is carried out by counting the crack-free fragments within a 50 mm x 50 mm mask at the point with the coarsest fracture structure (Fig. 2.4). All fragments only partially in the mask are counted as half a fragment. The specimen is classified as TTG if the number of fragments within the evaluation field is at least 40 (for glass thicknesses between 4–12 mm). In addition, the length of the longest fragment within the entire test sample (excluding the edge areas and the impact area) must not exceed 100 mm.

For the evaluation of the fracture pattern of HSG according to EN 1863-1 (2012), each fragment is classified based on its location and size. Ideally, large fragments with at least

one edge reaching the specimen edge are formed. In most cases, cracks propagate parallel to the edge in this region. In contrast to annealed float glass, HSG frequently exhibits island formation. These are fragments that do not touch the glass edge and are classified based on their area/mass equivalent. The *area/mass equivalent* is calculated from the fragment mass m using the glass thickness t and the glass density ($\rho = 2500$ kg/m^3) as shown in Equation (2.4).

$$\text{Area/mass equivalent} = \frac{m}{t\varrho} \tag{2.4}$$

Fragments with an area/mass equivalent larger than 100 mm^2 are classified as islands. Fragments with an area/mass equivalent to or smaller than 100 mm^2 are classified as particles. Fig. 2.5 illustrates the distinction between particles and islands on an exemplary fractured HSG specimen with evaluation areas. To be classified as HSG according to EN 1863-1 (2012), at least four out of five test specimens must satisfy the following criteria: no more than two island fragments per specimen should be present, and no individual island fragment shall have an area/mass equivalent to or exceeding 1,000 mm^2. Furthermore, the sum of the total area/mass equivalent of all particles must remain below 5,000 mm^2. If one of the five specimens fails to meet these criteria, acceptance may still be granted provided that the specimen contains no more than 3 island fragments and the combined area/mass equivalent of all islands and particles does not exceed 50,000 mm^2.

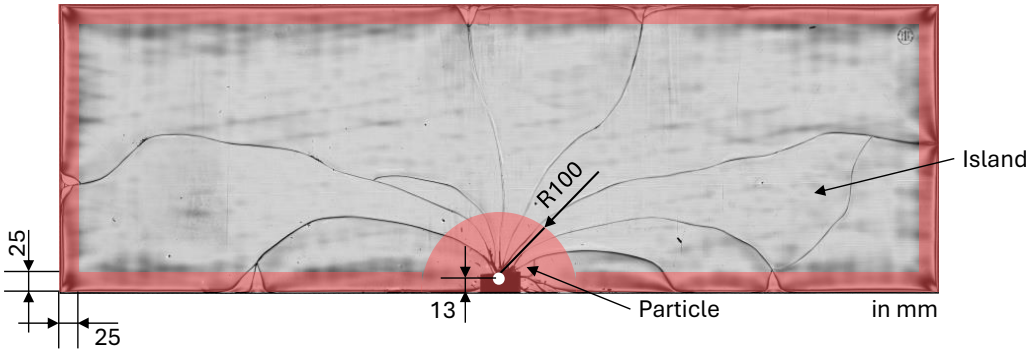

Figure 2.5: Evaluation of fracture pattern of heat-strengthened glass with representation of island and particle fragments. Red: from evaluation excluded area, center of circle: impact position 13 mm from glass edge

To illustrate the influence of tempering degree, three fracture patterns of 10 mm specimens are presented in Fig. 2.6. While Fig. 2.6a and Fig. 2.6c display typical fracture patterns for HSG and TTG, respectively, Fig. 2.6b exhibits a fracture pattern that is simultaneously too coarse for TTG and too fine for HSG, and therefore cannot be classified as either glass type according to EN standards.

2.2 Basics of photoelasticity

This chapter describes the basics of photoelasticity with the principles of the polariscope and the Wertheim's law in transparent materials under stress. Subsequently, the photoelastic measurement methods of PST, MWP, and scattered light were introduced, which form the

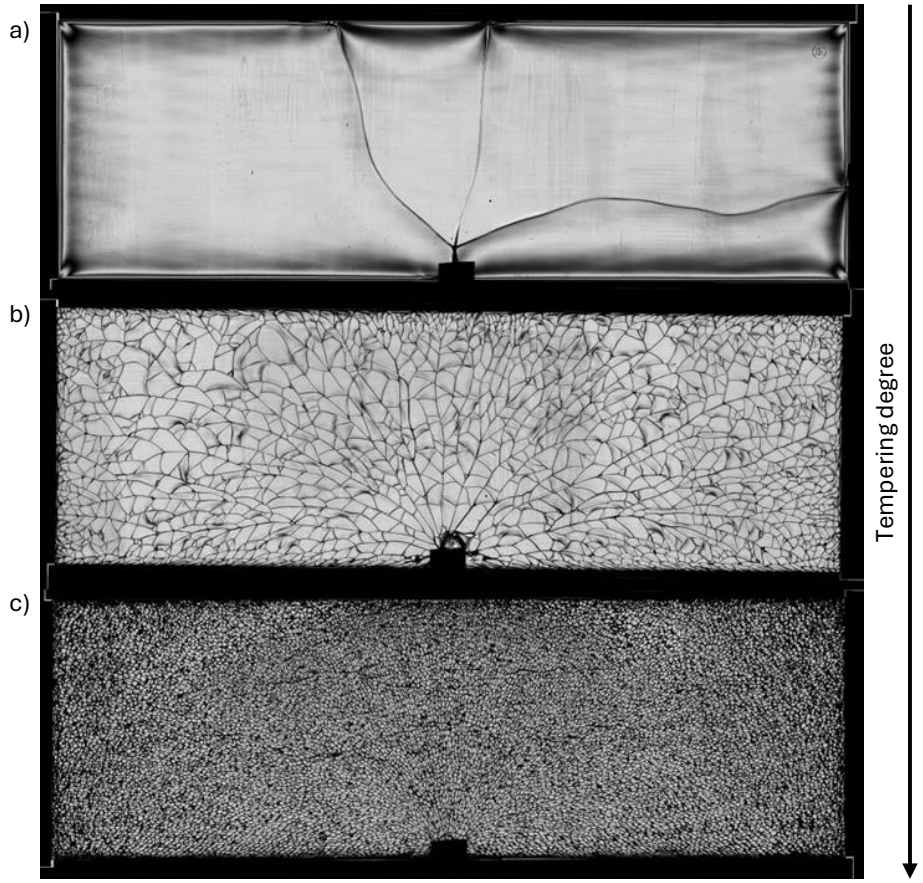

Figure 2.6: Typically fracture patterns with increasing tempering degree for a) conforming heat-strengthened glass, b) non-conforming heat-strengthened glass, c) conforming thermally toughened safety glass

basis of the measuring devices used in the subsequent investigations of this dissertation. Detailed descriptions of the measurement procedures and the operation of the respective devices are provided in Sections 3.2, 4.2, 4.3, and 5.3.1. The basics of photoelasticity and especially in the glass field can be found in Aben and Guillemet (1993), Ajovalasit et al. (2015a), Ramesh and Sasikumar (2020), Dix (2024), and Ramesh (2000).

Light propagation in space can be described as an electromagnetic wave with periodically oscillating electric and magnetic field vectors (Maxwell 1873). The amplitude of the electric field determines the light intensity, whereas the frequency defines the wavelength. Light with a single wavelength is referred to as monochromatic light, while light composed of a continuous spectrum of many wavelengths is referred to as white light. In a homogeneous, isotropic medium, light propagates in straight lines: reflection and refraction only change its direction and the spatial distribution of intensity. Polarization describes the direction of oscillation of the electric field vector of light (Paschotta 2006, Peatross and Ware 2015). Unpolarized light contains many oscillation directions, whereas linearly polarized light oscillates in a single fixed plane. Polarized light can be obtained naturally by reflection and scattering, or artificially by using polarizing filters or specific prisms. Based on linear polarized light, circularly and elliptically polarized light can be generated by inserting optical retardation elements, such as retardation plates or wave plates.

2.2.1 Stress-optical law and plane polariscope

Transverse light waves propagate in straight lines through air. When they encounter a different medium, their propagation velocity changes at the interface, causing refraction of the light ray. In an isotropic, transparent medium, light propagates according to Snell's laws of refraction and reflection and passes through the material as a single ray without splitting into separate components (Ramesh 2000). By contrast, when a transparent material is externally loaded or internally stressed, it becomes optically anisotropic, causing the incident light to split into two refracted rays. This phenomenon is known as birefringence or double refraction, which results in a visually apparent pattern of gray or colorful interference. Photoelasticity is a technique that allows for the calculation of the stresses that generate these patterns in transparent, birefringent materials (Neumann 1841, Maxwell 1873). In a photoelastic apparatus called a polariscope, see Fig. 2.7, the relationship between stresses and light retardation can be established. This setup consists of two linear polarizers and a loaded medium exhibiting birefringent properties. The second polarizer is typically referred to as the analyzer. In the so-called dark-field configuration, the polarization directions of the polarizer and analyzer are perpendicular to each other. Under this arrangement, light waves are extinguished in the absence of an intermediate specimen. However, the birefringent medium causes brightening depending on the specimen thickness, wavelength, and the angle between the polarizer axis and the principal stress directions within the specimen.

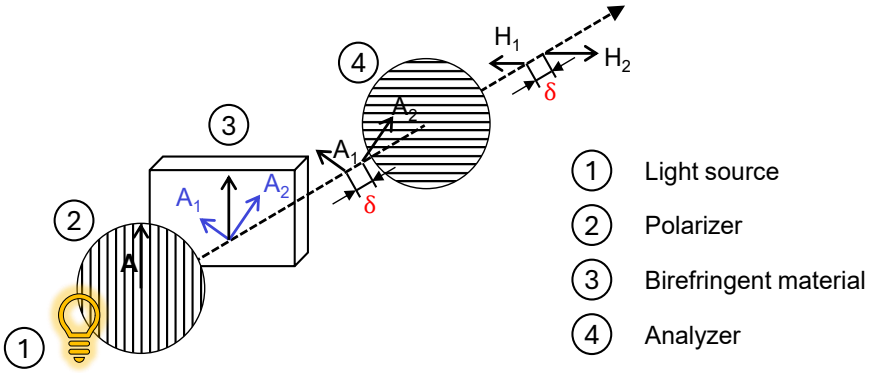

Figure 2.7: Design and measuring principle of plane polariscope

The first polarizer generates linearly polarized light oscillating vertically from the monochromatic light source, represented by vector A, by transmitting only light waves in a single polarization plane. When the light encounters the specimen, the amplitude of the vertical vector is decomposed into two orthogonal components, A_1 and A_2, corresponding to the two principal stresses σ_1 and σ_2, due to the load. These components possess different refractive indices, n_1 and n_2, respectively, depending on their stress states. Since the components have different propagation velocities, a phase difference or retardation δ occurs after the waves exit the specimen. The subsequently oriented horizontal analyzer transmits only the components H_1 and H_2, whose resultant wave determines the observed visibility. Due to the prior decomposition of A into A_1 and A_2 by the polarizer, these components possess equal amplitudes. When the principal stress difference equals zero, the retardation is also $\delta = 0$. In this case, the components H_1 and H_2 cancel each other because they are in opposite phase, resulting in darkness in the image. The same applies to integer multiples so called fringe orders of the wavelength under monochromatic light. At these locations,

no light reaches the detector. Conversely, when the retardation equals half a wavelength, the light wave oscillations constructively interfere and maximum brightness is observed in the image.

The retardations correlate with the stresses in the material according to the stress-optical law, also known as Wertheim's law, see Equation (2.5). It describes the relative retardation δ that occurs when polarized light with wavelength λ is directed perpendicular to a plate of thickness t and photoelastic material constant C, thereby splitting it into two components that can be directly related to the principal stress difference $\sigma_1 - \sigma_2$.

$$\delta = \frac{C}{\lambda} (\sigma_1 - \sigma_2) t \tag{2.5}$$

Connecting the dark points corresponding to integer retardations, they form dark lines known as isochromatics or fringes. These fringes represent loci of constant principal stress difference. The specific multiple of the retardation determines the order of the isochromatic m: the 0th, 1st, 2nd, and n^{th} isochromatic orders correspond to the 0th, 1st, 2nd, and n^{th} multiples of the ratio of retardation to the employed wavelength, respectively. This relationship can be expressed mathematically as $\delta = m\lambda$.

2.2.2 Phase-shifting technique

The principle of PST is the determination of retardation and stress patterns in birefringent material by digitally acquiring multiple images with different intensity levels. These intensity variations are obtained by systematically rotating optical elements within the photoelastic setup (Ramesh and Sasikumar 2020). The basic setup consists of a four-step plane polariscope or a six-step circular polariscope, but various combinations of steps are available (Ramesh and Ramakrishnan 2016). Compared to traditional fringe-based methods, phase-shifting techniques offer higher accuracy, improved noise resistance, and full-field quantitative results. However, classical implementations rely on mechanically rotating optical components. An important extension of this approach is the pixelated phase-shifting method, which employs micropolarizer arrays (Ramesh and Sasikumar 2020, Dix et al. 2022). In this method, the mechanical rotation of the analyzer is replaced by a polarization-sensitive camera, enabling the simultaneous acquisition of phase-shifted intensity information at each pixel.

Fig. 2.8 illustrates the arrangement of the photoelastic setup of the measuring device StrainScope flex (ilis gmbh 2023) which is employed in this work. The system comprises a monochromatic light source with a wavelength of 588 nm and a plane polarizer oriented at 45° with respect to the principal stress directions. A quarter-wave plate, parallel to the polarizing filter, is positioned between the glass sample and the analyzer. Its purpose is to convert the elliptically polarized light emerging from the birefringent specimen into linearly polarized light prior to analysis. The device determines the retardation on a per-pixel basis using the Sénarmont compensation method. For this purpose, the analyzer is rotated from the initial extinction position toward the orientation corresponding to maximum transmitted intensity, thereby measuring different degrees of polarization (Reichert and Katte 2005). From the measured analyzer rotation angle α and the known wavelength λ of the light source, the optical retardation R is calculated according to Equation (2.6). The

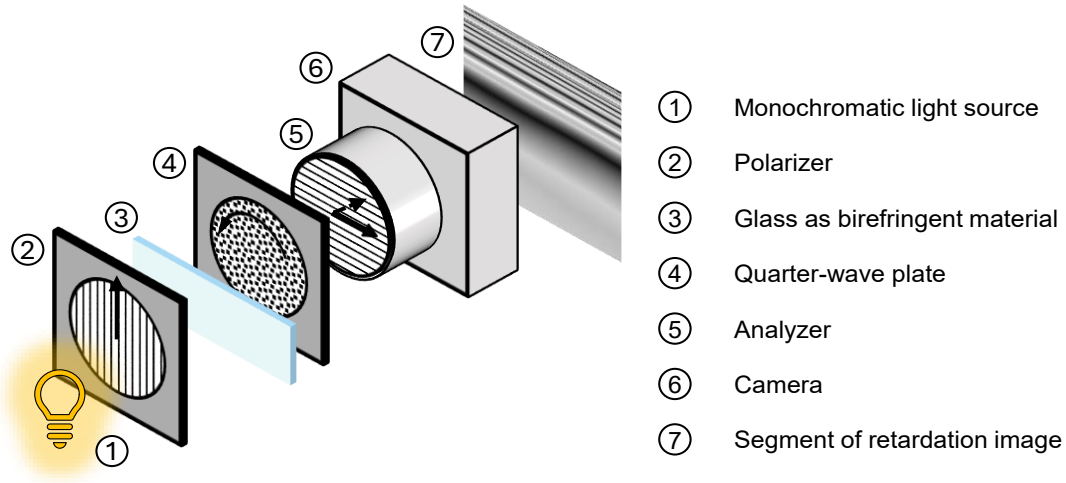

Figure 2.8: Photoelastic setup of phase-shifting technique as pixelated phase-shifting method with monochromatic light source from Efferz et al. (2024b)

output file of the StrainScope flex (ilis gmbh 2023) displays retardation values ranging from zero to half the wavelength and an intensity image without the retardation values.

$$R = \frac{\alpha\lambda}{180°} \tag{2.6}$$

2.2.3 Multiple-wavelength photoelasticity method

The MWP method is a development of the half-wavelength photoelasticity introduced by Voloshin and Burger (1983), which determines the retardations occurring in the model via a function of light intensity (Dix et al. 2022). One potential disadvantage of half-wavelength photoelasticity is that it can only detect retardations less than the 0.5^{th} fringe order. However, by combining multiple wavelengths of monochromatic light sources, relative retardations can be obtained using the MWP method in a fringe order of at least 1. This technique is already used in the production process using the commercial measuring device LineScanner (Softsolution GmbH 2023b) to measure retardations over the entire surface of the glass, and then evaluate optical anisotropy effects in tempered architectural glass. The basic configuration of this device corresponds to a bright-field circular polariscope and is shown in Fig. 2.9. Based on MWP, three monochromatic light-emitting diodes (LEDs) are used as light sources, emitting in the blue (442.35 nm), green (499.30 nm), and red (626.80 nm) wavelength ranges.

More comprehensive investigations of the measurement and assessment of optical anisotropy effects using MWP in tempered architectural glass can be found in Dix (2024), Hidalgo and Elstner (2018), Schuler et al. (2022). Furthermore, based on the acquired isochromatic images, the MWP method was employed to evaluate the influence of near-edge holes on the strength of point-fixed glass specimens (Dix et al. 2021, Efferz et al. 2023).

Fig. 2.9 shows the arrangement of the optical elements of the bright-field circular polariscope. In contrast to a dark-field polariscope configuration (see Section 2.2.1), the bright-field setup is characterized by parallel alignment of the polarizer and analyzer. As a result,

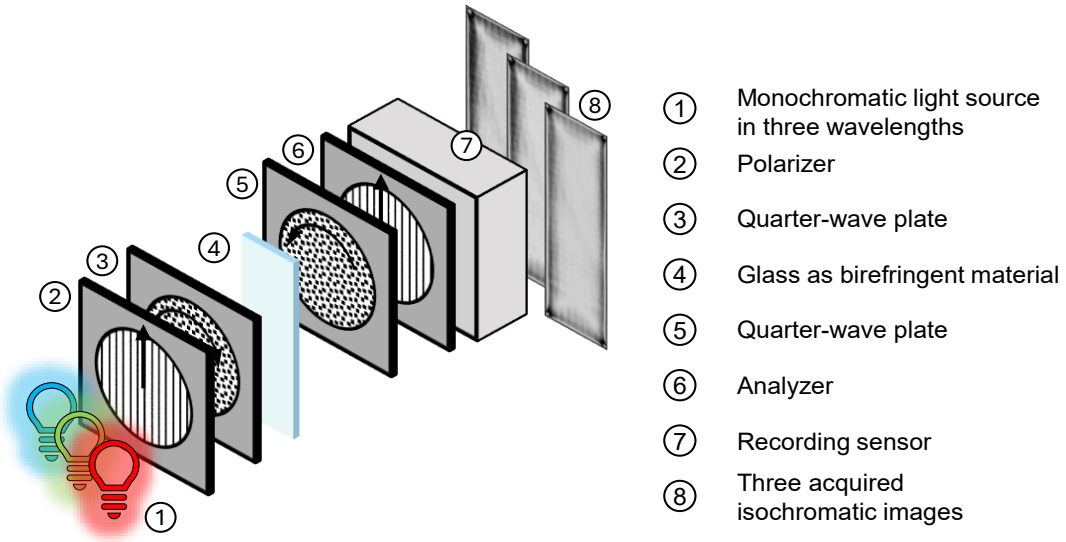

Figure 2.9: Photoelastic setup of a bright-field circular polariscope with telecentric LEDs in three wavelengths from Efferz et al. (2024a)

regions without optical retardation remain bright, whereas stress-induced retardation leads to partial or complete extinction of the transmitted light, appearing as darker regions in the image. The transmitted intensity I_t in the bright-field configuration is given by the incident light intensity I_0 and the stress-induced retardation δ, according to Equation (2.7).

$$I_t = I_0 \cos^2\left(\frac{\delta}{2}\right) \tag{2.7}$$

According to this relationship, zero transmitted intensity is obtained for the relative retardations equal to odd multiples of a half a wavelength, given by $\delta = (2m + 1)\pi$, with $m = 0, 1, 2, \ldots$. Consequently, the isochromatic fringes observed in the bright-field arrangement correspond to half-integer fringe orders of 0.5, 1.5, 2.5, and so forth (Ramesh 2000).

To obtain a circular polariscope, two additional quarter-wave plates are added before and after the sample to the plane polariscope shown in Fig. 2.7. This configuration converts linearly polarized light into circularly polarized light and back again, rendering the measurement insensitive to the orientation of the principal stress axes. As a result, only isochromatic information related to the magnitude of the principal stress difference is retained.

2.2.4 Scattered light method

The scattered light method is a photoelastic technique for determining the three-dimensional residual stress distribution (R. Weller 1941, Bateson et al. 1964, Ascough 1981). In this method, a focused, monochromatic laser beam is introduced into the medium under an oblique angle and the light scattered from stress-induced birefringent volume elements is recorded by a camera arranged perpendicular to the beam. As the laser beam propagates

through the medium, local residual stresses cause birefringence, which changes the polarization state of the light along the beam path. The scattered light emerging sideways is partially polarized and its intensity depends on the local optical retardation, which is proportional to the difference of the principal stresses according to the stress-optical law. Further details can be found in the reviews of Ramakrishnan and Ramesh (2016) and Dix et al. (2022).

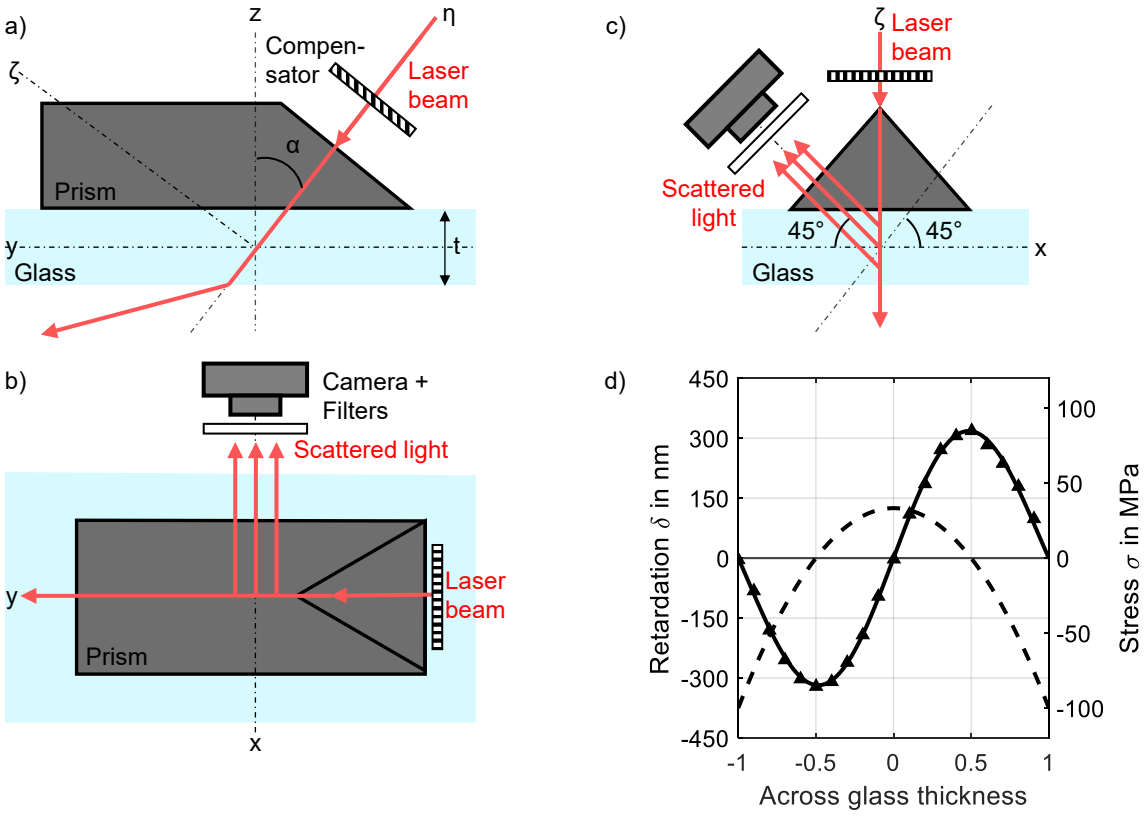

Figure 2.10: Design and measuring principle of SCALP-05 adapted from GlasStress Ltd. (2013), a) side view, b) top view, c) front view, d) retardation and stress distribution across the glass thickness

In the field of architectural glass, one of the most utilized devices is the portable scattered light polariscope, designated as the SCALP-05 (Aben et al. 2005, Aben et al. 2008, GlasStress Ltd. 2013). As shown in Fig. 2.10a-c, a linearly polarized laser beam enters the glass at an incidence angle α, while a CCD (charge-coupled device) camera with appropriate optics is positioned approximately perpendicular to the beam. By recording the intensity distribution of the scattered light for different polarization states, the retardation profile along the beam path can be reconstructed from the measured intensity variations. The through-thickness retardation is evaluated at discrete points along the visible beam trace inside the glass, and a smooth function, typically a 3rd degree polynomial, is fitted to these data to obtain a continuous retardation profile as a function of depth, see Fig. 2.10d. Differentiation of this profile and application of the stress-optical law yield the corresponding stress distribution across the glass thickness, from which the surface compressive stress and the position of the transition from compressive to tensile stresses can be determined.

2.3 Statistical approaches in experimental analysis

This section provides an introduction to the statistical methods and approaches applied in the subsequent analysis of the experimental investigations and determination of photoelastic stress limits. The focus is placed on descriptive statistics, classification performance metrics and various regression analyses. The methodological foundations are based on established statistical literature by Field (2013), Tabachnick and Fidell (2013), Backhaus et al. (2015), Kabacoff (2022), Hayes (2022), Hedderich and Sachs (2016), and Hox (2018).

2.3.1 Types of data and level of measurement

To conduct a statistical data analysis, it is essential to understand that data can exist in different types, each varying in how well it can be expressed numerically. Data can be classified into four levels of measurement (Fahrmeir et al. 2007, Backhaus et al. 2015) depending on the degree of information they provide. As the scale level ascends, the amount of information and the range of possible arithmetic and statistical operations also increase. In addition, the application of specific statistical analysis depends on the degree of information available.

The simplest level is the nominal scale, which categorizes data qualitatively in a non-metric form. Examples in this study include the manufacturer (A, B, C) and edge processing (ground and seamed edges). These categories do not imply any order, and therefore, only frequency counts can be determined, no arithmetic operations are applicable. The next level is the ordinal scale. Although the data type remains non-metric, the categories follow a specific order, i.e., ranking. An example used in this research is the conformity for TTG assessed by the fracture pattern for HSG in conforming and non-conforming. The ranking indicates that conforming glass typically exhibits a higher pre-stress level compared to non-conforming glass. However, the ordinal scale does not provide information about the magnitude of difference between ranks. The interval scale represents metric data with equal intervals between values but lacks an absolute zero point. An example could be temperature measured in degrees Celsius. In the broadest sense, the variable thickness of glass in this study can be regarded as an interval scale. The maximum level is the ratio scale, incorporating all information from preceding scales. It allows for ratio comparisons since it includes a true zero point. Most physical quantities as well as the variables measured here such as edge stress, surface stress, and bending stress belong to this scale (Backhaus et al. 2021).

2.3.2 Description of distributions

Descriptive statistics comprise techniques with measures of central tendency and variability used to summarize and graphically present datasets. The objective is to identify structural characteristics, such as patterns, distributions, and variability, within the data, without drawing conclusions about a larger population.

The arithmetic mean $\overline{x}$ represents the average value of a dataset and provides a first-order estimate of the expected magnitude of the measured quantity. It is calculated by dividing the sum of all observations x_i by the number of samples n according to Equation (2.8).

$$\overline{x} = \frac{1}{n}\sum_{i=1}^{n} x_i \tag{2.8}$$

The standard deviation *std* describes the variability of the data x_i around the mean $\overline{x}$ and thus reflects the degree of scatter within the dataset. A minimal standard deviation suggests that the observations are concentrated around the arithmetic mean, whereas a large standard deviation corresponds to a higher level of dispersion. The sample standard deviation is calculated as shown in Equation (2.9).

$$\text{std} = \sqrt{\frac{1}{n-1}\sum_{i=1}^{n}(x_i - \bar{x})^2} \tag{2.9}$$

Quantiles are statistical measures that divide an ordered dataset into equal-sized segments. The p-quantile is generally defined as the value below which p·100% of the data lie. The median $x_{0.5}$ delineates the data into two equal segments with 50% of the values falling below and 50% above this value. The first quartile, designated as $x_{0.25}$, signifies the 25th percentile, indicating that 25% of the values fall below this threshold. The third quartile $x_{0.75}$ is the 75% quantile, below which 75% of the values lie. For the statistical evaluation of material properties, the European standard EN 1990 2021 uses the 5% quantile as a characteristic value.

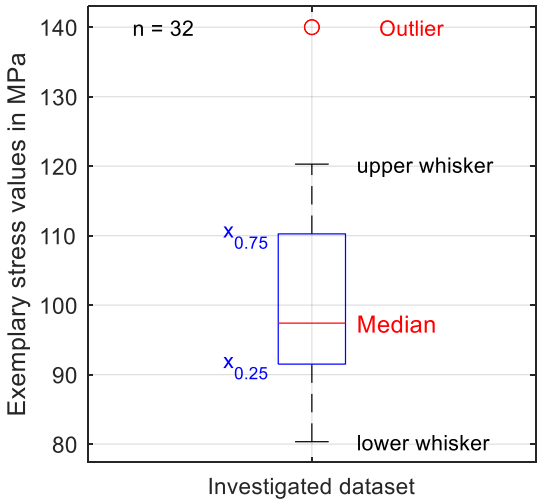

Figure 2.11: Schematic illustration of a box plot using exemplary data with 32 data points

A useful approach for rapidly evaluating the symmetry, dispersion, and potential outliers present within a dataset is the utilization of box plot to depict the data distribution and compare groups of data. Fig. 2.11 illustrates the basic structure of a box plot diagram. The box extends over the interquartile range (IQR), which measures the spread of the middle 50% of the data. The term is defined as the difference between the 3rd and 1st quartiles according to Equation (2.10).

$$\text{IQR} = x_{0.75} - x_{0.25} \tag{2.10}$$

The line within the box delineates the median. The whiskers frequently signify the minimum and maximum values within 1.5 x IQR of the box edges. Values that fall outside this range are designated as outliers. The required number of data points is minimum five (Krzywinski and Altman 2014).

2.3.3 Frequency distributions

Collected data can be described and analyzed with respect to their underlying frequency distribution. The normal distribution is one of the most frequently studied theoretical distributions in statistical data analysis, which exhibits symmetry and can assume negative values. The normal distribution is characterized by its mean μ and variance σ^2. The associated probability density function (PDF) in Equation (2.11) exhibits the characteristic bell-shaped curve and forms the basis of numerous inference procedures in classical statistics.

$$f_X(x) = \frac{1}{\sigma\sqrt{2\pi}} \exp\left(-\frac{(x-\mu)^2}{2\sigma^2}\right) \tag{2.11}$$

The corresponding cumulative distribution function (CDF) is obtained by integrating the density function as shown in Equation (2.12).

$$F_X(x) = \int_{-\infty}^{x} \frac{1}{\sigma\sqrt{2\pi}} \exp\left(-\frac{(t-\mu)^2}{2\sigma^2}\right) dt \tag{2.12}$$

The assumption of normality underlies many commonly used statistical procedures in data analysis. Before applying methods that are based on normal theory, it is important to check whether the observed data are reasonably consistent with a normal distribution. This assessment can be conducted through formal goodness-of-fit tests, such as the Shapiro-Wilk test or through graphical tools (Navarro 2026). A widely used graphical method is the quantile-quantile (Q-Q) plot, which plotted the empirical quantiles of the sample against the corresponding theoretical quantiles of a normal distribution. In the event of a close alignment with the 45° reference line, it is assumed that the observed data follows a normal distribution. Fig. 2.12 illustrates the probability density function and cumulative distribution function for an exemplary normal distribution based on random data, along with the corresponding Q-Q plot.

While the normal distribution is widely applicable, numerous other distribution functions exist to model data with different characteristics. One such distribution used in this work is the Weibull distribution. In contrast to the normal distribution, which can assume negative values, the Weibull distribution models only positive values, making it particularly suitable for material strength analysis (Schneider et al. 2016). The Weibull distribution (Weibull 1939, Rinne 2008) provides a statistical description of failure in brittle materials and is fundamentally based on the weakest-link theory. According to this concept, fracture occurs at the most critically stressed flaw within the material. Consequently, the mechanical strength of the entire specimen is governed by the weakest defect within the stressed volume or surface. This makes the Weibull distribution particularly suitable for modeling the strength of brittle materials, including glass (Madjoubi et al. 1999, Datsiou and Overend

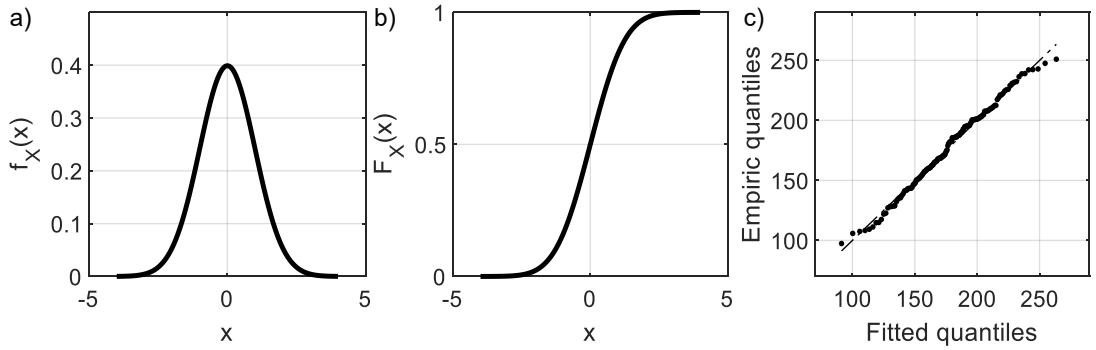

Figure 2.12: a) Probability density function, b) cumulative distribution function of a normal distribution and c) Q-Q plot of random data for a visual assessment of normal distribution

2018). The two-parameter Weibull distribution is defined by the scale parameter β and the shape parameter α, called Weibull modulus. The cumulative distribution function and probability density function (where $x > 0$, $\alpha > 0$, $\beta > 0$) are shown in Equations (2.13) and (2.14).

$$F(x) = 1 - \exp\left[-\left(\frac{x}{\beta}\right)^{\alpha}\right] \tag{2.13}$$

$$f(x) = \frac{\alpha}{\beta}\left(\frac{x}{\beta}\right)^{\alpha-1} \exp\left[-\left(\frac{x}{\beta}\right)^{\alpha}\right] \tag{2.14}$$

The scale parameter β determines the characteristic strength level of the material. By definition, at a failure probability of 63.21% (corresponding to $1–e^{-1}$), the stress equals the scale parameter. The shape parameter α controls the dispersion of strength values. A larger shape parameter indicates more homogeneous material with a narrower distribution of defect characteristics. If the measured values are assumed to be limited by a lower threshold x_0, the statistical evaluation is conducted using a three-parameter Weibull distribution, in which the parameter x_0 acts as a location parameter in Equation (2.15).

$$f(x) = \frac{\alpha}{\beta}\left(\frac{x}{\beta}\right)^{\alpha-1} \exp\left[-\left(\frac{x - x_0}{\beta}\right)^{\alpha}\right] \tag{2.15}$$

A graphical representation of the Weibull distribution is provided by the Weibull probability plot. By transforming the CDF and the failure stress into Weibull coordinates, the distribution is linearized, allowing the empirical failure data to be assessed in relation to a straight line, referred to as the Weibull line. The slope of this line corresponds to the shape parameter α, while its intercept is related to the scale parameter β. Fig. 2.13 illustrates a typical Weibull probability plot, showing the empirical failure data and the corresponding reference line.

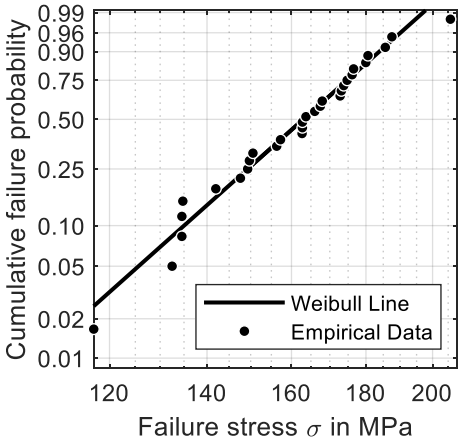

Figure 2.13: Weibull probability plot with empirical failure data and fitted regression line

2.3.4 Contingency tables and metrics

To assess the classification performance of a threshold-based criterion, the predicted class labels are compared with the actually observed categories. For a binary classification task for the categories "0" and "1", this comparison can be summarized using a 2x2 contingency table, commonly referred to as a confusion matrix.

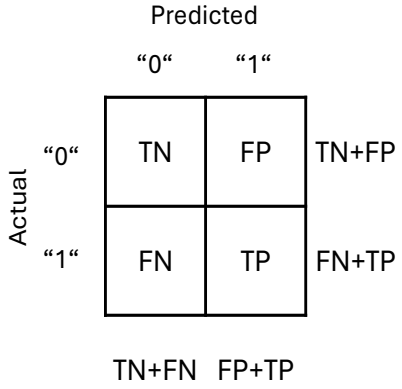

Figure 2.14: Contingency table notation for classification outcomes, including true negatives (TN), true positives (TP), false negatives (FN), and false positives (FP)

The confusion matrix is shown in Fig. 2.14 and distinguishes four possible classification outcomes:

- True positives (TP): Number of observations correctly classified as positive,
- True negatives (TN): Number of observations correctly classified as negative,
- False positives (FP): Number of observations incorrectly classified as positive,
- False negatives (FN): Number of observations incorrectly classified as negative.

The marginal sums of the contingency table represent the actual number of positive and negative cases (row sums) as well as the category distribution predicted by the threshold criterion (column sums). Based on the contingency table, several performance metrics can

be derived, which are used to evaluate and compare different threshold criteria. These metrics are dimensionless ratios with a range of 0 to 1, which can be expressed as percentages. In Equation (2.16), the precision is calculated as the proportion of correctly identified positive observations among all observations classified as positive.

$$\text{Precision} = \frac{TP}{TP + FP} \tag{2.16}$$

The recall represents the proportion of correctly classified positive observations relative to all actual positive cases, as shown in Equation (2.17). It is therefore also referred to as the true positive rate (TPR) or sensitivity.

$$\text{Recall} = \text{TPR} = \frac{TP}{TP + FN} \tag{2.17}$$

In the context of safety-relevant evaluations, it is essential to minimize the number of false positive classifications. The associated performance metric is the specificity, which describes the proportion of actual negative cases that are correctly identified, see Equation (2.18).

$$\text{Specificity} = \frac{TN}{TN + FP} \tag{2.18}$$

Closely related to specificity is the false positive rate (FPR), defined in Equation (2.19), which represents the proportion of actual negative cases that are incorrectly classified as positive. Unlike the other performance metrics indicated here, FPR should ideally be minimized to zero, whereas measures such as precision, recall, and specificity are preferred to be as close to one as possible.

$$\text{False Positive Rate} = \frac{FP}{TN + FP} = 1 - \text{Specificity} \tag{2.19}$$

2.3.5 Linear regression

Regression analysis enables the modeling and prediction of the relationship between the dependent variable Y and one or more independent variables X. The objective of classical linear regression analysis is to estimate a linear relationship. This is achieved by estimating regression coefficients using the Ordinary Least Squares (OLS) method, which minimizes the sum of squared deviations between the observed and predicted values. Basics for the linear regression can be found in Zdaniuk (2014), Field (2013), Hair et al. (2019), Backhaus et al. (2015), and Montgomery et al. (2021).

2.3.5.1 Model description

The linear regression model describes the relationship between a dependent metric variable Y and a set of explanatory variables X. In its general form of the multiple linear regression,

the model with k explanatory variables can be written as shown in Equation (2.20) and (2.21).

$$Y_i = f(X_i) + \varepsilon_i \tag{2.20}$$

$$f(X_i) = \beta_0 + \beta_1 X_{i1} + \ldots + \beta_k X_{ik} \tag{2.21}$$

Y_i denotes the dependent variable, $X_{i1}, \ldots, X_{ik}$ represent the predictor or independent, β_0 is the intercept, $\beta_1, \ldots, \beta_k$ are the regression coefficients, and ϵ_i is the error term for observation $i = 1, \ldots, n$ that captures random deviations of the observed values from the systematic component (Montgomery et al. 2021). In contrast to multiple linear regression, simple linear regression includes exactly one explanatory variable. Despite its inability to account for additional covariates or confounding effects, simple linear regression remains a highly effective method for the analysis of bivariate relationships and illustrative purposes.

Fig. 2.15 shows a scatter plot of an example dataset for which a regression line was fitted using OLS regression. The regression line represents the systematic relationship between the predictor variable and the dependent variable and is employed to predict the value of Y (Glantz et al. 2016).

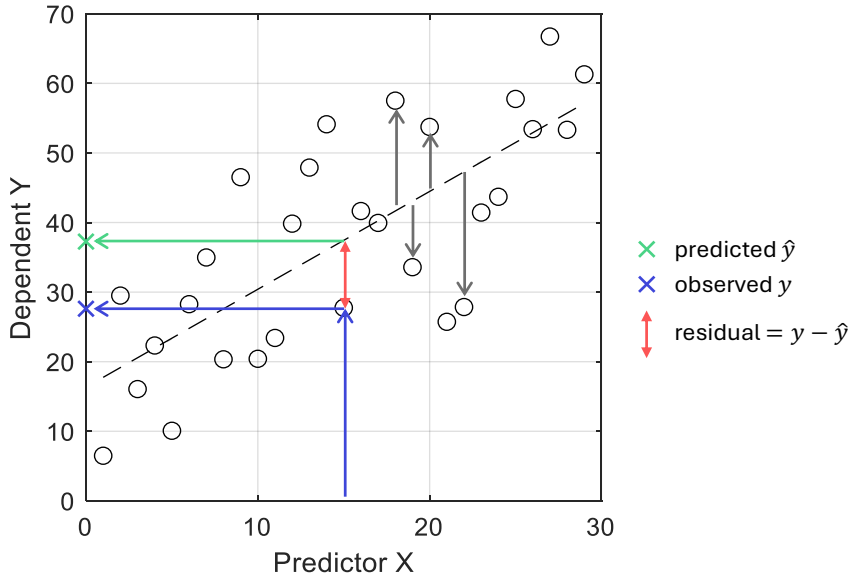

Figure 2.15: Linear regression using ordinary least squares (OLS) method on an exemplary dataset

Linear regression estimates the conditional mean of Y given X. That is, for a given set of predictor values, the regression model provides the expected value of the dependent variable. From a visual perspective, the primary objective of the simple linear regression with a single explanatory variable is to determine a regression line that best represents the relationship between the predictor variable and the dependent variable (Glantz et al. 2016). The residuals represent the deviations of the observed values from the fitted regression line (Lee 2014). They serve to quantify the portion of the outcome variable that is not

explained by the model. As illustrated in Fig. 2.15, each residual corresponds to the vertical distance between an observed data point and its predicted value on the regression line. Therefore, examining the pattern and distribution of residuals provides essential information for assessing the adequacy of the model and its underlying assumptions. The linear regression and the resulting regression line are estimated using the OLS method, which fits the model by minimizing the sum of errors (SSE). Squaring the residuals ensures that positive and negative deviations do not cancel each other out and assigns greater weight to larger deviations (Backhaus et al. 2015). This estimation criterion corresponds to the maximum likelihood solution under the assumption of normally distributed error terms.

2.3.5.2 Model interpretation

After estimating a linear regression model, its overall goodness-of-fit must be evaluated. The global assessment of the regression function typically includes the coefficient of determination R^2, the standard error of the estimate, and the F-statistic (Glantz et al. 2016). Together, these measures provide information about how well the model explains the observed variation in the dependent variable.

The statistical significance of the estimated regression model is commonly assessed using the F-statistic (Backhaus et al. 2021). This test evaluates whether the overall model explains a significant proportion of variance in the dependent variable compared to a model without predictors (Azen and Walker 2011). The F-statistic is based on the decomposition of total variance into explained and unexplained components and additionally considers the sample size and the number of predictors included in the model. The result of the F-test is typically reported using a p-value, which indicates whether the explained variance is statistically greater than it would be expected by chance. In addition to the global model fit, the precision of the model predictions can be evaluated using the standard error of the estimate, which reflects the average deviation of the observed values from the regression line. Further details on these evaluation criteria can be found in Backhaus et al. (2015).

Following the assessment of overall model fit, the individual regression coefficients are examined to evaluate the significance and direction of the effects of the predictor variables. The intercept β_0 represents the predicted value of Y when all predictors equal zero. The slope coefficients β_j indicate the expected change in Y for a one-unit increase in X_j, holding other predictors constant (Azen and Walker 2011). The sign of the coefficients indicates the direction of the relationship (positive or negative), while its magnitude reflects the strength of the relationship. The assessment of the regression coefficients is typically conducted using the t-statistic, which depends on the estimated regression coefficient and its associated standard error. In practice, statistical significance is commonly evaluated using the corresponding p-value for each coefficient. A regression coefficient is considered statistically significant if its p-value falls below a predetermined significance level, typically $\alpha = 0.05$. Then, this variable X contributes statistically significant to the prediction of the dependent variable Y.

To describe how well the model fits the observed data, the coefficient of determination, denoted R^2 is computed according to Equation (2.22).

$$R^2 = 1 - \frac{SSE}{SST} = \frac{SSR}{SST} = \frac{\sum_{i=1}^{n} \left(\hat{y}_i - \overline{\hat{y}}\right)^2}{\sum_{i=1}^{n} \left(y_i - \overline{y}\right)^2} \tag{2.22}$$

SSE is the sum of squared residuals (residual sum of squares), *SST* is the total sum of squares, and SSR is the regression sum of squares. For OLS regression with an intercept, the coefficient of determination R^2 is bounded between 0 and 1 when evaluated on the estimation data. Values of R^2 close to 1 indicate that the model explains a large proportion of the variability in the dependent variable, suggesting a good fit to the data. In contrast, values of R^2 close to 0 indicate that the model with the predictors explains little of the variability in the dependent variable. For example, an R^2 of 0.68 implies that 68% of the variance in the dependent variable is explained by the regression model.

In multiple linear regression, however, the inclusion of additional explanatory variables can inflate R^2, even if the added predictors contribute little explanatory power. Therefore, the adjusted coefficient of determination, adjusted R^2, is commonly reported. *Adjusted* R^2, defined in Equation (2.23), accounts for the number of observations n and the number of predictor variable p (excluding the intercept) by incorporating a penalty for model complexity. In contrast to R^2, the adjusted R^2 does not inherently increase with the inclusion of additional predictors. Its increase is only observed when these predictors contribute significantly to the explanation of the variability in the dependent variable. This makes adjusted R^2 particularly useful for model comparisons.

$$R^2_{\text{adj}} = 1 - (1 - R^2) \cdot \frac{n-1}{n-p-1} \tag{2.23}$$

2.3.5.3 Model assumptions

To ensure valid inference in OLS regression, several assumptions must be met. If these assumptions are violated, standard errors become biased, and OLS estimates may lead to misleading conclusions. Several assumptions pertain to the residuals of the regression model and can be visually assessed through residual diagnostic plots, as shown in Fig. 2.16 for an example dataset.

The linear regression model estimates a linear relationship between the predictors and the response variable. Accordingly, one fundamental assumption is that the relationship between the predictors and the conditional mean of the response is linear. This assumption can be visually assessed using a scatter plot between the predictor and dependent variable, or more formally using a residuals versus fitted values plot, as shown in Fig. 2.16a. The residuals should be randomly scattered around the horizontal zero line with no systematic pattern (Backhaus et al. 2021). The presence of a pattern may signify a non-linear relationship between the variables for which the OLS regression is not applicable.

Furthermore, for valid parametric inference, the residuals are typically assumed to be approximately normally distributed. This assumption can be visually assessed using a Q-Q plot, as illustrated in Fig. 2.16b. If the residuals follow a normal distribution, the points lie close to the diagonal reference line. In cases where this assumption is violated, for example due to non-normality or the presence of moderate outliers, bootstrap procedures

(see Section 2.3.9) can be employed to obtain more robust confidence intervals and standard errors without relying on the normality assumption.

An additional assumption of linear regression is homoscedasticity, which requires the residuals to exhibit constant variance across all levels of the predictor variables (Lee 2014). The violation of this assumption is referred to as heteroscedasticity, where the variance of residuals changes systematically with fitted values. Fig. 2.16c presents the Scale-Location plot, which displays the square root of the absolute standardized residuals against the fitted values and is specifically designed to assess homoscedasticity. Under homoscedasticity, the points should be randomly and diffusely scattered without any discernible systematic pattern. In contrast, funnel-shaped patterns or increasing or decreasing trends indicate heteroscedasticity. In the presence of heteroscedasticity, the application of robust heteroscedasticity-consistent standard errors can be used to correct the bias in standard errors without changing the coefficient estimates themselves. These adjustments ensure that hypothesis tests and confidence intervals remain valid even when the constant variance assumption is violated.

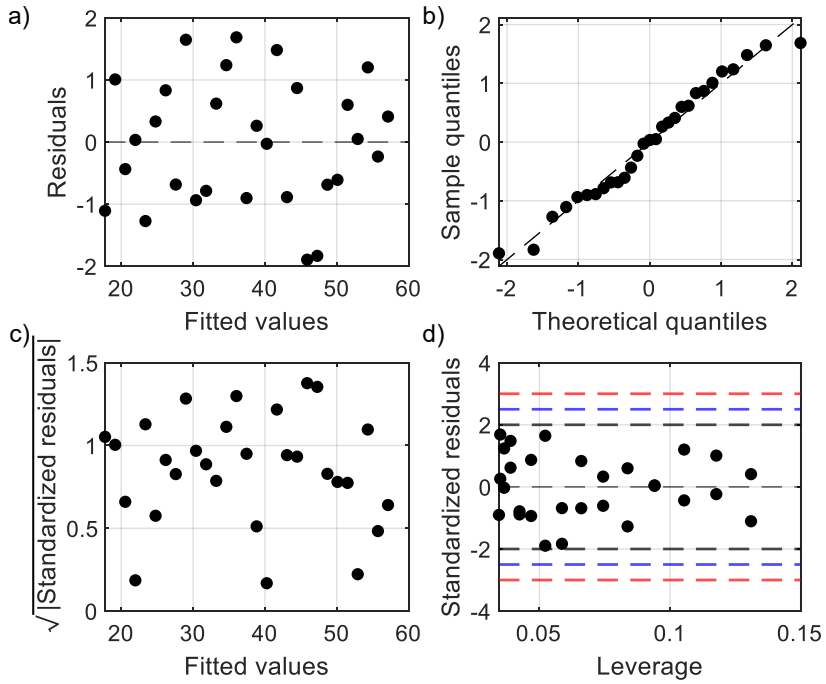

Figure 2.16: Residual diagnostic plots of model assumptions of OLS linear regression

Furthermore, outliers can adversely affect the model's estimates and overall fit. Potential outliers can be identified through the analysis of standardized residuals. General guidelines according to Field (2013) are: no more than 5% of observations should have standardized residuals greater than ±2; no more than 1% should exceed ±2.5; and no observation should exceed ±3. The standardized residuals are plotted in Fig. 2.16d, where the thresholds are marked as reference lines.

Additionally, the residuals are assumed to be independent of one another. This assumption ensures that no underlying structure in the data, such as temporal or spatial correlation, affects the results. Independence can be formally tested using the Durbin-Watson test. The Durbin-Watson test result ranges from 0 to 4, with a value near 2 indicating no

autocorrelation. Values substantially less than 2 suggest positive autocorrelation, while values greater than 2 indicate negative autocorrelation (Jansen 2020). Violations of this assumption, such as autocorrelation, commonly arise in clustered. In such cases, mixed-effects models or panel data models that explicitly account for the hierarchical structure of the data provide a more appropriate modeling framework.

When estimating multiple predictors in a so-called multiple regression, there should be no perfect multicollinearity among explanatory variables. Multicollinearity occurs when predictor variables are highly correlated with one another, which inflates the variance of the coefficient estimates (Backhaus et al. 2021) and can result in unstable and difficult-to-interpret regression coefficients. When multicollinearity is detected, only one of the correlated variables in the model is included or regularization techniques, such as ridge regression, are employed.

2.3.6 Moderation analysis

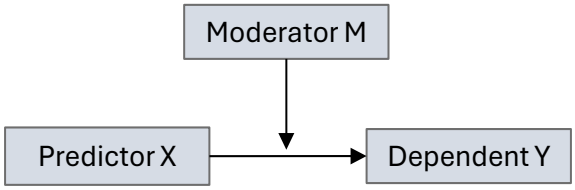

Figure 2.17: Moderation analysis with moderator influencing strength and direction of relation between X and Y according to Hayes (2022)

The moderation analysis examines linear relationships in which the dependent variable Y is predicted by one or more independent variables but is influenced by a third variable (Hair et al. 2021, Igartua and Hayes 2021, Hayes 2022), see Fig. 2.17. This additional variable serves as a moderator M that interacts with the predictor X. The defining feature that distinguishes moderation analysis from standard multiple linear regression is the explicit inclusion of an interaction term between the predictor and the moderator. This is illustrated in Fig. 2.17 and Fig. 2.18. The moderator variable captures under which conditions, or for which values of M, the strength and possibility the direction of the relationship between X and Y changes. Moderator variables can be either categorical or continuous.

2.3.6.1 Model description

The standard moderation model is expressed as a multiple linear regression including an interaction term with X as central predictor, M as the moderator and XM as their product term, as shown in Equation (2.24). Here, Y denotes the dependent variable, β_0 the intercept, β_1 the regression coefficient of the predictor X, β_2 the regression coefficient of the moderator M, β_3 the regression coefficient of the interaction term, and ε the error term.

$$Y = \beta_0 + \beta_1 X + \beta_2 M + \beta_3 (X \cdot M) + \varepsilon \tag{2.24}$$

As shown in Fig. 2.18, the product term represents the interaction of X and M. The corresponding estimate β_3 quantifies the moderating effect, indicating how much the effect of X on Y changes per unit increase in M. For ease of interpretation and reduce multicollinearity, continuous predictors and moderators are typically mean-centered prior to forming the interaction term (Olvera Astivia and Kroc 2019). After centering, β_1 represents the effect of X at the average value of M, β_2 the effect of M at the average value of X, and β_0 the expected value of Y when both centered variables are zero.

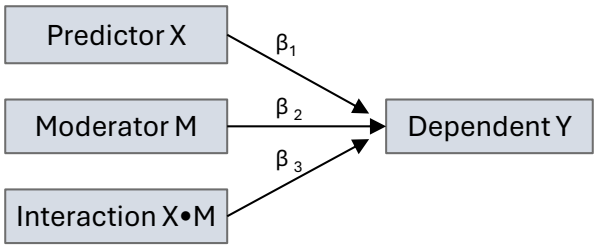

Figure 2.18: Model description of moderation with interaction term

2.3.6.2 Interpretation of the results

To evaluate the results of a moderation analysis, the key parameter of interest is the coefficient of the interaction term β_3. If the coefficient β_3 is statistically significant (e.g., $p < 0.05$), this indicates that the effect of the predictor X on the dependent variable Y varies as a function of the moderator M (SPSS Analysis 2024). For a continuous moderator, the moderation term is represented by a single interaction coefficient $\widehat{\beta_3}$. In contrast, for a categorical moderator with more than two levels, multiple interaction coefficients are estimated, allowing the effect of X on Y to be compared across categories.

Significant interactions were further examined using simple-slopes analysis and visualized in interaction plots. For continuous moderators, the conditional effect of X on Y is typically plotted at low, moderate, and high values of M. When the moderator is approximately normally distributed, these values are commonly defined as one standard deviation below and above the mean. For skewed distributions, Hayes (2022) recommends using the 16th, 50th, and 84th quantiles. For categorical moderators, separate regression lines are plotted for each category, making differences in slopes directly visible.

Such interaction or slope plots, as shown in Fig. 2.19, are well suited to illustrate moderation effects, as they visually depict how the relationship between the predictor X and the outcome Y changes across different values or categories of the moderator M (SPSS Analysis 2024). By comparing the slopes of the regression lines, these plots facilitate an intuitive interpretation of interaction effects, including differences in the strength or direction of the relationships. In addition to visual inspection, the explanatory value of the moderation effect can be quantified by examining the change in explained variance ΔR^2 resulting from the inclusion of the interaction term compared to the linear regression without moderator variable.

2.3.6.3 Model assumptions

The assumptions of a moderation model (SPSS Analysis 2024) correspond to those of multiple linear regression, including linear relationships between the predictors and the

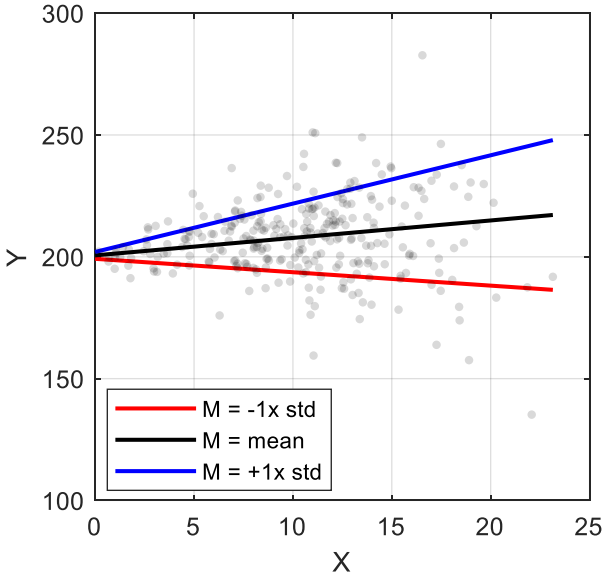

Figure 2.19: Exemplary simple-slope analysis of the interaction effect in a moderation analysis

dependent variable, approximately normally distributed and homoscedastic residuals, and independence of observations (see Section 2.3.5.3 for details).

When the normality assumption of the residuals is violated, bootstrap procedures can be used to obtain more robust confidence intervals for parameter estimates. In the presence of heteroscedasticity, heteroscedasticity-consistent robust standard errors (e.g., HC3) provide an appropriate alternative. Including interaction terms in the regression model often lead to increased multicollinearity. Mean centering the continuous predictors involved in the interaction reduces non-essential multicollinearity and facilitates the interpretation of regression coefficients.

2.3.7 Quantile regression

Koenker and Basset (1978) presented the concept of quantile regression as a further possibility for estimating the linear relationship between variables. The quantile regression extends the regression analysis by modeling the conditional distribution of the target variable on different quantiles τ rather than estimating the conditional mean of Y. This approach relaxes the assumption of constant regression slopes across the entire distribution. In other words, the effect of a predictor can vary at different points of the outcome distribution. While OLS assumes that the relationship between predictor and response is uniform across all levels of Y, quantile regression can capture heterogeneous effects.

Fig. 2.20 presents a scatter plot of simulated data with different regression lines. The plot includes the standard linear regression estimated using ordinary least squares, along with quantile regression models for selected quantiles (τ = 5%, 25%, 50%, 75%, and 95%). The OLS regression line represents the conditional mean of the outcome variable, whereas the quantile regression lines model different quantiles of the conditional distribution of Y (Koenker 2005). This demonstrates that quantile regression can capture not only the median, but also arbitrary parts of the distribution. In cases of heteroscedasticity or

asymmetric dispersion, the quantile regression lines exhibit distinct slopes and positions. Consequently, Fig. 2.20 illustrates how predictor effects can vary across the distribution.

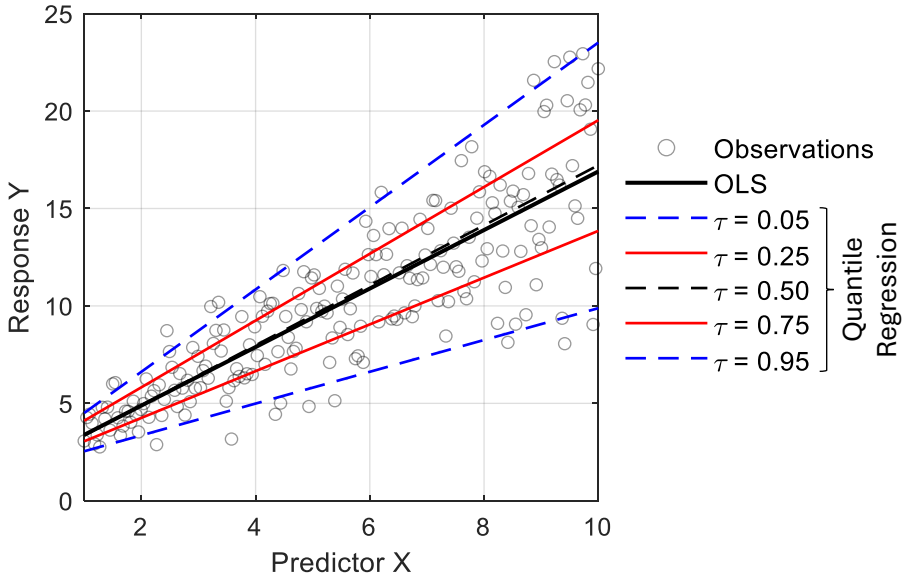

Figure 2.20: Scatter plot of simulated data evaluated by OLS linear regression and quantile regression for selected quantiles

Quantile regression is employed primarily when there is a focus on modeling the distribution of the dependent variable beyond the mean value. This is typically the case when analyzing extremes, such as risk assessments, income distributions, or evaluations in materials science. Quantile regression enables the examination of the differential effects of the independent variables on the various segments of the dependent variable's distribution (Koenker 2005).

2.3.7.1 Model description

For a given quantile level $\tau \in (0, 1)$ quantile regression specifies the conditional τ^{th} quantile of the dependent variable Y given the predictors $X_1, \ldots, X_p$ as shown in Equation (2.25).

$$Q_Y(\tau \mid X) = \beta_0(\tau) + \beta_1(\tau)X_1 + \cdots + \beta_p(\tau)X_p \tag{2.25}$$

$\beta_{\mathrm{p}}(\tau)$ denotes the vector of regression coefficients specific to quantile τ. Deviations of the observed values from the estimated conditional quantile can be interpreted as quantile-specific residuals but are not explicitly included in the model specification. Unlike linear regression estimated using OLS method, quantile regression directly models conditional quantiles of the response variable rather than the conditional mean (Porter 2015). Whereas OLS regression minimizes the sum of symmetric squared errors and therefore treats under- and overpredictions equally, quantile regression estimates regression coefficients by minimizing asymmetric loss function ρ_τ, referred to as the check loss (Koenker and Basset 1978), see Equation (2.26) and (2.27).

$$\min_{\beta(\tau)} \sum_i \rho_\tau(e_i) \tag{2.26}$$

$$e_i = y_i - x_i'\beta(\tau) \tag{2.27}$$

Positive residuals (overpredictions) are penalized by a factor of τ, while negative residuals (underpredictions) are penalized by a factor of 1 - τ. This asymmetric weighting yields estimates of the conditional τ^{th} quantile of the response variable, rather than its conditional mean. Intuitively, the loss function shifts the regression line, so that approximately a proportion τ of observations lie below the fitted line, characterizing the conditional τ^{th} quantile of the outcome distribution. Accordingly, the coefficients $\beta_{\text{j}}(\tau)$ indicate how much the conditional τ^{th} quantile of Y changes in response to a one-unit increase in the jth covariate, holding all other variables constant.

2.3.7.2 Model assumptions

Quantile regression relies on fewer and weaker assumptions compared to OLS linear regression. Both regression models assume linearity in the relationship between predictors and response, independence of observations, and no perfect multicollinearity among the explanatory variables. In contrast to OLS, quantile regression does not impose assumptions of normally distributed or homoscedastic error terms. Consequently, it provides a more flexible modeling framework and is less sensitive to outliers, non-normality, and heteroscedasticity, making it particularly useful when the conditional distribution of the response variable is skewed or exhibits unequal variance (Xu 2023).

2.3.8 Logistic regression

Logistic regression is a statistical method that is used for the analysis of categorical dependent variables. If the response can be expressed as a binary outcome $Y \in \{0, 1\}$ the model is referred to as a binary logistic regression model, which is the focus of this section. In contrast to the application of linear regression, which is utilized for the prediction of metric responses, logistic regression is employed for the modeling of the probability that a specific event, typically denoted as $Y = 1$, will occur, given a specified set of explanatory variables.

2.3.8.1 Model description

The model is based on a non-linear transformation of conditional probability, see Equation (2.28).

$$\pi(x) = \Pr(Y = 1 \mid x) \tag{2.28}$$

While probabilities are restricted to values between 0 and 1, the logit transformation in Equation (2.29) maps these values onto the entire real line.

$$\text{logit}\{\pi(x)\} = \log\left(\frac{\pi(x)}{1 - \pi(x)}\right) = \eta(x) \tag{2.29}$$

The transformed quantity represents the linear predictor, which is expressed as a linear combination of the intercept β_0, the regression coefficients β_i, and the predictor variables x_i in Equation (2.30).

$$\eta(x) = \beta_0 + \beta_1 x_1 + \cdots + \beta_k x_k \tag{2.30}$$

Unlike linear regression, the linear predictor in logistic regression does not directly estimate the dependent variable itself, but rather the logarithm of the odds that the event Y = 1 occurs. Applying the inverse of the logit transformation yields the logistic function, as shown in Equation (2.31).

$$\pi(x) = P(Y = 1 \mid x) = \frac{1}{1 + \exp(-(\beta_0 + \beta_1 x_1 + \cdots + \beta_k x_k))} \tag{2.31}$$

This function takes values strictly between 0 and 1 and follows a sigmoid, a so called S-shaped curve. It can be interpreted as a cumulative distribution function that links the linear predictor to the underlying probability space. Consequently, the logistic regression model ensures that predicted probabilities remain bounded within the unit interval while preserving a linear relationship on the log-odds scale. The transformation from the linear predictor $\eta(x)$ to the probability $\pi(x)$ can be visualized by plotting both relationships in the same coordinate system. As illustrated in Fig. 2.21, the linear predictor increases linearly with the explanatory variable, whereas the logistic transformation yields an S-shaped curve that approaches 0 and 1 asymptotically. This curve represents the characteristic non-linear link between the predictor and the probability of the outcome.

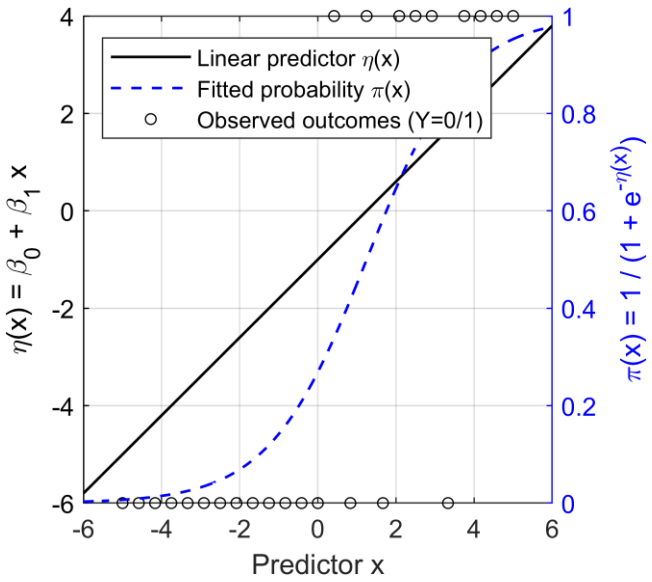

Figure 2.21: Transformation of the linear predictor $\eta(x)$ with intercept β_0, regression coefficient β_1 and explanatory variable x into the corresponding logistic probability function

2.3.8.2 Assessment of model fit

Since the parameters of the logistic regression model are estimated by the maximum likelihood method, the value of the maximized log-likelihood (LL) provides the basis for assessing model fit. The likelihood-ratio (LR) test compares the constant-only (null) model with the full model and evaluates whether the more complex model provides a significantly better fit to the data. The constant-only model (or null model) includes only the intercept term and no predictor variables. Its log-likelihood is denoted by LL_{null}. The full model, by contrast, contains all predictor variables specified in the regression equation, and its log-likelihood is denoted by LL_{full}. The likelihood-ratio test statistic is computed using Equation (2.32), which involves the difference between the null deviance and the residual deviance.

$$\chi^2_{\mathrm{LR}} = 2\left(\mathrm{LL}_{\mathrm{full}} - \mathrm{LL}_{\mathrm{null}}\right) = D_{\mathrm{null}} - D_{\mathrm{full}} \tag{2.32}$$

The deviance is defined as D = *-2LL*. Under the null hypothesis, which stipulates that the inclusion of additional predictors does not enhance the model's fit, the observed statistic conforms to a chi-squared distribution with p degrees of freedom. Here, p denotes the number of predictors present in the full model. A statistically significant result, typically indicated by a p-value less than 0.05, signifies that the full model provides a substantially superior explanation of the data in comparison to the null model. This observation suggests that at least one of the predictors contributes significantly to the prediction of the outcome (Backhaus et al. 2015).

2.3.8.3 Interpretation of the results

In the context of logistic regression, a positive regression coefficient β_{i} signifies that an increase in the corresponding predictor variable $\mathrm{x_i}$ results in an increase in the log-odds of the event occurring. Conversely, a negative coefficient functions to reduce the log odds. For a more intuitive interpretation, the coefficients are usually exponentiated to obtain odds ratios (OR), as shown in Equation (2.33).

$$\mathrm{OR}_i = \exp(\beta_i) \tag{2.33}$$

For continuous predictors, the magnitude of the OR depends on the measurement scale of the variable and is therefore less informative when interpreted in isolation. In contrast, the interpretation is straightforward for binary predictors. An OR of 1 indicates no association between predictor and outcome, values greater than 1 indicate increased odds of the event for the exposed group, and values less than 1 indicate decreased odds.

In linear regression, the coefficient of determination R^2 provides an intuitive measure of model fit, quantifying the proportion of variance in the dependent variable explained by the model (Glantz et al. 2016). However, given that the dependent variable in logistic regression is categorical rather than metric, a direct analogue of R^2 does not exist. To address this limitation, several pseudo-R^2 measures have been proposed. These indices are not based on explained variance but on likelihood comparisons between the null model and the full model. Among these, the Nagelkerke's R^2 is one of the most reported. It

extends the Cox and Snell's R^2, which cannot reach the value of 1 even for a perfectly fitting model. Nagelkerke rescaled this measure to ensure values range between 0 and 1, where higher values indicate a better model fit. In applied research, a Nagelkerke's R^2 value of approximately 0.50 or higher is typically considered indicative of a well-fitting model (Backhaus et al. 2015).

To further assess the predictive performance of the model, a confusion matrix is commonly employed. It cross-tabulates the number of true positives, true negatives, false positives, and false negatives based on a predefined classification threshold with the desired probability. Based on the confusion matrix as described in Section 2.3.4, several performance metrics can be derived, including accuracy, precision, recall, and the F1-score.

Another widely used diagnostic tool is the Receiver Operating Characteristic (ROC) curve. As illustrated in Fig. 2.22, an exemplary ROC curve is presented in blue. This curve was derived from the fitted probabilities of the logistic regression and represents the true positive rate as a function of the false positive rate for the corresponding classification thresholds. In contrast, the diagonal gray line signifies random classification, which is denoted as the no-skill line. The ROC analysis offers a comprehensive evaluation of the model's classification ability across all possible probability thresholds. A well-performing model is characterized by a ROC curve that rises sharply towards the upper-left corner of the plot, indicating a high proportion of correctly classified positive cases with a minimal number of false positives. An additional evaluation criterion is the area under the curve (AUC) which serves as a summary measure of the model's discriminative performance and quantifies the model's accuracy to correctly distinguish between the outcome categories across all possible classification thresholds. The AUC value ranges from 0 to 1, where a value of 0.5 is assigned to random classification, indicating no discriminatory ability, while values closer to 1 indicate better discrimination.

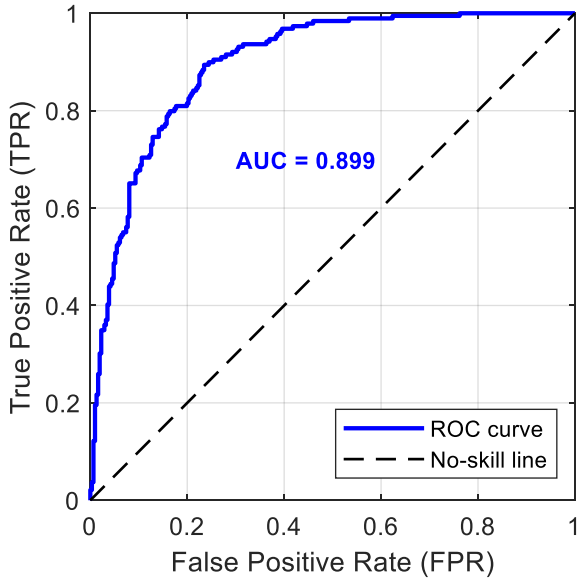

Figure 2.22: Receiver Operating Characteristic (ROC) curve derived from the fitted probabilities of the logistic regression model with area under the curve (AUC) value

2.3.8.4 Model assumptions

Compared to linear regression, logistic regression relies on a reduced set of statistical assumptions. However, several assumptions of linear regression (see Section 2.3.5.3) also apply to logistic regression. These include the independence of observations, the absence of perfect multicollinearity when multiple predictors are included, and the absence of influential outliers. Outliers can be identified using the same diagnostic criteria as described by Field (2013). The central assumption of the logistic regression model is that the categorical dependent variable represents a random variable following a Bernoulli distribution in case of binary outcomes (Backhaus et al. 2015). A further assumption of logistic regression is the linear relationship between the metric independent variables and the logit of the dependent variable (Tabachnick and Fidell 2013). The linearity of logit can be verified most readily using the Box-Tidwell test (Hosmer and Lemeshow 2000), in which a significant interaction term suggests a violation of the assumption. Furthermore, stable parameter estimation requires an adequate sample size. A commonly cited rule recommends at least ten observations of the less frequent outcome category per independent variable included in the model (Peduzzi et al. 1996).

2.3.9 Bootstrapping as a resample method

Bootstrapping, introduced by Efron and Tibshirani (1994), is a resampling method that allows statistical inference without relying on strict parametric distributional assumptions. It is used to estimate the variability and uncertainty of a statistic by repeatedly resampling from the observed data and relies solely on the information contained in the available sample.

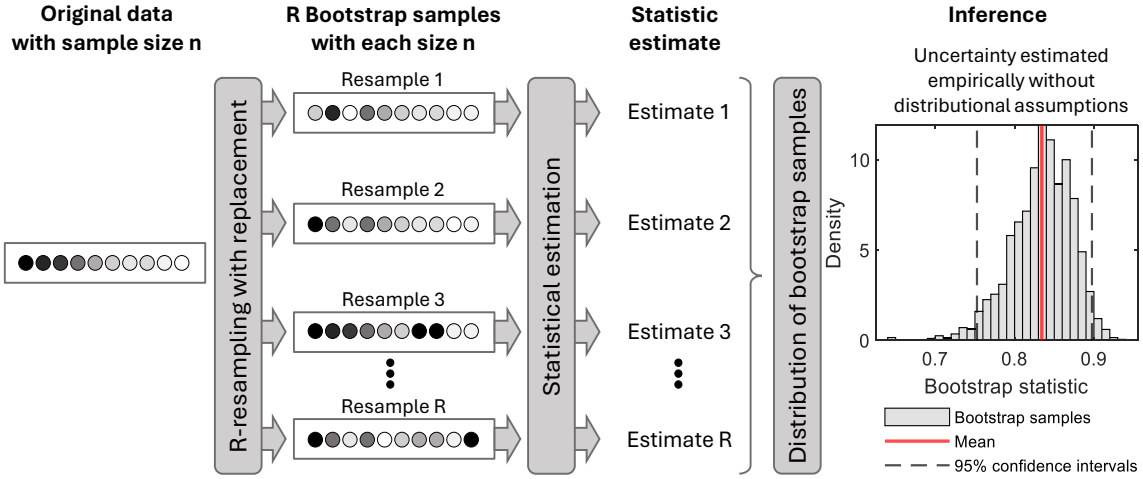

Figure 2.23: Approach of bootstrapping as resample method

The approach of the bootstrapping method is illustrated in Fig. 2.23. The original dataset contains a sample size of n. From this database, bootstrap resamples are constructed by randomly selecting data with replacement to achieve resampling sizes that equal the sample size n. This process results in the recurrence of data points within a resample. The number of bootstrap resamples R can be selected. Kabacoff (2022) sets the number of resamples to

minimum 1000, taking advantage of the resample method but not unnecessarily prolonging the calculation time. For each bootstrap resample, the statistical value of interest is re-estimated, such as the mean, correlation coefficient, or regression estimates. By repeating this process for all resamples, the resulting statistics can be summarized and combined into a single distribution diagram of the bootstrap samples. From this bootstrap distribution, various measures of uncertainty can be derived, including the standard error and confidence intervals, typically at the 95% level. These confidence intervals provide information about the precision and uncertainty of statistical estimates. In addition, differences between datasets can be formally assessed by examining the confidence interval of the difference between the corresponding estimates.

In contrast to parametric inference methods, bootstrapping does not require any assumptions regarding the form of the underlying population distribution. It thus provides a systematic approach to assess uncertainty, which is particularly advantageous in situations where theoretical sampling distributions are unknown or classical assumptions, such as normality, are violated. The bootstrap approach is widely applied in both exploratory and confirmatory data analysis, particularly when analytical derivations of standard errors are complex or unavailable. In this thesis, the bootstrap method is applied in regression models, as it allows for assessing the stability of estimated coefficients. In correlation analysis, it provides robust estimates of confidence intervals even under non-normal conditions.

3 Residual stresses and non-destructive measurements of tempered glass

Residual stresses introduced into glass during the tempering process play a significant role in influencing the fracture behavior and the bending strength of tempered glass (Nielsen 2009). During thermal tempering, the glass is heated above its glass transition temperature and subsequently cooled rapidly. This non-uniform cooling leads to the development of a characteristic residual stress profile, with compressive stresses at the surfaces and tensile stresses in the core of the glass plate. The presence of these residual stresses causes a stress-induced anisotropy in the refractive index of the glass, resulting in stress birefringence (Aben and Guillemet 1993). Consequently, tempered glass exhibits birefringent behavior, meaning that the refractive index becomes direction dependent. Photoelastic measurement methods exploit this birefringent behavior to enable non-destructive evaluation of residual stresses in tempered glass. When polarized light passes through tempered glass, the stress-induced birefringence causes retardations of the light waves, which can be visualized as characteristic fringe patterns. Photoelastic measurement techniques utilize this phenomenon to non-destructively quantify residual stresses, enabling the quantitative determination of stresses at the surface and edge.

This chapter compares the different measurement and evaluation methods for surface and edge stress reported in literature. In addition, the relationship between mechanical properties and residual stresses is investigated, and existing photoelastic limit values from standards and research are reviewed.

Basics, reviews, and in-depth research on residual stresses and non-destructive measurement techniques in glass can be found in Vivek and Ramesh (2015), Ramesh and Ramakrishnan (2016), Ramesh and Sasikumar (2020), Laufs (2000), Dix (2024), Nielsen (2009), Pour-Moghaddam 2020, and Aben and Guillemet (1993).

3.1 Distribution of residual stresses within tempered glass

Residual stresses in a tempered glass plate can be divided into thickness stresses, which are variable in depth, and membrane stresses, which are constant in depth (Aben and Guillemet 1993). In addition, Laufs (2000) divides the plate of tempered glass into four zones: central, edge, corner, and hole area. Zone 1 is the main body of the glass, sufficiently far from edges, corners, or holes, where a parabolic stress distribution develops across the thickness, as shown in Fig. 3.1 and Fig. 3.2 (right). The stress distribution $\sigma(z)$ as a function of depth z, measured from the mid-plane of the glass, can be expressed as seen in Equation (3.1).

$$\sigma(z) = -\frac{\sigma_s}{2}\left(1 - \frac{6z}{t}\right) \tag{3.1}$$

The compressive stress at the surface σ_s is approximately twice as high as the tensile stress σ_m in the core due to the rapid cooling process. The depth of the compressive zone at the surface is typically about 20% of the glass thickness t.

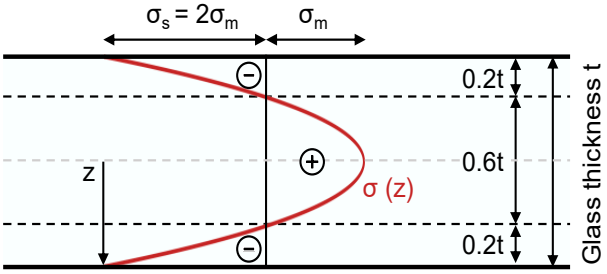

Figure 3.1: Parabolic stress distribution in an undisturbed glass plate

The residual stress state of the compressive stresses at the surfaces of the glass can be described by the principal stresses σ_1 and σ_2. In the undisturbed area of the glass plate, these principal stresses are approximately equal and the measured retardations are typically low, minor as 300 nm, which corresponds to about 0.5^{th} fringe order (Dix et al. 2022). From the perspective of photoelastic measurement, differences between the two principal stresses σ_1 and σ_2 cause optical retardations. Due to the non-constant, parabolic stress distribution, the relative retardation δ is expressed in Equation (3.2) by integrating Wertheim's law from Equation (2.5) across the glass thickness.

$$\delta = C \int_0^t (\sigma_1(z) - \sigma_2(z))\, dz \tag{3.2}$$

The stress state at the edges of a tempered glass plate differs from that in the central region. In addition to the two main surfaces of the pane, the edges represent an additional free surface that is directly exposed to the cooling medium. Due to the three-dimensional cooling behavior, a compressive membrane stress forms around the edges of the glass since the edges tend to cool faster than the center of the pane. The resulting stress distribution in the edge region, designated as zone 2 according to Laufs (2000), is illustrated in Fig. 3.2 (left).

Due to mechanical equilibrium, one of the two in-plane principal stresses oriented perpendicular to the edge direction reduces to zero directly at the edge as shown as σ_1 in Fig. 3.2. This boundary condition leads to an uniaxial stress state in the pre-stress zone of the edge, with the remaining principal stress acting parallel to the edge and corresponding to the compressive membrane stress σ_e induced during tempering.

Towards the edge within the compressive stress area, the optical retardation increases continuously and reaches its maximum value directly at the outermost edge of the glass pane. The width of this pre-stress zone is governed by tempering level and glass thickness. According to Laufs (2000), the characteristic width of the compressive edge stress zone amounts to approximately 1.0 t for TTG and 1.5 t for HSG.

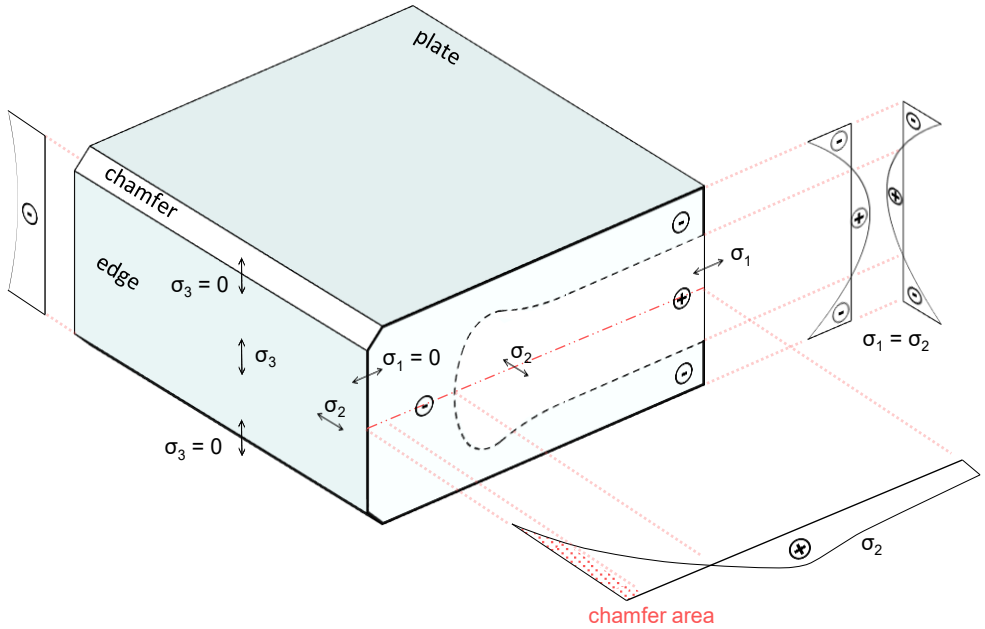

Figure 3.2: Pre-stress zones of the glass edge and plate with stress distribution of σ_1 and σ_2 and pressure and tension areas from Efferz et al. (2024a)

Within this area, the stress state progressively approaches a uniaxial condition at the free edge, with the directions of the principal stresses being known from the boundary conditions. Under these conditions, the stress component acting parallel to the edge can be determined using Wertheim's law from Equation (2.5). The edge stress σ_e can be determined using the maximum retardation R at the edge, the glass thickness t and the photoelastic constant C, as outlined in Equation (3.3).

$$\sigma_2 = \sigma_e = \frac{\delta\lambda}{tC} = \frac{R}{tC} \tag{3.3}$$

The photoelastic constant C depends on the material of the specimen. For glass, the material constant C is ranging from 2.61 to 3.03 TPa^{-1} (Dix 2024). The wavelength λ corresponds to the light of the photoelastic measuring device used to detect the relative retardation δ at the edge.

The residual stress state is stored in the glass in the form of elastic energy (Pourmoghaddam and Schneider 2018a, Pourmoghaddam et al. 2019). When the tempered glass fractures, part of this stored energy is released. In the case of TTG, the high level of residual stresses leads to a rapid and extensive release of elastic energy, resulting in the characteristic fine, crumbly fracture pattern composed of numerous small, relatively blunt fragments. HSG, with its lower residual stress level, releases less energy and therefore exhibits a coarser fracture pattern with larger fragments. The elastic energy U with Poisson's ratio ν (0.23), Young's modulus E (70,000 MPa), glass thickness t and surface stress σ_s is calculated as shown in Equation (3.4).

$$U = \frac{1}{5}\frac{(1-\upsilon)}{E}\, t\, \sigma_s^2 \tag{3.4}$$

3.2 Measuring methods for surface stress

Surface stress measurement is a commonly used method in glass analysis by researchers. As described in the previous section, surface stresses vary across the glass thickness, meaning that direct transmission-based measurement of stresses is not feasible. The reason is that stress components must be oriented appropriately relative to the light propagation direction to obtain meaningful optical measurements. Additionally, the parabolic stress distribution with compressive stresses at the surface and tensile stresses in the core would cause cancellation effects over the parabolic stress profile (Ramakrishnan and Ramesh 2016).

To measure surface stress, alternative methods are employed. The primary approaches include differential refractometry and surface guided wave methods, such as the mirage method and grazing angle surface polarimetry. The GASP (Grazing Angle Surface Polarimeter) by Strainoptics. Inc. (2025), which utilizes a quartz wedge compensator, is one of the most widely recognized instruments using the mirage principle. The method exploits the presence of tin ions from the float process, which form a thin layer of approximately 10 μm at the surface (Aben et al. 2008). These tin ions create a refractive index gradient toward the glass interior, which causes slight deflection of polarized light rays. This effect is combined with optical retardation measurements to determine residual surface stresses. Notably, this measurement method can only be applied on the tin side of float glass. This measuring method is also used in ASTM C1279 (2023).

Another method widely used for surface stress measurement is the scattered light method (introduced in Section 2.2.4. The scattered light polariscope SCALP-05, manufactured by GlasStress Ltd. (GlasStress Ltd. 2013), is widely utilized for stress measurement in tempered glass. To determine the principal stresses σ_1 and σ_2 at the surface under an unknown stress state, the SCALP-05 manual recommends measurements in four directions at 0°, 45°, 90°, and 135°, spaced 45° apart, as shown in Fig. 3.3.

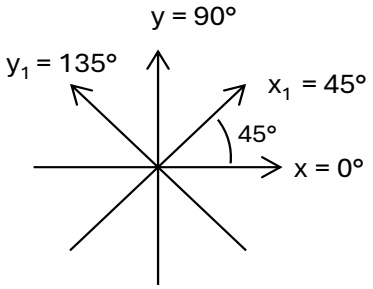

Figure 3.3: Recommended measurement directions of SCALP-05 adapted from GlasStress Ltd. (2013)

First the shear stress τ_{xy} can be calculated via Equation (3.5) from the measurements at 45° and 135°. The principal stresses σ_1 and σ_2 are then determined from Equation (3.6), where σ_1 represents the larger principal stress in terms of magnitude.

$$\tau_{xy} = \frac{1}{2}\left(\sigma_{x1} - \sigma_{y1}\right) \tag{3.5}$$

$$\sigma_{1,2} = \frac{\sigma_x + \sigma_y}{2} \pm \sqrt{\left(\frac{\sigma_x - \sigma_y}{2}\right)^2 + \tau_{xy}^2} \tag{3.6}$$

The azimuthal angle ϕ of the principal stress direction relative to the 0° measurement line can be calculated as shown in Equation (3.7).

$$\tan\varphi = \frac{2\tau_{xy}}{\sigma_x - \sigma_y} \tag{3.7}$$

Thiele et al. (2022a) investigated various evaluation methods for surface stress measurement using SCALP-05 (GlasStress Ltd. 2013). In addition to the approach described in the SCALP-05 manual using four directions, they compared two alternative methods that require only three measurement directions at 0°, 45°, and 90°. The first method solves an eigenvalue problem to directly obtain the principal stress components showing the highest accuracy in this investigation.

The second method represents a simplified approach in which a plane stress state is assumed at the surface. Normal stresses are evaluated for the three measurement directions, while the material is assumed to be optically isotropic. Based on these directional stress components, Mohr's stress circle is applied to determine the principal stresses using Equations (3.8) to (3.12). Even if slightly different results are obtained, this approach still returns valid results, which saves time by eliminating the fourth measurement direction.

$$\tau_{xy} = \sigma_{x1} - \frac{\sigma_y - \sigma_x}{2} \tag{3.8}$$

$$\varphi_1 = \frac{1}{2}\arctan\left(\frac{2\tau_{xy}}{\sigma_x - \sigma_y}\right) \tag{3.9}$$

$$\varphi_2 = \varphi_1 + \frac{\pi}{2} \tag{3.10}$$

$$\sigma_1 = \frac{\sigma_x + \sigma_y}{2} + \frac{\sigma_x - \sigma_y}{2}\cos(2\varphi_1) + \tau_{xy}\sin(2\varphi_1) \tag{3.11}$$

$$\sigma_2 = \frac{\sigma_x + \sigma_y}{2} + \frac{\sigma_x - \sigma_y}{2}\cos(2\varphi_2) + \tau_{xy}\sin(2\varphi_2) \tag{3.12}$$

3.3 Relation of surface stress to destructive tests

This section reviews the current state of the art on the relationship between surface stress, mechanical strength, and fracture behavior in tempered glass. Several key studies have investigated the correlations between surface stress and strength characteristics (Aben et al. 2010, Mognato et al. 2018, Pourmoghaddam and Schneider 2018b, Mognato et al. 2019), while others have focused specifically on the relationship between surface stress

and fragmentation behavior (Mognato et al. 2011, Lee et al. 2012, Pourmoghaddam and Schneider 2018b, Pour-Moghaddam 2020).

Aben et al. (2010) conducted a study examining five glass specimens each of HSG, fully tempered glass (FTG), and tempered safety glass, all with a thickness of 6 mm in standard format (360 mm x 1100 mm). The mean surface compressive stress values were 62 MPa for HSG, 121 MPa for FTG, and 157 MPa for safety glass, with corresponding average bending stresses of 120 MPa, 183 MPa, and 210 MPa, respectively. These results demonstrated a clear linear relationship between surface stress and bending strength. In additional investigations on specimens which are produced under the identical cooling parameter of the tempering process, however, the authors found no significant correlation between surface stress and the number of fragments.

Mognato et al. (2011) studied TTG in standard format (360 mm x 1100 mm) with thickness values ranging from 4 to 15 mm. The measured surface stresses ranged from approximately 75 to 120 MPa. The findings indicated that a minimum surface stress of 90 MPa was necessary for glass thicknesses $\leq$ 10 mm and minimum 85 MPa for glass thicknesses $\geq$ 12 mm to achieve the fracture pattern requirements specified in EN 12150-1 (2020). A linear relationship was observed between surface stress and the number of fragments. For glasses with thickness from 4 to 8 mm, no influence of the glass thickness was recognizable. However, this relationship became thickness-dependent for specimens $\geq$ 10 mm glass thickness. The relationship between surface stress and bending strength showed general agreement, although several outliers were observed where specimens with high surface stress failed to meet the required bending tensile strength. For HSG, the authors identified a surface stress range of 35 to 55 MPa as necessary to achieve acceptable fracture patterns.

Lee et al. (2012) conducted investigations on thin glass specimens with thicknesses less than 4 mm, obtaining surface stress values between approximately 90 and 140 MPa. These findings demonstrated that thin glasses require disproportionately higher compressive stress levels to achieve the fragmentation standards specified for safety glass (EN 12150-1 2020). In surface stress measurements on HSG, Veer and Rodichev (2016) investigated specimens with thicknesses ranging from 4 mm to 12 mm, measuring 800 mm x 400 mm, and exhibiting surface stress values between 43 MPa and 61 MPa. However, no statement regarding the fracture pattern was made.

In investigations on TTG using SCALP-05 (GlasStress Ltd. 2013), Nehring (2018) reported characteristic surface stress values of approximately 107-120 MPa for test series with nominal glass thicknesses of 2-6 mm. However, one test series with a thickness of 2.25 mm showed considerably lower values of approximately 86 MPa. The specimens from this series also exhibited a coarser fracture pattern, indicating that lower residual stress levels can be associated with a reduced fragment count, particularly for glass thicknesses below 3 mm. Some specimens did not fulfil the fracture pattern requirements for TTG according to EN 12150-1 (2020). For thin HSG with a glass thickness of 2 mm, Nehring (2018) reported surface stress values of approximately 68–88 MPa for specimens measured using the SCALP-05 (GlasStress Ltd. 2013). Measurements of 2 mm specimens using the SCALP-04 (GlasStress Ltd. 2013) yielded considerably higher values. The author therefore considered this device unsuitable for this glass thickness. The findings indicated that thin HSG can exhibit the required fracture characteristics according to EN 1863-1 (2012) even at comparatively low residual stress levels.

Pourmoghaddam and Schneider (2018a) examined glass specimens in standard format (360 mm x 1100 mm) with three different thicknesses (4 mm, 8 mm, and 12 mm) and surface stress values ranging from approximately 50 to 120 MPa. They found that higher surface stresses were required for thinner glass to achieve the same degree of fragmentation. This thickness dependence can be related to the elastic strain energy stored in the glass. For a given residual stress distribution, thicker glass stores a higher amount of elastic strain energy. Since the fragmentation pattern is related to the available elastic strain energy, a higher surface stress is therefore required in thinner glass to achieve a comparable degree of fragmentation.

Mognato et al. (2019) conducted measurements on both coated and uncoated specimens in dimensions 360 mm x 1100 mm using the devices SCALP-05 (GlasStress Ltd. 2013) and GASP (Strainoptics. Inc. 2025). For specimens exhibiting conforming fracture patterns for TTG, surface stress values were measured at $\geq$ 86 MPa. In contrast, HSG specimens meeting fracture requirements showed surface stress values in the range of 29 to 57 MPa.

3.4 Measuring methods for edge stress

This section reviews the relevant literature and the current state of the art, with a focus on measurement methods and commercial measuring devices used to determine retardation in the edge area of tempered glass. Subsequently, different extrapolation techniques applied across the chamfer to derive edge stress values are compared. Finally, measured edge stress data corresponding to different pre-stress levels are presented and related to destructive test results reported in the literature.

3.4.1 Retardation measurement at the edge

To determine the edge stress at a specific location using Equation (3.3), both the retardation profile in the edge area and its maximum value directly at the edge must be accurately identified. Since edge stresses in tempered glass are thickness-constant residual stresses, several photoelastic methods can be employed to measure the retardation distribution perpendicular to the edge. Scafidi et al. (2015),Ajovalasit et al. (2014), Ramesh and Ramakrishnan (2016) investigated edge stress measurement using photoelastic methods. Ajovalasit et al. (2011) and Ajovalasit et al. (2014) provided a comprehensive review of automated photoelastic approaches suitable for edge stress analysis.

Spectral content analysis

One technique is the spectral content analysis (Redner 1985, Ajovalasit et al. 2015a), in which a spectrophotometer measures the color spectrum of white light emitted from a circular polariscope. The recorded intensity spectrum is compared to a set of theoretical spectra computed for various retardation values. The actual retardation is determined by identifying the theoretical curve that minimizes the deviation from the measured (Ajovalasit et al. 2012b). A commercial implementation of this method is the Automated Edge-Stress Meter PES-100 developed by Strainoptics Inc. (2026) and described in Redner (2003) and Feingold and Redner (2003).

Phase-shifting techniques

The following methods rely on classical transmission photoelasticity. The basics of PST are described in Section 2.2.2 (Yoneyama et al. 2003). Automated PST have been refined to replace labor-intensive manual compensation methods such as Tardy and Sénarmont's goniometric compensation or Babinet and Babinet-Soleil compensators. Using this approach, Ajovalasit et al. (2014) measured the retardation until the chamfer offering more consistent and accurate retardation data at the edge for controlling car windows. Aben et al. (2013) and Aben et al. (2015) employed PST in their investigations and measured edge stress in window and automotive glass using the AP-07 measuring device from GlasStress Ltd. (2026). Furthermore, Lohr (2019) and Lohr and B. Weller (2019) used the measuring device StrainScope flex by ilis gmbh (2023), which is also employed in this thesis. Additional details about this device and its associated measurement method are provided in Section 4.2.

RGB photoelasticity

RGB photoelasticity employs a color camera within a dark-field circular polariscope using white light to capture a single image displaying colored isochromatics. As described by Ajovalasit et al. (1995) and Ajovalasit et al. (2015b), each pixel's response is decomposed into its red, green, and blue components. Through calibration, typically implemented as a look-up table (LUT), these color intensities are mapped to corresponding retardation values. The addition of a tint plate (full-wave retardation plate) enhances sensitivity in low-retardation regions. However, because such plates are wavelength-specific, their use under white light may introduce measurement errors due to chromatic dispersion. A modified RGB method proposed by Ajovalasit et al. (2012b) and Ajovalasit et al. (2015b) eliminates the need for a separate calibration pattern, enabling direct retardation measurement near the edge. This approach showed good agreement with the more precise but experimentally cumbersome method of PST, indicating its potential for practical applications. Despite this, no commercial system based on RGB photoelasticity is currently available for industrial edge stress measurement in tempered glass.

Carrier fringe method

The carrier fringe method is another transmission technique for measuring retardation in the edge area of glass. This approach employs a circular polariscope setup in combination with a carrier and is particularly suitable for low retardations (Vivek and Ramesh 2015, Ramesh and Ramakrishnan 2016). As carriers, periodic phase plates, retarders, or compensators are used to generate a defined reference interference pattern. The method assumes that the principal stress directions of the carrier and the glass specimen are either parallel or perpendicular, as is the case for edge stress conditions. Ajovalasit et al. (2012a) demonstrated that this method is well suited for determining edge stress. In this technique, the introduction of the carrier causes composite fringes, which are displayed as a displacement of the fringes within tempered glass due to the residual stresses. The retardation can then be quantified by evaluating the spatial deviation of the glass fringe pattern with respect to the reference carrier fringes.

Other methods

To determine the mean edge membrane stress, Laufs (1998), Laufs (2000) used the Edge Stress Meter by Sharples (2026). The underlying measurement principle belongs to the analog methods of classical photoelasticity and is based on the Sénarmont's compensation

technique, in which the analyzer is rotated until the transmitted light intensity reaches a minimum. The extinction angle is proportional to the optical retardation and, according to the Wertheim's law from Equation (2.5), enables a quantitative determination of stress. Another manual measuring device based on double-wedge compensation is the GES-100 by Strainoptics Inc. (2012) which operates according to the principles described in Procedure B of ASTM C1279 (2023). One additional measuring device on the market is the NES-T Automatic Edge Stress Meter by Ayrox SRL. (2026) using quartz wedge compensator method. The approach of MWP (basics in Section 2.2.3) to measure edge stress in-line during the production process of tempered glass was first described by Schaaf et al. (2017). Since this measurement method is applied in this work, its methodology is elaborated in Sections 2.2.3 and 4.3.

3.4.2 Extrapolation techniques across the chamfer

The edges of architectural glass are chamfered before tempering to reduce the risk of breakage during the tempering process. Cutting the glass can produce sharp and irregular edges with surface defects and microcracks that may act as fracture initiation sites under the thermal stresses induced during tempering. Accordingly, EN 12150-1 (2020) and EN 1863-1 (2012) require the edges to be chamfered, with at least a seamed edge, before tempering. For measuring retardations, the incidence angle of light waves of the used measuring devices must be perpendicular to the surface to obtain accurate photoelastic measurements of residual stress in the glass. However, in the case of chamfers in architectural glass, the sloping surface causes reflection of the light, leading to errors in the data output from the retardation measurement. Therefore, it is not possible to measure the retardation and, as consequence, evaluate the edge stress accurately at the furthest point on the edge. The measurement of retardation values is reliable only until the start of the chamfer (Aben et al. 2015). Consequently, the available retardation curve must be extrapolated to determine the retardation values across the chamfer and to obtain the maximum retardation at the edge. This section indicates different extrapolation techniques and polynomial degrees.

Simplified extrapolation method by ASTM C1279 (2023)

The ASTM C1279 (2023) provides a simplified technique for determining the maximum retardation on the edge with chamfer. Therefore, the retardations R_1 and R_2 at two specific measurement points x_1 and x_2 are measured using a hand-held polarimeter with a wedge compensator. Then, the maximum retardation on the edge is calculated as in Equation (3.13), using a linear extrapolation method.

$$R = 3.8\,R_1 - 2.8\,R_2 \tag{3.13}$$

Table 3.1 shows the location of these measurement points x_1 and x_2. The distance of the edge depends on the thickness of the glass. For glass thicknesses between 3 and 5 mm, the size of the chamfer is also decisive: if the values $x_1 = 0.6$ mm and $x_2 = 1.0$ mm fall within the chamfer region, the alternative values $x_1 = 0.8$ mm and $x_2 = 1.3$ mm should be used.

Table 3.1: Position of measurement points for retardation according to ASTM C1279 (2023)

	Glass thickness [mm]		
Distance of the edge [mm]	3 to 5	6 to 10	12 to 24.5
x_1	0.6 or 0.8 *	1.0	2.0
x_2	1.0 or 1.3 *	1.6	3.0

* In case of broad chamfer

Extrapolation with polynomial of 2nd degree

The method of MWP introduced by Schaaf et al. (2017) and used in this thesis is, at this stage, still based on a 2nd degree polynomial fitting function.

Extrapolation with polynomial of 3rd degree

Laufs (2000) conducted experimental and numerical investigations on edge stresses. Using the Edge Stress Meter by Sharples (2026) based on the Sénarmont's compensation technique, the retardation was measured at multiple points perpendicular to the edge, resulting in an increasing retardation profile in the pre-stress zone. The retardation distribution was then extrapolated towards the edge using a 3rd degree polynomial fit. This was verified by a numerical simulation of the residual stresses on the edge. For the fitting function passing through the measurement points, Laufs (1998) reports high coefficients of determination ($R^2 > 0.9990$). A comparison with higher or lower polynomial degrees, however, is not provided. Based on Laufs (2000) and Lohr (2019), a 3rd degree polynomial extrapolation was applied for demonstrating the impact of regrinding edges for edge stress and strength. To facilitate extrapolation, Lohr (2019) developed conversion factors to transform the measurable stress value at the beginning of the chamfer into the corresponding edge stress directly at the glass edge. The conversion factors depend on both glass thickness and glass type, with specific values defined for thicknesses of 6 mm, 8 mm, and 10 mm as well as for TTG and HSG. These conversion factors are applicable to a chamfer width of 1 mm.

Extrapolation with polynomial of 4th degree

Aben et al. (2013) and Aben et al. (2015) conducted experimental measurements on edge stress in tempered glass using PST methods (see Section 2.2.2). They extrapolated the retardation curve with a 4th degree polynomial. However, no justification for the choice of the polynomial degree was provided, nor was an analysis of the fitting function conducted.

Other extrapolation techniques

The remaining methods mentioned in Section 3.4.1 (Ajovalasit et al. 2011, Ajovalasit et al. 2012b, Ajovalasit et al. 2012a, Ajovalasit et al. 2014, Ajovalasit et al. 2015b) do not provide any statements regarding the fitting procedure or the extrapolation towards the edge.

In summary, the reviewed extrapolation methods differ considerably, and there is currently no clear evidence or justification supporting the appropriateness of any specific approach, which is why these methods are further investigated in Section 4.2.2.

3.5 Relation of edge stress to destructive measurements

Most of the studies discussed in the previous two sections focus primarily on the photoelastic measurement techniques of edge retardation and do not provide extrapolated values for edge stress. Consequently, only a few investigations have examined the relationship between edge stress, bending strength, or fracture pattern.

As described before, Laufs (1998) and Laufs (2000) calculated edge stress values by extrapolation using a 3rd degree polynomial. For TTG consisting of 84 samples with a thickness of 10 mm, edge stress values ranged from 63 MPa to 117 MPa, with a mean value of 91 MPa. For 15 mm thick TTG (68 samples), the mean value was 102 MPa, with a minimum of 81 MPa and a maximum of 124 MPa. The specimens originated from four to five different manufacturers. Furthermore, he also showed exemplary retardation curves in the edge area with extrapolated values for glass thicknesses ranging from 6 to 15 mm, yielding edge stress values between approximately 70 and 82 MPa. For HSG, a wider scatter was observed for thicknesses between 4 and 12 mm, with edge stress values ranging from 45 to 85 MPa. Although Laufs (2000) performed four-point bending tests, the subsequent investigation did not explore the relationship between the resulting bending stresses and the edge stress. Instead, the difference between pre-stress and bending stress was used to determine the inherent glass strength.

Lohr (2019) investigated the influence of regrinding edges on edge stress and strength for TTG and HSG with thicknesses of 6 mm, 8 mm, and 10 mm. For the samples before regrinding, the tests yielded edge stress values (at the fracture origin determined by four-point bending tests) ranging from 64 to 76 MPa for 6 mm TTG, 54 to 71 MPa for 6 mm HSG, 61 to 80 MPa for 8 mm TTG, 58 to 70 MPa for 8 mm HSG, 52 to 69 MPa for 10 mm TTG, and 46 to 61 MPa for 10 mm HSG. As described before, these values were extrapolated using a 3rd degree polynomial. Across all thicknesses, TTG exhibited slightly higher edge stress levels than HSG, with a relatively small and consistent difference of approximately 5 to 10 MPa. The four-point bending tests were carried out about the strong axis, resulting in a linear correlation between edge stress and bending stress considering glass thickness and pre-stress level.

3.6 Relation between edge stress and surface stress

It is reasonable to assume a correlation between edge stress and surface stress, as both originate from the residual stress state introduced during the tempering process. The relation between surface stress and edge stress was investigated by Aben et al. (2015). By determining edge stress with an extrapolation of 4th polynomial degree, they identified a one-to-one correlation between surface stress and edge stress, indicating a direct relationship between the two residual stress measures.

The photoelastic results based on the mean values of the test series reported by Lohr (2019) show that edge and surface stress values lie within a similar range for HSG. In contrast, Laufs (2000) reported noticeably higher edge stress values than surface stress for HSG. For TTG, the results reported by Lohr (2019) reveal a different trend: the measured surface stress values exceed the corresponding edge stress values by a factor of approximately 1.4.

3.7 Existing photoelastic limit values

As part of factory production control, the European standards EN 12150-1 (2020) and EN 1863-1 (2012) permit the use of the scattered light method to verify the bending strength. However, these standards do not specify any exact or generally applicable surface stress limits, nor do they consider edge stress measurements.

In contrast, the American standard ASTM C1048 (2025) defines photoelastic limit values for use in factory production control, a practice established already in the early 1990s. The corresponding measurement methods of surface and edge stress for tempered glass are specified in ASTM C1279 (2023). Surface stress measurements are conducted at five measurement points distributed across the specimen surface in accordance with ASTM C1048 (2025). At each location, the surface stress is measured in two orthogonal directions, resulting in a total of ten surface stress values per specimen. The standard uses the measuring device GASP (Strainoptics. Inc. 2025) employing the mirage effect to determine the stress state at the glass surface.

According to ASTM C1279 (2023), edge stress is evaluated using the linear extrapolation method based on two retardation measurements perpendicular to the edge (see Section 3.4.2). The corresponding measuring device used for this method is the PES-100 Automated Edge-Stress Measurement System (Strainoptics Inc. 2026). Edge stress measurements are performed at the midpoint of each edge, yielding four edge stress values per glass specimen. The location and distribution of these measurement points are illustrated in Fig. 3.4. Importantly, ASTM C1048 (2025) does not impose format restrictions on the glass specimens for photoelastic measurements, so they can be performed on specimens of any size or aspect ratio.

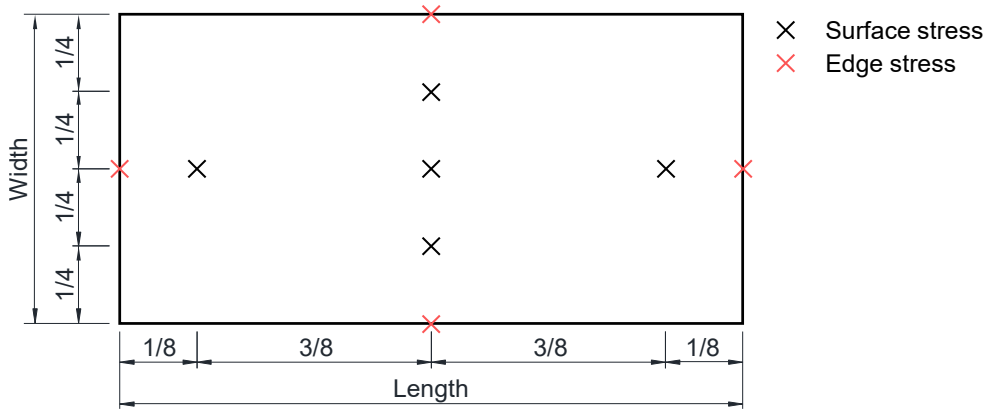

Figure 3.4: Position of measurement points for surface stress and edge stress according to ASTM C1279 (2023) and ASTM C1048 (2025)

For fully tempered glass, ASTM C1048 (2025) does not provide any specifications regarding restrictions on glass thickness that would limit the photoelastic limit values. According to the standard, the range of glass thicknesses for the glass types described therein is from 3 mm to 19 mm. The ASTM C1048 (2025) standard specifies a minimum surface stress of 69 MPa and a minimum edge stress of 67 MPa for fully tempered glass, which nominally corresponds to the European thermally toughened safety glass. However, fully tempered glass according to ASTM C1048 (2025) is defined based on bending tensile strength, while

the fracture pattern is governed by a separate standard (ANSI Z 97.1 2015) and not by a photoelastic stress criterion. Previous studies (Mognato et al. 2011, Mognato et al. 2017, Mognato et al. 2018) have shown that the photoelastic limit values defined in ASTM C1048 (2025) do not ensure compliance with the fracture pattern required by EN 12150-1 (2020).

The international standard ISO 12540 (2017) acknowledges this discrepancy and differentiates the surface stress limits for TTG according to mechanical requirements: a minimum of 80 MPa is required to meet the strength criterion, whereas a minimum of 90 MPa is necessary to satisfy the fracture pattern requirement. These values for surface pre-stress is valid for glass thicknesses from 4 mm to 12 mm. Edge stress values are not specified in ISO 12540 (2017).

From the literature, few photoelastic limit values for surface stress measurements are reported: Mognato et al. (2011) examined glass samples with thicknesses ranging from 4 to 15 mm and identified minimum surface stresses of 90 MPa for $t \leq 10$ mm and 85 MPa for $t \geq 12$ mm as photoelastic limits corresponding to a safe fracture pattern defined in EN 12150-1 (2020). The relationship between bending strength and surface stress was further investigated by Mognato et al. (2017) who proposed a lower limit of 85 MPa to ensure the required bending strength of clear TTG. In a subsequent study, Mognato et al. (2018) refined these findings and recommended a minimum surface stress of 90 MPa for clear TTG to simultaneously satisfy both the strength and fracture pattern requirements. The different photoelastic limit values for clear TTG reported in the standards and literature are summarized in Table 3.2.

Table 3.2: Surface and edge stress limit values for thermally toughened glass / fully tempered glass to fulfill strength requirements and fracture pattern from various references

		Surface stress [MPa]		Edge stress [MPa]	
Reference	Glass thickness [mm]	Bending strength	Fracture pattern	Bending strength	Fracture pattern
ASTM C1048 (2025)	3–19	69	–	67	–
ISO 12540 (2017)	4–12	80	90	–	–
Mognato et al. (2018)	4–15	90	90	–	–

HSG represents a critical pre-stress stage, as two limiting conditions must be satisfied. The residual stress state must be sufficiently high to achieve a bending tensile strength of 70 MPa, yet not excessively high to maintain the characteristic coarse fracture pattern (EN 1863-1 2012). For the control of HSG using surface stress measurements, ASTM C1048 (2025) specifies a range of 24 and 52 MPa for glass thicknesses ≤ 6 mm. For glass thicknesses ≥ 6 mm, the standard recommends consulting the glass manufacturer to determine appropriate surface stress limits. The ISO 22509 (2020) provides a similar range of 25 to 52 MPa, but for glass thicknesses ranging from 4 mm to 12 mm. However, it should be noted that this standard specifies a minimum value of 65 MPa for bending strength of HSG. No limit values for edge stress are specified for HSG in either ISO 22509 (2020) or ASTM C1048 (2025).

Laufs (2000) recommended a surface stress of 35 to 50 MPa for HSG to ensure a sufficient fracture pattern while maintaining high strength. Mognato et al. (2018) reported a surface stress range of 35 to 60 MPa for uncoated HSG to ensure compliance with both fracture

pattern and bending strength requirements, valid for glass thicknesses of 4–12 mm. No literature sources were found specifying edge stress limits for HSG. The different limit values for clear HSG reported in the literature are summarized in Table 3.3.

Table 3.3: Surface and edge stress limit values for heat-strengthened glass to fulfill strength requirements and fracture pattern from various references

		Surface stress [MPa]		Edge stress [MPa]	
Reference	Glass thickness [mm]	Bending strength	Fracture pattern	Bending strength	Fracture pattern
ASTM C1048 (2025)	3–6	24	52	–	–
ISO 22509 (2020)	4–12	25	52	–	–
Mognato et al. (2018)	4–12	35	60	–	–
Laufs (2000)	–	35	50	–	–

4 Developing a method for evaluating edge stress

This chapter develops a photoelastic methodology for determining edge stress. The initial step was to record the retardation of the light source of the measuring device in the compressive area of the edge. This was conducted using two distinct measurement approaches: PST and MWP. The ASTM C1279 (2023) method for measuring the retardation values on two specific points could not be applied due to the broad chamfer width of architectural tempered glass specimens. Since photoelastic measurements could not be performed directly in the chamfer area, the retardation curve must be extrapolated across the chamfer towards the edge to ascertain the edge stress. To identify the appropriate degree of the interpolation and extrapolation function, different fittings were compared by means of PST measurements. This was achieved by employing continuous retardation curves, which were locally measured with the StrainScope flex by ilis gmbh (2023). The second measuring device under consideration was the LineScanner, developed by Softsolution GmbH (2023b). This device is currently used in production control to evaluate anisotropy effects at the end of the tempering process (Dix 2024) and its potential advantage lies in the possibility of an automating edge stress control. Nevertheless, the evaluation employing MWP is presently confined to a limited number of edge isochromatics. To enhance the reliability of edge stress determination, the curve parameters of the interpolation function obtained by PST were adapted for the method of MWP. By comparing edge stress values measured with both techniques, a reliable methodology for online edge stress assessment was established. This formed the basis for the subsequent investigations. Parts of this chapter have already been pre-published in Efferz et al. (2024a) und Efferz et al. (2024b).

4.1 Characterization of the chamfer issue

Under polarized light, differences between the two principal stresses σ_1 and σ_2 in a transparent material cause optical retardations. In the region of the undisturbed area of the glass, far enough away from the edge, corner, or cut-outs, the measured retardations are typically low, minor as 300 nm, which corresponds to about 0.5^{th} fringe of the used wavelength (Dix et al. 2022). Towards the edge in a width of approximately the glass thickness (Laufs 2000), the retardation increases steadily, typically attaining values in excess of 0.5 fringe order of the wavelength. The maximum retardation is reached at the outermost edge. Isochromatics parallel to the edge can be recognized under polarized light conditions. Fig. 4.1 shows photoelastic images of the same pre-stress level TTG, but of different glass thicknesses, acquired by a bright-field setup using the blue wavelength of the device of MWP. As can be seen, the number of isochromatics increases with glass thickness within the same pre-stress level.

After the characteristic cutting process of glass to the desired dimensions, the edges of glass are sharp and irregular. The product standards EN 12150-1 (2020) for TTG and EN 1863-1 (2012) for HSG specified that the edges must be chamfered for safety and strength, particularly before tempering. Edge finishing standards are detailed in DIN 1249-11 (2023) and vary based on the glass application. Edge processing for tempered glass ranges from a basic 45° chamfer with a coarse finish to a highly polished, transparent edge for aesthetic applications. The width of the chamfer is usually between 0.5 and 2.0 mm, depending on glass thickness, to ensure safety during and after the tempering process.

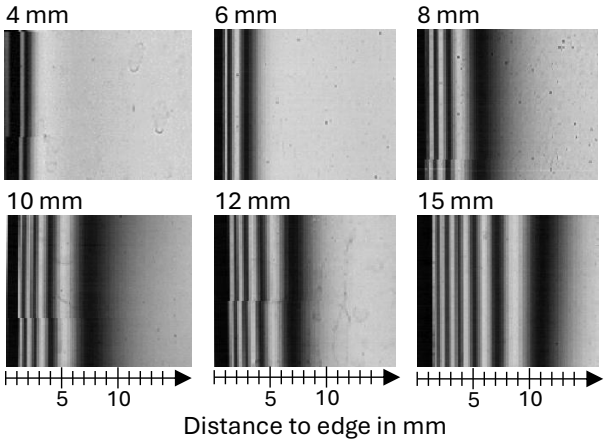

Figure 4.1: Monochromatic isochromatic images obtained by multiple-wavelength photoelasticity (blue wavelength, 442.35 nm): isochromatic fringes parallel to the glass edge are shown for thermally toughened glass with increasing thickness from 4 mm to 15 mm at a surface pre-stress level of 100–110 MPa from Efferz et al. (2024b)

However, the chamfer of architectural glass causes issues for photoelastic measurements in the area of the edge. The incidence angle of light waves of the used measuring device must be perpendicular to the glass surface to obtain accurate photoelastic measurements of residual stress in the glass. However, the sloping surface of the chamfer results in the reflection of the incoming polarized light, as illustrated in Fig. 4.2a. This phenomenon leads to errors in the data output of the retardation measurement. Fig. 4.2b and Fig. 4.2c illustrate the chamfer issue exemplary shown on a 10 mm TTG specimen, using the intensity image acquired by PST (b) and the photoelastic image recorded by MWP (c). As displayed in Fig. 4.2b, the intensity image by PST demonstrates the scattering of incoming light at the chamfer, thereby hindering precise transmission. Fig. 4.4d shows exemplary the corresponding disturbed retardation curve in the chamfer area. In contrast, the photoelastic image in Fig. 4.2c recorded by MWP shows that the chamfer no longer permits light transmission, and the area is shown as a black area due to the absence of light intensity. As demonstrated by the use of two distinct measuring devices, it was not feasible to accurately evaluate the retardation at the furthest point on the edge.

ASTM C1279 (2023) provides a linear extrapolation method, whereby retardations R_1 and R_2 are to be measured at the fixed points x_1 and x_2, the location of which depends on glass thickness. A more detailed description of the measurement method can be found in Section 3.7. The analysis of retardation values by means of this method can be challenging due to the size of the chamfer of architectural glass. As can be seen in Fig. 4.2b and c, one or both of the measurement points x_1 and x_2 fell within or near the chamfer. Therefore, the ASTM

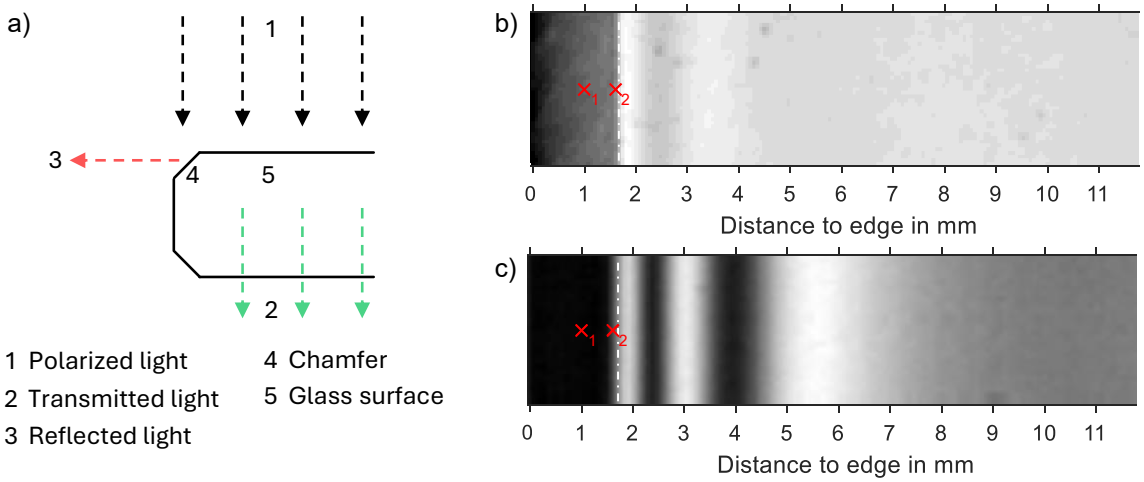

Figure 4.2: a) Reflection of the incident light at the chamfer in a glass cross-section, b) intensity image obtained using phase-shifting technique, and c) isochromatic image obtained using multiple wavelength photoelastic on thermally toughened glass (t = 10 mm) with measurement points $x_1 = 1.0$ mm and $x_2 = 1.6$ mm; chamfer is indicated by a dashed line, from Efferz et al. (2024a)

method could not be used for the test specimens available for analysis in this research. Consequently, alternative extrapolation methods were required to determine the edge stress. In the following sections, two different methods for measuring retardation in the edge region were investigated as alternatives to ASTM C1279 (2023). In addition, various extrapolation approaches were systematically compared to identify a reliable method for assessing edge stress.

4.2 Evaluation with phase-shifting technique

To develop an evaluation method for edge stress using PST, a total of 82 glass specimens of TTG and HSG with a size of 360 mm x 1100 mm, ground edges, and nominal glass thicknesses of 4, 6, 8, 10, and 12 mm were initially analyzed. The measurements were carried out using the StrainScope flex from ilis gmbh (2023) displayed in Fig. 4.3.

4.2.1 Experimental setup

The method of PST was used to measure the retardation locally at three selected measurement areas per longitudinal edge of the specimen. These areas were selected in the center and in the quarters of the longitudinal edges (see Fig. 4.4a). The measuring device StrainScope flex by ilis gmbh (2023) generates csv files for the measurement area in retardation values and intensity values shown as corresponding images in Fig. 4.4c and d. The following analysis were conducted with MATLAB (The MathWorks, Inc. 2024b). Fig. 4.4b illustrates that five cuts were made through a measurement area. The retardation values of a section through the edge are in a range from 0 nm to half the wavelength of the light. For the light source with a wavelength of 588 nm, this means that the retardation increases up to 294 nm and then decreases again to 0 nm, see Fig. 4.4d as a zigzag pattern. To

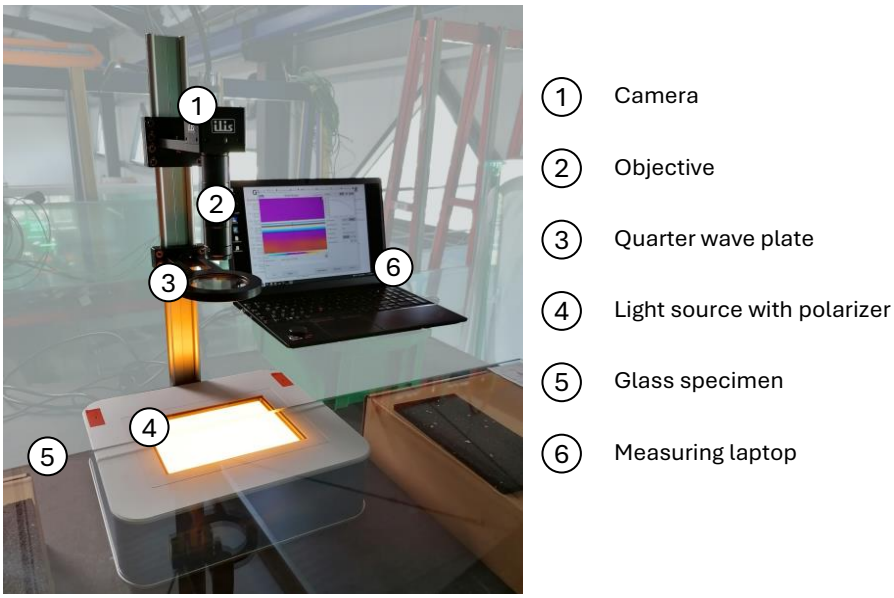

Figure 4.3: Measuring device StrainScope flex by ilis gmbh (2023) using phase-shifting technique

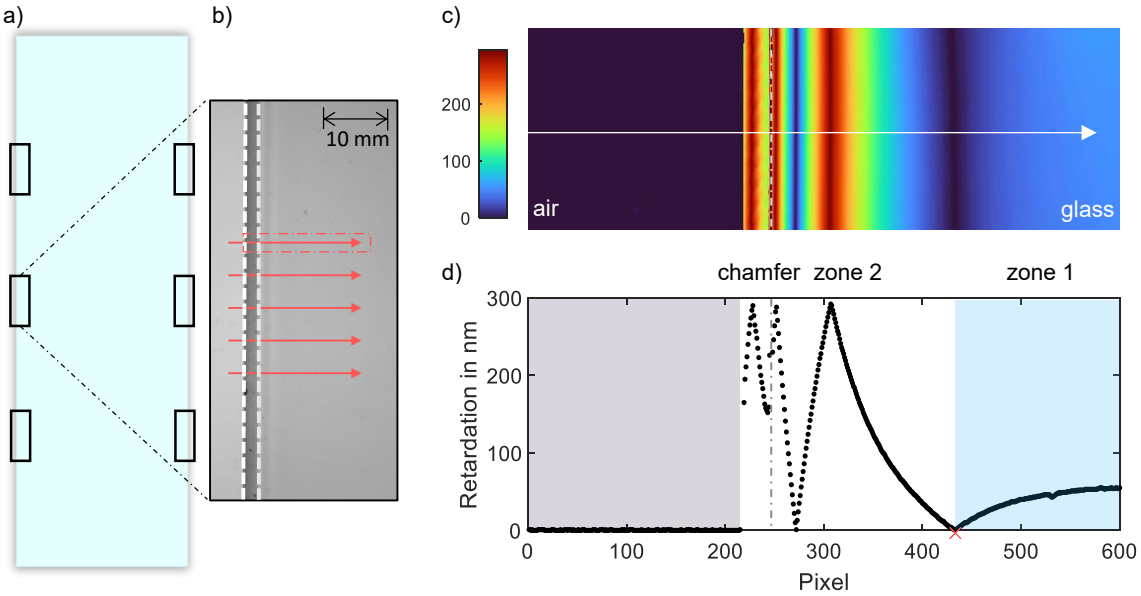

Figure 4.4: Evaluation method based on the phase-shifting technique: a) six measurement areas per glass specimen, b) five sections per measurement area, from Efferz et al. (2024a), c) retardation image of a 10 mm heat-strengthened glass, and d) corresponding retardation curve showing a zigzag pattern between 0 and 294 nm

determine higher retardations beyond 294 nm, a plane stress state in the model with known principal stress directions is necessary. This condition is fulfilled at the compressive zone at the edge where one of the principal stresses becomes zero due to the cooling behavior of the tempering process. In the area near the edge of the glass, the fringe order increases towards the edge. To obtain the maximum retardation at the edge, the discrete retardation steps associated with the half-fringe order were accumulated. To ascertain the position at which pre-stress zone 1 of the glass plate begins, the entire section (Fig. 4.4d) must be observed within a measurement area of the retardation (Fig. 4.4c) to find a wider minimum peak: behind the zero-fringe point, the retardation rises only slowly and stabilizes at a certain value in direction of zone 1. Up to this point, the individual retardation increments could be summed. After this procedure, the 0th isochromatic order is equivalent to the zero-crossing of the curve thus formed. This delineates the transition from zone 2 of the edge to zone 1 of the plate, where the parabolic stress distribution is applied over the glass thickness.

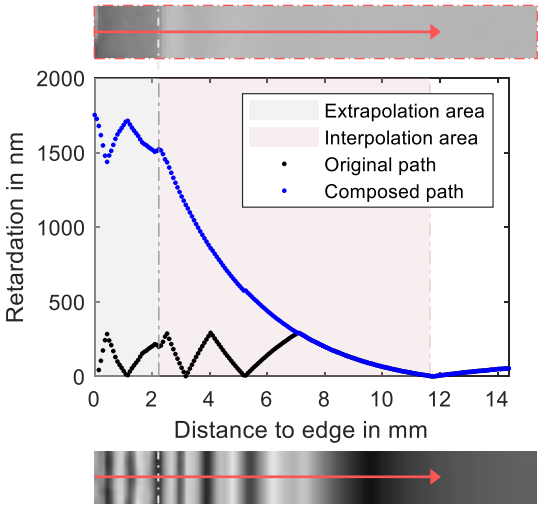

Figure 4.5: Phase-shifting technique applied to the glass edge: schematic diagram showing the chamfer and the fitting area used for extrapolation to the edge; original retardation data points exhibiting $\lambda/2$ increments and the accumulated composed retardation curve; and the corresponding intensity and retardation images of the edge section, shown for 12 mm thermally toughened glass, from Efferz et al. (2024a)

Fig. 4.5 shows the composed retardation path of a 12 mm TTG, which was formed of the zigzag curve labelled as original path. Across the chamfer, transmission losses led to distorted retardation values, resulting in a non-uniform path, as shown in Fig. 4.5 in the chamfer area. Therefore, these retardation values acquired at the chamfer were excluded from the evaluation, and extrapolation to the edge of the glass was required. The area from zero-crossing to the start of the chamfer was referred to as the interpolation area wherein the measured points were fitted into a polynomial function. The width of the chamfer constituted the extrapolation area.

4.2.2 Interpolation of retardations

The PST is characterized by its ability to provide a more precise observation of the gradient and selection of extrapolation, since the measurement points can be described as a continuous curve, in contrast to the MWP method, see Section 4.3.1. The formation of an interpolation function was achieved by utilizing measurement points that fell within the range from the 0th isochromatic order to the start of the chamfer. This chapter describes the comparison of the fitting functions of 2nd, 3rd and 4th degree polynomials.

The first step was to get an appropriate interpolation fit of the measured retardation values. There were various ways to create a fitting function for data points. The fit connected the available data points as a steady mathematical function. Standard fitting functions can be polynomials of different degrees, exponential, spline, or trigonometric functions. Laufs (2000) and Aben et al. (2013) used different investigation methods to measure the retardation towards the glass edge. Additionally, they used polynomials of different degrees to describe the increase in retardations.

The choice of polynomial degree significantly influences the accuracy of the interpolation of data points and the reliability of the extrapolation over the chamfer to the edge to obtain the edge stress. Although a higher degree polynomial may offer a more accurate fit to the data points, it also carries the risk of overfitting, leading to unwanted deviations in the extrapolation. Additionally, experimental inaccuracies can lead to significant errors in the calculated stress distribution (Aben and Guillemet 1993). Therefore, it was crucial to carefully select the polynomial degree to achieve a balanced interpolation between the data points of retardation and ensure a realistic extrapolation for the edge stress.

Ideally, the interpolation function should run precisely through all data points to have the fewest deviations. To assess the quality of the fit, it is possible to compare goodness-of-fit parameters. Fig. 4.6 and Fig. 4.7 illustrate the factors of SSE and adjusted R^2 of the interpolation functions depending on the different polynomial degrees for five investigated glass thicknesses divided by glass types TTG and HSG. The polynomial behaviour was evaluated based on five cuts per measurement area.

A thorough evaluation of the goodness-of-fit parameters showed that all three polynomial degrees generally provided satisfactory fits. However, the comparison indicates that the 2nd degree polynomial showed a notable discrepancy from the 3rd and 4th degree polynomials across all glass thicknesses. The statistical parameters SSE and adjusted R^2 indicate that the 2nd degree polynomial is generally less suitable for fitting the measured retardations than the 3rd and 4th degree polynomials. For samples with thicknesses between 4 mm and 10 mm, the HSG specimens exhibited a poorer fit with the 2nd degree polynomial, whereas for the 12 mm glass, the pattern was reversed: here, the 2nd degree polynomial produced worse fitting parameters for TTG.

Furthermore, differences between glass thicknesses were also evident. For the 4 mm samples, several outliers in adjusted R^2 values were observed, reaching down to 0.83. These outliers are omitted from the figures for clarity. Similar outliers also occurred with the 3rd degree polynomial, suggesting that both degrees may be insufficient to describe the measured retardations in some cases. Although a higher-degree polynomial might improve the fit, the limited number of retardation values available across the narrow interpolation width of thin glass may reduce extrapolation reliability and cause the curve to diverge at its upper end. Consequently, the evaluation of 4 mm glass was particularly challenging and

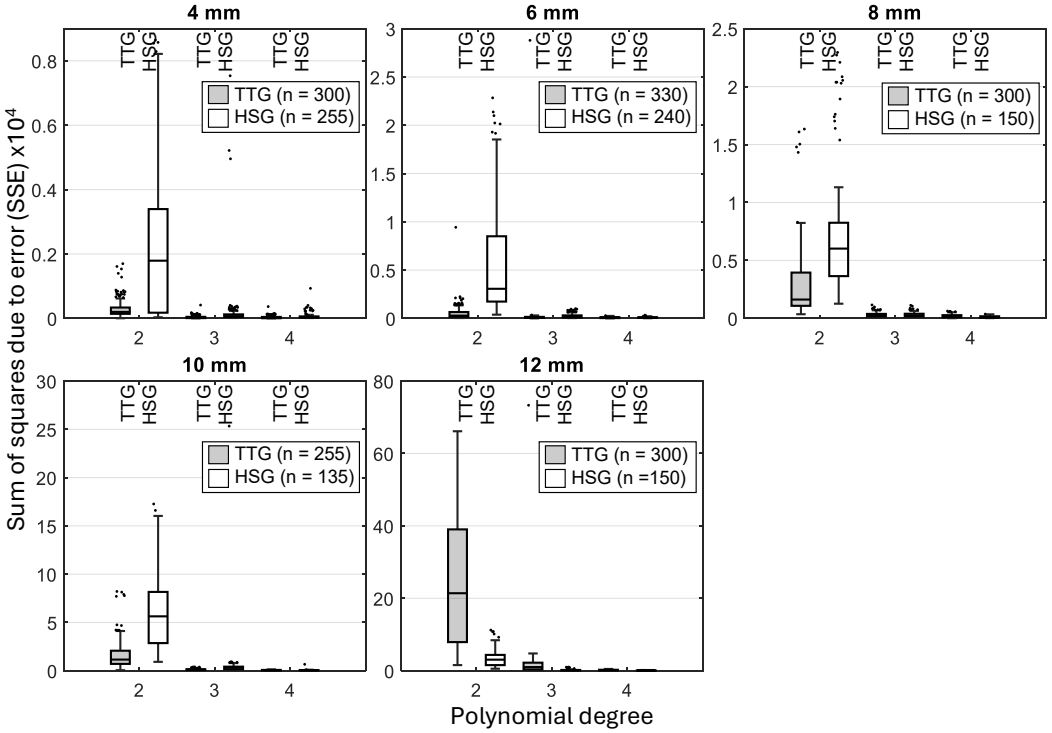

Figure 4.6: Evaluation of polynomial degrees for interpolation fit using phase-shifting technique: comparison of sum of squared errors for glass thicknesses from 4 mm to 12 mm for thermally toughened and heat-strengthened glass

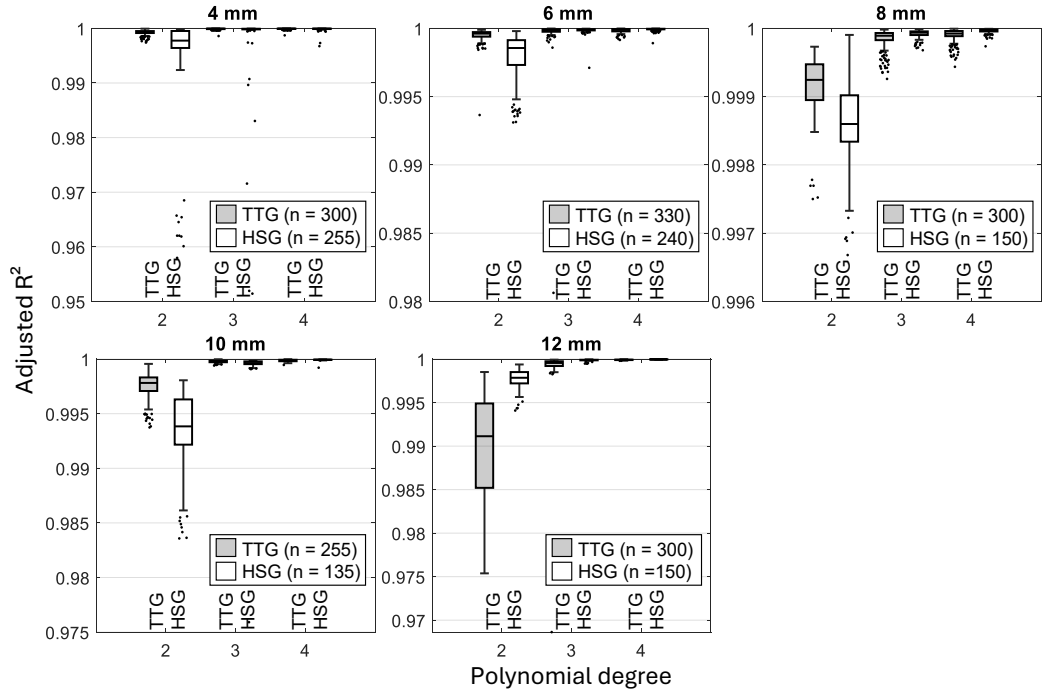

Figure 4.7: Evaluation of polynomial degrees for interpolation fit using phase-shifting technique: comparison of adjusted R^2 for glass thicknesses from 4 mm to 12 mm for thermally toughened and heat-strengthened glass

less robust. The differences between polynomial degrees were most pronounced for the 10 mm and 12 mm glass samples. In these cases, the 2nd degree polynomial tended to yield comparatively lower adjusted R^2 values and higher SSE, indicating a poorer fit. From this, it could be concluded that a 2nd degree polynomial was generally unsuitable as an interpolation function for these glass thicknesses. Overall, the polynomial degree must be selected by balancing goodness of fit against the risk of overfitting and reduced extrapolation reliability, particularly for thin glass.

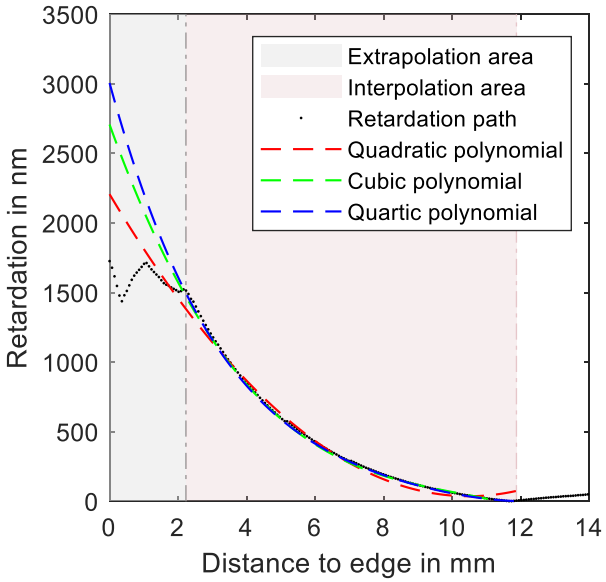

Figure 4.8: Comparison of interpolation curves and extrapolation behavior of polynomials of 2nd, 3rd, and 4th degree based on phase-shifting measurements, exemplified for thermally toughened glass with a thickness of 12 mm

This behaviour can also be seen in Fig. 4.8 on a specimen with a thickness of a 12 mm TTG. Here, the retardation curve of one section through the edge measured by PST showed that a 2nd degree polynomial could not provide an accurate fit to the data points. This polynomial degree was too low and therefore unsuitable for describing the retardation curve towards the edge. For all test specimens, the interpolation curve and the statistical measures of SSE and adjusted R^2 of the 3rd and 4th degree polynomials did not notably differ when fitted within the measured data points. As shown in Fig. 4.8, the two polynomials of the 3rd and 4th degree demonstrated a precise fit to the measured curve within the interpolation range in comparison to the 2nd degree polynomial.

4.2.3 Ratio of interpolation and extrapolation width

By extrapolation, values are inferred for points outside the interpolation range, which are no longer supported by measurement data. For the analysis using PST, the interpolation width extends from the chamfer to the zero crossing, while the extrapolation region corresponds to the width of the chamfer. The corresponding widths are shown in Fig. 4.9.

If the chamfer is too wide compared to the interpolation range, the extrapolation tends to exhibit stronger oscillations outside the interpolation interval. The farther the extrapolation extends, the less reliable the result becomes. Therefore, in this section, the ratio between

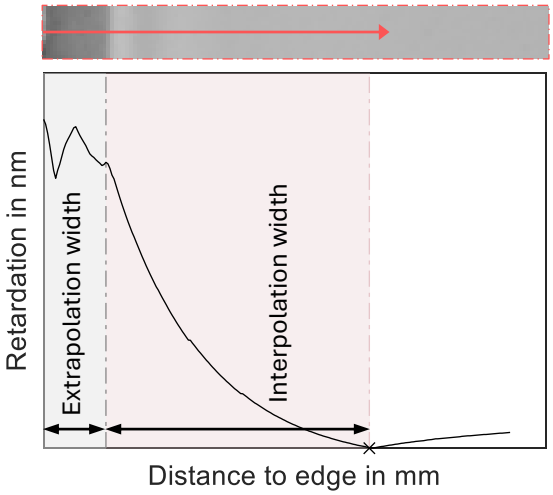

Figure 4.9: Schematic visualization of interpolation and extrapolation widths for phase-shifting technique

interpolation and extrapolation width was investigated, calculated as factor $f_{ex/int}$, see Equation (4.1).

$$f_{ex/int} = \frac{\text{extrapolation width}}{\text{interpolation width}} \tag{4.1}$$

Fig. 4.10 shows the ratio between interpolation and extrapolation width per measurement area, separated by the glass thickness and glass types TTG and HSG. In some cases of 4 mm and 6 mm TTG, the ratio between interpolation and extrapolation width exceeded 1, indicating that the extrapolation width was larger than the interpolation width, which was unfavorable for robust extrapolation. With increasing glass thickness from 6 mm to 12 mm, the TTG samples exhibited a decreasing trend of this factor $f_{ex/int}$. This behavior occurred because the interpolation width increases with glass thickness. The zero crossing of the retardation curve defines the width of the pre-stressed zone of the edge area, which depends on the glass thickness, as shown by Laufs (2000). For 4 mm and 6 mm TTG, the ratio between interpolation and extrapolation width were within a similar range. A closer inspection of the chamfer revealed that it was smaller for the 4 mm samples, leading to comparable ratios to those of the 6 mm samples.

For HSG, the factor $f_{ex/int}$ was consistently smaller than for TTG. The maximum values reached about 0.5, indicating that the interpolation width is approximately twice the extrapolation width. For HSG, a slightly decreasing trend of the factor could also be observed starting from 6 mm glass thickness. As already observed with TTG, the 4 mm HSG samples also exhibited a narrower chamfer compared to the other glass thicknesses. However, in this case, the change from 4 mm to 6 mm glass thickness appeared to have little effect on the width of the interpolation zone, resulting in a slightly larger factor for the 6 mm HSG samples compared to the 4 mm ones.

In conclusion, the results indicated that the HSG samples generally provided a more favorable ratio between interpolation and extrapolation width than TTG for the PST method. Although the 4 mm and 6 mm TTG samples exhibited similar factors in this study, it should be noted that the interpolation zone for the 4 mm glass was narrower due

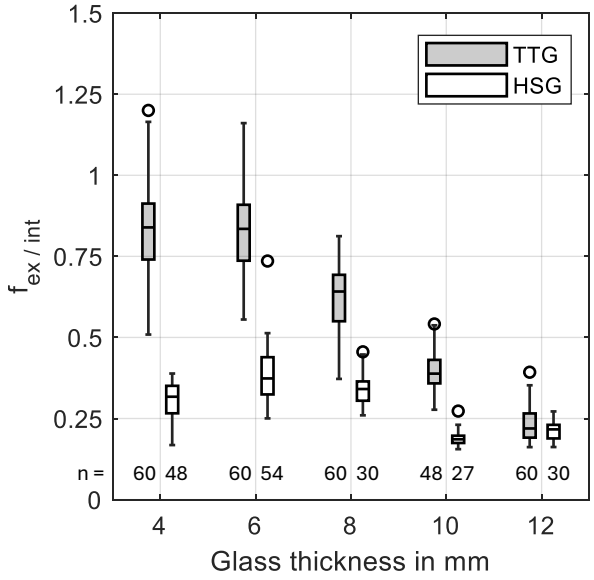

Figure 4.10: Ratio between interpolation and extrapolation width determined using phase-shifting techniquee

to its smaller thickness, resulting in fewer available retardation measurement points. In the context of thin glass with wide edge processing, it is imperative to exercise caution when interpreting the extrapolation results. This evaluation was carried out in the next section.

4.2.4 Extrapolated edge stress values

For selecting the suitable fitting function, it is essential to compare the extrapolated edge stress, as this is the value used to guarantee the glass properties in production control. Therefore, the retardation curves were extrapolated over the chamfer to the end of the edge, and the edge stress obtained at this point was calculated using Equation (3.3) with the actual measured glass thickness.

Fig. 4.11 demonstrates that polynomial degrees resulted in significantly different edge stress values. The diagram shows box plots of the extrapolated edge stress determined by the 3rd and 4th degree polynomials, depending on the glass type and the glass thickness for each measurement area. The extrapolation curve towards the glass edge is no longer defined by any measurement points. The extrapolated value is contingent upon the selected mathematical interpolation function. The extrapolation of 4th degree polynomial resulted in higher edge stress values or more scatter than the 3rd degree. This can be explained by the higher rise resulting from the greater polynomial and an increased adaptability of the 4th degree polynomial due to the additional coefficient.

The evaluation of the interpolation range demonstrated that the 3rd and 4th degree polynomials functions exhibited comparable efficacy for describing the data points. This finding indicated that a conclusive preference for either polynomial degree could not be determined based on this current evaluation. Additionally, the practical validation of extrapolated edge stress values against actual values is not infeasible due to the presence of an unavoidable chamfer, which complicates accurate stress measurement at the edge.

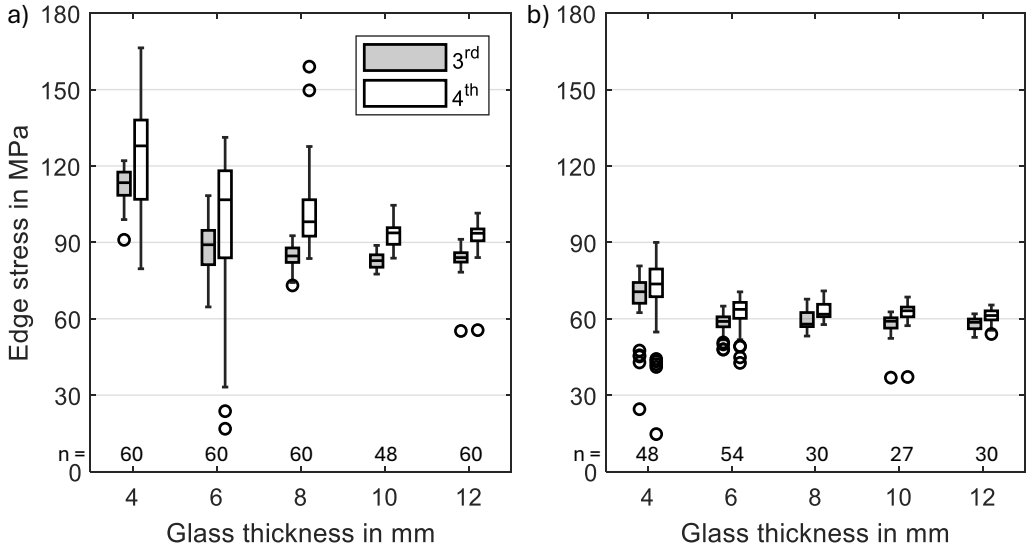

Figure 4.11: Edge stress values extrapolated with 3rd and 4th degree polynomials for a) thermally toughened glass and b) heat-strengthened glass, evaluated using phase-shifting technique

The primary objective was to establish a reliable method for evaluating edge stresses to ensure the integrity of glass properties within the context of automated production control. Using a 4th degree polynomial for this purpose carries the risk of overestimating edge stress values due to extrapolating, which poses a significant safety concern. Such overestimation is particularly problematic in the context of determining the safety characteristics of the glass products and ensuring compliance with the standards. Therefore, to avoid potential risks and comply with more stringent limit criteria, a 3rd degree polynomial was employed in the following evaluations. This approach was safer and more suitable for ensuring the safety and accuracy of controlling the pre-stress quality.

As demonstrated in the previous sections, the interpolation of retardation values measured using the PST method for 4 mm glass were not consistent. Furthermore, Fig. 4.11 shows that the 4 mm samples exhibited not only greater scatter but also significantly higher edge stress values compared to the glass thicknesses 6–12 mm. Due the associated measurement uncertainties of this thin glass thickness, the validity of these results could not be objectively assessed. Consequently, 4 mm thick glass was considered less suitable for measuring edge stress with the PST method and will therefore not be further evaluated in the subsequent chapters.

4.2.5 Constraints for cubic polynomial coefficients

The behavior of a cubic polynomial depends on the values of the coefficients and is described as the mathematical function shown in Equation (4.2).

$$f(x) = P_1 x^3 + P_2 x^2 + P_3 x + P_4 \tag{4.2}$$

Characterizing the behavior of the cubic function is difficult due to the interaction of its parameters. However, it is possible to make specific observations about the characteristics

of the curve. The value of P_1 is crucial in determining the asymptotic behavior of the graph, while the coefficient P_2 affects the degree of curvature: a higher value results in a more pronounced curvature. Parameter P_3 determines the tangent slope of the function at $x = 0$ and affects the curve's displacement along the x and y axes. The recorded retardation measurement points were adjusted so that the outer glass edge falls on $x = 0$. Therefore, parameter P_4 represents the required retardation value at the edge to determine the edge stress according to Equation (3.3).

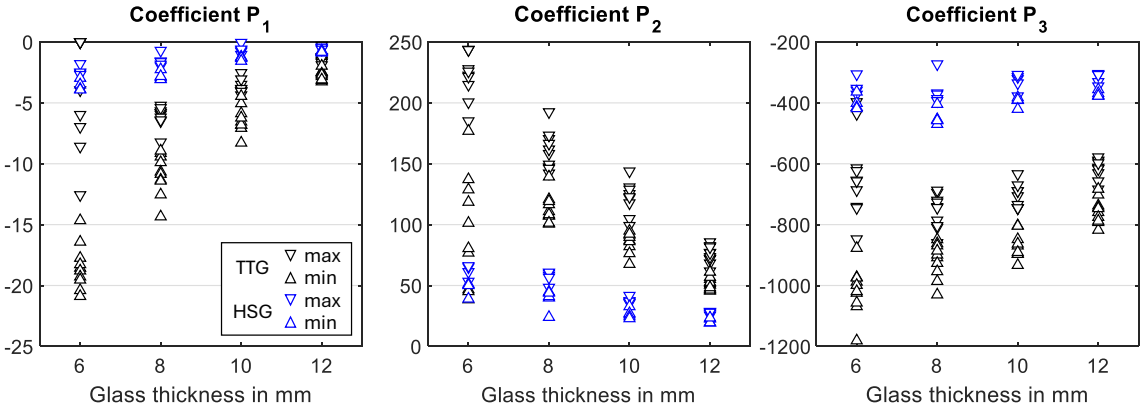

Figure 4.12: Coefficients P_1 to P_3 of the polynomial fitting function of 3rd degree depending on glass thickness evaluated using phase-shifting technique

For the previous investigations, the coefficients P_1 to P_3 of different specimens examined by the PST were compared. For this purpose, the minimum and maximum values of each parameter were determined from the five sections within each of the six measurement areas per specimen. Fig. 4.12 displays these minimum and maximum coefficients P_1 to P_3 on the respective y-axis of the three diagrams, divided by glass thickness and glass type. A significant difference between the coefficients was particularly evident in the glass type. The interpolation curves of HSG were generally flatter and did not increase as much as those of TTG. Additionally, HSG exhibited less scattering. The influence of thickness was less pronounced for HSG than for TTG. The coefficients P_1 and P_3 generally increased, while P_2 decreased as thickness increases.

Table 4.1: Range of constrained coefficients of 3rd-degree polynomial for thermally toughened glass and heat-strengthened glass depending on glass thickness, determined using phase-shifting technique

Glass type	t [mm]	P_1	P_2	P_3
TTG	6	[-22.974, 0.000]	[42.293, 268.202]	[-1299.210, -440.000]
	8	[-15.781, 0.000]	[110.649, 211.772]	[-1133.330, -756.316]
	10	[-9.114, 0.000]	[74.282, 158.246]	[-1026.652, -696.949]
	12	[-3.583, 0.000]	[44.000, 94.251]	[-899.481, -660.000]
HSG	6	[-4.400, 0.000]	[28.294, 73.111]	[-463.947, -300.587]
	8	[-3.380, 0.000]	[26.365, 66.865]	[-516.999, -299.796]
	10	[-1.722, 0.000]	[25.193, 45.854]	[-462.612, -338.061]
	12	[-0.977, 0.000]	[21.367, 31.403]	[-415.206, -334.751]

In the MATLAB (The MathWorks, Inc. 2024b) environment, constraints for the parameters can be defined under options when utilizing the *fit* function. As illustrated in Fig. 4.12,

with a safety factor of 10% applied, the following lower and upper limits were determined for the coefficients that describe the cubic curve of the retardation in the area of the glass edge. These limits are detailed in Table 4.1 for TTG and HSG, and formed the foundation for the subsequent evaluation of the edge stress in Chapters 5, 6 and 7.

4.3 Evaluation with multiple-wavelength photoelasticity

This section develops a measuring method for edge stress based on MWP, using the same 82 TTG and HSG specimens investigated in the preceding Section 4.2. The TTG and HSG specimens with a size of 360 mm x 1100 mm, ground edges, and nominal glass thicknesses of 4, 6, 8, 10, and 12 mm were scanned with the measuring device LineScanner by Softsolution GmbH (2023b).

4.3.1 Experimental setup

The test specimens were scanned over their entire format using the LineScanner by Softsolution GmbH (2023b) which is displayed in Fig. 4.13. The LEDs are telecentric and provide a high spatial resolution of 200 dpi. During each scanning process, three monochromatic isochromatic images are recorded simultaneously in the wavelengths blue (442.35 nm), green (499.30 nm), and red (626.80 nm). A complete isochromatic image of the pane in the blue wavelength is displayed in Fig. 4.13a.

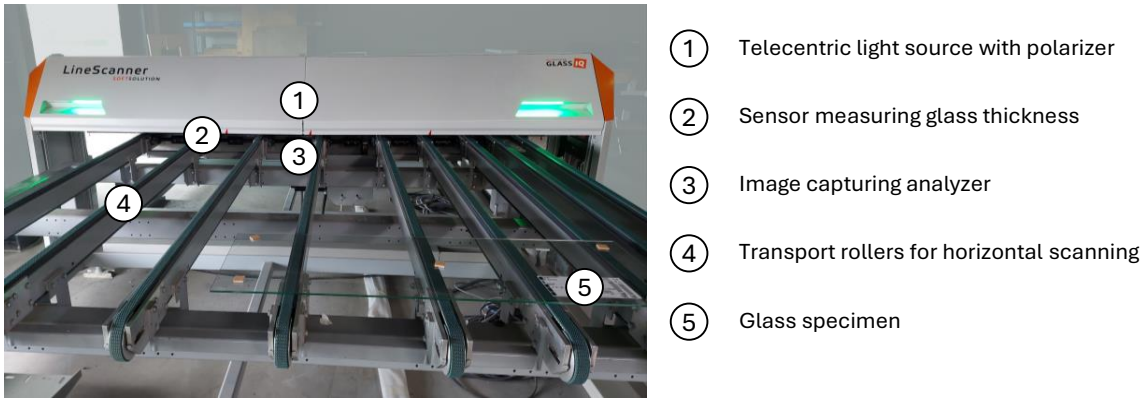

Figure 4.13: Measuring device LineScanner by Softsolution GmbH (2023b) using multiple-wavelength photoelasticity

To determine the retardation in the edge area, a section was extracted at the same position from the recorded isochromatic intensity images across the glass edge. The length of this section was defined as 2t, depending on the glass thickness of the specimen. The extracted section exhibits a wave-like intensity pattern, as illustrated in Fig. 4.13b for all three wavelengths. Based on this intensity distribution, the corresponding fringe order of the isochromatics can be determined. The intensity peaks of the edge isochromatics were subsequently detected automatically using a MATLAB script (The MathWorks, Inc. 2024b). Due to the bright-field configuration of the LineScanner, Fig. 4.13b indicates that fringe counting begins with the first dark isochromatic, which is assigned a fringe order of 0.5. In the next step, the detected fringe orders of the relative retardations were multiplied

by their respective wavelengths blue (442.35 nm), green (499.3 nm), and red (626.8 nm) and combined into a single diagram for all three wavelengths, as shown in Fig. 4.13c. These data points served as the basis for subsequent interpolation. In total, 50 cross-sections through the edge were analysed for each isochromatic image along each longitudinal edge per specimen, corresponding to one measurement point approximately every 22 mm, as depicted in Fig. 4.14a.

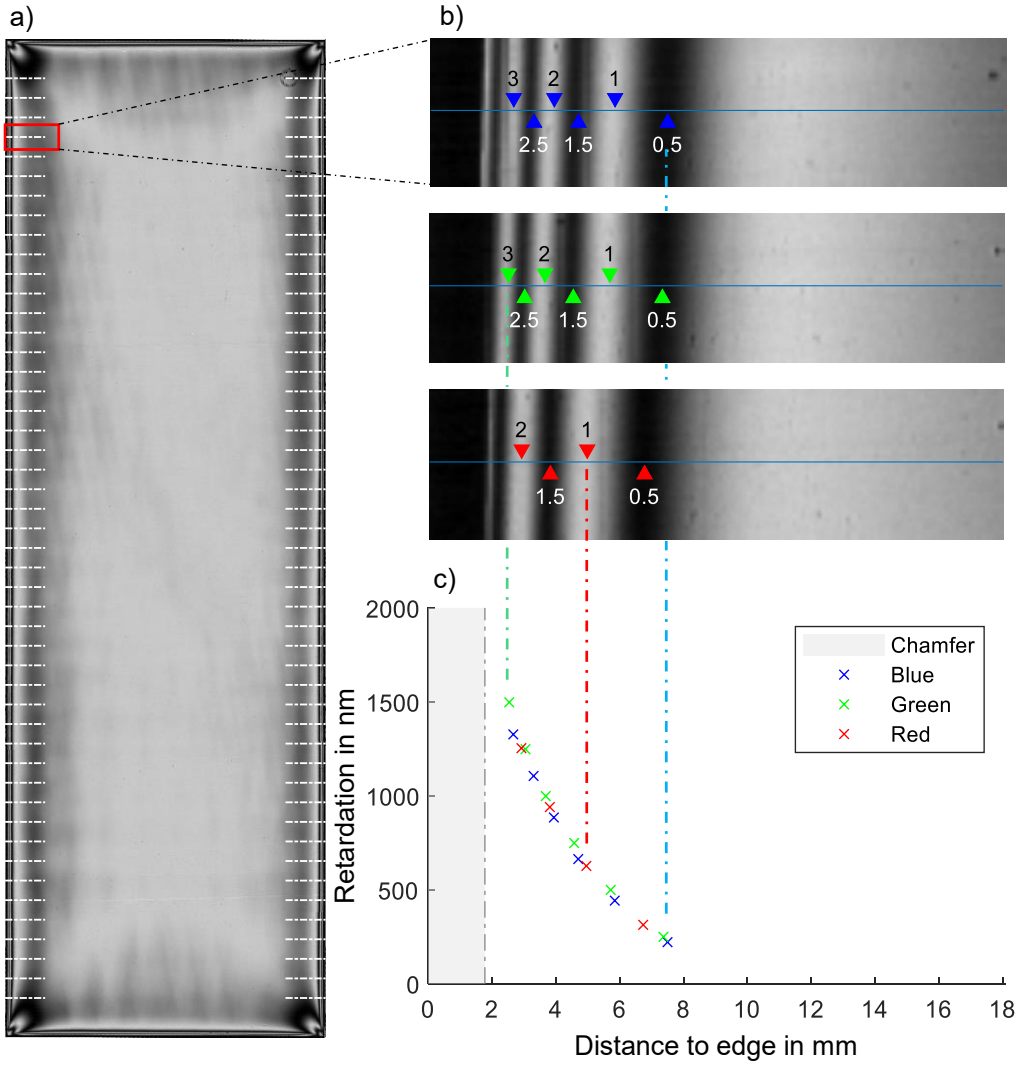

Figure 4.14: Experimental setup of multiple-wavelength photoelasticity: a) 100 sections per glass specimen, b) detection of peaks in three isochromatic images, and c) assignment of fringe order to corresponding wavelength for retardation values, shown for a 12 mm thermally toughened glass, from Efferz et al. (2024a)

4.3.2 Peak detection

Errors in peak detection may occur due to contaminants such as dust particles or impurities on the glass sample surface. These contaminants can affect the isochromatic image and cause a shift in intensity maxima and minima positions on a pixel-by-pixel basis. Additionally, it is essential to note that data preparation, specifically cropping and aligning images,

can cause discontinuities in the image matrix. This can make it challenging to accurately superimpose peaks over the three analyzed wavelengths.

Furthermore, when analyzing intensity maxima near the edges of samples, it was impossible to determine if they represented actual isochromatics or if they would continue if the chamfer were absent. To avoid potential distortions of the extrapolation curve, maxima that are too near to the edge of the sample were not included in the analysis. In addition, the identification of the chamfer can be complicated, especially when using the MWP measuring device where the chamfers are displayed as black areas, the exact position of the intensity minima in the vicinity of the chamfer cannot be determined, and the chamfer is optically magnified.

4.3.3 Combination of single cuts

Fig. 4.15a–c displays the retardation values of the peaks, color-coded according to the three wavelengths for a single edge cut, the interpolation curves, and the extrapolated edge stress including R^2, exemplarily shown for an 8 mm TTG sample exhibiting a surface stress of 104.4 MPa.

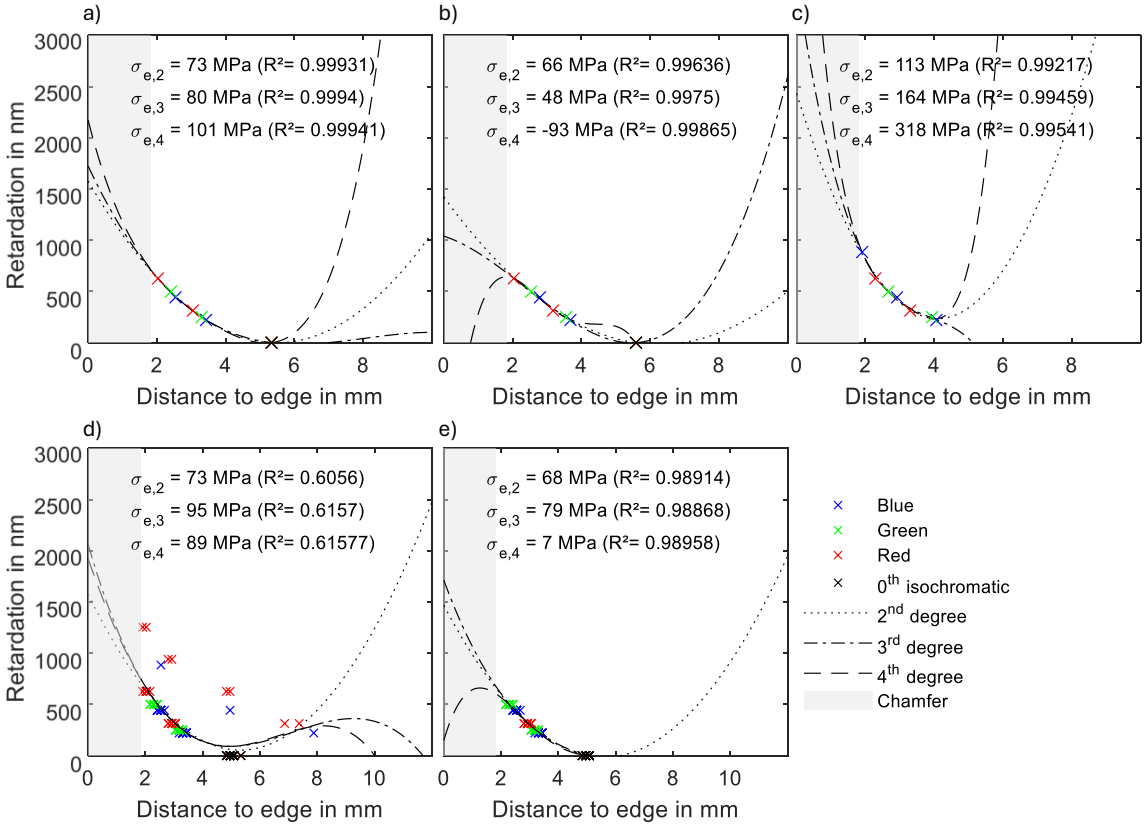

Figure 4.15: Peak identification using multiple-wavelength photoelasticity: a)–c) single cuts, d) combination of single cuts, and e) combined cuts after outlier elimination, exemplified for an 8 mm thermally toughened glas)

The diagrams revealed that the extrapolated edge stress values differed considerably within one sample among the three polynomial degrees, even though all interpolated functions

achieved R^2 values greater than 0.99. In Fig. 4.15a, the overall curve progression appeared reasonable and the resulting edge stress values seemed physically realistic. In contrast, Fig. 4.15b shows only minor differences in the peak positions, yet noticeably lower edge stress results are obtained. The extrapolation of the 4th degree polynomial even led to a strongly negative edge stress value. In Fig. 4.15c, no 0th isochromatic order was found, resulting in overestimated high edge stress values.

Due to the large variations in edge stress values within one sample obtained from individual cuts, a section-by-section extrapolation was not considered feasible and practical for determining edge stress values using the MWP method. This applied particularly to thinner glass samples, which exhibited only a few isochromatics and peak points so that the interpolation was more challenging. To reduce these strong deviations in edge stress values within a single sample, the individual cuts along the specimen's longitudinal edge were grouped into three measurement regions, as shown in Fig. 4.16. Accordingly, the peaks from 16 individual cuts were combined and plotted together in a single diagram.

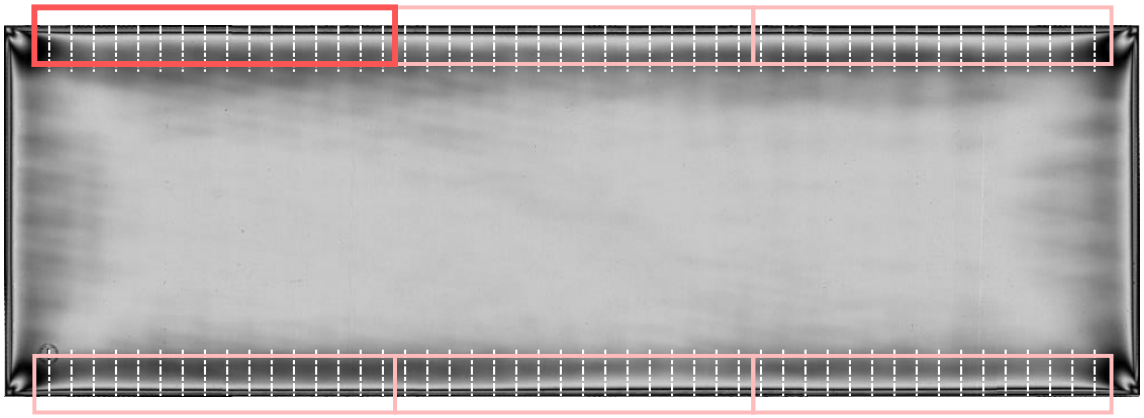

Figure 4.16: Six evaluation areas per 360 mm x 1100 mm specimen obtained by combining 16 single cuts shown in an isochromatic image acquired using multiple-wavelength photoelasticity

However, as illustrated in Fig. 4.15d, several outliers among the peak values could be observed, which adversely affected the interpolation behavior. In the example of the 8 mm TTG in Fig. 4.15d, this was reflected in relatively low coefficients of determination with R^2 values around 0.62. To ensure a more robust and less error-prone extrapolation, these outliers were systematically removed. The procedure followed a clear rule: for each peak all corresponding data values were examined, and those exceeding 1.5 x IQR were identified as outliers and subsequently excluded from further analysis. Furthermore, each peak was required to contain at least five valid data points to avoid inaccuracies in the interpolation process.

After the data cleaning step, the extrapolation was repeated using the refined set of peak values. As exemplarily shown in Fig. 4.15e, this led to significantly improved fits, with R^2 values again reaching approximately 0.99. Nevertheless, even with the cleaned data, it becomes evident that a 4th degree polynomial is not suitable for extrapolation when using MWP method. This is due to the fact that it leads to a more oscillating interpolation behavior and results in unrealistic edge stress values, as illustrated in Fig. 4.15e with a value of 7 MPa. This highlights that while data cleaning improves the reliability of the

fitting process, the choice of polynomial degree remains a critical factor for obtaining physically plausible edge stress values.

Fig. 4.17 illustrates the determination method for edge stress using the MWP method: the summarized and cleaned data points were interpolated with a polynomial of 3rd degree over the chamfer to read the maximum retardation at the edge. This retardation was used to calculate the edge stress according to Equation (3.3). As an additional evaluation criterion for all glass thicknesses, when interpolating the data points, the goodness-of-fit value R^2 was considered. For the MWP method, it should be at least 0.95 to ensure reliable interpolation and extrapolated edge stress values. Measurement areas with R^2 below 0.95 were not included in the further evaluation.

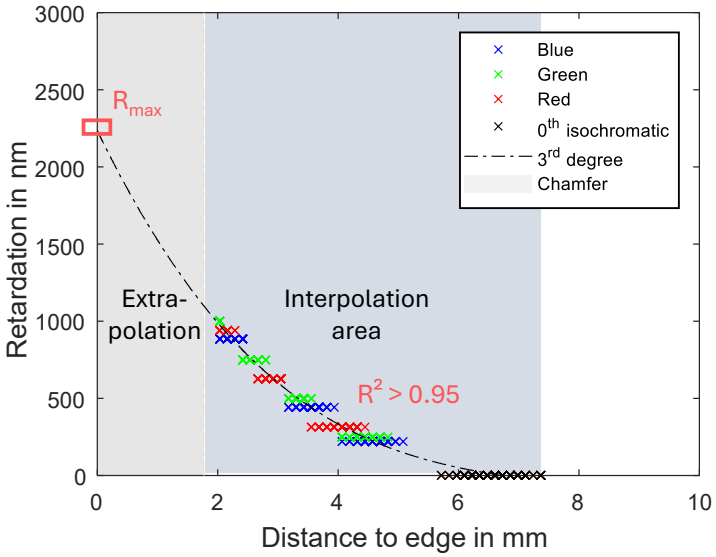

Figure 4.17: Determination method for edge stress using multiple-wavelength photoelasticity method with 3rd degree polynomial interpolation ($R^2 > 0.95$)

4.3.4 Influence of 0th isochromatic order

Due to its bright field setup, the 0th isochromatic order in the images acquired by MWP method was not as clearly visible as the distinctly separated edge isochromatics in the isochromatic image or as for PST. This is because the retardations, which should ideally be 0 nm in the field, are shown as a bright color. However, upon closer inspection of the section from the edge into the field, an irregular gradient was revealed after the 0.5th isochromatic order which corresponded to the maximum brightness of the image (see Fig. 4.18). Beyond this point, the brightness often decreases. The diffuse field of pre-stress zone 1 begins, characterized by minor principal differences and retardations. Therefore, the 0th isochromatic order was determined to be at this maximum intensity value.

Fig. 4.19 illustrates the behavior of the extrapolation curve with and without considering the 0th fringe order on a TTG sample with a thickness of 8 mm. When the peaks of 0th isochromatic orders are included, the curve has a fixed point and a steeper, steady rise (Fig. 4.19b). In contrast, excluding the peaks of the 0th isochromatic order causes the inflection points of the polynomial function to shift, which can negatively affect the extrapolation behavior. This tendency is further confirmed in Fig. 4.19a, where the 0th

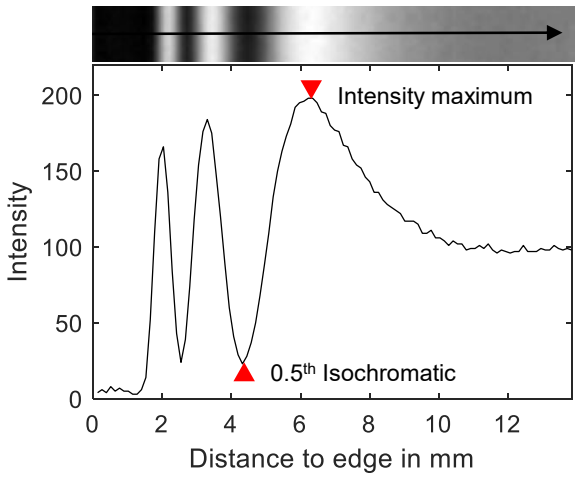

Figure 4.18: Identification of the 0th isochromatic order based on the intensity maximum using multiple-wavelength photoelasticity, exemplified for 10 mm thermally toughened glass, from Efferz et al. (2024a)

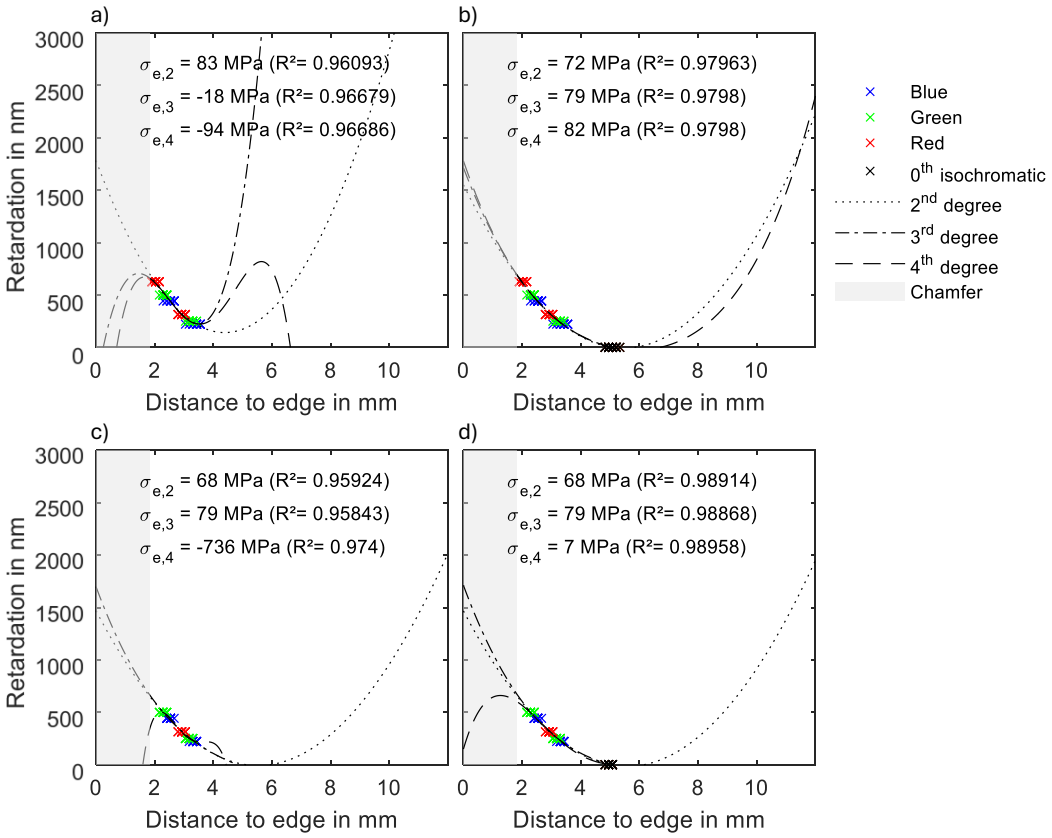

Figure 4.19: Comparison of extrapolation-curve behavior in multiple-wavelength photoelasticity: a) and c) without and b) and d) with inclusion of the 0th isochromatic order, exemplified for 8 mm thermally toughened glass

isochromatic orders were not considered and the interpolation function was constructed with free coefficients. In this case, the resulting edge stress values within this measurement area were not reliable.

However, this effect was not universal. In most cases, comparable edge stress values were obtained both with and without the inclusion of the 0th isochromatic orders by the 3rd degree polynomial, as shown in Fig. 4.19c and d. This indicates that the inclusion of the 0th fringe order generally contributed to more reliable edge stress values but was not strictly necessary, particularly when the interpolation coefficients were constrained (see Section 4.3.7). Therefore, whenever the peaks of the 0th isochromatic order could be clearly identified, they were included in the subsequent evaluations.

4.3.5 Influence of number of peaks

Since the MWP method operates with a few discrete peaks in the interpolation region, which do not form a continuous retardation curve as from the PST method, the number of peaks becomes a decisive factor for reliable interpolation and, consequently, extrapolation for obtaining edge stress values. In addition, for thin glass, both the width of the interpolation region and the chamfer width must be considered. An extrapolation with 3rd degree polynomial requires mathematically at least four data points. The grouping of data points of the single cuts into measurement regions, as explained in Section 4.3.3, allowed for extrapolation even with fewer supporting points. This is due to the fact that all data points contributed to the interpolation calculation, even if they shared the same y-coordinate. This behavior can be seen in Fig. 4.20a which displays the peaks and fitting functions with extrapolated edge stress values for a 4 mm TTG sample with a surface stress of 112 MPa.

Fig. 4.20a shows a measurement area of the sample containing only two supporting points, each consisting of several data points. This formally allowed extrapolation of higher order. However, from a mathematical perspective, this was invalid, as no true interpolation function could be established and the resulting extrapolated values could not be considered reliable. Fig. 4.20b shows the peaks of the same sample at a different measurement area. Here, four supporting points were available, enabling mathematically valid interpolation. Nevertheless, the extrapolated edge stress values were unrealistically high.

Fig. 4.20c presents a 4 mm HSG sample with a surface stress of 49 MPa. In this case, no 0th isochromatic order was detected, but three supporting points were present. However, the extrapolated edge stress values were considered too high for HSG. Fig. 4.21a and b show the corresponding edge isochromatics on fringe images captured in blue wavelength. Comparing the two 4 mm samples of TTG and HSG revealed that the edge isochromatics of 4 mm HSG extended further into the plate, but no distinct transition corresponding to the 0th isochromatic order could be identified. In contrast, in the 4 mm TTG sample, the intensity maximum corresponded to the 0th isochromatic order, while the 0.5^{th} isochromatic order laid very close to the chamfer, indicating that the compression zone of TTG was narrower.

In comparison, Fig. 4.20d shows a 6 mm TTG sample with a surface stress of 107 MPa and Fig. 4.20e presents a 6 mm HSG sample with a surface stress of 52 MPa. The corresponding isochromatic images are shown in Fig. 4.21c and d. Compared to the 4 mm TTG, both the 0th and 0.5^{th} isochromatic orders of the 6 mm samples extended further into the plate.

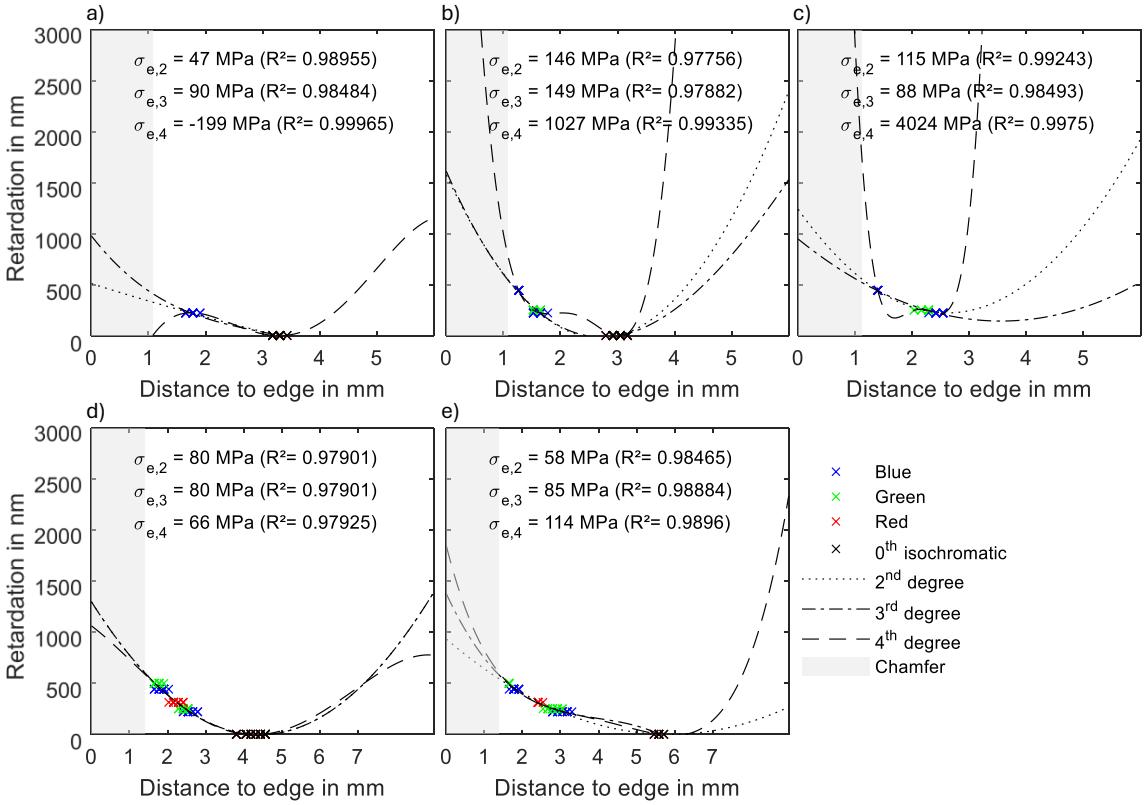

Figure 4.20: Retardation curves and extrapolated edge stress values determined using multiple-wavelength photoelasticity exemplary for a) 4 mm thermally toughened glass, b) 4 mm thermally toughened glass (same sample), c) 4 mm heat-strengthened glass, d) 6 mm thermally toughened glass, and e) 6 mm heat-strengthened glass

The six peaks, the interpolation fit, and the third-order extrapolated value of the 6 mm TTG sample in Fig. 4.20d exhibited acceptable behavior.

In contrast, the 6 mm HSG sample showed a different trend. While the fitting functions with six peaks yield good R^2 values, the value extrapolated with a 3rd degree polynomial was too high for HSG compared to the surface stress value. The fact that the 6 mm HSG sample also exhibited a wider compression zone can be seen from the peak distribution and the comparison of the isochromatic images in Fig. 4.21d.

Fig. 4.22 shows the median number of supporting points divided by glass type and glass thickness. The number of supporting points corresponds to the peaks of the three wavelengths and the 0th isochromatic fringe. With increasing glass thickness, the number of supporting points also increases, since the pre-stress zone of the edge becomes broader and the retardations rise. This phenomenon has been previously observed in isochromatic images in Fig. 4.1. For TTG samples, the number of supporting points increased almost linearly, except for the 8 mm TTG sample, which deviated from this trend. HSG also showed an increase in supporting points. However, HSG samples resulted in a lower number of supporting points compared to TTG.

The analysis of the number of supporting points in comparison with the extrapolated edge

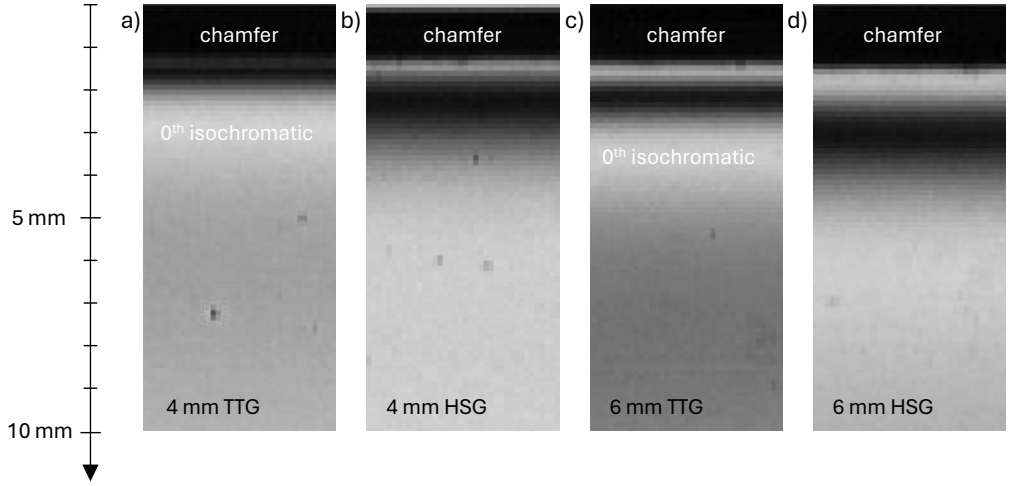

Figure 4.21: Edge isochromatic patterns acquired using multiple-wavelength photoelasticity, corresponding to the extrapolation curves shown in Fig. 4.20 for specimens of a) 4 mm thermally toughened glass, b) 4 mm heat-strengthened glass, c) 6 mm thermally toughened glass, and d) 6 mm heat-strengthened glass

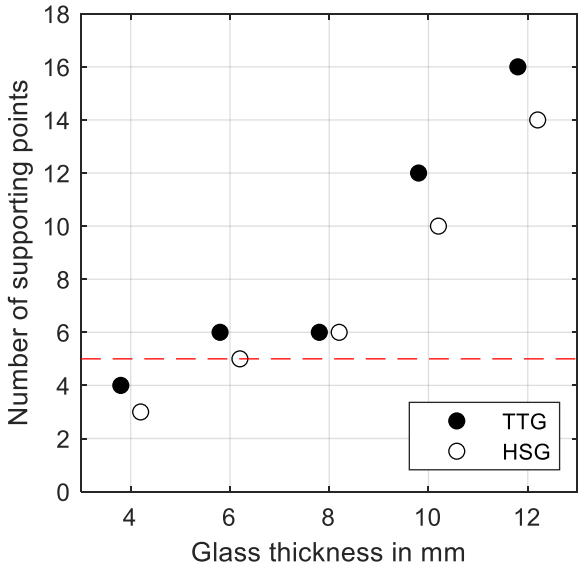

Figure 4.22: Number of supporting points determined using multiple-wavelength photoelasticity method, evaluated as median of each measurement area and organized by glass thickness and glass type thermally toughened and heat-strengthened glass

stress values showed that at least five distinct supporting points were required to obtain a reliable extrapolated edge stress value. Evaluation regions with fewer supporting points were not considered in the further evaluation. This also implies that thin glass samples with a thickness of 4 mm cannot be analyzed using the MWP method. The reasons are that the number of edge isochromatics is too low (see Fig. 4.20) and the compression zone at the edge is very narrow due to the small glass thickness. As a result, the interpolation region is not sufficiently large compared to the extrapolation region. A more detailed investigation of this ratio is presented in the following section.

Therefore, the edge stress values of 4 mm TTG and HSG were not analyzed using the MWP method in the subsequent investigations. The determination of edge stress in 6 mm HSG specimens must also be regarded critically, since, although the HSG samples usually reached the required number of five supporting points, the extrapolated values were often not reliable, particularly when the 0th isochromatic could not be detected. The reason for this is the lower pre-stress level in HSG. This could be observed in the spacing of the edge isochromatics, which were further apart, indicating a less steep increase and thus leading to uncertainties in the extrapolation behavior due to the less pronounced interpolation region.

4.3.6 Ratio of interpolation and extrapolation width

As already carried out for the PST method, the ratio of interpolation to extrapolation width was also analyzed for the MWP method. The extrapolation region corresponded to the width of the chamfer, i.e., the dark area in the isochromatic image, while the theoretical interpolation region extended from the end of the chamfer to the 0th isochromatic order, which appears as the maximum intensity. The difference between the MWP and PST method is that, although the interpolation zone in the MWP can be defined in the same manner, the actual interpolation region is narrower. This is because the MWP method provides only a few discrete supporting points and no continuous retardation profile. It should be noted that the actual interpolation region therefore extends from the 0th isochromatic order to the last peak before the chamfer, as shown in Fig. 4.23a. To investigate the ratio between the chamfer width as extrapolation area and the possible interpolation width, the same factor $f_{ex/int}$, as defined for the PST method in Equation (4.1), was used.

Fig. 4.23b shows the ratio between interpolation and extrapolation width for each measurement area obtained by the MWP method, separated by glass thickness and glass type TTG and HSG. In comparison to PST, the values were less than a factor of 1. However, a decreasing trend of the factor with increasing glass thickness was also observed here, particularly for TTG. The 6 mm TTG start with an average ratio of 0.57 and decreased to 0.19 for 12 mm TTG. The factors for HSG were lower, meaning that the proportion of the chamfer relative to the interpolation region was smaller. The values started at 0.33 for 6 mm HSG and decreased to 0.18 at 12 mm HSG. Similar to the PST method, the values for TTG and HSG converged to a comparable level at a glass thickness of 12 mm.

Although the evaluation of the ratio of interpolation to extrapolation width appears more favorable for interpolation at HSG samples due to the wider compression zone, it should be noted that this ratio does not reflect the number of peaks. Because of the lower compressive pre-stress at the edge in HSG, fewer supporting points for interpolation are present in this

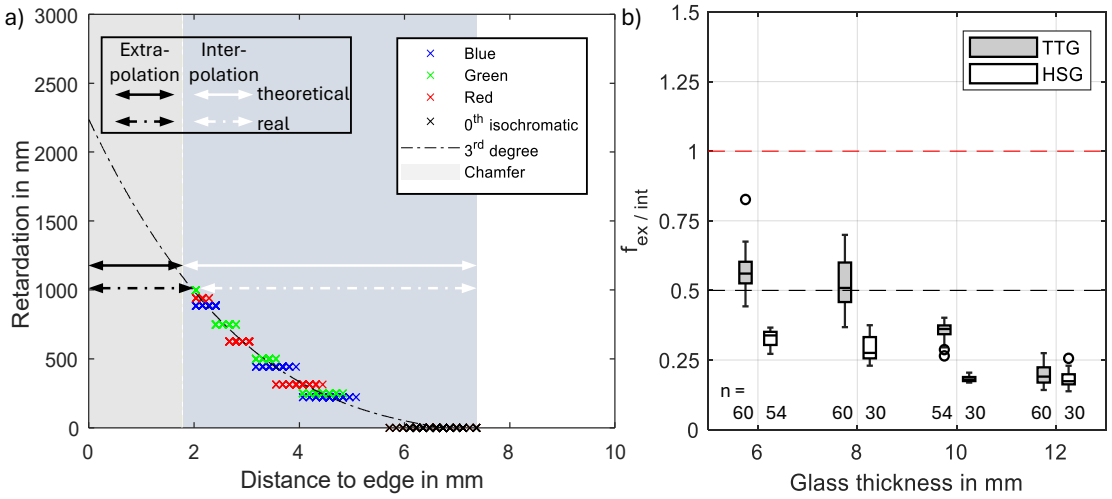

Figure 4.23: a) Schematic visualization of interpolation and extrapolation widths for multiple-wavelength photoelasticity separated as theoretical and real width depending on the highest peak and b) factor between extrapolation and interpolation width for glass thickness and glass type thermally toughened and heat-strengthened glass

region, as previously shown in Fig. 4.22. For thinner HSG samples, this relationship of fewer peaks resulting in a less steep retardation increase is particularly unfavorable for a reliable interpolation.

4.3.7 Extrapolation with constrained coefficients

As described in the sections before, the retardation data obtained as supporting points by MWP were inconsistent and resulted in a greater scatter when extrapolating to the edge than was realistic. To address this issue, constraints could be used for extrapolating the data points of MWP. To do this, the coefficients of the 3rd degree polynomial from Table 4.1, which were obtained by PST, are suitable. Using the MATLAB (The MathWorks, Inc. 2024b) environment, the coefficients P_1 to P_3 were defined as the upper and lower boundary constraints in the *fit* function for the 3rd degree polynomial interpolation for the evaluation of the edge stress of the MWP. The lower limit of P_4 was set as the maximum measured retardation because the retardation is rising towards the edge and prevents the extrapolation curve from flattening out.

Fig. 4.24 illustrates the comparison of the edge stress values per measurement area, which were determined either with free coefficients or with constrained coefficients. It can be observed that the 6 mm samples of both TTG in Fig. 4.24a and HSG in Fig. 4.24b showed outliers in the free fitting. In general, the use of constrained coefficients resulted in reduced dispersion.

For thicker glass samples, the difference between free and constrained interpolation was very small. In most cases, it was observed that both methods obtain the same edge stress values. This finding indicates that the constraints were redundant, suggesting that the free curve was within the established limits. Consequently, it can be concluded that the curve's progression was not inherently constrained but rather establishes a framework that

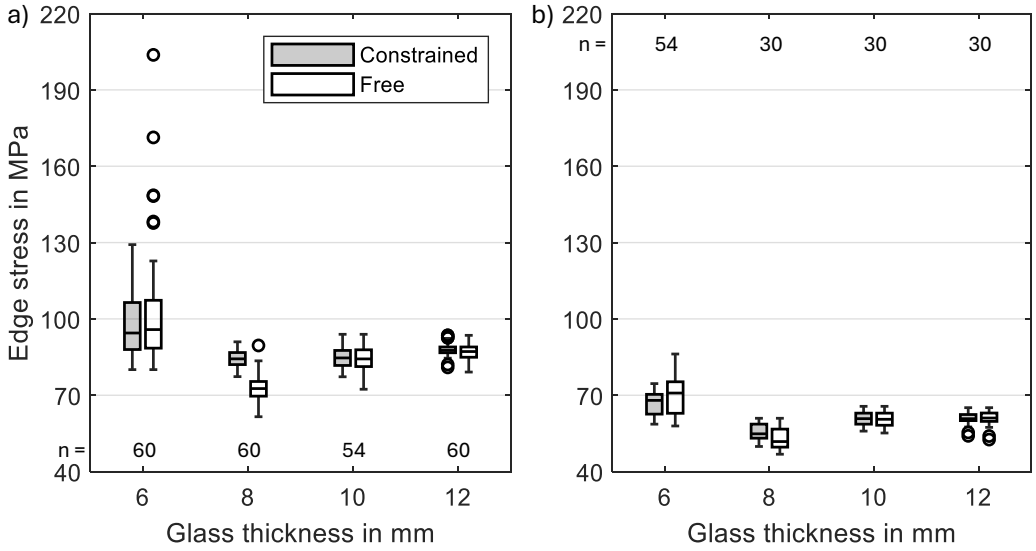

Figure 4.24: Comparison of edge stress values determined by multiple-wavelength photoelasticity method for a) thermally toughened glass and b) heat-strengthened glass extrapolated with free and constrained coefficients per measurement area

guarantees its safety. Therefore, the utilization of the introduced constraints facilitated a more precise extrapolation of the edge stress if measured by MWP.

4.4 Comparison of edge stress values measured with both photoelastic methods

As the samples in this chapter were measured using both photoelastic methods, this section provides a comparative evaluation of the PST and MWP method. To quantify how both measurement approaches differ, a discrepancy factor between MWP and PST was defined for each specimen, as indicated in Equation (4.3).

$$\text{factor}_{\text{MWP}-\text{PST}} = \left| \frac{\sigma_{\text{edge},\, MWP}}{\sigma_{\text{edge},\, PST}} - 1 \right| \tag{4.3}$$

For both the PST and MWP methods, the edge stress values were calculated using the constrained coefficients determined by PST from Table 4.1. Subsequently, the mean value was computed for each specimen based on the six measurement areas. It is important to note that the measurement locations differed between the two methods. The MWP evaluation method summarized single cuts into measurement areas over the entire glass edge, whereas PST measurements were performed at localized points.

The discrepancy factor between MWP and PST is shown in Fig. 4.25. For glass thicknesses between 8 mm and 12 mm, the discrepancy factors remained within ±10%. However, 6 mm specimens exhibited noticeably higher discrepancies, particularly in HSG. As discussed in previous sections, the MWP method showed uncertain extrapolation behavior for thin glass due to the limited number of supporting points, which reduced the reliability of

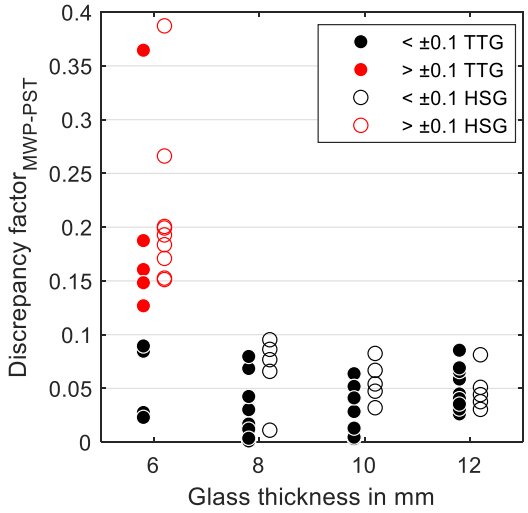

Figure 4.25: Discrepancy factor between multiple-wavelength photoelasticity and phase-shifting technique for each sample

edge stress determination. The PST method was also limited for thin glass because of the small interpolation area, especially when compared to the broader chamfer. Nevertheless, the comparison confirms that the MWP can reliably reproduce the edge stress values determined by PST, when the same constrained coefficients were applied.

4.5 Conclusions

Due to the chamfer of architectural glass, retardation could not be measured close to the edge, as most measuring devices require perpendicular light incidence, which was not present due to the beveled surface of the chamfer. ASTM C1279 (2023) provides an evaluation method in which retardation is measured at two points and then linearly extrapolated to the edge. However, the specimens examined in this research had a chamfer that was too wide. The measurement points specified by ASTM C1279 (2023) were located in the chamfer area where reliable retardation values could not be obtained, since the light from the measuring devices was scattered by the inclined chamfer surface. Consequently, alternative evaluation methods were required to establish an extrapolation approach for determining edge stress. The aim of this chapter was to establish the basis for measuring to develop an automated method for evaluating edge stresses in the production process. The procedure addresses the issue of the chamfer by applying a suitable extrapolation method. The experiments were carried out on 82 standard-size glass panes (360 mm x 1100 mm) of TTG and HSG with thicknesses ranging from 4 to 12 mm. Two photoelastic methods were employed: PST using the StrainScope flex by ilis gmbh (2023) and MWP using the LineScanner by Softsolution GmbH (2023b).

The PST device enables pixel-by-pixel measurement of retardation as a continuous curve up to the chamfer, allowing for reliable interpolation between points. However, the measurement cannot be performed over the entire surface but only at discrete points. For the investigations, three measurement areas per longitudinal edge were analyzed. To determine a suitable interpolation function, differences of polynomials of 2nd, 3rd, and 4th

degree of the interpolation function and the influence on the extrapolation were analyzed. The interpolation area extends from the zero crossing to the beginning of the chamfer. The evaluation of the goodness-of-fit parameters adjusted R^2 and SSE showed that the 2nd degree polynomial was not appropriate for the fitting function. The other two degrees had both a good similar fit for the measurement area, but they differed in the amount of the extrapolated edge stress values on the edge. Polynomial extrapolation is inherently sensitive to scatter, as it attempts to represent behavior beyond the available data range. The scatter range of edge stress values increased with the degree of the polynomial. Despite the nearly continuous retardation curves up to the chamfer obtained by PST, the extrapolated edge stress values still showed a tendency to scatter. Consequently, the 3rd degree polynomial was considered a good compromise between accuracy and reliability and therefore provides a safe basis for the non-destructive quality control of tempered glass. The coefficients of the cubic polynomial fitting function were analyzed, revealing a clear distinction between TTG and HSG. These coefficients of the cubic function were subsequently used for the second measurement method as well.

The second method using MWP enables the acquisition of three isochromatic images at three different wavelengths over the entire surface of the glass pane. The data points for interpolation were derived from the half and integer fringe orders corresponding to the wavelengths of the three isochromatic images. The fringe orders of the peaks were counted and assigned to the respective wavelengths to obtain retardation values. Peak detection was performed on 50 sections per longitudinal edge. To achieve a robust fitting of the measurement points from the fringe orders in the MWP method, several corrective approaches were implemented to compensate for variations in extrapolation due to the limited number of peaks. A section-by-section extrapolation was not considered feasible for determining edge stress values, as the interpolation and extrapolated values were found to be unreliable and exhibited higher scatter due to the increased influence of inaccuracies. Therefore, 17 sections were combined into one measurement area. These data points were cleaned out of outliers. Additionally, the goodness-of-fit R^2 of the interpolation function was set to at least 0.95 to exclude measurement areas that yielded unreliable results due to inconsistent peak detection. The interpolation was further performed using constrained coefficients obtained from the PST method, depending on glass thickness and glass type. Especially for thin glass samples, the use of constrained coefficients prevented unrealistic edge stress values. Investigations of the number of supporting points and the ratio of interpolation to extrapolation width showed that at least five supporting points are required for determining edge stress using MWP. This means that the MWP method cannot determine edge stress values for 4 mm TTG and HSG samples.

The comparison of the edge stress values measured by PST and MWP demonstrated a generally good agreement between both measurement methods. For glass thicknesses ranging from 8 to 12 mm, the relative deviations remained within 10%, confirming the reliability of the MWP method when referenced to constrained coefficients obtained by PST. Higher discrepancies were observed in 6 mm specimens, particularly in HSG, indicating that the MWP method was not accurate for thin glasses. Overall, the results confirm that MWP method provided a valid and consistent approach for non-destructive edge stress evaluation.

5 Experimental investigations on standard-size specimens

This chapter presents the experimental investigations conducted on standard-size specimens, which are well suited for this analysis because their dimensions correspond to those required for the destructive tests in factory production control according to EN 12150-1 (2020) and EN 1863-1 (2012). This allows photoelastic stress measurements to be directly linked to the mechanical properties determined through destructive testing.

In the first part of this chapter, the destructive tests, including four-point bending tests for determining bending tensile strength and fracture-pattern analysis, are presented to classify the specimens according to their conformity with the respective product standards EN 12150-1 (2020) and EN 1863-1 (2012). This is followed by the photoelastic measurements of surface stress using scattered light method and edge stress using PST and MWP. After analyzing the effects of glass thickness, manufacturer, and pre-stress level, the investigation proceeds to assess the homogeneity of the residual stresses. For the edge stress, the width of the pre-stress zone at the glass edge was also examined. In addition, the reproducibility of the MWP measurements was evaluated. Subsequently, the relationship between destructive and non-destructive results will be examined. Correlation analyses were employed to ascertain the suitability of photoelastic measurements for describing mechanical properties. Furthermore, regression models were utilized to assess the influence of the manufacturer and glass thickness on these relationships. Finally, the correlation between the two photoelastic measurements surface stress and edge stress was evaluated. Parts of the experimental program have already been published in Efferz et al. (2024b) and Efferz et al. (2025c), and in the associated NEMA final report (Efferz et al. 2025a).

5.1 Approach and specimens

The specimens investigated in this chapter had dimensions of 360 mm x 1100 mm, which correspond to the standard format defined in EN 12150-1 (2020) and EN 1863-1 (2012) for use in quality control testing. All specimens originated from the research project NEMA (Efferz et al. 2025a). They were manufactured from clear float soda-lime-silicate glass supplied by three different glass manufacturers. For each test series, ten specimens were tempered together by each manufacturer. In the experimental program, the following parameters were systematically varied:

- Glass thickness: 4 mm, 6 mm, 8 mm, 10 mm, and 12 mm
- Edge finishing: ground edge for all thicknesses; in addition, seamed edge for specimens with thicknesses between 4 mm and 8 mm

- Glass type and pre-stress level: TTG and HSG, each at two different pre-stress levels, referred to as “low” and “high”
- Glass manufacturer: three different suppliers, labeled A, B, and C

This work examined a total of 955 specimens. The categorization by glass thickness and pre-stress level is shown in Table 5.1. All glass thicknesses specified in this thesis refer to nominal glass thicknesses rather than actual measured thicknesses. As the specimens originated from the NEMA research project, the experimental work was divided between the research institutions of TUDa and HM.

Table 5.1: Number of specimens (360 mm × 1100 mm), divided by glass thickness and pre-stress level

Glass type	Pre-stress level	4 mm	6 mm	8 mm	10 mm	12 mm
Thermally toughened glass	Low	60	60	60	30	30
	High	60	58	60	30	30
Heat-strengthened glass	Low	60	60	60	30	30
	High	60	60	57	30	30
Total		240	238	237	120	120

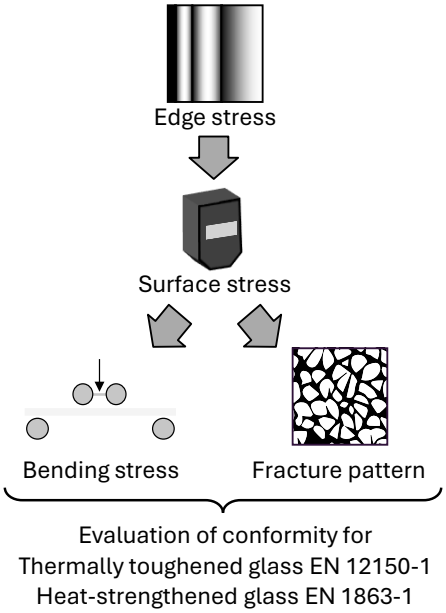

Figure 5.1: Workflow of the experimental investigations conducted on the standard-size glass specimens

The experimental procedure followed the sequence illustrated in Fig. 5.1. First, both research institutions performed photoelastic measurements. For all specimens, the edge stress was determined, and for at least four specimens per test series, the surface stress was additionally measured. Subsequently, destructive tests were carried out to evaluate the conformity for the glass products TTG according to EN 12150-1 (2020) and HSG according to EN 1863-1 (2012). Half of the specimens of one series were subjected to four-point bending tests to determine the bending stress. These experiments were conducted at HM.

The remaining half was examined at TUDa to analyze the fracture patterns. The detailed procedures are described in the following chapters.

5.2 Destructive testing

The chapter on destructive testing is structured as follows. First, the methodology and results of the bending strength tests are presented, followed by the evaluation of the fracture patterns. Subsequently, the destructive test series, which consist of jointly tempered specimens, are compared to evaluate the conformity of the test series and assign them to the glass products in accordance with EN 12150-1 (2020) and EN 1863-1 (2012).

5.2.1 Bending strength

The bending strength tests on the standard-format glass samples were carried out entirely at HM as part of the NEMA project (Efferz et al. 2025a).

5.2.1.1 Test procedure

The bending stress was determined using four-point bending tests with the universal testing machine ZPM-E from ift Messtec, see Fig. 2.3. During the experimental investigation, a minimum of five test specimens were examined for each test series until the glass broke. The test speed was selected based on the glass thickness, as outlined in EN 1288-3 (2000) and Table 2.2. The bending stress was determined following the Equations (2.1) and (2.2) specified in EN 1288-3 (2000), considering the breaking force F_{max} and the measured geometries for the width B, thickness of the glass t, and the dead weight. The correction factor was assumed to be $k = k_s = 1$.

Since the bending strength of glass exhibits considerable scatter, the European product standards (EN 1863-1 2012, EN 12150-1 2020) require a minimum of ten specimens for the evaluation of the characteristic bending tensile strength. According to the statistical approach, which determines the 5% quantile at a 95% confidence level, the number of test specimens is a critical parameter. In the research project NEMA, the fracture stress was generally measured on only five specimens per test series. Therefore, the limited sample size can significantly influence the reliability of the calculated 5% quantile. To increase the number of test specimens, the test series for the different edge finishes, ground and seamed, were combined when the specimens were prestressed together.

Therefore, the bending stress was first evaluated as individual test values, followed by the characteristic bending tensile strength as a 3-parameter Weibull distribution, considering test strength including the residual stress due to thermal pre-stressing. Based on Equation (2.15), the residual stress x_0 was estimated using the mean surface stress for each test series. The characteristic strength was then defined as the 5% quantile of a fitted Weibull distribution, whose parameters were estimated by maximum likelihood using MATLAB's *wblfit* function (The MathWorks, Inc. 2024b). To quantify statistical uncertainty, one-sided 95% confidence bounds of the 5% quantile were obtained by non-parametric bootstrap resampling. The resulting Weibull parameters for each test series are listed in Appendix Table A.1.

5.2.1.2 Results

The bending stress results from the four-point bending tests are shown in Fig. 5.2 and Fig. 5.3 as a function of glass thickness and the two pre-stress levels “low” and “high”, grouped by manufacturer. Fig. 5.2 presents the test series tempered according to heating and cooling parameters for TTG, while Fig. 5.3 shows the two pre-stress levels produced using tempering settings related to HSG. In each diagram, the required characteristic strength limits of 120 MPa according to EN 12150-1 (2020) and 70 MPa according to EN 1863-1 (2012) are indicated. As can be seen in both figures, all individual specimens exceeded the required characteristic values for their respective glass type.

In Fig. 5.2, slight differences between the TTG test series of the individual manufacturers could be observed, although no consistent trend was apparent. For manufacturers A and C, a slightly increasing trend in bending stress with increasing glass thickness could be identified. In contrast, manufacturer B showed a peak in bending stress in the 8 mm test series. The difference between the two pre-stress levels of TTG was small for manufacturers A and C. In some cases, the series that were nominally tempered to a higher level even exhibited lower bending stresses, as seen for the 8 mm and 10 mm specimens from manufacturer A. The largest differences between the pre-stress levels low and high TTG occurred for manufacturer B. This manufacturer also showed the greatest scatter in the results. For example, the 8 mm TTG low series from manufacturer B exhibited a standard deviation of 32 MPa.

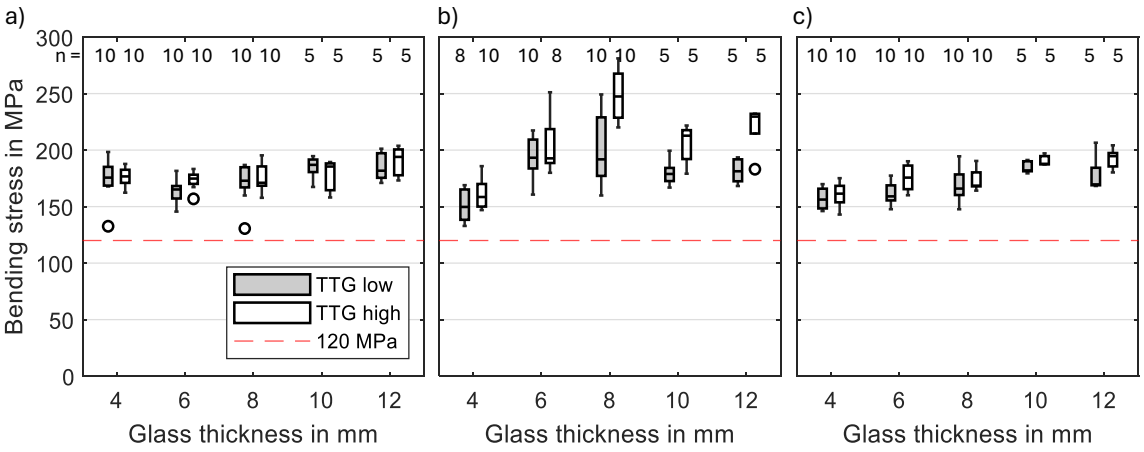

Figure 5.2: Results of bending stress depending on glass thickness and pre-stress level for standard-size thermally toughened glass of manufacturer a) A, b) B, and c) C

Fig. 5.3 similarly demonstrates only negligible disparities between the HSG pre-stress levels, particularly for the thinner glass specimens. In some cases, individual panes tempered to the high level even exhibited lower bending stress values than those tempered to the low HSG level. The largest separations between the high and low pre-stress levels occurred for the 10 mm specimens from manufacturer C and the 12 mm specimens from manufacturer B. No influence of glass thickness could be identified.

Fig. 5.4 shows the characteristic bending tensile strength of the low and high tempered test series as a function of glass thickness, grouped by manufacturer. The pre-stress levels of HSG are presented in Fig. 5.4a. A notable exception was found in the 12 mm low-tempered HSG series from manufacturer A, which showed a characteristic strength

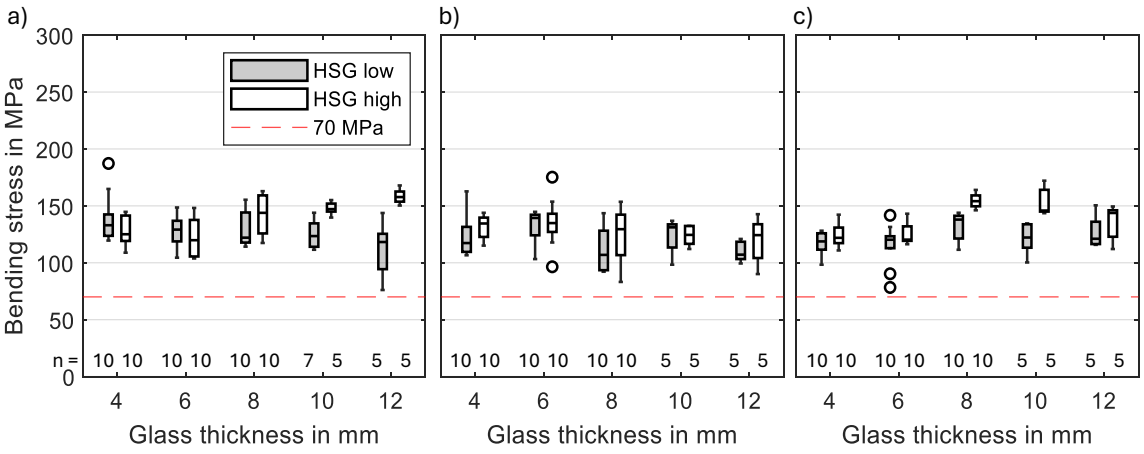

Figure 5.3: Results of bending stress depending on glass thickness and pre-stress level for standard-size heat-strengthened glass of manufacturer a) A, b) B, and c) C

of 61.4 MPa and therefore fell below the required limit of 70 MPa specified in EN 1863-1 (2012). However, this series was based on only five specimens, so the representativeness of this characteristic value must be questioned. Notably, the high tempered HSG test series of 6 mm HSG high tempered from manufacturers A and B and 12 mm HSG high tempered from manufacturer B achieved lower characteristic bending strength values than their corresponding low tempered HSG series. In addition, some high tempered HSG series in the thickness range of 8–12 mm reached characteristic strengths more typical of TTG.

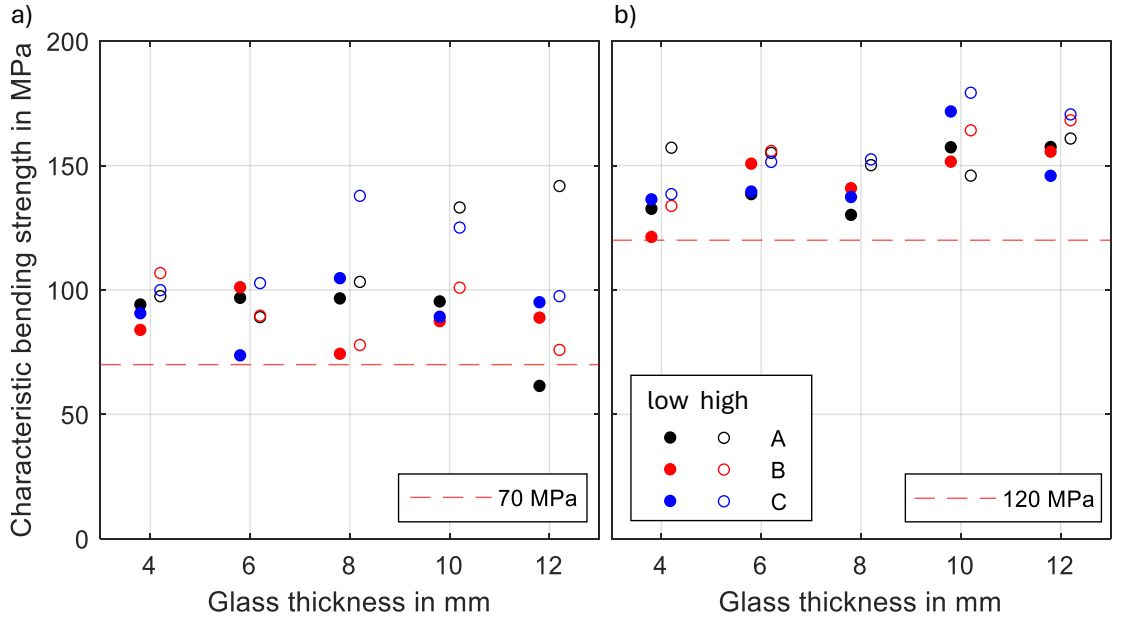

Figure 5.4: Characteristic bending strength (5% quantile, 95% confidence interval) derived from 3-parameter Weibull analysis for standard-size a) heat-strengthened glass and b) thermally toughened glass

The characteristic bending strength values of TTG are shown in Fig. 5.4b. The 4 mm low tempered TTG series from manufacturer B exhibited a tensile strength of 121 MPa, thereby meeting narrowly the stipulated requirement of 120 MPa as outlined in EN 12150-1

(2020). All remaining TTG test series met the specifications by a large margin. However, similar to the HSG results, the 10 mm low tempered TTG from manufacturer A, exhibited a lower characteristic strength than the corresponding low-tempered series.

It can be concluded that the evaluation of characteristic bending strength based on Weibull statistics indicates that one HSG test series fell below the required limit of 70 MPa. However, this result is regarded as non-representative due to the extremely small sample size of five specimens.

For the context of non-destructive quality control, however, these characteristic values are of limited practical relevance. Although the Weibull approach incorporates the scatter of the strength data, the characteristic value is highly sensitive to the number of tested specimens. In contrast, the individual bending strength values, which will later be linked directly to the photoelastic measurements in the regression models, are all above the required limits. Thus, the assessment of quality on the level of individual panes is more meaningful for the intended methodology than evaluating characteristic strength values derived from small or heterogeneous test series.

5.2.2 Fracture pattern

The evaluation of the fracture patterns of the small-format specimens was conducted within the framework of the NEMA project (Efferz et al. 2025a) and was carried out entirely by TUDa.

5.2.2.1 Test procedure

The tests were performed as described in Section 2.1.2.2 according to EN 12150-1 (2020) and EN 1863-1 (2012) on five specimens per series. A spring-loaded center punch was used to induce fracture. Fig. 5.5 shows the CulletScanner from Softsolution GmbH (2023a) which was used to evaluate the fracture pattern. The scanner uses light with a wavelength of 940 nm and captures the fracture pattern in a high resolution. In case of TTG, the algorithm searches automatically for the area with the coarsest fracture pattern and counts the fragments at this point in a 50 mm x 50 mm. In addition, the length and position of the longest fragment are output. For HSG, the conformity of the fracture pattern is not evaluated by the algorithm of the CulletScanner from Softsolution GmbH (2023a). Instead, the recorded fracture pattern images are assessed manually by the operator according to the criteria specified in EN 1863-1 (2012), see Section 2.1.2.2.

5.2.2.2 Results

For TTG, the results of the fracture pattern evaluation, expressed as the automatically determined number of fragments within a counting mask of 50 mm x 50 mm area obtained by the CulletScanner from Softsolution GmbH (2023a), are shown in Fig. 5.6 as a function of glass thickness for both pre-stress levels of TTG. Differences between manufacturers were evident in the fragment counts. Therefore, the data are presented in three separate diagrams, each corresponding to one manufacturer. Although variations with glass thickness were visible, no consistent trend could be identified.

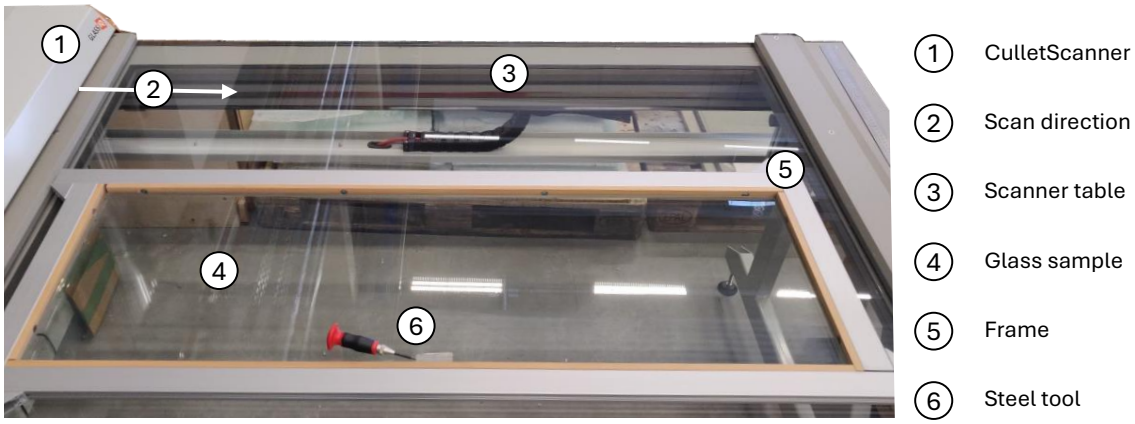

Figure 5.5: Scanner table of the CulletScanner by Softsolution GmbH (2023a) with glass sample, courtesy of Miriam Schuster, adapted from Efferz et al. (2024b)

As expected, all TTG high series exhibited a higher number of fragments, and thus a finer fracture pattern, compared to the TTG low series. While the differences between pre-stress levels were minor for manufacturer A, the series from manufacturers B and C showed distinctly larger variations in the fracture pattern. This indicates that the test series were tempered under substantially different tempering parameters. Moreover, it could be observed that the scatter within a test series decreased with increasing glass thickness, although this effect may also be related to the number of specimens tested. The maximum standard deviation of 25 fragments was found in the TTG low 6 mm series from manufacturer B and in the TTG low 4 mm series from manufacturer A. Within the series of TTG low 4 mm, seven specimens from manufacturer B and one specimen from manufacturer C exhibited less than 40 fragments.

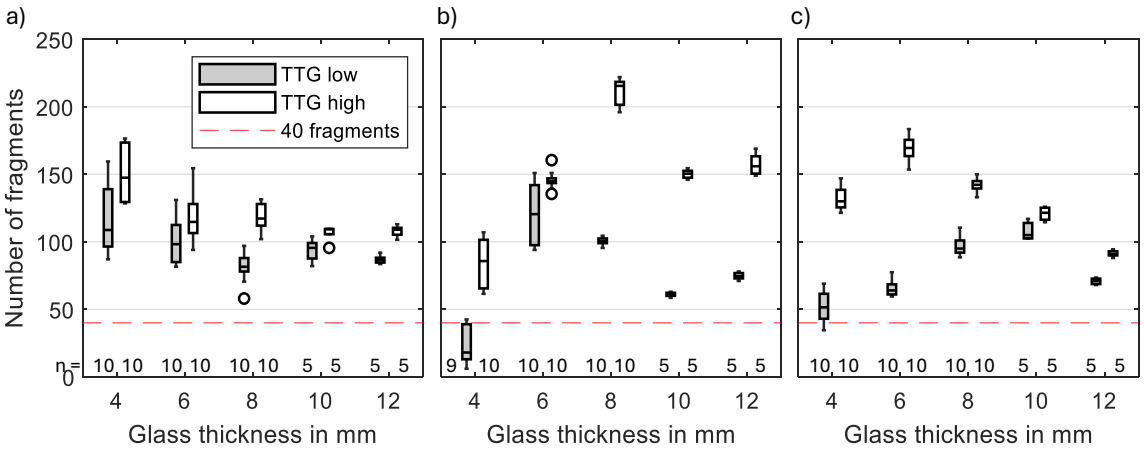

Figure 5.6: Results of number of fragments depending on glass thickness and pre-stress level for standard-size thermally toughened glass of manufacturer a) A, b) B, and c) C

The results of fracture pattern of the series tempered as HSG could not be presented in the same manner as above, since the evaluation was performed qualitatively as conforming or non-conforming according to EN 1863-1 (2012), see Section 2.1.2.2. Nevertheless, to illustrate the number of specimens that met the fracture pattern requirements defined

in EN 1863-1 (2012), Fig. 5.7 presents the proportion of conforming specimens for each manufacturer and glass thickness in a stacked bar chart.

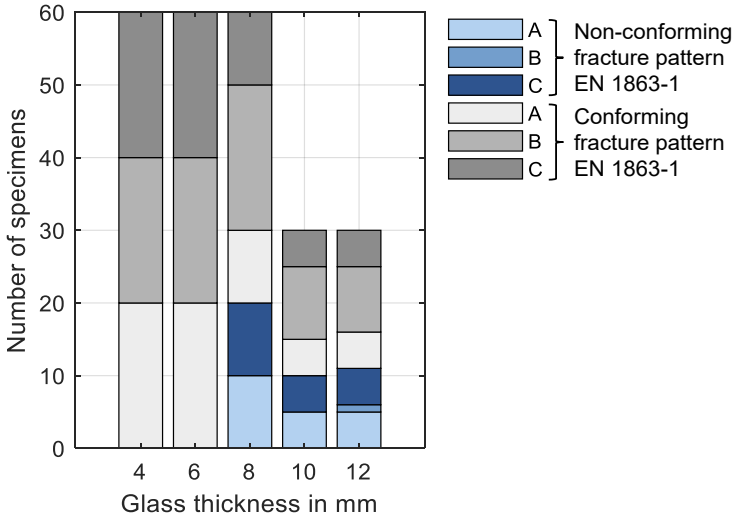

Figure 5.7: Number of standard-size specimens of the pre-stress level HSG low and high with evaluation of fracture pattern conformity according to EN 1863-1 (2012) depending on glass thickness and manufacturer

All specimens with glass thicknesses of 4 mm and 6 mm met the HSG fracture pattern requirements. For glass thicknesses of 8 mm and 10 mm, there were 10 and 5 specimens, respectively, from manufacturers A and C that did not exhibit an HSG-compliant fracture pattern and were therefore tempered to an excessively high level for HSG conformity. At 12 mm thickness, in addition to five non-conforming specimens each from manufacturers A and C, there was one further specimen from manufacturer B that did not meet the HSG criteria. Notably, this specimen was the sole non-conforming element within its test series, whereas the rest demonstrated the requisite fracture pattern.

5.2.3 Evaluation of conformity for glass type

The results of bending strength and fracture pattern could not be directly compared on a per-specimen basis, since only one destructive test could be performed on each specimen. To nevertheless establish a relationship between bending strength and fracture pattern, the results of the two destructive tests were aggregated for each test series. Each series consisted of ten specimens that were tempered together and subsequently divided into two groups of five for the two destructive tests. The test series of ground and seamed edges were combined if tempered together. The arithmetic mean was calculated for the number of fragments, while the characteristic bending strength was calculated as the 5% quantile with a 95% confidence interval (see Section 5.2.1.2). The calculation of mean and quantile values was feasible for the metric variables number of fragments and bending strength, which were measured for TTG specimens. However, this approach was not applicable to HSG, as the evaluation of the fracture pattern was based on a qualitative assessment of conformity rather than a quantitative fragment count.

Fig. 5.8 compares the 5% quantiles of the bending strength with the mean number of fragments for the TTG test series, including the two limit criteria of 40 fragments and

120 MPa bending tensile strength. The plot shows that the pre-stress levels low and high could be clearly distinguished only when considering the number of fragments. In contrast, the characteristic bending strength exhibited substantial overlap between the pre-stress levels. This indicates that the four-point bending tests display considerably higher scatter within the same pre-stress level than the fragmentation counts.

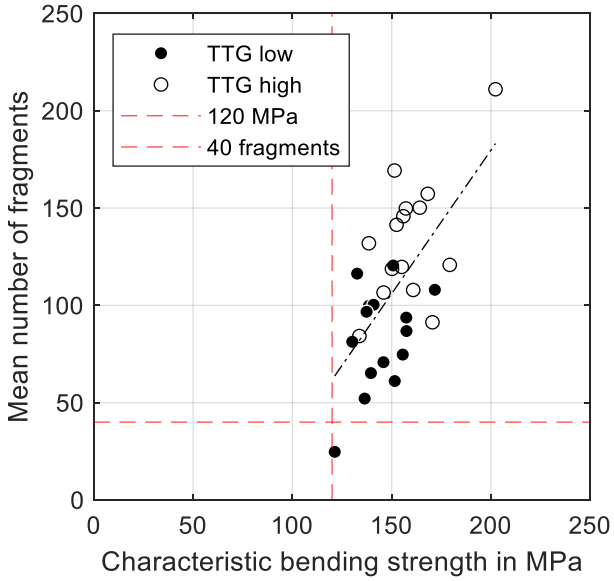

Figure 5.8: Relationship between characteristic bending strength and mean fragment count per standard-size test series, showing the conformity limits of 120 MPa bending strength and 40 fragments per 50 mm x 50 mm

The relationship between the number of fragments and the bending strength is illustrated in Fig. 5.8 by a fitted linear trend line. The line's slope, as indicated by the data, was found to be 1.47. However, the data points exhibited significant scatter around this line, suggesting a weak and highly variable correlation between the two destructive test results.

One TTG test series with a glass thickness of 4 mm failed to meet the minimum fragment count of 40, while the minimum bending tensile strength of 120 MPa was narrowly satisfied. For the evaluation presented in the following chapters, a TTG specimen was considered conforming only if both criteria are fulfilled simultaneously. Consequently, the specimens of this 4 mm TTG low test series were classified as non-conforming TTG. All other TTG test series exceeded both the required strength limit and the required fracture pattern specified in EN 12150-1 (2020).

For the evaluation of the HSG specimens, Fig. 5.9 shows the spreading of characteristic bending strength across the two categories conforming and non-conforming fracture pattern according to EN 1863-1 (2012). For completeness, the diagram also includes the assessment of the fracture pattern according to EN 12150-1 (2020) for TTG test series to provide an overall comparison of the distribution of bending strength values. Accordingly, the two strength limits of 70 MPa and 120 MPa are indicated in the plot. The color-coding of the data points highlights the two pre-stress levels, high and low, for each glass type, allowing a direct visual comparison. As described earlier in Section 5.2.1.2, one HSG test series fell below the required limit of 70 MPa, but regarded as not representative, as it was derived from a limited series of five specimens. Seven test series tempered at the HSG high level

did not exhibit a conforming HSG fracture pattern. Due to the higher pre-stress level, these specimens demonstrated fracture patterns that were too fine to be classified as HSG. These series exhibited bending strength values ranging from 75.9 MPa to 141.8 MPa, with four of the HSG high series demonstrating bending strengths that exceeded 120 MPa, thus surpassing the threshold for TTG.

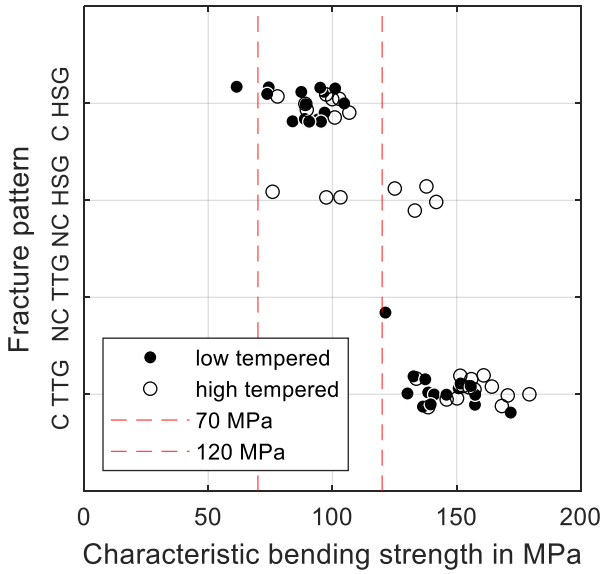

Figure 5.9: Relationship between characteristic bending strength and mean fracture-pattern conformity per standard-size test series for thermally toughened glass and heat-strengthened glass, showing the conformity limits of 70 MPa and 120 MPa bending strength

Table 5.2: Total number of investigated standard-size specimens depending on conformity and glass thickness

Conformity	Glass type		4 mm	6 mm	8 mm	10 mm	12 mm
Conforming	EN 12150-1 (2020)	C TTG	104	118	120	60	60
Non-conforming		NC TTG	16	0	0	0	0
Conforming	EN 1863-1 (2012)	NC HSG	0	0	37	20	21
Non-conforming		C HSG	120	120	80	40	39

These observations demonstrated that the characteristic bending strength cannot serve as a clear discriminating criterion between the different tempering levels. The conforming HSG series with a typical fracture pattern achieved characteristic bending strength values below approximately 106.8 MPa. The conformity for HSG according to EN 1863-1 (2012) and for TTG according to EN 12150-1 (2020) was, in this research, determined primarily by the fracture pattern. This categorization formed the basis for the datasets used in the subsequent photoelastic analysis of edge and surface stress. Table 5.2 provides an overview of the number of specimens in each conformity category and glass thickness. In the subsequent analysis, the categories "C HSG" (conform) and "NC HSG" (non-conforming) were used for HSG in accordance with EN 1863-1 (2012). Likewise, "C TTG" (conform) and "NC TTG" (non-conforming) denoted TTG complying with EN 12150-1 (2020). The number of test specimens examined varied depending on the photoelastic measurement.

5.3 Photoelastic measurement of surface stress

The surface stress measurements were carried out within the NEMA research project (Efferz et al. 2025a) by the two research institutions HM and TUDa.

5.3.1 Test procedure

The SCALP-05 (GlasStress Ltd. 2013), shown in Fig. 5.10b, was used to measure the surface stress of at least four specimens per series. The device operates based on the scattered light method, which determines the stress distribution from the depolarization of light passing through the glass surface. By means of a local regression method with fit closeness of 0.5, the SCALP-05 approximated the measured retardation by splines of 3rd degree polynomials and can thus calculated the parabolic curve across the glass thickness.

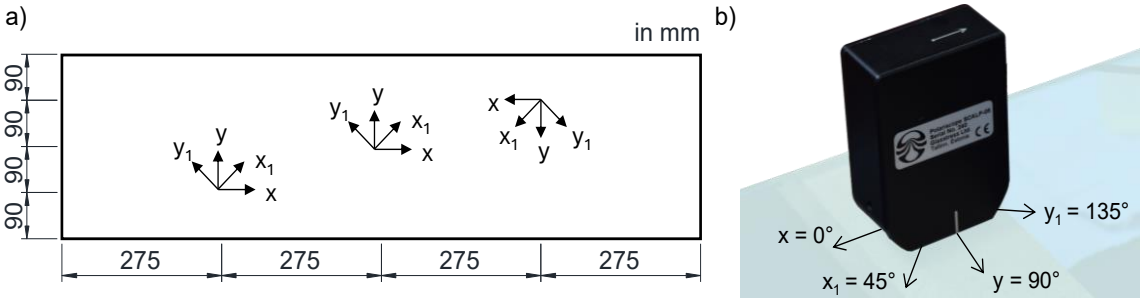

Figure 5.10: a) Locations of the surface stress measurement points on a standard-size specimen with dimensions in mm and b) measuring device for surface stress SCALP-05 (GlasStress Ltd. 2013) showing the measurement directions

Surface stresses can vary significantly within a tempered glass. High differences in the surface stresses can indicate strong optical anisotropy effects, visible in anisotropy scans. Three measurement points were selected on a diagonal of the upper side of the test specimen, see Fig. 5.10a, to be able to detect any strongly scattered surface stresses on a test specimen. Care was taken to ensure that a sufficiently large distance to the edge was maintained to prevent the edge stress from influencing the measurement results. Furthermore, a sufficiently large distance to the edge simplified the measurement, because the reflection of the laser at the edge of the specimen did not reach the measurement field.

To calculate the principal stresses in the plate plane, it was necessary to employ different measurement directions for each measurement point. The x- and y-directions run parallel to the edges of the specimen, with direction x_1 positioned at a 45° angle in between and direction y_1 in a 135° angle, as can be seen in Fig. 5.10. Whether three or four directions were measured per measurement point depended on the research institute. Since Thiele et al. (2022b) showed only slight deviations between the two methods, no distinction is made below between the measurement methods.

Using the stresses measured at these directions, the principal surface stresses σ_1 and σ_2 were calculated according to Equations (3.5) to (3.6), provided in the SCALP-05 manual (GlasStress Ltd. 2013) or based on the principles of Mohr's stress circle using Equations (3.8) to (3.12), see Section 3.2. For the subsequent evaluations, σ_1 was defined as the larger stress in absolute value.

5.3.2 Analysis of surface stress measurements

The subsequent section will present the results of the surface stress measurements. The initial section examines the mean value of σ_1 per specimen, which were subsequently employed as an evaluation criterion for production control. The ensuing section focuses on the three individual measurement points and evaluates the homogeneity of the pre-stress within the glass pane. The principal stress difference also functioned as a criterion for evaluating the pre-stress quality.

5.3.2.1 Results of surface stress measurements

As in the destructive tests, the results from the surface stress measurements are shown in Fig. 5.11 for the pre-stress levels of HSG and in Fig. 5.12 for the pre-stress levels of TTG, depending on the glass thickness and divided by manufacturer. The evaluation in this section includes the arithmetic mean of σ_1 of the three measurement points per specimen.

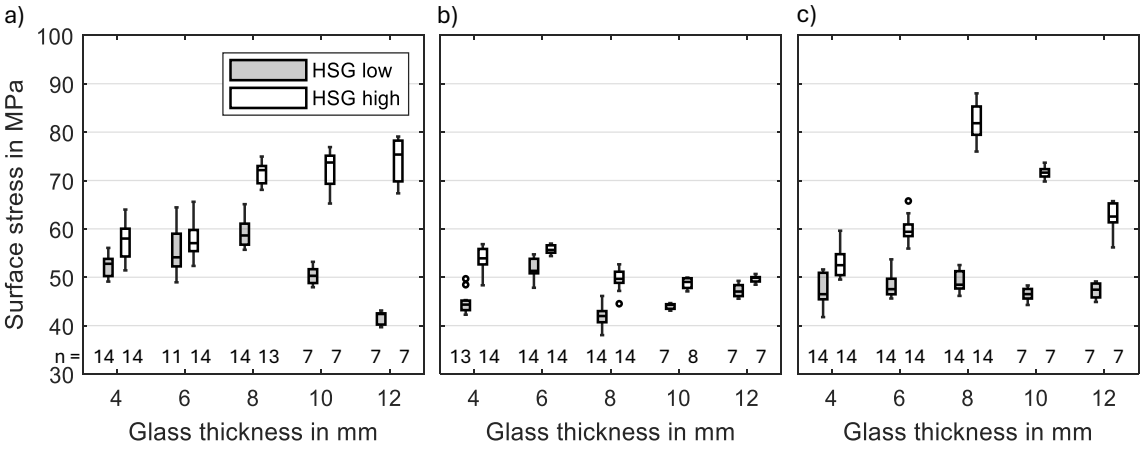

Figure 5.11: Results of surface stress of standard-size specimens, depending on glass thickness and pre-stress level for heat-strengthened glass of manufacturer a) A, b) B, and c) C

TTG specimens generally exhibited greater variations within a test series than HSG. The standard deviation of 10.4 MPa for 4 mm TTG high from manufacturer A demonstrated the greatest variation within a test series. The maximum standard deviation measured for the HSG was 4.6 MPa for 12 mm HSG high test series from manufacturer A. As demonstrated in both figures of Fig. 5.11 and Fig. 5.12, the high-tempered test series exhibited higher median values in comparison to the low-tempered ones across all test series. However, in many test series, the ranges of high- and low-tempered samples overlapped. As observed in the 4 mm and 6 mm HSG samples and in the samples of all glass thicknesses of TTG from manufacturer A, the technically highly tempered samples exhibited lower surface stress values. As already observed in the destructive tests, the 8 mm TTG high series produced by manufacturer B stood out again in the non-destructive measurements, exhibiting exceptionally high surface stress values of up to 171 MPa.

In the next step, each test series was classified according to its conformity with the relevant European standards of the glass products. Fig. 5.13 illustrates these conformity categories

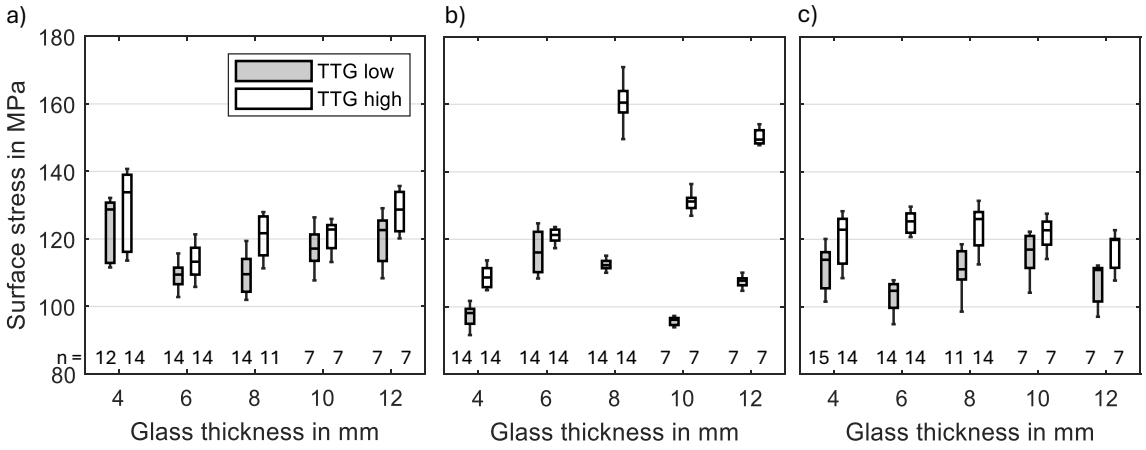

Figure 5.12: Results of surface stress of standard-size specimens depending on glass thickness and pre-stress level for thermally toughened glass of manufacturer a) A, b) B, and c) C

for the measured surface stress, with a color-coded differentiation by glass thickness to improve readability and highlight thickness-specific trends. The corresponding number of points n per box plot, depending on conformity and glass thickness th, is listed in Table 5.3.

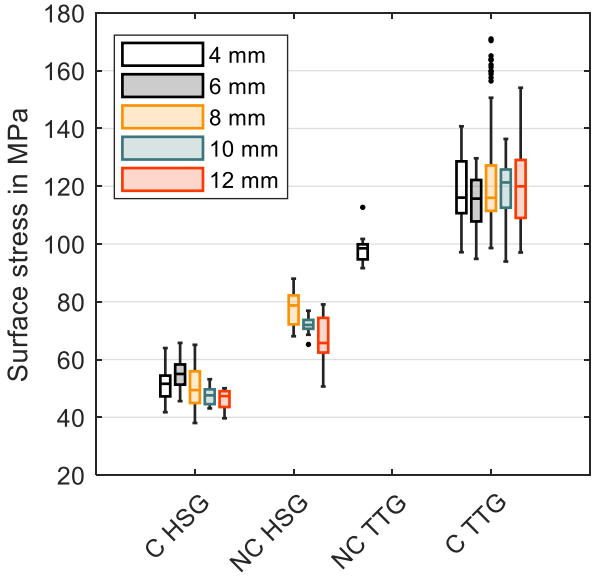

Figure 5.13: Evaluation of surface stress measurements on standard-size specimens classified into conforming and non-conforming heat-strengthened glass according to EN 1863-1 (2012) and conforming and non-conforming thermally toughened glass according to EN 12150-1 (2020)

A clear distinction between the categories of conforming HSG and conforming TTG specimens could be observed, independent of glass thickness. This indicates that surface stress measurements were generally suitable for a coarse differentiation of the conforming glass types. When considering the glass types separately, the following trends emerged: For HSG, a precise and unambiguous distinction could be identified between C HSG and NC

Table 5.3: Number of specimens per box plot depending on conforming and non-conforming heat-strengthened glass and thermally toughened glass, corresponding to surface stress measurements in Fig. 5.13

	C HSG					NC HSG			NC TTG	C TTG				
t [mm]	4	6	8	10	12	8	10	12	4	4	6	8	10	12
n	83	84	53	28	27	25	14	15	12	71	81	83	43	42

HSG when analyzing each glass thickness individually. Within a given thickness, the surface-stress distributions showed sufficiently separated ranges to reliably discriminate between conforming and non-conforming samples. However, across different glass thicknesses, such a clear distinction was no longer evident, as the measured surface stresses overlapped within a common range of 50 to 65 MPa. This overlap across thicknesses reduced the ability of the method to discriminate when specimens of different dimensions were analyzed together. For TTG, the assessment of conformity was only possible for the 4 mm test series, as thicker non-conforming specimens were not available in the database. In this case, however, there was an overlap between conforming and non-conforming samples in the range of 97 to 102 MPa, aside from a single outlier at 112 MPa. Overall, no systematic trend with respect to glass thickness could be identified when evaluating conformity based on surface stress measurements.

5.3.2.2 Homogeneity of pre-stress at the surface

To ensure the homogeneity of the tempering process within pre-stress zone 1 of the glass plate, two aspects were evaluated during the surface stress measurements. Initially, the standard deviations of σ_1 among the three measurement points across the specimen were examined. Secondly, the principal stress difference $(\sigma_1 - \sigma_2)$ at each individual point was evaluated.

Fig. 5.14a presents the standard deviation of σ_1 of the three measurement points for each specimen in the form of box plots. The majority of specimens exhibited only minor variation across the plate, with deviations of less than 5 MPa. A few outliers show higher variation, yet all remained below 9 MPa. The conformity for a glass product did not appear to influence the degree of within-specimen scatter. This suggests that, for most samples including those that did not conform to the specified standards, the stress distribution across the measured area was relatively uniform, indicating a sufficiently homogeneous tempering process.

In a uniformly tempered glass pane, the stresses in the two orthogonal principal stress directions, σ_1 and σ_2, should be approximately equal. Increasing deviation between these principal stresses indicates a higher degree of inhomogeneity in the tempering process. Such inhomogeneities in surface stress within the pre-stress zone of the glass plate could lead to reduced mechanical strength or irregular fracture patterns as well as a higher risk for observing anisotropy effects. For this reason, monitoring the principal stress difference between σ_1 and σ_2 could be a meaningful metric in quality control. Fig. 5.14b shows the principal stress difference $(\sigma_1 - \sigma_2)$ at each measurement point of the specimens, presented as box plots. A slightly decreasing trend with increasing glass thickness could be observed. Once more, no discernible influence of conformity status, particularly for the NC HSG

specimens, could be identified. The maximum principal stress difference reached 17.83 MPa, while the majority of values remained below 10 MPa. This suggests that, despite some variation, most specimens exhibited sufficiently homogeneous stress states with respect to the principal stress difference.

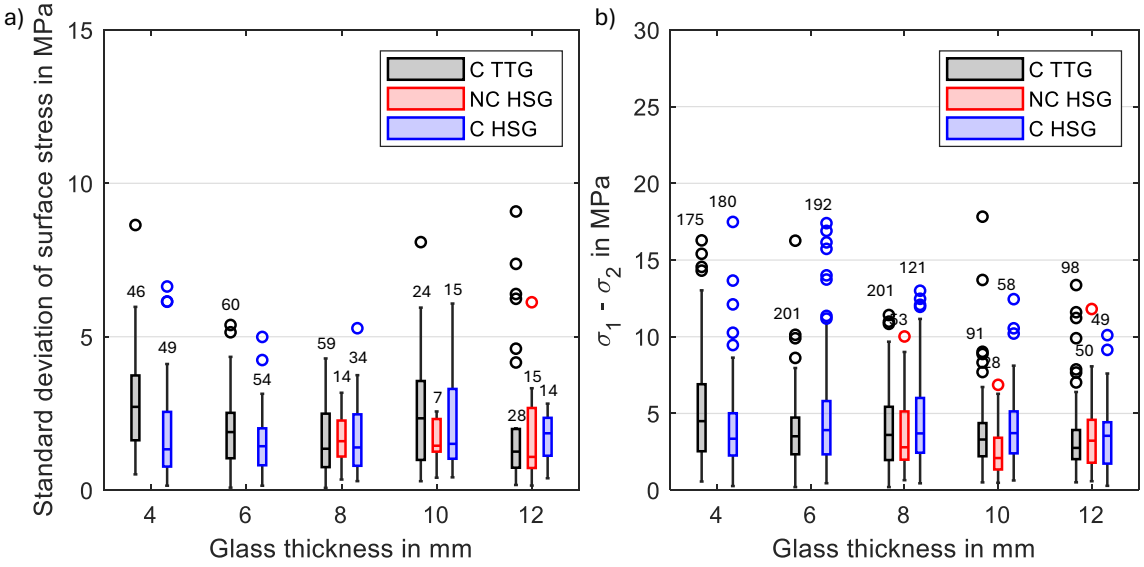

Figure 5.14: a) Standard deviation of σ_1 of the three individual surface stress measurement, b) principal stress difference σ_1–σ_2 of measuring points for surface stress measurement on standard-size specimens with indication of the number of points per box plot

5.4 Photoelastic measurement of edge stress

The photoelastic edge stress measurements were carried out using both PST and MWP. While all PST measurements were performed exclusively at HM, the rest procedure of MWP measurements were conducted within the NEMA research project (Efferz et al. 2025a) by the two collaborating institutions, HM and TUDa.

5.4.1 Test procedure with phase-shifting technique

For determining the edge stress using the PST, a subset of the specimens was examined at HM, using the StrainScope flex measuring device by ilis gmbh (2023). The detailed procedure has already been described in Section 4.2. Since the device is suitable only for local measurements, the retardation was recorded at six measurement areas per specimen, as shown in Fig. 5.15a. Within each measurement area, five closely spaced sections through the glass edge were analyzed (see Fig. 5.15b), and the retardation was measured from 0 nm up to half the wavelength of the device's light source. After aligning the half-wavelength increments, a 3rd degree polynomial fitting function was generated from the nearly continuous retardation curve in the interpolation region starting at the zero-fringe point to the chamfer. This function was extrapolated across the chamfer and the maximum retardation value R_{max} was used to calculate the edge stress according to Equation (3.3)

, as illustrated in Fig. 5.15c. For each measurement area, the five values obtained from the individual sections were averaged, resulting in six measurement values per specimen available for evaluation. As described in Section 4.2.3, specimens with glass thickness of 4 mm were excluded from evaluation with PST. The subsequent analysis therefore included only specimens with a glass thickness from 6 to 12 mm, all supplied exclusively by manufacturer A.

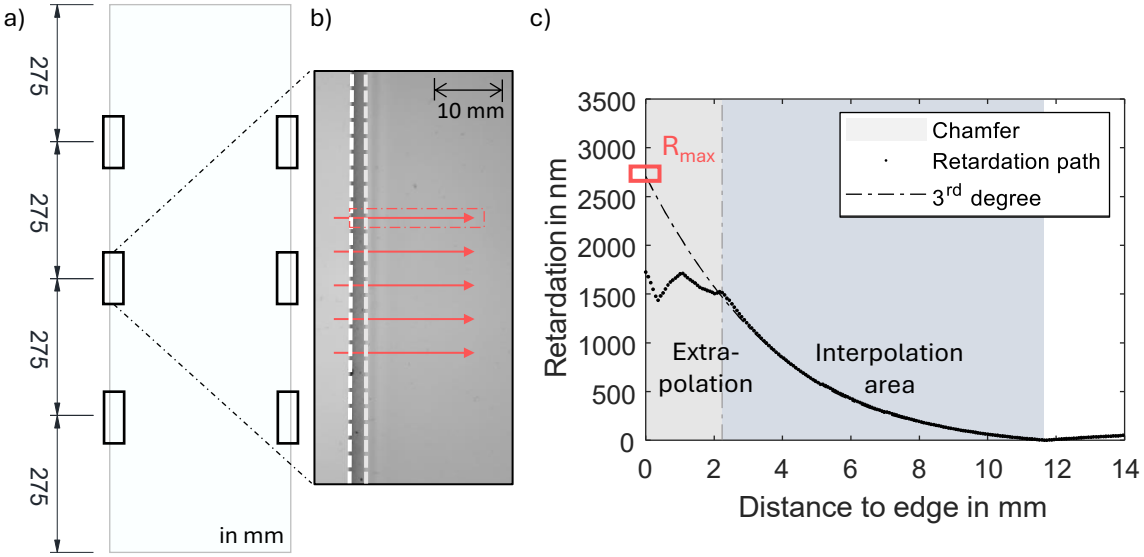

Figure 5.15: Test procedure with phase-shifting technique a) six measurement areas for edge stress measurement on standard-size specimen, b) five sections per measurement area shown on the intensity image, and c) measured retardation path with fitted extrapolation polynomial 3rd degree and maximum retardation

5.4.2 Test procedure with multiple-wavelength photoelasticity

In addition, all glass samples were investigated, using the measuring instrument LineScanner by Softsolution GmbH (2023b) which is based on the MWP method. The measuring device located at HM acquired three isochromatic images simultaneously in wavelengths of blue, green, and red. After a software change in the measuring device of the CulletScanner (Softsolution GmbH 2023a) at TUDa, the isochromatic images could be recorded with the same measuring system as that of HM, with the difference that this measuring device was equipped with only two wavelengths of blue and green. The evaluation method for determining edge stress is described more detailed in Section 4.3. The peaks of the intensity of the two or three isochromatic images were analyzed on 50 sections on both longitudinal edges of the specimen with sufficient distance from the corner. The data obtained was not evaluated per section because of significant deviations, but 17 sections were then grouped into three measurement areas per longitudinal edge. Accordingly, each specimen contained six edge stress values, as illustrated in Fig. 5.16. After extrapolating the fitting curve over the chamfer towards the edge of the glass with a polynomial of 3rd degree and constrained coefficients from Table 4.1, the maximum retardation value was read and used in Equation (3.3) for the calculation of the edge stress. As described in Section 4.3.5, measurements on 4 mm specimens did not yield reliable results. Therefore, the evaluation of edge stress

using the MWP method was limited to glass thicknesses from 6 to 12 mm for TTG and 8 to 12 mm for HSG.

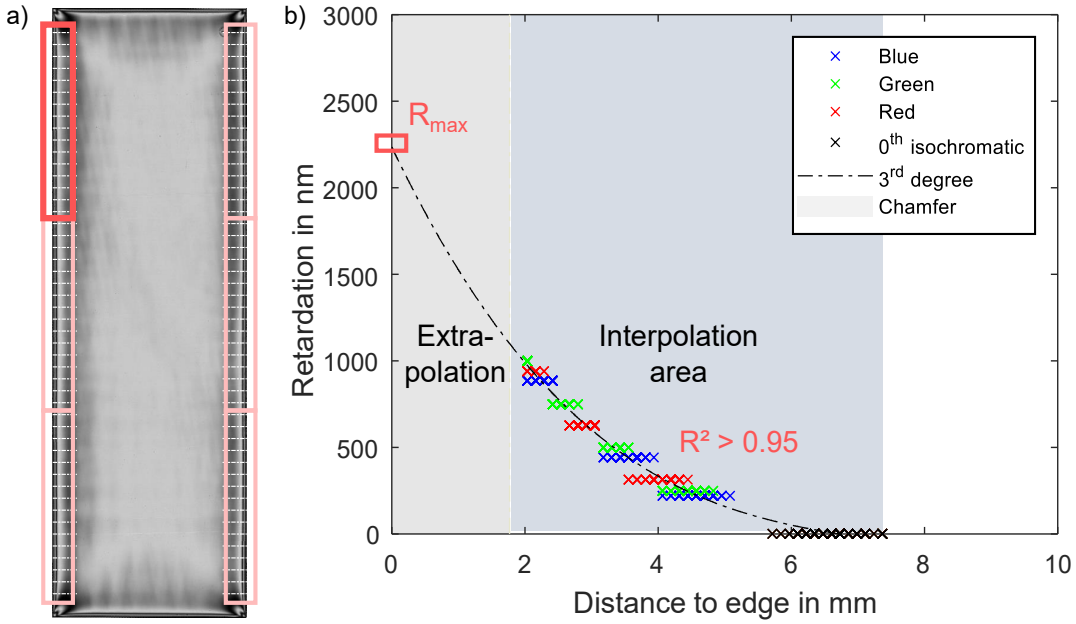

Figure 5.16: Test procedure for multiple wavelength photoelasticity a) of six evaluation areas for edge stress measurement on standard-size specimen shown on isochromatic image and b) composed data points of one measurement area of three isochromatic image with fitted extrapolation polynomial 3rd degree and maximum retardation, adapted from Efferz et al. (2024b)

5.4.3 Analysis of edge stress measurements

The following sections present the results of the edge stress measurements obtained using PST and MWP. First, the parameters related to manufacturer, glass thickness, pre-stress level and measurement method were compared. This is followed by an evaluation of the width of the compressive zone at the glass edge. As in the analysis of the surface stress, the homogeneity of the tempering process was then assessed by examining the variation between the individual measurement points along the edge. Finally, the reproducibility of the MWP measurements was evaluated based on samples that were scanned twice in different alignments with the LineScanner (Softsolution GmbH 2023b).

5.4.3.1 Results of edge stress measurements

The edge stress results presented in this section are based on the mean value of the six measurement areas calculated for each specimen. The values obtained using PST were provided by manufacturer A and are shown in Fig. 5.17a for HSG and in Fig. 5.17b for TTG. The diagrams are organized by glass thickness and pre-stress levels low and high. For HSG, no direct influence of glass thickness could be identified in Fig. 5.17a. For TTG, the data indicated a slight decreasing trend in edge stress with increasing glass thickness. The largest scatter within a test series occurred for the 6 mm TTG specimens: the low tempered

series showed a standard deviation of 6.4 MPa, while the high tempered series exhibited 4.5 MPa. The TTG edge stress values ranged between 75 and 98 MPa and were clearly separated from the values of HSG series, which fell between 50 MPa and 65 MPa. When comparing low and high pre-stress levels, the higher-tempered series generally exhibited higher edge stress values, although this trend was not consistent. In some cases, such as the 6 mm TTG and HSG specimens, there was substantial overlap between the tempering levels, meaning that particular specimens nominally tempered at the higher level showed relatively low edge stress values.

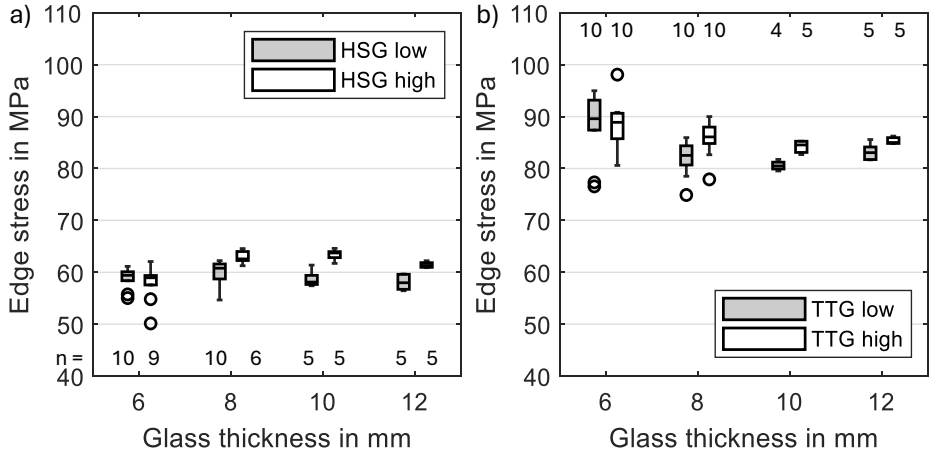

Figure 5.17: Results of edge stress determined by phase-shifting technique depending on glass thickness and pre-stress level for standard-size a) heat-strengthened glass and b) thermally toughened glass

The edge stress results determined by MWP are presented in the diagrams in Fig. 5.18 for TTG and in Fig. 5.19 for HSG, differentiated by manufacturer and further organized by glass thickness and tempering level. In Fig. 5.19, it becomes apparent that the 12 mm HSG specimens from manufacturer A showed lower edge stress values in the series nominally tempered at the higher level. This behavior was not observed in the PST measurements nor in the surface stress or bending stress results. A similar tendency was found for the 12 mm TTG specimens from manufacturer C, where the series declared as high also exhibits slightly lower edge stress values. Apart from these cases, larger overlaps between the tempering levels were present, but the median value of the higher tempered series generally remained higher. Overall, the differences between the tempering levels were small.

The largest scatter was found in the 6 mm TTG series. Here, the 6 mm TTG high series from manufacturer A showed the highest standard deviation, reaching 9.2 MPa. Among the HSG series, the greatest scatter occurred in the 8 mm HSG high series from manufacturer C, with a standard deviation of 5.5 MPa. In general, the HSG series exhibited lower variability than the TTG series. Differences between the manufacturers were evident. While manufacturer B showed variations across the glass thicknesses with an edge stress maximum at the 8 mm TTG series, the TTG edge stress values of manufacturer C remained at a more consistent level. For the HSG specimens, manufacturer C showed a trend across the thicknesses, whereas manufacturer A, in this case, exhibited similar values across all glass thicknesses. Regardless of manufacturer and glass thickness, a clear separation between the HSG and TTG test series could not be achieved, as the two categories overlapped within the range of 72 MPa to 82 MPa. This overlap was exclusively caused

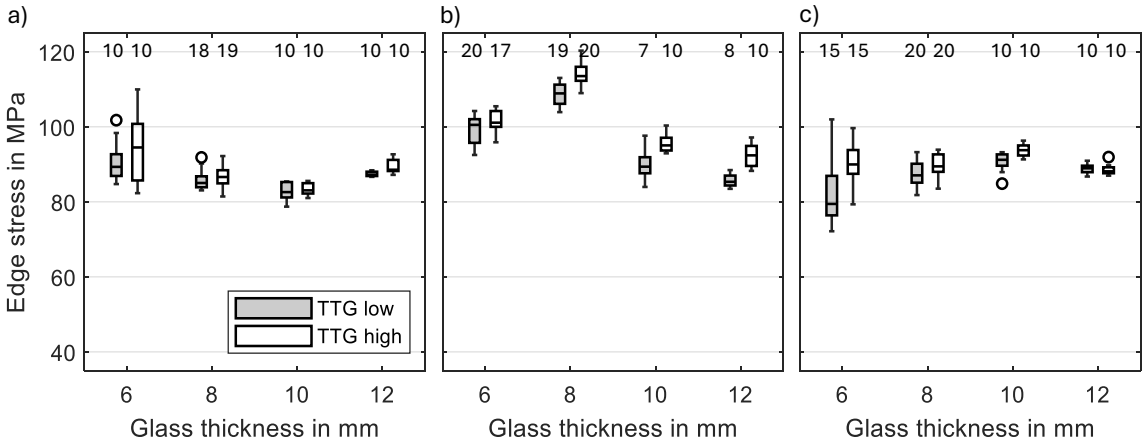

Figure 5.18: Results of edge stress determined by multiple-wavelength photoelasticity depending on glass thickness and pre-stress level for standard-size thermally toughened glass of manufacturer a) A, b) B, and c) C

by the specimens from manufacturer C. For manufacturers A and B, a clear distinction between the HSG and TTG test series could be observed.

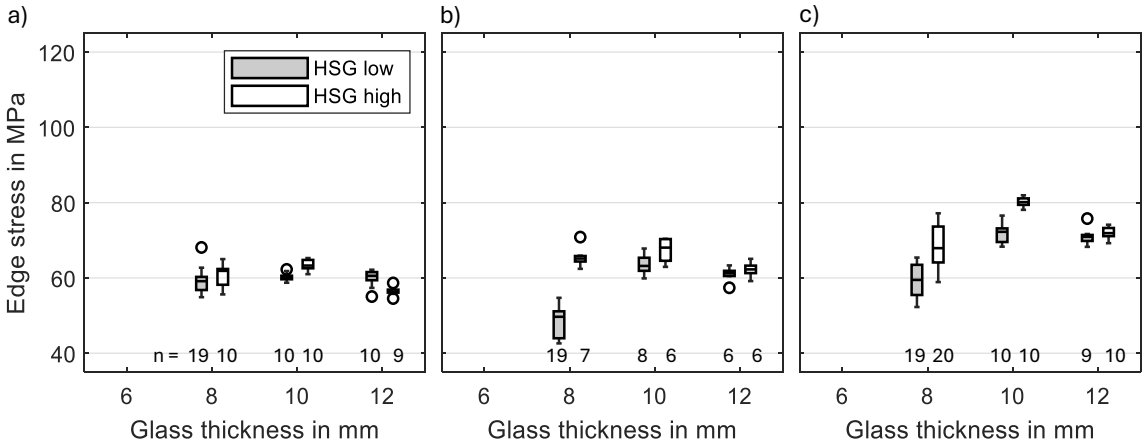

Figure 5.19: Results of edge stress determined by multiple-wavelength photoelasticity depending on glass thickness and pre-stress level for standard-size heat-strengthened glass of manufacturer a) A, b) B, and c) C

Fig. 5.20 evaluates the edge stress values measured with a) PST and b) MWP, differentiated by conformity for both glass products HSG and TTG. Table 5.4 indicates the number of specimens n per box plot. A direct comparison of the two measurement techniques showed that the box plots of PST exhibited less scatter than those of MWP. Several factors may contribute to this: first, the PST dataset contained fewer specimens and included specimens from only one manufacturer. Second, the continuous retardation curve used in PST may allow for more precise interpolation and as consequence edge stress extrapolation. In addition, the PST method yielded slightly lower edge stress values across all glass thicknesses and tempering levels. Using the PST method, TTG could be clearly separated from both conforming and non-conforming HSG specimens, with a difference of approximately 10 MPa. Although the NC HSG specimens, which did not exhibit a conforming HSG fracture pattern, show higher edge stress values, distinguishing between C

and NC HSG remained difficult and was largely independent of glass thickness. While the 10 mm and 12 mm HSG test series could be separated with a narrow margin, the 8 mm series showed a small overlap of about 2 MPa.

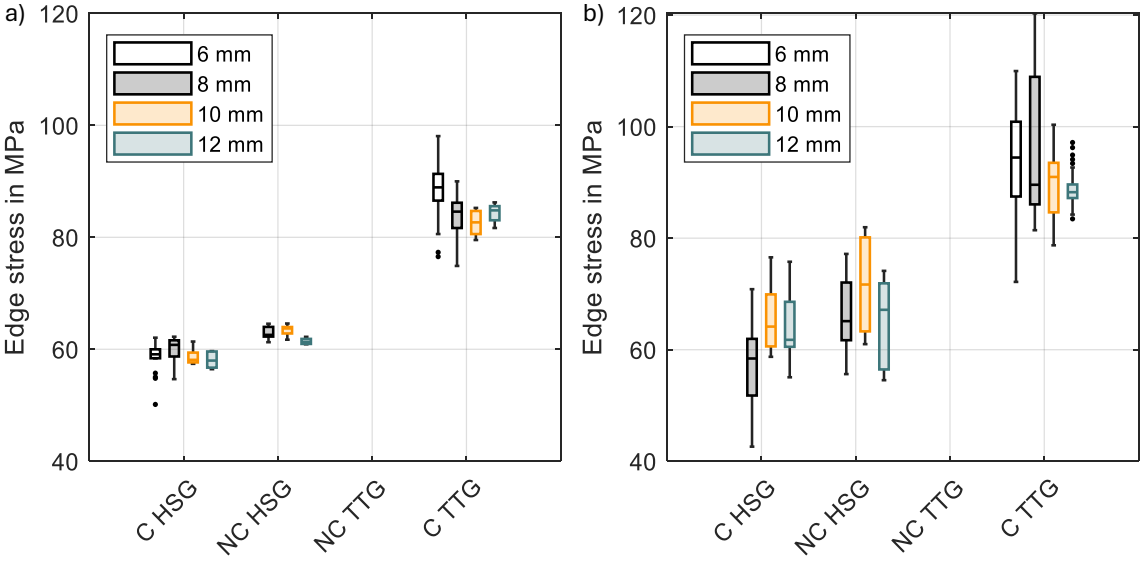

Figure 5.20: Evaluation of edge stress measurements by a) phase-shifting technique, b) multiple-wavelength photoelasticity on standard-size specimens: classified into conforming and non-conforming heat-strengthened glass according to EN 1863-1 (2012), and conforming and non-conforming thermally toughened glass according to EN 12150-1 (2020)

Table 5.4: Number of specimens per box plot depending on conforming and non-conforming heat-strengthened glass and thermally toughened glass, corresponding to edge stress measurements using phase-shifting technique and multiple wavelength photoelasticity from Fig. 5.20

	C HSG				NC HSG			C TTG			
t [mm]	6	8	10	12	8	10	12	6	8	10	12
n_{PST}	19	10	5	5	6	5	5	20	20	9	10
n_{MWP}	–	64	34	30	30	20	20	87	116	57	58

Fig. 5.20 demonstrates that no clear separation of the edge stress values measured using the MWP method could be established between the two conforming categories C HSG and C TTG, regardless of glass thickness. This is mainly due to the fact that the 6 mm TTG specimens showed lower edge stress values down to 72 MPa, while the highest values of the C HSG specimens reached up to 77 MPa. As a result, the ranges of both conforming categories partially overlapped. When considering the individual glass thicknesses, no comparison could be made for 6 mm because no reliable HSG edge stress values were obtained for this thickness. As previously discussed in Section 4.3.5, the MWP measurements for 6 mm HSG were not sufficiently robust to allow for evaluation. Excluding the 6 mm series, a distinction between C TTG and C HSG would be possible, as the remaining thicknesses showed separated value ranges. There was, however, a small overlap of approximately 3 MPa between non-conforming HSG and conforming TTG. The 10 mm NC HSG specimens reached edge stress values of up to 82 MPa, while the lowest value recorded for the 10 mm

TTG specimens was 79 MPa. In contrast, the edge-stress values within the HSG test series of C and NC HSG exhibited substantial overlap. The medians of the box plots can be separated only marginally: the medians of the three NC HSG series exceeded 65 MPa, whereas the highest median of the C HSG series reached 64 MPa. This demonstrates that, within HSG conformity could not be reliably distinguished based on edge stress values measured by MWP alone. In comparison, the PST method provided a clearer separation and therefore offers greater potential for performing conformity assessments.

5.4.3.2 Homogeneity of pre-stress at the edge

For both methods of PST and MWP, the edge stress was determined at six predefined measurement locations per standard-size specimen. Based on these individual measurements, the mean value was calculated, thereby providing a simplified assessment of the pre-stress at the edge. Concurrently, it was important to investigate the extent to which these individual measurement areas differ from one another. This variation could serve as an indicator of the homogeneity of edge stress and may therefore be used as a criterion in production control. Accordingly, Fig. 5.21 presents the standard deviation of the six measurement areas for each specimen, differentiated by glass thickness and by conformity classification for the glass products of TTG and HSG.

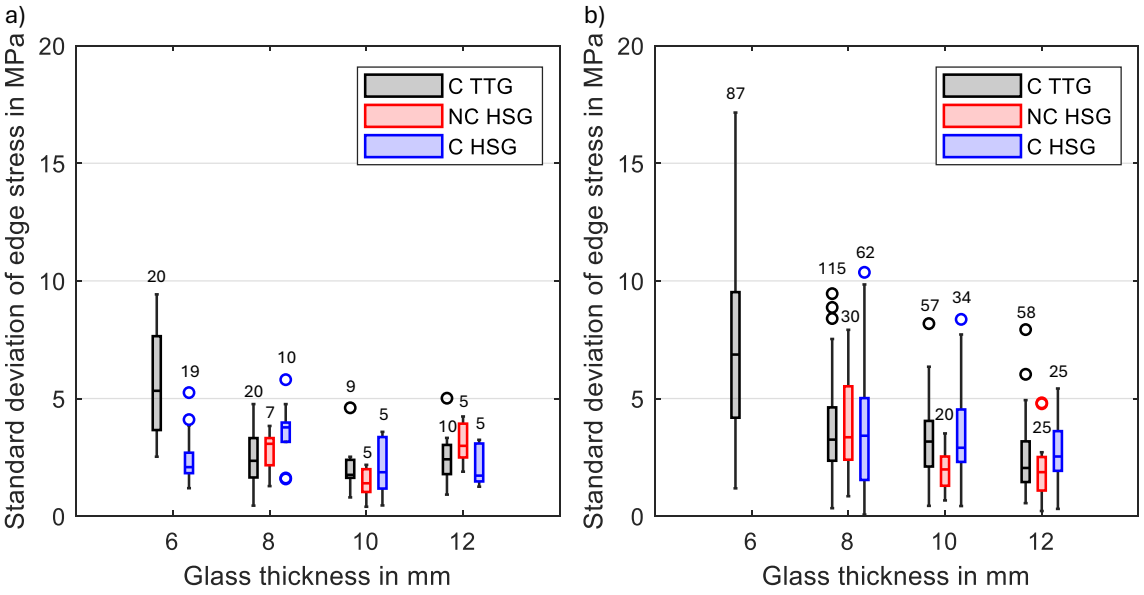

Figure 5.21: Standard deviation of the six individual edge stress measurement locations per standard-size specimen determined by a) phase-shifting technique and b) multiple-wavelength photoelasticity depending on glass thickness and conformity for heat-strengthened glass according to EN 1863-1 (2012) and thermally toughened glass according to EN 12150-1 (2020)

Fig. 5.21a shows that using PST measurements resulted in low standard deviation per specimen, with all specimens exhibiting values below 10 MPa. Most specimens with glass thicknesses of 8 to 10 mm even showed standard deviations below 5 MPa, whereas thinner 6 mm specimens displayed higher variability, reaching up to 10 MPa. The non-conforming

HSG specimens did not show increased standard deviations, indicating that the criterion of homogeneity did not appear to influence the conformity classification.

Fig. 5.21b shows the standard deviations of the six measurement edge stress values obtained using MWP. These standard deviations were higher than those from the PST method. In particular, the 6 mm TTG specimens exhibited comparatively large within-specimen scatter, even though each individual edge stress value met the interpolation quality requirement for the retardation curve with a $R^2 \geq 0.95$. However, the IQR for 8–12 mm were below 5 MPa. With increasing glass thickness, the scatter within a specimen decreased, indicating more stable measurement behavior for thicker glass. For both measuring methods, no influence of standard deviation on conformity classification, especially for the non-conforming HSG specimens, could be observed. It would be reasonable for production control to introduce a limit for the standard deviation of the individual edge stress measurements within a glass, to detect measurement errors and tempering inhomogeneities. However, the present analysis showed that the non-conformity of the NC HSG specimens was not associated with higher standard deviations than for conforming specimens. Therefore, this criterion cannot be used effectively to identify non-conforming specimens based on the measured level of edge stress.

5.4.3.3 Width of pre-stress zone of the edge

Laufs (2000) divided a tempered glass pane into four zones. According to this model, tempering zone 1 occupies the largest part of the pane, while zone 2 is defined by the membrane compressive stress at the glass edge. The width of the pre-stress zone of the edge is bounded by the 0th fringe-order isochromatic, which represents the transition point between the edge compression and the parabolic stress distribution of zone 1. In the evaluation of edge stress using MWP, the 0th isochromatic order was determined by identifying the location of maximum light intensity in the bright-field setup of the LineScanner (Softsolution GmbH 2023b). As discussed in Section 4.3.4, this identification could be challenging in some cases. In contrast, the PST method allowed the 0th isochromatic order to be identified more clearly through the retardation curve. Laufs (2000) stated that the width of the pre-stress zone of the edge is influenced by both the tempering level and the glass thickness. His research indicated that, for TTG, the pre-stress zone of the edge corresponds to a width of approximately 1.0 t, whereas for HSG a width of 1.5 t is expected. Therefore, this section investigates and compares the pre-stress width at the edge obtained using MWP and PST, examining their dependence on glass thickness and glass type.

Based on glass thickness and separated by conformity category, Fig. 5.22a shows the width of the pre-stress zone at the edge for each measurement area obtained with the PST method. All specimens originated from manufacturer A. A clear influence of the tempering level could be observed: as expected, the HSG specimens exhibited a wider edge-tempered zone than the TTG specimens. The width of the pre-stress zone also increased with glass thickness. For the TTG specimens in particular, a pronounced increase in zone width with increasing glass thickness could be seen, an increase that appeared to exceed a linear trend. This behavior was not observed for HSG specimens. For the thickness of 12 mm, the TTG and HSG specimens exhibited nearly identical values.

Fig. 5.22b shows the width of the pre-stress zone determined with the MWP method, plotted as a function of glass thickness and separated according to conformity, combining

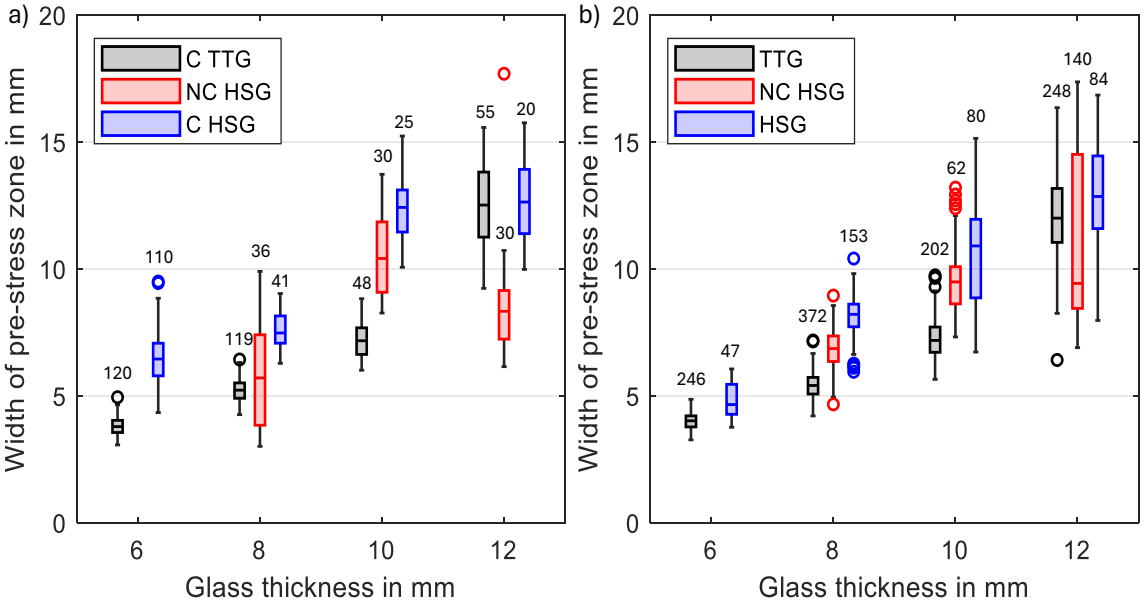

Figure 5.22: Width of the edge pre-stress zone on standard-size specimens determined by a) phase-shifting technique and b) multiple-wavelength photoelasticity, depending on glass thickness and conformity for heat-strengthened glass according to EN 1863-1 (2012) and thermally toughened glass according to EN 12150-1 (2020)

all manufacturers. For the evaluation of pre-stress width, the 6 mm HSG specimens were included, even though their edge stress values were not analyzed for this thickness. For several specimens, particularly those from manufacturer B, the 0th isochromatic order could not be identified. Inspection of the isochromatic images suggests that retardation patterns originating from the center of the plate interacted with those near the edge, making detection of the 0th isochromatic order based on maximum intensity difficult and therefore not well suited for these particular specimens. As can be seen in Fig. 5.22b, there was no clear separation between the glass types. Although the HSG series consistently exhibited higher median values than the TTG series, substantial overlap persisted. This overlap was particularly pronounced for the 12 mm specimens, which showed wide interquartile ranges. In contrast, the 8 mm and 10 mm specimens displayed a clearer distinction between TTG and HSG.

To analyze the influence of glass thickness on the width of the pre-stress zone of the edge in more detail, a thickness-normalized factor was determined by Equation (5.1).

$$\text{Factor}_{w/t} = \frac{\text{Width of prestress zone}}{\text{Glass thickness}} \tag{5.1}$$

Fig. 5.23a presents this factor for PST measurements depending on glass thickness and glass type. The TTG specimens showed considerably less scatter than the HSG and NC HSG specimens. The TTG specimens with thicknesses from 6 to 10 mm showed similar factors with an average value of approximately 0.67 t, whereas the 12 mm TTG specimens differed markedly with a median factor of 1.04 t. The HSG specimens exhibited greater variation but showed no consistent trend across the thickness. In fact, the 4 mm HSG specimens partly reached higher factors than some of the thicker panes.

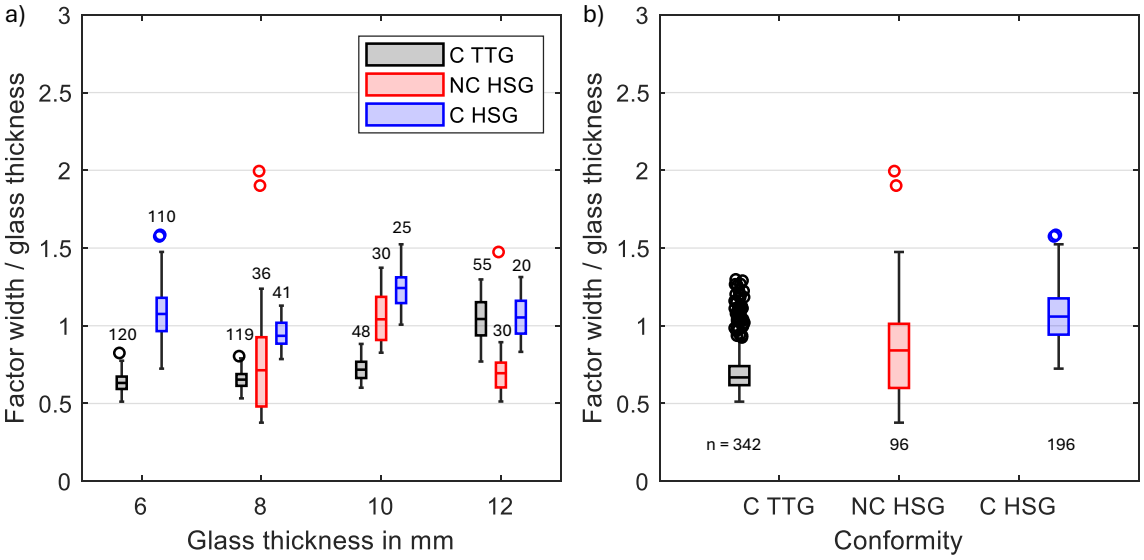

Figure 5.23: Thickness-normalized factor for width of the edge pre-stress zone on standard-size specimens determined by phase-shifting technique a) depending on glass thickness and conformity and b) summarized for conformity for heat-strengthened glass according to EN 1863-1 (2012) and thermally toughened glass according to EN 12150-1 (2020)

Fig. 5.23b combines all thicknesses and presents the factor$_{w/t}$ for PST measurements, separated by conformity. Even though the IQR in the box plots did not overlap, the overall ranges of TTG and HSG could not be clearly separated. Most TTG specimens laid between 0.51 t and 0.92 t with a median of 0.67 t and outliers reaching up to 1.30 t. The HSG specimens ranged from 0.72 t to 1.52 t with a median of 1.06 t and a few outliers extending to 1.59 t. The non-conforming HSG specimens were dispersed across almost the entire combined range of both TTG and HSG.

Fig. 5.24a shows the thickness-normalized factors of the pre-stress zone obtained with the MWP method, separated by glass thickness. Considerable overlap remained between the 12 mm TTG and HSG specimens, The TTG specimens of 6 and 8 mm thickness exhibited median factors of approximately 0.67 t, while the 10 mm TTG specimens reached a slightly higher value of 0.72 t. In contrast, the 12 mm TTG specimens showed a markedly increased factor of around 1.0 t. The HSG specimens displayed an increasing trend with thickness: the 6 mm HSG specimens showed a factor of about 0.78 t and only from 8 mm onward did the HSG specimens exceed a factor of 1.0 t. When combining all glass thicknesses, as illustrated in Fig. 5.24b, the resulting overall factors as medians amounted to approximately 0.70 t for TTG and 1.03 t for HSG. Although the interquartile ranges of TTG and HSG were offset from one another, the overlap between the two glass products persisted, indicating that the glass types cannot be clearly separated based on this factor alone.

To evaluate the results obtained by both measuring methods, the mean pre-stress zone widths were calculated for each glass thickness and glass type. Fig. 5.25 presents these mean widths for TTG and HSG measured with PST and MWP. The two glass types were plotted on a common axis so that the absolute values of TTG and HSG could be directly compared, with color-coding used to distinguish between them. In all cases, the pre-stress zone at the edge was wider for HSG than for TTG. The difference between the

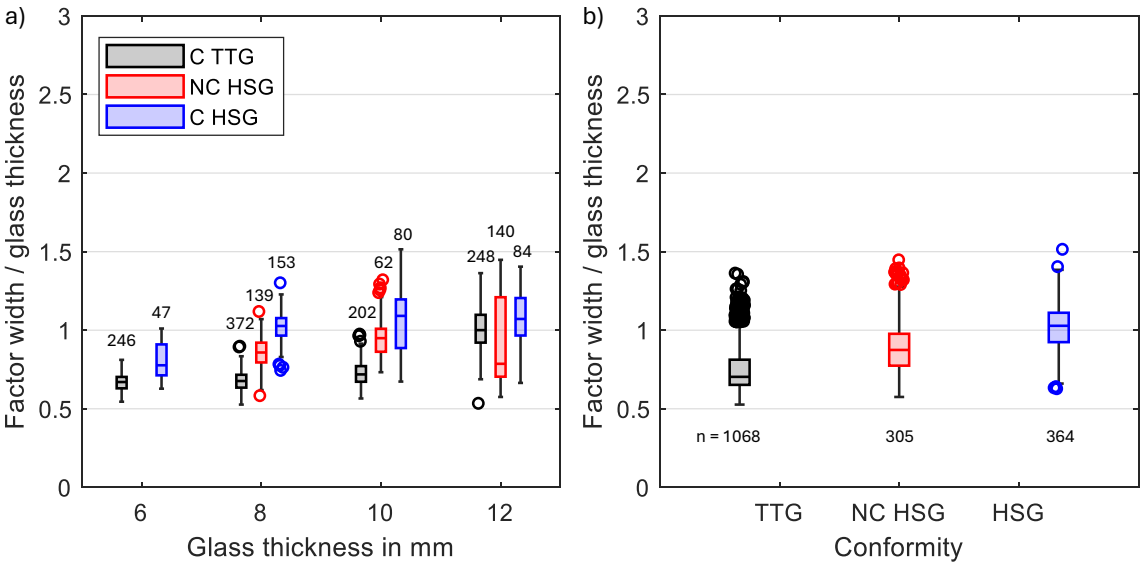

Figure 5.24: Thickness-normalized factor for width of the edge pre-stress zone on standard-size specimens determined by multiple-wavelength photoelasticity a) depending on glass thickness and conformity and b) summarized for conformity for heat-strengthened glass according to EN 1863-1 (2012) and thermally toughened glass according to EN 12150-1 (2020)

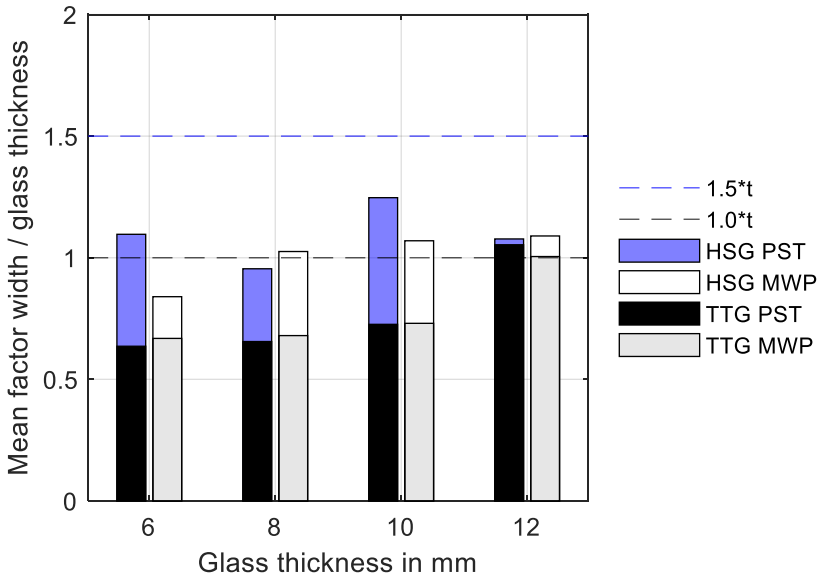

Figure 5.25: Bar chart of the mean thickness-normalized factor for the width of the edge pre-stress zone per glass thickness, comparing the measurement methods multiple-wavelength photoelasticity and phase-shifting technique and the tempering types heat-strengthened glass and thermally toughened glass for standard-size specimens, including the reference widths according to Laufs (2000): 1.5 t for heat-strengthened glass and 1.0 t for thermally toughened glass

two tempering levels was smallest for the 12 mm specimens. The best agreement between PST and MWP measurements was observed for 6 to 10 mm TTG as well as for 12 mm HSG, whereas the largest discrepancies occurred for the 6 and 10 mm HSG specimens.

Only the 12 mm TTG specimens approached the factor for the pre-stress widths reported by Laufs (2000), which are also indicated in Fig. 5.25. For this thickness, the mean factor obtained from both PST and MWP measurements was 1.03 t. The remaining thicknesses of TTG showed much lower values with similar factors around 0.68 t. When averaging across all thicknesses and both measurement methods, TTG reached an overall factor of 0.77 t. The corresponding mean factor for HSG was 1.05 t, which also fell short of the value of 1.5 t reported by Laufs (2000). The highest individual value in this investigation was 1.25 t, measured for the 10 mm HSG specimens using PST.

In summary, the evaluation of the pre-stress zone at the edge demonstrates that the width could not be expressed as a consistent thickness-dependent factor. In most cases, HSG specimens exhibited a wider pre-stress zone than TTG specimens. However, the reference values proposed by Laufs (2000) could not be confirmed. Both MWP and PST measurements indicated considerably smaller zone widths than those reported in Laufs (2000). A similar conclusion was reached by Lohr (2019), who investigated the width of the pre-stress zone at the edge using the StrainScope Flex on specimens with glass thicknesses of 6, 8, and 10 mm. For specimens before the regrinding edge processing, the author reported increasing factors for TTG. The TTG factors ranging from 0.65 t to 0.78 t were in good agreement with the factors derived in the present work. In contrast, Lohr (2019) observed decreasing factors for HSG ranging from 1.42 t to 1.04 t which were not consistent with the factors obtained here. A reliable distinction between TTG and HSG based on the width of the pre-stress zone at the edge was therefore not feasible. Likewise, the width could not be used to identify non-conforming HSG specimens. Nevertheless, for specimens with glass thicknesses from 8 to 10 mm, the mean values for TTG and HSG differed sufficiently to provide indicative reference ranges. For the 12 mm specimens, however, TTG and HSG showed nearly identical zone widths.

5.4.3.4 Reproducibility of MWP measurements

The measurement of edge stress must be reproducible if it is to be used for production control of tempering quality. To examine the reproducibility of the measurements obtained with the MWP method, a subset of specimens originating from manufacturer A were scanned twice with the LineScanner (Softsolution GmbH 2023b) at HM. First, each specimen was scanned in one direction, referred to in this section as the initial scan. The specimen was then rotated by 180°, thereby swapping the longitudinal edges, and scanned again. This second measurement was referred to as the repeat scan, as illustrated in Fig. 5.26. For each of the two scan directions, the edge stress was evaluated in six measurement areas, as described in Section 5.4.2, and subsequently averaged to obtain the mean value per specimen. Since this mean value was intended to serve as the evaluation criterion in production quality control, it was also used for assessing measurement reproducibility.

The edge stress results of the initial scan are plotted on the x-axis and those of the repeat scan on the y-axis in Fig. 5.27a. The specimens are additionally color-coded according to glass thickness. It can be observed that the 6 mm TTG specimens showed considerable scatter from the diagonal. The absolute deviations in edge stress between the initial scan

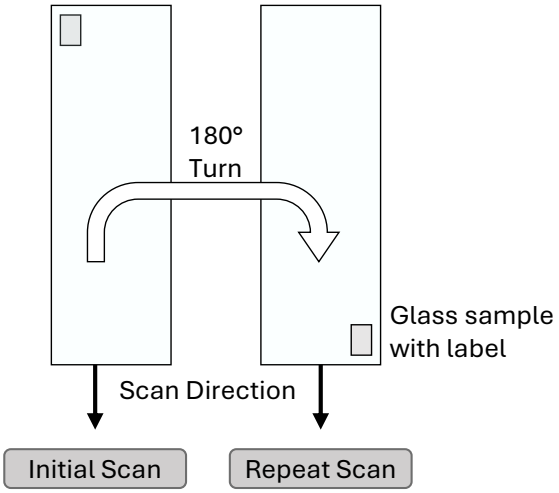

Figure 5.26: Scan directions for the reproducibility analysis of multiple-wavelength photoelasticity measurements on standard-size specimens: initial and repeat scan after a 180° rotation

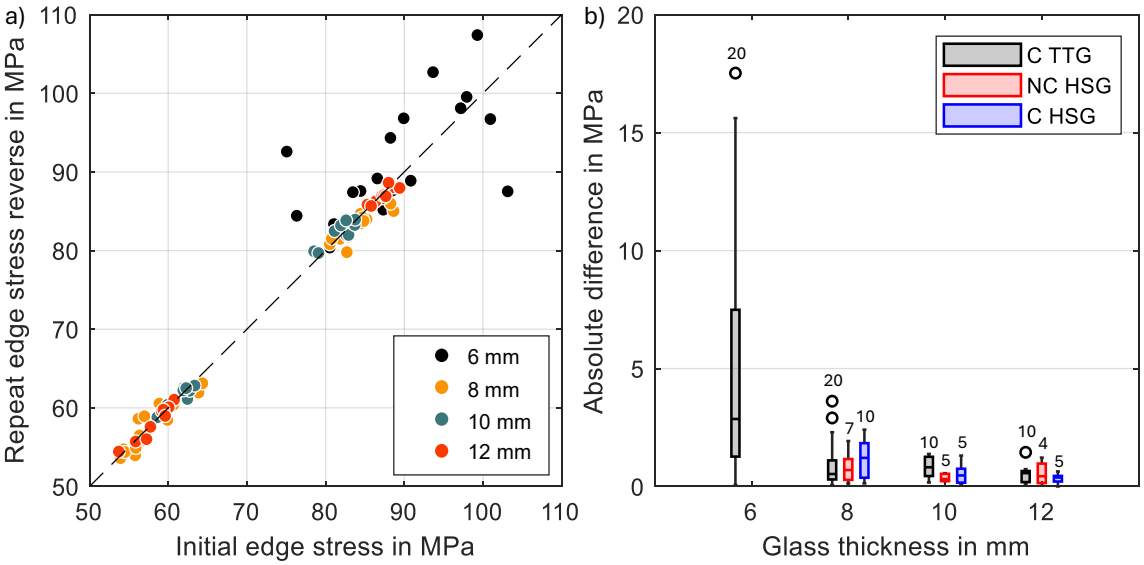

Figure 5.27: Reproducibility analysis of edge stress measurements obtained with the multiple-wavelength photoelasticity on standard-size specimens: a) scatter plot of results for initial versus repeat scan and b) box plots illustrating the absolute deviations between the two scan directions

and the repeated scan, separated by conformity category and further subdivided by glass thickness, are shown in Fig. 5.27b. Although the median deviation for the 6 mm TTG specimens was 2.9 MPa, several panes exhibited deviations of up to 17.5 MPa. In contrast, edge stress results of the other glass thicknesses laid close to the diagonal in Fig. 5.27a, independent of conformity. Also, the absolute deviations in Fig. 5.27b were small for the thicknesses between 8 and 12 mm with a maximum of 3.6 MPa for the 8 mm TTG specimens.

In summary, the edge-stress measurements obtained with the MWP method showed very good reproducibility for glass thicknesses between 8 and 12 mm, whereas the 6 mm specimens exhibited substantially larger deviations between the two scan directions.

5.5 Relation between photoelastic and destructive test results

Based on the results previously delineated in this chapter, the following models were investigated to evaluate the relation between photoelastic and destructive variables:

- Number of fragments vs. Surface stress
- Number of fragments vs. Edge stress (MWP)
- Bending stress vs. Surface stress
- Bending stress vs. Edge stress (MWP)
- Bending stress vs. Edge stress (PST)

In this framework, Pearson correlation analyses were conducted to examine the linear relationship between the photoelastic measurements and the destructive test results. The purpose was to evaluate the suitability of photoelastic measurements of edge and surface stress for destructive testing of bending stress and number of fragments. Following the correlation analysis, regression models were calculated for the five relations to examine the relationship between the photoelastic and destructive tests in greater detail, with a particular focus on assessing the influence of manufacturer and glass thickness on these relationships. Parts of the chapter have already been pre-published in Efferz et al. (2025c).

5.5.1 Method of correlation analysis

Correlation analysis is suitable for measuring the magnitude and direction of a linear relationship between two continuous variables (Schober et al. 2018). The correlation coefficient r, defined as the ratio of the covariance to the product of the standard deviations, is evaluated and found to vary between -1 and 1. A hypothesis test determines whether there is a correlation between the two sets of data. The null hypothesis H_0, that there is no correlation between the results of the two test variables, is tested at a significance level of 0.05 to determine whether the observed data are sufficient to reject this hypothesis. The test for statistical significance considers the scatter in the data and makes it possible to distinguish between random variability and true correlation. There are several methods of correlation analysis, each requiring specific assumptions regarding the distribution of the data.

In the following sections, the Pearson correlation (Kirch 2008), a parametric technique, was employed. One assumption is a normal distribution for both variables which were tested visually by Q-Q plots. Furthermore, the relationship between the variables must be linear. This can be verified by a scatter plot, in which the presence of a curve would indicate non-linearity. To estimate the Pearson correlation coefficient r with a reasonable degree of certainty, the function *boot()* from the *boot* package (version 1.3.31) in R (R Core Team 2024) was used with 2000 resamples, resulting in 95% confidence intervals. Since the confidence intervals were used to compare the different correlations, the bootstrapping method was chosen over other ways of addressing the issue of a possible non-compliance with the normal distribution, such as data transformations or other correlation types.

5.5.2 Method of moderation analysis

After investigating a simple linear regression model for each relationship, the effect of nominal glass thickness as a categorical moderator was evaluated. For the OLS regressions, the *lm()* function from the *stats* package (version 4.4.1) in R (R Core Team 2024) was used, applying the notation *Destructive variable* $\sim$ *Photoelastic variable*. The moderation analyses were conducted using the same function, but including an interaction term: *Destructive variable* $\sim$ *Phototelastic variable* $*$ *Glass thickness.*

To account for potential violations of normality, linearity, and the presence of outliers, both the linear regressions and the moderation analyses were bootstrapped using R = 2000 resamples with the *boot()* function from the *boot* package (version 1.3.31) in R (R Core Team 2024). The resulting 95% confidence intervals were of the bias-corrected and accelerated (BCa) type. After evaluating the significance of the interaction terms, interaction plots were generated for each glass-thickness category. These plots corresponded to the individual, thickness-specific OLS regressions but supported the interpretation of the moderation analysis. Because a categorical moderator requires defining a reference category, each glass thickness was in turn treated as the reference in separate moderation models in a contrast analysis. The bootstrapped confidence intervals of the interaction terms were then interpreted to determine which thickness categories differ significantly from one another.

5.5.3 Method of intraclass correlation

Due to the tempering process, the three manufacturers may induce a hierarchical data structure: specimens from the same manufacturer were expected to be more similar to each other than to specimens from other manufacturers. Such clustering violates the independence assumption of OLS regression and motivates the use of mixed-effects models. To account for clustering at the manufacturer level (Level 2), linear mixed-effects models were employed with manufacturers included as a random intercept. This specification captured between-manufacturer variability while estimating within-manufacturer relationships among the predictors and outcomes (Tabachnick and Fidell 2013, Hox 2018).

To statistically assess whether a relevant hierarchical structure was present, the intraclass correlation coefficient (ICC) was computed. The ICC is a group-level correlation-type measure that quantifies the proportion of the total variance that is attributable to differences between groups. In this section, the ICC was obtained from a linear mixed model with

a random intercept for manufacturer: *Destructive variable* $\sim$ *Photoelastic variable* + (1 | Manufacturer). The ICC was determined in R (R Core Team 2024) using the function *ICC()* from the package *performance* (version 0.15.2). The ICC can be computed directly from the variance components of the model as the ratio of the random-intercept variance ${\sigma^2}_{\text{Manufacturer}}$ to the sum of the random-intercept and residual variances ${\sigma^2}_{\text{Manufacturer}} + {\sigma^2}_{\epsilon}$, as indicated in Equation (5.2).

$$\text{ICC} = \frac{\sigma^2_{\text{Manufacturer}}}{\sigma^2_{\text{Manufacturer}} + \sigma^2_{\varepsilon}} \tag{5.2}$$

The resulting value indicates how large the share of total variance explained by differences between manufacturers is. A higher ICC implies that measurements within the same manufacturer are more similar than measurements across manufacturers, suggesting that manufacturer is an important source of variability in the relationship under study. Following Vajargah and Masoomehnikbakht (2015), an ICC greater than 0.10 was taken to indicate substantial clustering, in which case a mixed-effects model should be preferred because the influence of the random grouping structure is considerable. For ICC values below 0.10, the grouping structure is often regarded as negligible, and a classical linear regression model without random effects can be used.

5.5.4 Comparison of correlation analysis

Before the correlation analysis, histograms were used to gain insight into the underlying data distribution and to evaluate these assumptions. Fig. A.1 and Fig. A.3a in Appendix provide a visual representation of the frequency distribution. The normal distribution for each correlation model was controlled by means of Q-Q plots in Fig. A.2 and Fig. A.3b in Appendix. A visual evaluation of the diagrams indicated that not all variables were distributed normally. However, the application of the bootstrapping method did not compromise the validity of the Pearson correlation. The scatter plots in Sections 5.5.5.2 to 5.5.5.6 demonstrate that the data was predominantly consistent with the condition of linearity.

To ascertain whether the correlation models exhibit significant differences and to identify which correlations represent a stronger relationship, the 95% confidence intervals of the correlation coefficient r were compared. The confidence intervals were derived from the bootstrapping process and, in conjunction with the averaged correlation coefficient r, provided insight into the strength of the relationship between the photoelastic and the destructive measured variables. Appendix Table A.2 presents the statistical values of the correlations. H_0 could be rejected for all correlation models investigated, as the p-values were below the significances level of 0.05. Therefore, all Pearson correlations were statistically significant, thereby indicating a robust relationship between the photoelastic measurements and the destructive test results.

Fig. 5.28 compares the confidence intervals for each of the five correlation models regarding the correlation between the (a) number of fragments or (b) bending stress and the photoelastic variables. The 95% confidence intervals for the correlation models of *Fragments vs. Surface stress* und *Fragments vs. Edge stress* determined by MWP were not overlapping, as illustrated in Fig. 5.28a. It could thus be concluded that the two correlation models of

number of fragments were significantly disparate. Given the higher Pearson correlation coefficient of r = 0.85 with confidence interval [0.81, 0.88], indicating a very large effect, the number of fragments could be described with greater precision by surface stress than by edge stress, for which the correlation was r = 0.57 with confidence interval [0.42, 0.68].

It can be seen in Fig. 5.28b, all models showed very high, significant correlations with bending stress. Because the 95% confidence intervals of the correlation coefficients overlapped, no statistically significant differences could be identified between the models *Bending stress vs. Surface stress*, *Bending stress vs. Edge stress (MWP)*, and *Bending stress vs. Edge stress (PST)*. Consequently, no definitive conclusion could be drawn as to which model exhibited the strongest correlation with bending strength, indicating that all three models are suitable for describing this relationship.

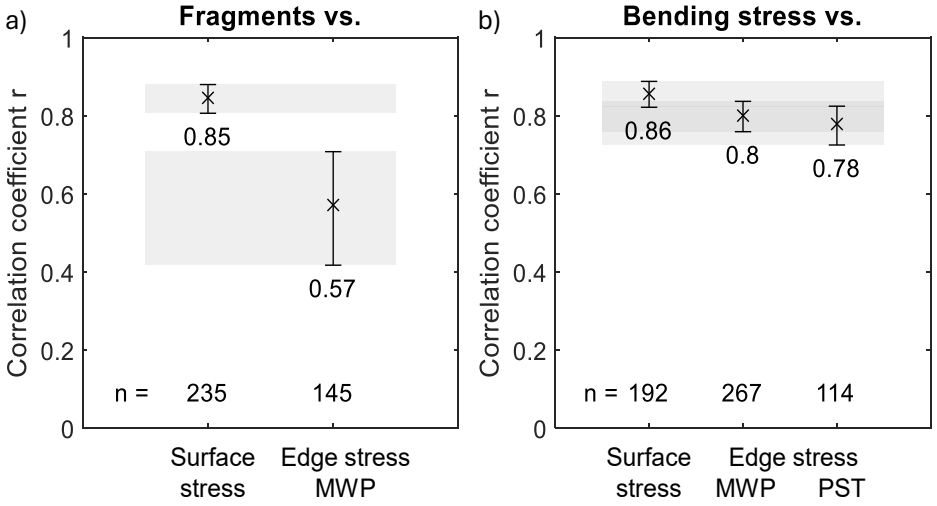

Figure 5.28: Comparison of the 95% confidence intervals of the correlation analyses for standard-size specimens according to Pearson with bootstrapping a) Fragments vs. Surface stress and Fragments vs. Edge stress and b) Bending stress vs. Surface stress and Bending stress vs. Edge stress, adapted from Efferz et al. (2025c)

5.5.5 Influence of glass thickness and manufacturer

5.5.5.1 Investigation of manufacturer-level clustering

To investigate a possible hierarchical data structure regarding the manufacturers, Table 5.5 reports the ICC values of the four relationships estimated using mixed-effects models. The edge stress models were based on the MWP method, as for PST, all specimens originate from a single manufacturer, so no manufacturer-level clustering needed to be examined. All ICC values were clearly below 0.10, indicating that no pronounced manufacturer structure needed to be accounted for in the regression analysis.

Table 5.5: Intraclass correlation coefficient for testing a possible manufacturer structure within standard-size specimens using mixed model, edge stress measured by multiple-wavelength photoelasticity

Mixed model	ICC
Fracture pattern ∼ Surface stress + (1 | Manufacturer)	0.033
Bending stress ∼ Surface stress + (1 | Manufacturer)	0.059
Fracture pattern ∼ Edge stress (MWP) + (1 | Manufacturer)	0.002
Bending stress ∼ Edge stress (MWP) + (1 | Manufacturer)	0.021

5.5.5.2 Number of fragments ∼ Surface stress

Fig. 5.29 illustrates the relationship between the number of fragments and surface stress, separated by glass thicknesses ranging from 4 mm to 12 mm with the corresponding OLS regression lines. Additionally, the three manufacturers A, B and C are color-coded to assess a potential influence of manufacturer-specific effects within each glass thickness. For thickness-specific models, Table 5.6 reports the intercepts, estimates, and R^2 values, along with bootstrapped 95% confidence intervals, to indicate the statistical significance of the estimated coefficients.

Glass thicknesses of 6 mm, 8 mm, and 12 mm exhibited very high R^2 values above 0.927, indicating a significant, high proportion of variance explained by the models. Together with the good visual agreement observed in the plots, this suggests that the manufacturer had no substantial influence on the relationship between the number of fragments and surface stress at these thickness levels. For the 10 mm specimens, manufacturer dependence was also minimal. However, the model fit is comparatively lower with an R^2 of 0.79.

Table 5.6: Statistical details of intercept, estimates, and R^2 with 95% confidence intervals for the linear regression model Number of fragments ∼ Surface stress of standard-size specimens, divided by glass thickness with sample size

t [mm]	n	Intercept + CI	Estimate + CI	R^2 + CI
4 *	59	-270.48 [-309.70, -225.85]	3.06 [2.71, 3.38]	0.755 [0.629, 0.836]
6 *	57	-420.37 [-460.71, -383.62]	4.64 [4.32, 4.97]	0.927 [0.890, 0.947]
8 *	59	-171.78 [-190.39, -151.77]	2.36 [2.21, 2.51]	0.950 [0.914, 0.967]
10 *	30	-149.60 [-194.58, -108.28]	2.15 [1.77, 2.53]	0.788 [0.499, 0.897]
12 *	30	-152.69 [-178.37, -121.09]	2.02 [1.75, 2.22]	0.929 [0.866, 0.963]
4–12 *	235	-193.89 [-215.85, -173.84]	2.52 [2.35, 2.70]	0.716 [0.647, 0.774]

* Predictor statistically significant based on bootstrap confidence intervals

The lowest R^2 was observed for the 4 mm thickness model. Furthermore, Fig. 5.29a clearly reveales manufacturer dependence: data points from different manufacturers are distinctly separated and do not fit well to the regression line of all 4 mm specimens. When analyzed separately by manufacturer, the regression lines exhibite similar slopes but are horizontally shifted, as shown in Fig. 5.30. However, compared to the regression line including all 4 mm specimens, these manufacturer-specific regression lines are substantially steeper. The steep slopes of the manufacturer-specific regression lines corroborate practical experience that producing 4 mm tempered glass is challenging. The gradual variation in pre-stressing within

the glass pane strongly affected the number of fragments, making manufacturer-related differences more pronounced.

As illustrated by the differing slopes of the thickness-specific regression lines in Fig. 5.29, an effect of glass thickness on the relationship between number of fragments and surface stress was suspected. Without accounting for glass thickness, the OLS regression decreased the explained variance to a mean R^2 of 0.715, and the estimated slope of the regression line was 2.52. This regression line is shown in Fig. 5.30a. Although the regression was computed independently of glass thickness, the data points were color-coded according to their respective thicknesses.

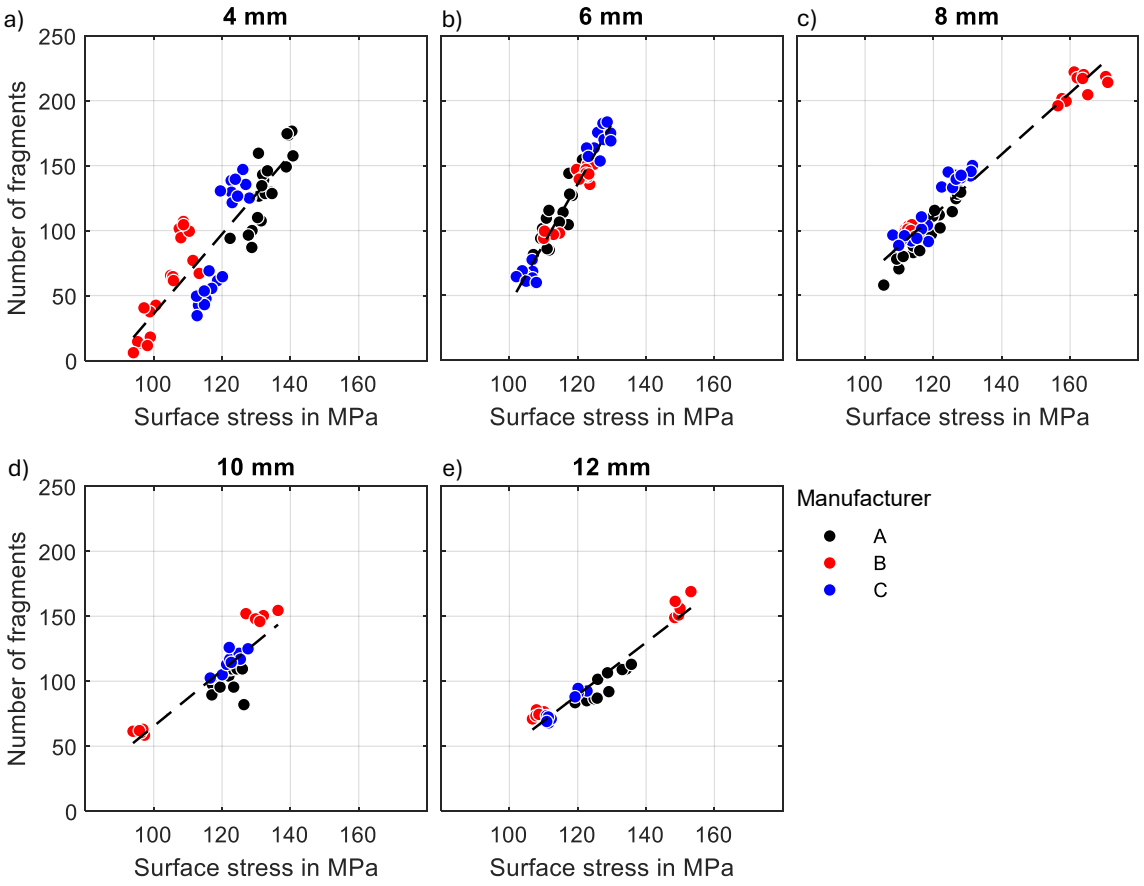

Figure 5.29: Comparison of ordinary least squares regression Number of fragments ~ Surface stress of standard-size specimens for different glass thicknesses (a-e); manufacturers are distinguished by color

To formally test the influence of glass thickness, a moderation analysis was conducted using the model *Number of fragments* ~ *Surface stress* * *Glass thickness*. The interaction regression model demonstrated a significantly improved explained variance with an R^2 of 0.874. The contrast analysis, performed by alternating the reference category, revealed that especially the 4 mm and 6 mm thicknesses differed significantly from the other glass thicknesses, see Section 5.5.5.7.

The interaction plot in Fig. 5.30b displays the thickness-specific regression lines. Due to the manufacturer effect observed in the 4 mm thickness group, the 4 mm data was further split by manufacturer. The slopes of the regression lines indicate that the estimated

relationship between surface stress and number of fragments decreases with increasing glass thickness. This suggests that changes in pre-stress at the surface have a stronger impact on the fracture pattern for thinner glass. While the regression lines for 8 mm, 10 mm, and 12 mm thicknesses appeared to shift vertically without a clear intersection point, the 6 mm regression line stood out by crossing the others. A similar behavior was observed for the 4 mm regression lines: one of the 4 mm lines aligned closely with the 6 mm line, while the other two were shifted horizontally to the right, towards higher surface stress values.

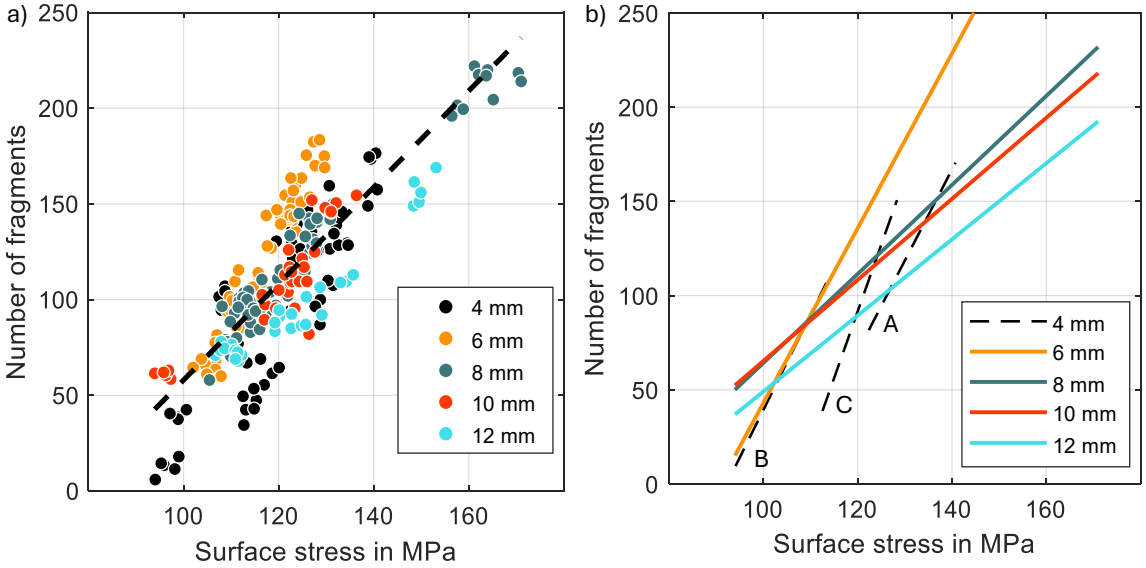

Figure 5.30: Number of fragments ∼ Surface stress a) ordinary least squares regression color-coded by glass thickness and b) interaction plot illustrating the moderating effect of glass thickness; for standard-size specimens

5.5.5.3 Number of fragments ∼ Edge stress (MWP)

As shown by the correlation analysis in Section 5.5.4, the relationship between number of fragments and edge stress determined by MWP was weak. This trend was also reflected in the OLS regression analysis shown in Fig. 5.32a, which was performed for the aggregated model of glass thicknesses ranging from 6 to 12 mm. The explained variance was low with only $R^2 = 0.347$ with a 95% confidence interval of [0.180, 0.481], as reported in Table 5.7. In Fig. 5.32a, the data points are color-coded by glass thickness, suggesting a potential influence of thickness on the relationship between number of fragments and edge stress measured by MWP.

However, the regression models in Fig. 5.31, calculated separately for each glass thickness from 6 mm to 12 mm, also showed low R^2 values. As detailed in Table 5.7, the 95% confidence intervals for the estimates were quite wide. Nevertheless, the predictor edge stress measured by MWP was significant for thicknesses between 8 mm and 12 mm and the overall model including glass thicknesses from 6–12 mm, as indicated by 95% confidence intervals for the estimates that did not include zero. The 6 mm regression model showed a confidence interval ranging from -0.23 to 2.31, indicating that edge stress did not significantly contribute to explaining this model.

Table 5.7: Statistical details of intercept, estimates, and R^2 with 95% confidence intervals for the linear regression model Number of fragments ~ Edge stress (determined by multiple-wavelength photoelasticity) of standard-size specimens, divided by glass thickness with sample size

t [mm]	n	Intercept + CI	Estimate + CI	R^2 + CI
6	30	-9.99 [-97.27, 164.39]	1.44 [-0.23, 2.31]	0.212 [0.002, 0.565]
8 *	52	-148.52 [-244.43, -33.18]	2.81 [1.58, 3.82]	0.350 [0.146, 0.547]
10 *	29	-150.06 [-307.55, -9.87]	2.83 [1.22, 4.53]	0.237 [0.032, 0.453]
12 *	29	-855.02 [-1009.65, -556.50]	10.72 [7.35, 12.46]	0.789 [0.549, 0.907]
6–12 *	140	-118.30 [-178.03, -49.32]	2.50 [1.76, 3.13]	0.347 [0.180, 0.481]

* Predictor statistically significant based on bootstrap confidence intervals

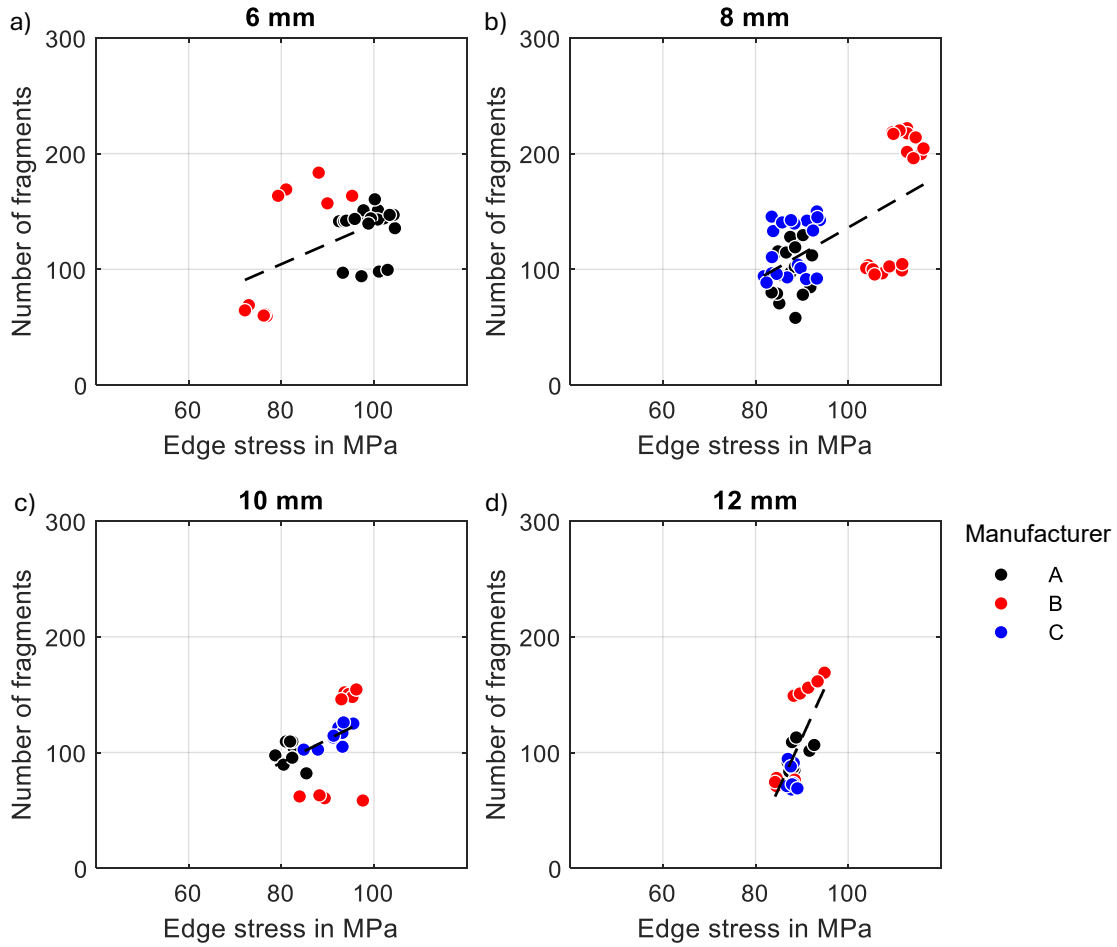

Figure 5.31: Comparison ordinary least squares regression Number of fragments ~ Edge stress (determined by multiple-wavelength photoelasticity) of standard-size specimens for different glass thicknesses (a-d); manufacturers are distinguished by color

As described in Section 5.1, TTG was produced at two distinct pre-stress levels: low-tempered and high-tempered TTG. From the perspective of the dependent variable (number of fragments) these pre-stress levels could be clearly distinguished for each manufacturer. However, these differences in number of fragments could not be explained by edge stress. In particular for thicknesses between 6 mm and 10 mm, specimens with widely varying numbers of fragments showed similar levels of edge stress values, which was reflected in the relatively low R^2 values ranging from 0.212 to 0.350. In Fig. 5.31, clustering of the data points by manufacturer could also be observed, rather than a close fit to the regression line. However, subdividing the data by manufacturer did not lead to an increase in explained variance. In contrast, the model for 12 mm glass thickness demonstrated the best explained variance with $R^2 = 0.789$ [0.549, 0.907] and a significantly steeper slope with an estimate of 10.72 [7.35, 12.46]. This pattern was also visible in the interaction plots shown in Fig. 5.32b. Moderation by glass thickness improved the relationship between number of fragments and edge stress measured by MWP, increasing the adjusted R^2 to 0.407 [0.255, 0.512]. However, only the 12 mm thickness differed significantly from all other thicknesses.

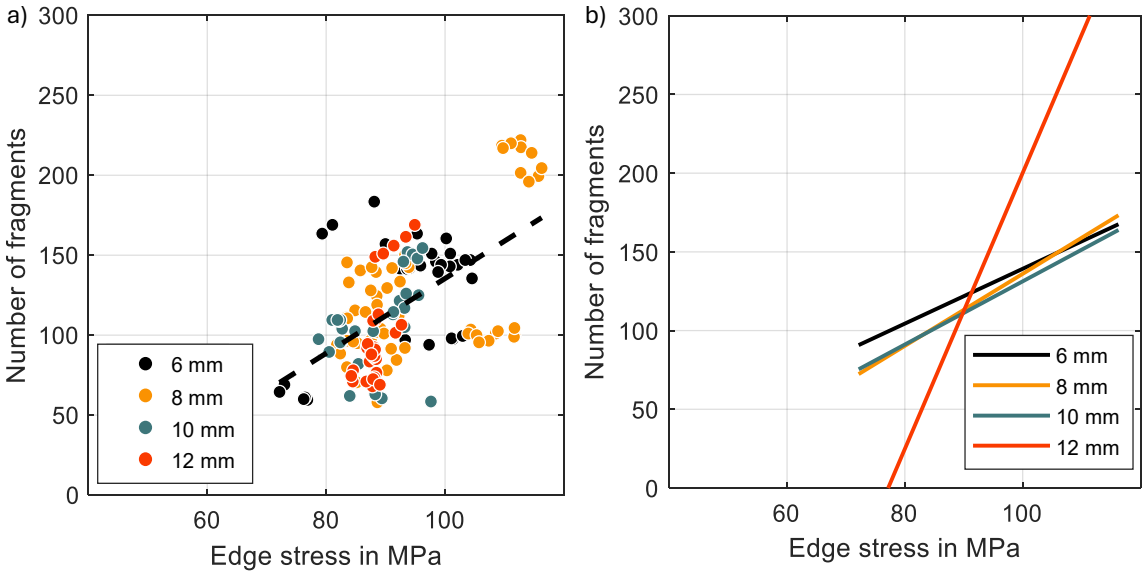

Figure 5.32: Number of fragments ~ Edge stress (determined by multiple-wavelength photoelasticity) a) ordinary least squares regression color-coded by glass thickness and b) interaction plot illustrating the moderating effect of glass thickness for standard-size specimens

5.5.5.4 Bending stress ~ Surface stress

Fig. 5.33 displays the regression models for bending stress and surface stress, analyzed separately for each glass thickness from 4 mm to 12 mm, with manufacturers distinguished by color. In each model, the OLS regression line, calculated independently of the manufacturer, is shown. The corresponding intercepts, estimates, and R^2 values with 95% confidence intervals are provided in Table 5.8. Across all thickness-specific models as well as the aggregated model, the predictor surface stress contributed significantly to explaining the dependent variable bending stress.

Regression models of 4 mm, 10 mm, and 12 mm glass thicknesses showed little manufacturer

Table 5.8: Statistical details of intercept, estimates, and R^2 with 95% confidence intervals for the linear regression model Bending stress ~ Surface stress of standard-size specimens divided by glass thickness with sample size

t [mm]	n	Intercept + CI	Estimate + CI	R^2 + CI
4 *	49	93.88 [84.72, 105.07]	0.64 [0.52, 0.75]	0.680 [0.459, 0.778]
6 *	48	81.83 [67.27, 94.13]	0.89 [0.71, 1.12]	0.671 [0.550, 0.760]
8 *	46	70.12 [51.49, 84.99]	1.02 [0.85, 1.27]	0.766 [0.589, 0.846]
10 *	25	89.31 [73.96, 103.04]	0.82 [0.67, 1.01]	0.817 [0.647, 0.879]
12 *	24	83.86 [68.83, 100.78]	0.89 [0.67, 1.06]	0.847 [0.698, 0.921]
4–12 *	192	82.12 [75.08, 88.06]	0.87 [0.79, 0.97]	0.729 [0.658, 0.778]

* Predictor statistically significant based on bootstrap confidence intervals

influence. In contrast, the 6 mm and 8 mm thicknesses, especially for manufacturer B, exhibited greater deviations from the regression line. Consequently, the poorest prediction of bending stress by surface stress was observed for the 6 mm model with $R^2 = 0.671$ [0.550, 0.760].

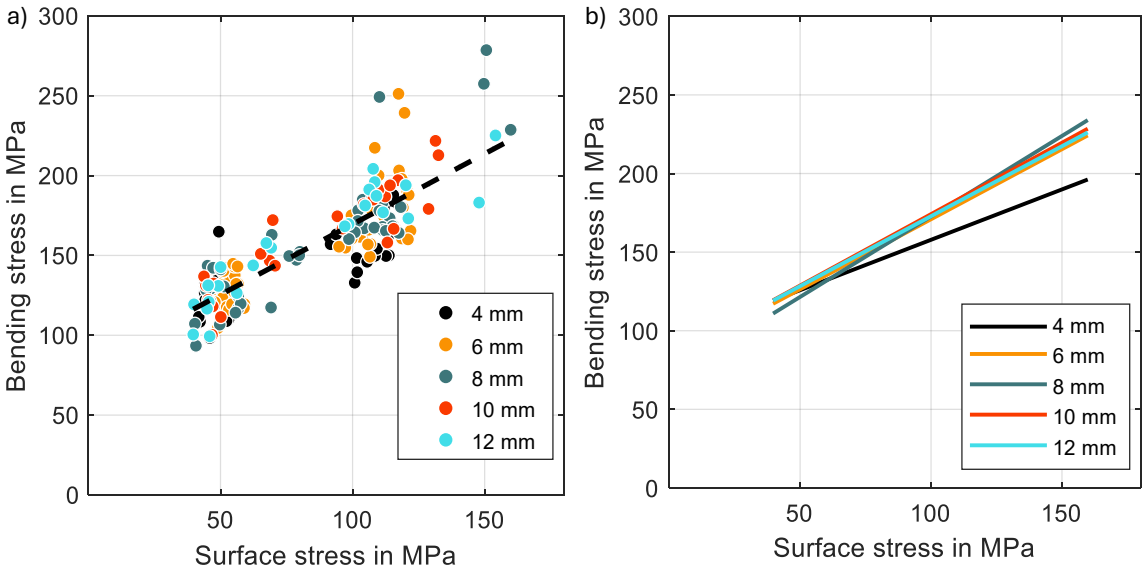

Figure 5.33: Comparison of ordinary least squares regression Bending stress ~ Surface stress of standard-size specimens for different glass thicknesses (a-e), manufacturers are distinguished by color

Fig. 5.34a presents a scatter plot of surface stress relative to bending stress for all glass thicknesses. The OLS regression, performed independently of manufacturer and glass thickness, yielded a high R^2 of 0.729 [0.658, 0.778]. Additionally, the data points were color-coded by glass thickness to facilitate interpretation of the interaction plot shown in Fig. 5.34b. No clear trend with respect to glass thickness could be identified, a finding that aligned with the outcomes of the moderation analysis. The moderator glass thickness, as revealed by contrast analysis, indicated that only the 4 mm thickness differed significantly from the 6 mm and 8 mm thicknesses. The explained variance of the interaction model was 0.747 [0.669, 0.788], representing a slight improvement over the OLS regression model.

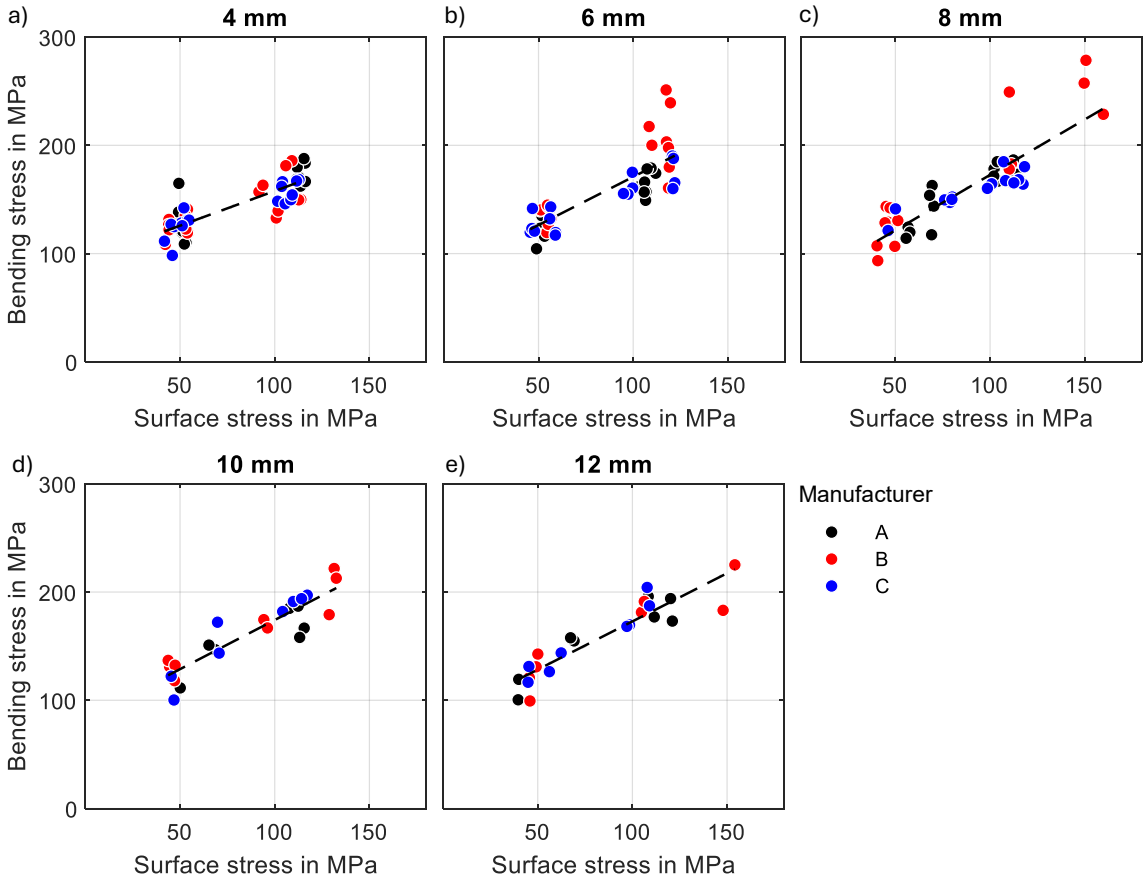

Figure 5.34: Bending stress ∼ Surface stress: a) OLS regression color-coded by glass thickness and b) interaction plot illustrating the moderating effect of glass thickness, for standard-size specimens

5.5.5.5 Bending stress ∼ Edge stress (MWP)

The OLS regressions of the relationship between bending stress and edge stress determined by MWP were computed separately for each glass thickness. The thickness-specific scatter plots, in which the three manufacturers are color-coded, along with the regression lines calculated independently of the manufacturer, are shown in Fig. 5.35. The statistical details are listed in Table 5.9.

Notably, for the 6 mm thickness, the specimens of manufacturer A exhibited a pronounced deviation from the overall trend. Due to the lack of 6 mm HSG specimens in the available dataset, the regression analysis for the 6 mm glass thickness could not reliably characterize the relationship between bending stress and edge stress determined by MWP. In fact, the data points from manufacturer A even indicated a negative slope, which substantially weakened the model fit and results in a low R^2 value of 0.349 [0.159, 0.526] for the 6 mm model that includes all three manufacturers. Nevertheless, all models were statistically significant. The remaining thickness-specific models showed higher R^2 values, up to a maximum of 0.747 [0.659, 0.813] for the 8 mm model with only minor manufacturer-related scatter.

Table 5.9: Statistical details of intercept, estimates, and R^2 with 95% confidence intervals for the linear regression model Bending stress ∼ Edge stress (determined by multiple-wavelength photoelasticity) of standard-size specimens, divided by glass thickness with sample size

t [mm]	n	Intercept + CI	Estimate + CI	R^2 + CI
6 *	57	51.92 [-6.60, 98.03]	1.33 [0.81, 1.98]	0.349 [0.159, 0.526]
8 *	104	30.38 [12.72, 47.76]	1.69 [1.45, 1.93]	0.747 [0.659, 0.813]
10 *	55	-11.77 [-41.89, 20.68]	2.15 [1.77, 2.50]	0.676 [0.544, 0.765]
12 *	52	-18.92 [-66.42, 36.59]	2.31 [1.69, 2.90]	0.649 [0.469, 0.774]
6–12 *	268	26.79 [12.60, 40.24]	1.69 [1.52, 1.87]	0.652 [0.588, 0.708]

* Predictor statistically significant based on bootstrap confidence intervals

The regression model including all glass thicknesses yielded an R^2 of 0.652 [0.588, 0.708] and is displayed with its regression line in the scatter plot in Fig. 5.36a. The color-coding facilitated the interpretation of the interaction plot from the moderation analysis, where glass thickness was the moderator. The thickness-specific regression lines are shown in Fig. 5.36b. The models of 10 mm and 12 mm thicknesses exhibited very similar slopes and differed only slightly by vertical shift.

Overall, the following glass-thickness-dependent behavior could be observed: with increasing thickness, the influence of the predictor variable edge stress on the dependent variable bending stress increased. The regression lines for the individual thicknesses intersected in the range of approximately 56 MPa to 89 MPa, driven by the steeper slopes of the 6 mm and 8 mm thickness lines. In the higher edge stress range, associated with TTG, the regression lines were arranged in ascending order according to thickness. Due to the intersection, the arrangement in the HSG range was approximately reversed. Including glass thickness as a moderator increased the R^2 to 0.682 [0.599, 0.729] for the relationship between edge stress (determined by MWP) and bending stress.

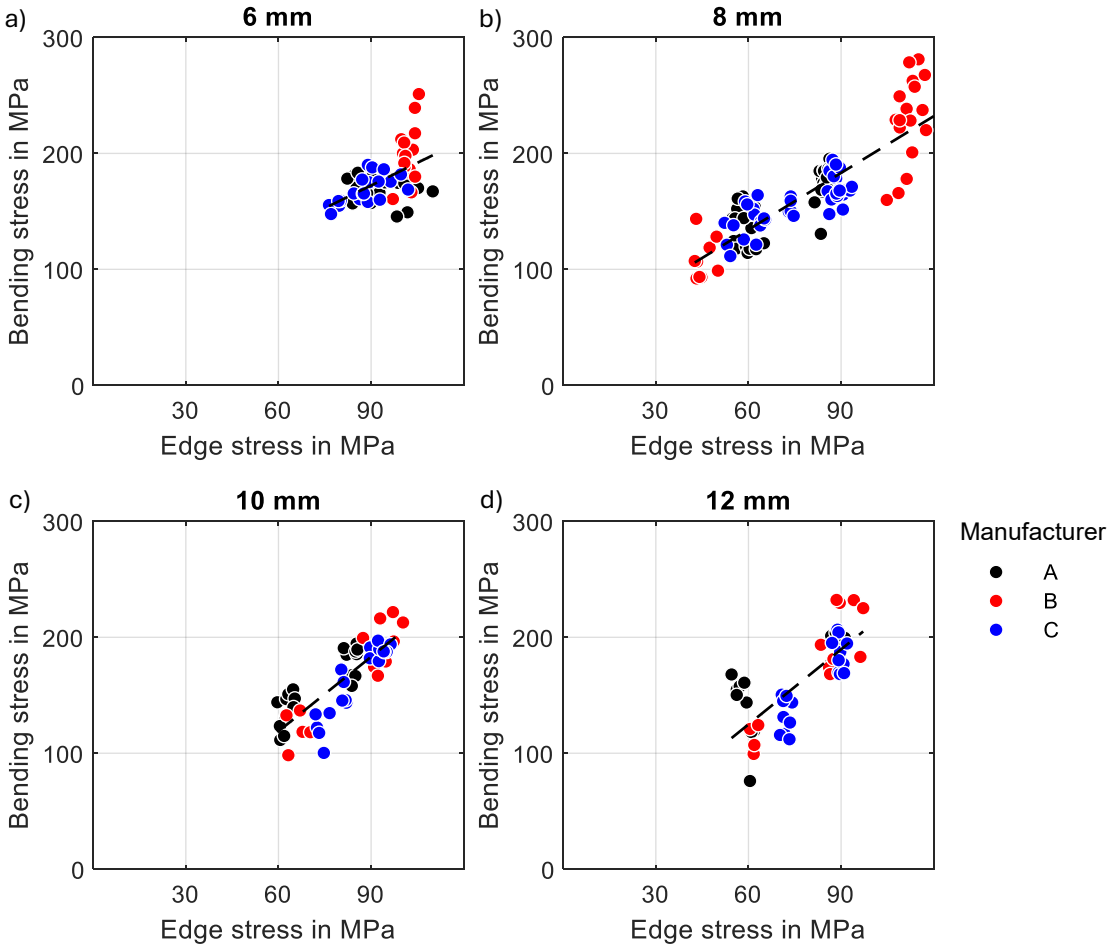

Figure 5.35: Comparison of OLS regression Bending Stress ∼ Edge stress (determined by multiple-wavelength photoelasticity) of standard-size specimens for different glass thicknesses (a-d), manufacturers are distinguished by color

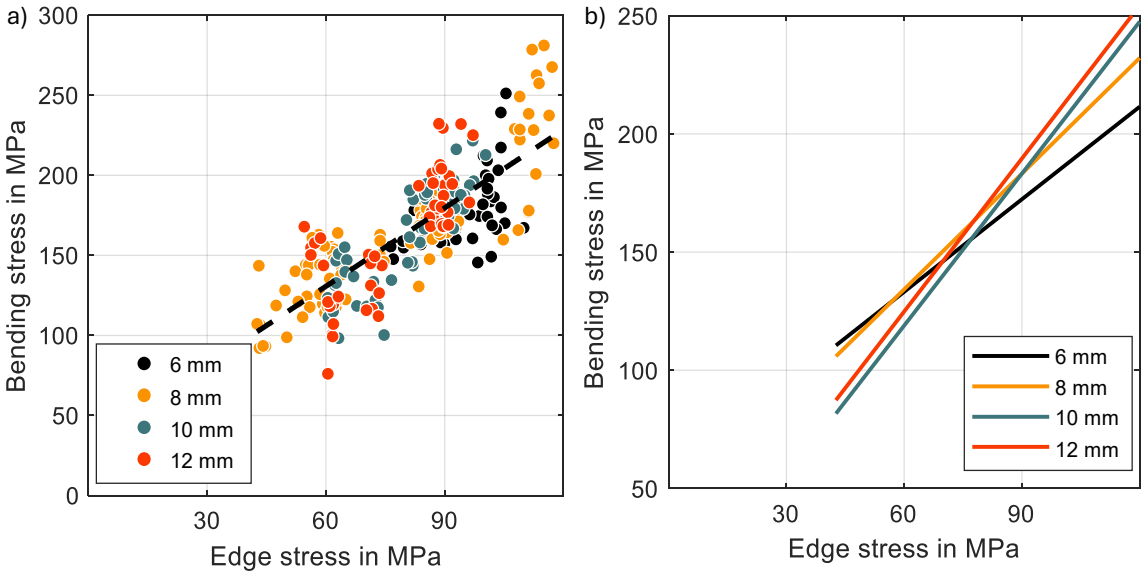

Figure 5.36: Bending stress ∼ Edge stress (determined by multiple-wavelength photoelasticity): a) ordinary least squares regression color-coded by glass thickness and b) interaction plot illustrating the moderating effect of glass thickness, for standard-size specimens

5.5.5.6 Bending stress ∼ Edge stress (PST)

For the relationship between bending stress and edge stress measured by PST, the influence of the manufacturer could not be assessed, as the specimens analyzed originated from only one manufacturer. Nevertheless, OLS regression models were calculated for each glass thickness, which are shown as scatter plots with regression lines in Fig. 5.37. The corresponding intercepts, estimates, and R^2 values with 95% confidence intervals derived from bootstrapping are presented in Table 5.10. The model of 10 mm thickness showed a high R^2 of 0.751 [0.494, 0.876]. The poorest model fit was observed for the 12 mm model, where the HSG specimens with values between 54 to 62 MPa edge stress exhibited a wide range of measured bending stresses, spanning from 76 MPa to 167 MPa. All thickness-specific models were statistically significant.

Table 5.10: Statistical details of intercept, estimates, and R^2 with 95% confidence intervals for the linear regression model: Bending stress ∼ Edge stress (determined by phase-shifting technique) of standard-size specimens, divided by glass thickness with sample size

t [mm]	n	Intercept + CI	Estimate + CI	R^2 + CI
6 *	39	46.99 [27.57, 69.42]	1.39 [1.11, 1.64]	0.726 [0.584, 0.811]
8 *	37	49.22 [19.77, 80.77]	1.49 [1.05, 1.88]	0.572 [0.348, 0.725]
10 *	19	13.25 [-24.51, 59.29]	2.08 [1.37, 2.61]	0.751 [0.494, 0.876]
12 *	20	-2.55 [-75.98, 52.64]	2.31 [1.62, 3.22]	0.668 [0.498, 0.791]
6–12 *	115	39.53 [20.97, 56.96]	1.61 [1.38, 1.86]	0.604 [0.518, 0.674]

* Predictor statistically significant based on bootstrap confidence intervals

The OLS regression model including glass thickness ranging from 6 to 12 mm was shown

in the scatter plot with the regression line in Fig. 5.38a. Results showed a moderate R^2 of 0.604 [0.518, 0.674]. The color-coding of glass thickness in Fig. 5.38a did not suggest a strong effect of thickness. However, the moderation analysis increased the R^2 to 0.666 [0.536, 0.721].

Similar to the regression model of bending stress and edge stress determined by MWP, described in Section 5.5.5.5, a comparable glass-thickness-dependent behavior could be observed for the TTG specimens: as glass thickness increases, the slopes of the individual regression lines also increased. Thus, the influence of edge stress on bending stress grew with thickness. Unlike Section 5.5.5.5, however, the intersection of the regression lines occurred in the lower range of HSG.

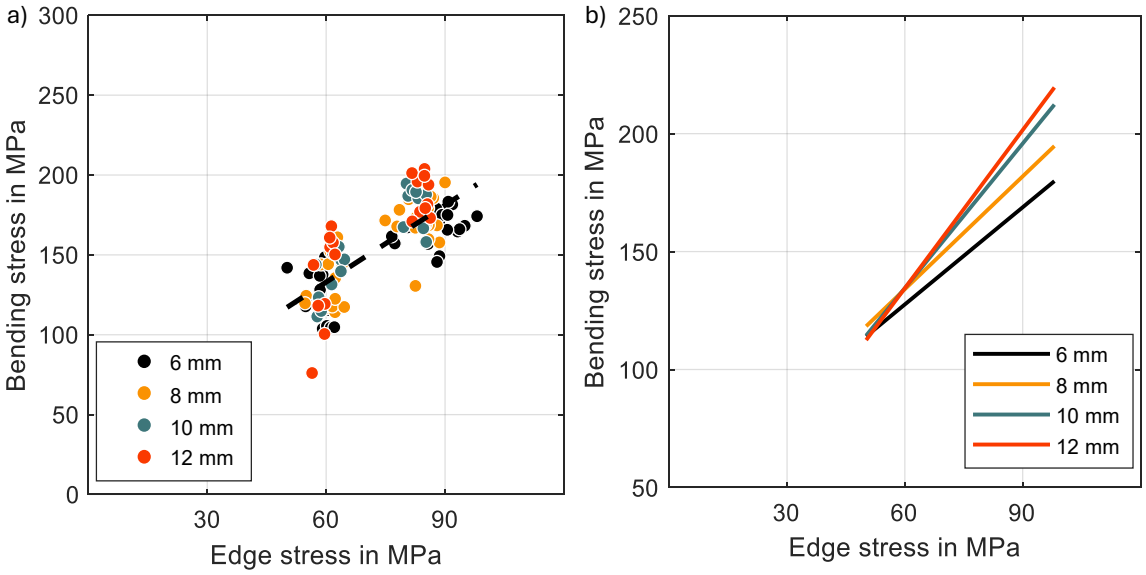

Figure 5.37: Comparison of ordinary least squares regression Bending Stress ~ Edge stress (determined by phase-shifting technique) of standard-size specimens for different glass thicknesses (a-d)

5.5.5.7 Comparison of moderation analysis

The moderation analyses presented in previous Sections 5.5.5.2 to 5.5.5.6 examined the explanatory performance of photoelastic values in relation to the destructive test results with nominal glass thickness considered as a moderating variable. For each of the five relationships including all glass thicknesses, the R^2 values obtained from the simple linear OLS regressions and the adjusted R^2 values derived from the corresponding moderation models are summarized in Table 5.11.

The comparison of the predictive performance of the linear regression and moderation models was performed using the analysis of variance *anova()* function in R (R Core Team 2024) from package *stats* (version 4.4.1). This model comparison statistically evaluates whether a more complex model, here the moderation model including the interaction term, offers a significantly improved fit to the data compared to a simpler model. This is tested by comparing the reduction in residual sum of squares, accounting for the additional

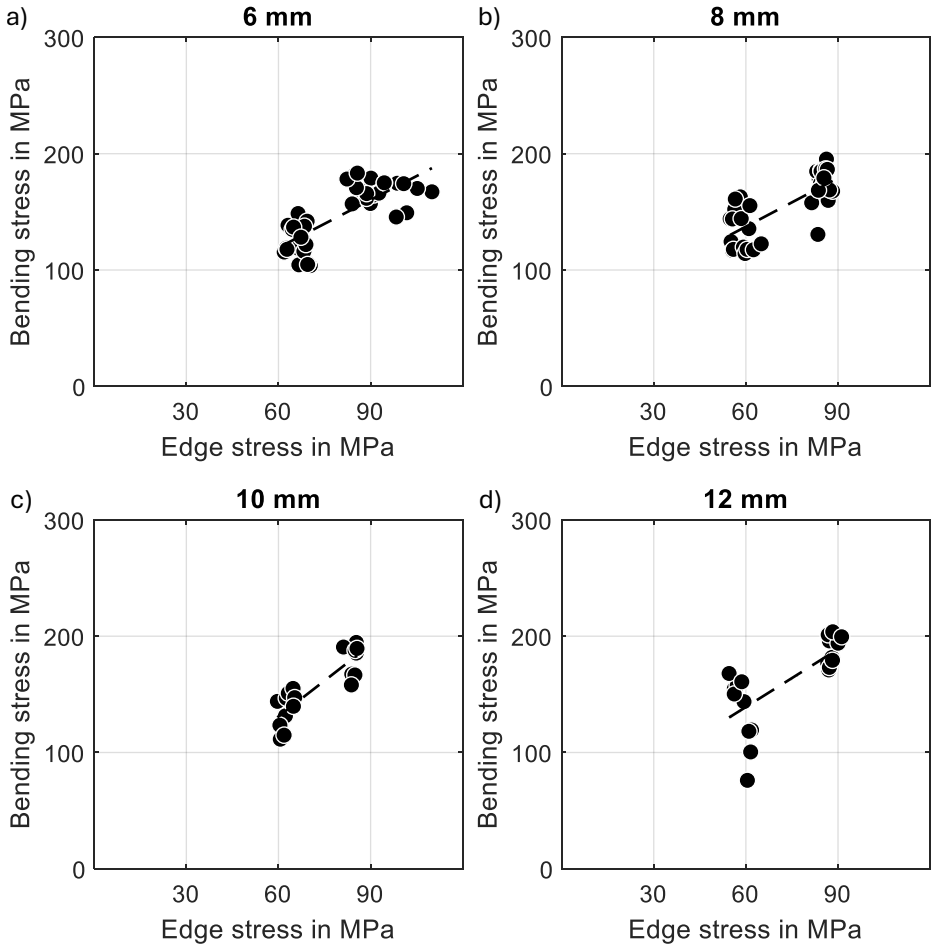

Figure 5.38: Bending stress ∼ Edge stress (determined by phase-shifting technique): a) ordinary least squares regression color-coded by glass thickness and b) interaction plot illustrating the moderating effect of glass thickness, for standard-size specimens

degrees of freedom introduced by the interaction. A significant result indicates that the moderation model explains significantly more variance than the simple OLS model.

The comparisons *anova(linear regression model, moderation model)* showed significant improvements for all relationships when glass thickness was included as a moderator. However, the magnitude of improvement varied across the relationships. Therefore, Table 5.11 also reports the ΔR^2, representing the increase in explained variance attributable to the moderation effect.

The corresponding complete contrast analysis of the different glass thickness categories is presented in Table 5.12. This analysis lists all pairwise comparisons of glass thickness and indicates which thickness as moderator differed significantly from one another. As previously described, this was performed by repeatedly estimating the moderation model while rotating the reference category. The 95% confidence intervals of the moderation models were then compared, which are listed in Table A.4 to Table A.8 in Appendix. If a particular glass thickness showed no overlap in the confidence intervals, it was assumed that there was a consistently significant difference from all other thickness categories. This

is reported in Table 5.11 in the column titled "Thickness effect".

Table 5.11: Comparison of R^2 with 95% confidence intervals for ordinary least squares regression and moderation analysis of standard-size specimens with glass thickness as moderator

Relation	R^2 (OLS) + CI	adj.R^2 (Mod) + CI	ΔR^2	Thickness effect*
Fragments ∼ Surface stress	60.716 [0.647, 0.774]	0.874 [0.830, 0.903]	+0.158	4 mm, 6 mm
Fragments ∼ Edge stress (MWP)	0.347 [0.180, 0.481]	0.407 [0.255, 0.512]	+0.060	12 mm
Bending stress ∼ Surface stress	0.729 [0.658, 0.778]	0.747 [0.669, 0.788]	+0.018	No clear trend
Bending stress ∼ Edge stress (MWP)	0.652 [0.588, 0.708]	0.682 [0.599, 0.729]	+0.030	No clear trend
Bending stress ∼ Edge stress (PST)	0.604 [0.518, 0.674]	0.666 [0.536, 0.721]	+0.062	No clear trend

* Statistically significant distinct effect of glass thickness

The contrast analysis for the relationship *Fragments ∼ Surface stress ∗ Glass thickness* showed that, although several pairwise combinations differ significantly, the 4 mm and 6 mm thicknesses differed not only from all other thicknesses but also from each other. In addition, with a ΔR^2 of +0.158, this relationship benefitted the most from including glass thickness as a moderator. Because the 95% confidence intervals of the R^2 (OLS) and the adjusted R^2 from the moderation model did not overlap, a clear and substantial moderating effect of glass thickness could be confirmed.

For the model *Fragments ∼ Edge stress (MWP) ∗ Glass thickness*, the 12 mm thickness clearly differed from the other thicknesses regarding the effect of edge stress on fragment count. However, the R^2 values from the OLS and moderation models did not show a distinct separation. Thus, the moderating role of glass thickness could not be considered as strong.

Table 5.12: Overview of all significant pairwise contrasts of glass thicknesses for moderation analysis of standard-size specimens, indicating statistically significant differences, based on 95% confidence intervals indicated in Table A.4 to Table A.8 in Appendix

Glass thickness [mm]	4 vs. 6	4 vs. 8	4 vs. 10	4 vs. 12	6 vs. 8	6 vs. 10	6 vs. 12	8 vs. 10	8 vs. 12	10 vs. 12
Fragments ∼ Surface stress	✓	✓	✓	✓	✓	✓	✓	-	✓	-
Fragments ∼ Edge stress (MWP)	N/A	N/A	N/A	N/A	-	-	✓	-	✓	✓
Bending stress ∼ Surface stress	✓	✓	-	-	-	-	-	-	-	-
Bending stress ∼ Edge stress (MWP)	N/A	N/A	N/A	N/A	-	✓	✓	-	-	-
Bending stress ∼ Edge stress (PST)	N/A	N/A	N/A	N/A	-	-	✓	-	✓	-

For the remaining moderation models *Bending stress ∼ Surface stress*, *Bending stress ∼ Edge stress (MWP)*, and *Bending stress ∼ Edge stress (PST)*, several significant pairwise

differences between individual thickness combinations were identified, as summarized in Table 5.12. However, these differences did not follow a systematic or consistent pattern across thickness levels. Accordingly, no clear thickness-dependent trend could be inferred for these relationships which are labeled as "no clear trend" in Table 5.11. For these models, although the inclusion of glass thickness as a moderator led to only a modest increase in explained variance, with the largest improvement observed for the relationship *Bending stress ~ Edge stress (PST)* amounting to $\Delta R^2 = 0.062$. The 95% confidence intervals of the R^2 (OLS) and the adjusted R^2 from the corresponding moderation models overlapped in all three cases. Taken together, these results indicate that the observed differences were not sufficiently systematic to support a meaningful moderating effect of glass thickness.

In the interaction plots, a further difference in the behavior of the photoelastic measurements with respect to the destructive test results was observed. In the model *Fragments ~ Surface stress,* the thinner glass thicknesses showed steeper regression slopes than the thicker ones. This means that thin glass responded more sensitively to changes in surface stress: even a moderate increase in surface stress led to a large increase in the number of fragments, whereas a decrease in surface stress resulted in a rapid loss of fragmentation fineness due to the position of the regression lines. This effect is likely related to the higher process sensitivity of thin glass during thermal tempering. Thin glass develops more easily variations in cooling rate and stress distribution across the thickness, which amplifies the influence of surface stress changes on the resulting fracture pattern.

In contrast, the regression model *Bending stress ~ Surface stress* showed the opposite trend. In particular, the 4 mm glass exhibited a flatter slope and the position of its regression line indicated that it could not reach bending stresses as high as those of the thicker glass types. This suggests that increases in surface stress in thin glass were only partially translated into higher bending stresses. Thicker glass, on the other hand, exhibited steeper regression slopes, meaning that identical changes in surface stress were more strongly reflected in bending stress.

This pattern was also observed in the regression models *Bending stress ~ Edge stress* for both measurement methods: with increasing glass thickness, the regression slopes became steeper and the vertical arrangement of the lines showed a thickness-dependent behavior, at least in the TTG range.

5.6 Relation between edge stress and surface stress

As described in Section 5.5.4 for the relationship between destructive and non-destructive measurements, a Pearson correlation analysis with bootstrapping (2000 resamples) was also performed for analyzing the relation between edge stress and surface stress. The relationship between edge stress and surface stress exhibited a significant, very strong positive correlation for both measurement methods, MWP and PST, with correlation coefficients of r = 0.875 (MWP) and r = 0.941 (PST). The narrow 95% confidence intervals for MWP [0.854, 0.898] and PST [0.918, 0.966] indicated high precision in the estimated correlation coefficients and reflected the low variability within the datasets.

Surface stress measurements are widely established in both research and industry. Therefore, to illustrate the relationship between the two photoelastic measurements surface stress and edge stress obtained on the same specimen, the surface stress is placed on the x-axis in

Fig. 5.39 for the edge stress measurement methods (a) PST and (b) MWP. The coloring of the data points differentiates between the conformity of the glass products HSG and TTG, providing additional insight into how the glass type influences the relationship of both residual stresses.

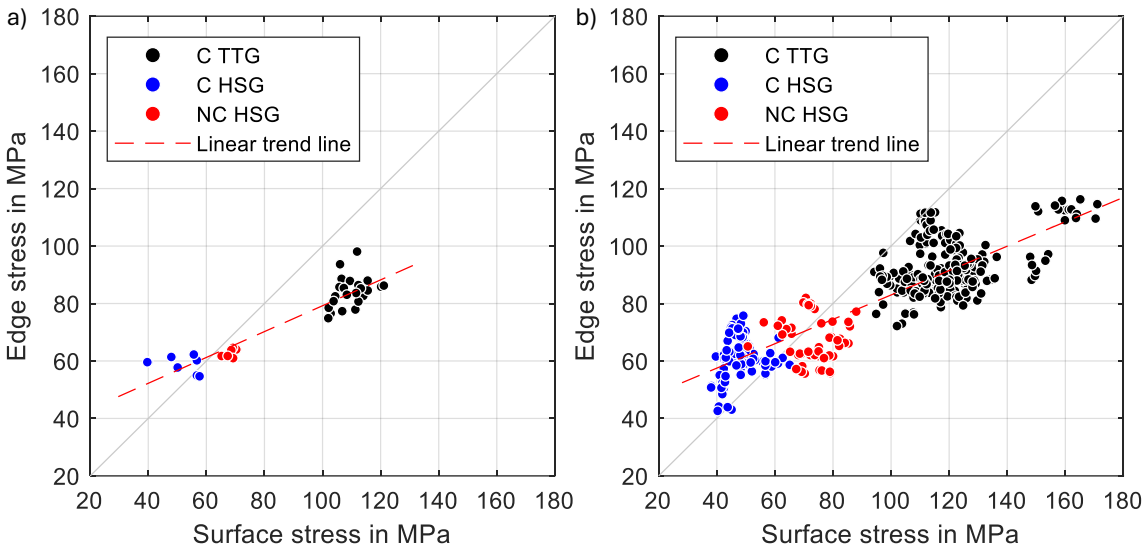

Figure 5.39: Relation between surface stress and edge stress determined by a) phase-shifting technique and b) multiple-wavelength photoelasticity, for standard-size specimens

The axis limits were chosen to be identical, which allows Fig. 5.39b to show that the surface stress covered a wider range from 38 MPa to 171 MPa, while the edge stress spanned a narrower interval from 42 MPa to 116 MPa for the MWP method. When examining conformity from the perspective of the x-axis, a good separation could be observed based on the surface stress measurements. In contrast, when conformity was evaluated by edge stress measurement using MWP along the y-axis, no distinct separation, particularly between NC and C HSG, could be identified. The reference line with a slope of 1, drawn in both diagrams in Fig. 5.39, further illustrates that the two photoelastic stress variables did not exhibit a one-to-one relationship, contrary to what has been suggested by Aben et al. (2015).

A linear trend line based on an OLS regression was also added to the diagrams to illustrate the relationship between surface stress and edge stress. The slope of this regression line was similar with 0.42 for MWP and 0.45 for PST. It could be observed that the intersection point between the reference line with slope 1 and the regression line laid within the range of the NC HSG specimens. Furthermore, the following observations could be made for the conforming glass products TTG and HSG: almost all C HSG specimens laid above the reference line with slope 1, whereas the C TTG specimens laid below this line. This indicates that the HSG specimens exhibited higher edge stress values than surface stress values, whereas for the TTG specimens, the opposite pattern was observed, with surface stress values exceeding edge stress values. The NC HSG specimens evaluated with the MWP method in Fig. 5.39b were located both above and below the 1:1 reference line, with the majority lying below the line. This behavior was also observed in Fig. 5.39a for the PST method.

To enable a potential conversion from surface stress to edge stress, the ratio of edge stress

to surface stress was calculated for each specimen. These resulting factors are presented in Fig. 5.40 for (a) PST and (b) MWP, depending on the glass thickness and with color-coding to distinguish conformity.

For the TTG specimens, a slight decrease in the factor could be observed with increasing glass thickness. The median decreased from 0.82 for 6 mm to 0.73 for 12 mm for the edge stress values determined by MWP. The specimens measured by PST showed a very similar trend with median factors decreasing from 0.81 for 6 mm to 0.73 for 12 mm TTG. For both methods, the factors for TTG exhibited IQR than those of the HSG specimens, although several outliers were visible for the glass thicknesses of 8 mm and 10 mm.

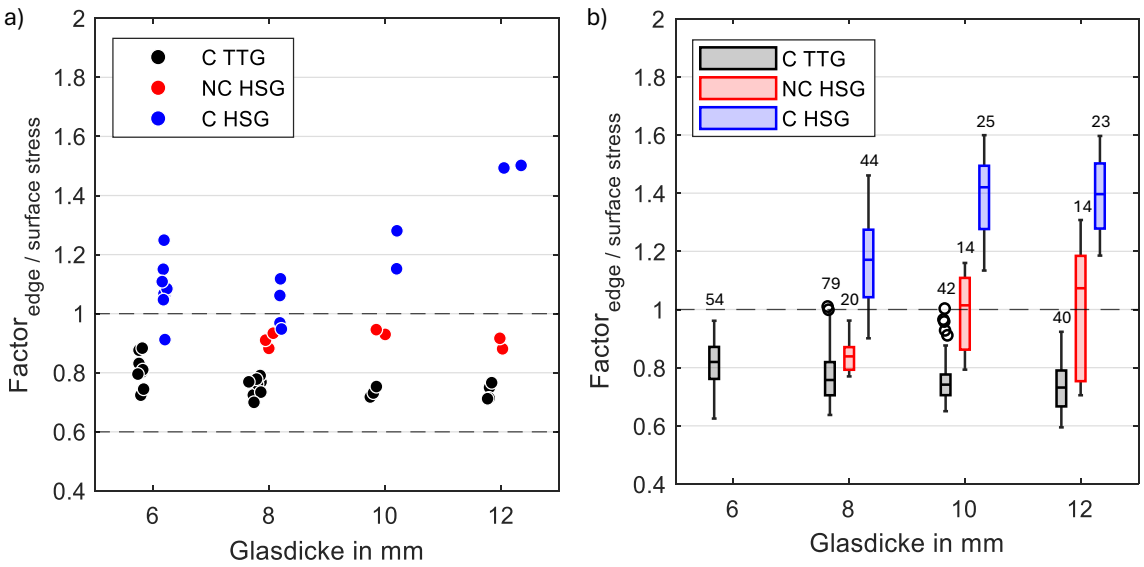

Figure 5.40: Factors from surface stress to edge stress determined by a) phase-shifting technique and b) multiple-wavelength photoelasticity, per standard-size specimen

For the HSG specimens evaluated using MWP, an increasing trend of the factors with increasing glass thickness was observed. A similar behavior was seen for HSG measured by PST starting from a glass thickness of 8 mm, whereas the 6 mm specimens showed a higher median of 1.08 compared to 1.02 for the 8 mm specimens. However, the edge stress measurement methods differed considerably with respect to the median values for the HSG specimens. PST yielded a median factor of 1.50 for 12 mm, which was based on only two data points, while MWP resulted in a factor of 1.40, which was close to the value of 1.42 obtained for the 10 mm specimens. PST, in contrast, yielded a lower value of 1.22 for the 10 mm specimens.

Averaged over glass thickness, an approximate conversion factor of 1.21 could be derived for HSG and 0.77 for TTG, although the spread of values was considerable. In summary, edge stress and surface stress measurements showed a strong, significant correlation. However, the relationship between edge stress and surface stress differed for TTG and HSG. As a general guideline, surface stress was typically higher than edge stress in TTG, whereas the opposite pattern was observed for HSG.

5.7 Summary and conclusions

This chapter presented the test results performed on standard-size specimens in dimensions of 360 mm x 1100 mm with glass thicknesses ranging from 4 mm to 12 mm and various pre-stress levels, produced by three manufacturers within the framework of the research project NEMA (Efferz et al. 2025a). The destructive tests were conducted in accordance with the European product standards EN 12150-1 (2020) for TTG and EN 1863-1 (2012) for HSG. This allowed for the classification of specimens based on their mechanical performance in bending strength and fracture pattern.

Four conformity categories were defined: specimens tempered according to heating and cooling parameters for TTG and fulfilling the requirements of EN 12150-1 (2020) were classified as conforming TTG, while those not meeting the fracture pattern and bending strength requirements were classified as non-conforming TTG. Similarly, for HSG, specimens were classified as conforming HSG if they fulfilled the requirements of EN 1863-1 (2012), and non-conforming HSG if they exhibited an inadequately fine fracture pattern.

Prior to destructive testing, non-destructive photoelastic measurements were conducted on the specimens' surfaces and edges. Surface compressive stress was measured at three distributed points across the surface using the SCALP-05 device (GlasStress Ltd. 2013), and the mean value of σ_1 of these points was used for further analysis. The results of the surface stress measurements demonstrated a clear ability to distinguish between conforming TTG and conforming HSG specimens across all glass thicknesses. However, this differentiation was not possible for separating non-conforming HSG from conforming HSG when considering all thicknesses collectively. When analyzed separately by glass thickness, a marginal but non-overlapping distinction between NC and C HSG specimens could be made. For the only NC TTG series with a glass thickness of 4 mm, there was overlap with the C TTG specimens, indicating that the surface stress measurement could not reliably distinguish between these groups in this case.

To assess the homogeneity of pre-stressing across the surface, two metrics were used: the standard deviation of the three measurement points and the principal stress difference σ_1–σ_2. The measurement points exhibited low standard deviations below 10 MPa, and the principal stress differences were also mostly under 10 MPa, with some outliers reaching approximately 18 MPa.

Edge stress measurements were performed on specimens with $t \geq 6$ mm using two devices. While specimens from all three manufacturers were scanned with the LineScanner by Softsolution GmbH (2023b) using the MWP method, a subset of specimens from one manufacturer was measured with the StrainScope Flex by ilis gmbh (2023) using the PST method. For each specimen, six measurement areas were evaluated and subsequently averaged to a single value per pane for further analysis.

Regarding the distinction of conformity based on edge stress measurements, the PST method demonstrated clear advantages. PST measurements showed less variability within the test series than the MWP measurements. Additionally, edge stress values measured by PST enabled a clear differentiation between the two conforming glass types, TTG and HSG, whereas differentiation based on MWP edge stress was less pronounced. For MWP, only values above 82 MPa consistently indicated conforming TTG. When considering individual glass thicknesses, differentiation between conforming and non-conforming HSG based on

PST edge stress values was possible but very narrow. In contrast, MWP edge stress values exhibited substantial overlap, with some non-conforming HSG specimens showing lower edge stress values than conforming HSG specimens.

The homogeneity of pre-stress at the edge was evaluated by the standard deviation of the six measurement points. Here, the MWP method showed greater variability, especially for 6 mm TTG specimens, with a range up to approximately 18 MPa. Other specimens mostly showed standard deviations below 10 MPa. Specimens measured with PST had standard deviations mostly below 5 MPa, except for 6 mm TTG specimens, which reached a maximum of 9 MPa. Furthermore, it was found that the standard deviation of the measurement points did not influence the conformity classification of the glass panes.

The width of the pre-stress zone at the edge was evaluated using the position of the 0th isochromatic order. The analysis revealed that the zone width does not follow a consistent pattern with respect to glass thickness. Generally, HSG tends to have a wider pre-stress zone than TTG, but the reference values reported by Laufs (2000) could not be confirmed. For TTG, zone width factors of approximately 0.68 t were determined for glass thicknesses from 6 to 10 mm valid for both measurement methods, while for 12 mm TTG, a factor of 1.03 t was found. For HSG specimens with glass thicknesses between 6 and 10 mm, the mean zone width factors differ between the two measurement methods. For 12 mm glass, zone widths measured by HSG and PST methods are nearly indistinguishable. Therefore, using width of the pre-stress zone at the edge to reliably differentiate between TTG and HSG or to identify non-conforming HSG specimens is not clearly feasible.

To assess reproducibility in measuring edge stress, a subset of specimens was measured twice using the MWP device, with the second measurement taken after rotating the specimens by 180 degrees. The results reveal clear thickness-dependent behavior: for glass thicknesses between 8 and 12 mm, the results of the initial and repeat scans show excellent agreement with only minor deviations. This indicates that, for these thicknesses, the MWP method provides a stable and robust measurement of edge stress. In contrast, the 6 mm TTG specimens exhibit noticeably larger differences between the initial and repeat scans.

The correlation between the photoelastic and destructive tests was analyzed with the Pearson correlation analysis in combination with a bootstrapping method: all the investigated correlations were significant. The comparison of the 95% confidence intervals showed that the relationship between *Number of fragments vs. Surface stress* has a significantly higher correlation coefficient than *Number of fragments vs. Edge stress.* On the other hand, for the relations involving bending stress, no clear advantage of the photoelastic measurement can be identified due to overlapping 95% confidence intervals.

The predictor variables of the photoelastic measurements included in the regression models were significant for analyses based on the entire dataset as well as for models stratified by glass thickness, except for the 6 mm model for *Number of fragments* $\sim$ *Edge stress (MWP).* While the cluster analysis did not reveal any manufacturer-related structure due to low ICC values (< 0.1), the separation by individual glass thickness indicated manufacturer influences for some relations. Notably, for the 4 mm specimens in the relation *Number of fragments* $\sim$ *Surface stress*, a clear manufacturer effect was observed: individual manufacturers exhibited steeper regression slopes that were not captured by the overall regression line for the full 4 mm dataset. Nonetheless, despite these manufacturer-specific differences observed in some subsets, the overall influence of the manufacturer on the relationships examined appears limited and does not substantially affect the main

regression results. Therefore, manufacturer effects were considered secondary and not explicitly accounted in the final models.

The conducted moderation analysis revealed significant thickness-dependent relationships between photoelastic measurements and destructive test results. Notably, the number of fragments showed a stronger sensitivity to surface stress changes in thinner glass, indicating that fracture patterns in thin glass are more affected by variations in residual stresses during the tempering process. Conversely, in models predicting bending stress from surface or edge stress, thicker glass specimens exhibited steeper regression slopes, reflecting their higher flexural rigidity. Moderation analysis confirmed that glass thickness significantly influences these relationships, with the strongest effects observed for the relation *Number of fragments* $\sim$ *Surface stress*. In contrast, relations involving edge stress and bending stress showed moderate improvements in explanatory power when thickness was considered, but with overlapping confidence intervals suggesting less distinct differentiation. While moderation by glass thickness improved the model's explained variance in all cases, absolute differences between glass thicknesses were only observed for the relation between *Number of fragments* $\sim$ *Edge stress (MWP)* in the 12 mm specimens as well as for *Number of fragments* $\sim$ *Surface stress* in the 4 mm and 6 mm specimens.

Edge stress and surface stress show a very strong positive correlation for both measuring methods, although the one-to-one relationship from Aben et al. (2015) could not be confirmed. Surface stress spans a wider range and provides clearer separation of conformity. The ratio of edge stress to surface stress differs systematically between glass types. TTG generally shows higher surface stress than edge stress, while HSG exhibits higher edge stress than surface stress.

Based on these results and findings, the following chapter will establish statistical limit values for edge stress and surface stress, which are intended to be used in production control to ensure the mechanical properties of bending strength and fracture pattern.

6 Statistical definition of photoelastic stress limits

The key parameter for the non-destructive quality control of tempered glass is the definition of photoelastic limit values that characterize the conformity of the glass type of TTG and HSG according to the European standards EN 12150-1 (2020) and EN 1863-1 (2012). This chapter employs a statistical approach to ascertain reliable limit values for surface and edge stress measurements using quantile regression models and binary logistic regression models. Furthermore, the necessity of distinct limits based on glass thickness was assessed. Following the implementation of a statistical validation method, a comparative analysis of the limits derived from the various regression models was conducted. Parts of this chapter were pre-published with a reduced database in Efferz et al. (2025c).

6.1 Methodological approach

The procedure for acquiring photoelastic limit values using regression models depends on the glass types of TTG and HSG and is displayed in Fig. 6.1. For the higher pre-stress level TTG according to EN 12150-1 (2020), one lower limit value is required for each photoelastic measurement of surface stress and edge stress. This limit value should comply with both mechanical properties of TTG: the bending strength, which must reach a minimum of 120 MPa, and the characteristic fracture pattern, which is evaluated by counting more than 40 fragments within a 50 mm x 50 mm counting mask placed in the area of the coarsest fracture pattern. Both destructive test results are metric variables, enabling quantile regression analysis. In this case, the results of the photoelastic and destructive tests could be directly related to determining a lower photoelastic stress value.

Conversely, the assessment of the quality of HSG according to EN 1863-1 (2012) necessitates the determination of two photoelastic limit values. The lower stress limit is defined by the bending strength of 70 MPa. Given that bending stress is a metric value, ascertaining a photoelastic limit value using quantile regression model is feasible. The situation is different for assessing the fracture pattern: for HSG, it is essential to ensure that the fracture pattern is sufficiently rough to maintain residual load-bearing capacity. The evaluation of the fracture pattern is based on a visual assessment of the cracks and fragments, as described in Sections 2.1.2.2 and 5.2.2. Therefore, the predicted variable for the fracture pattern conformity is nominal and describes whether HSG conforms or not. Consequently, binary logistic regression can be employed with a nominal variable to ascertain a photoelastic stress limit and differentiate between two categories.

Additionally, it is possible to transform metric variables into nominal. To provide a basis for comparison with quantile regression, logistic regression was also analyzed for TTG. In this case, the categorical variable was determined based on the outcomes of destructive tests.

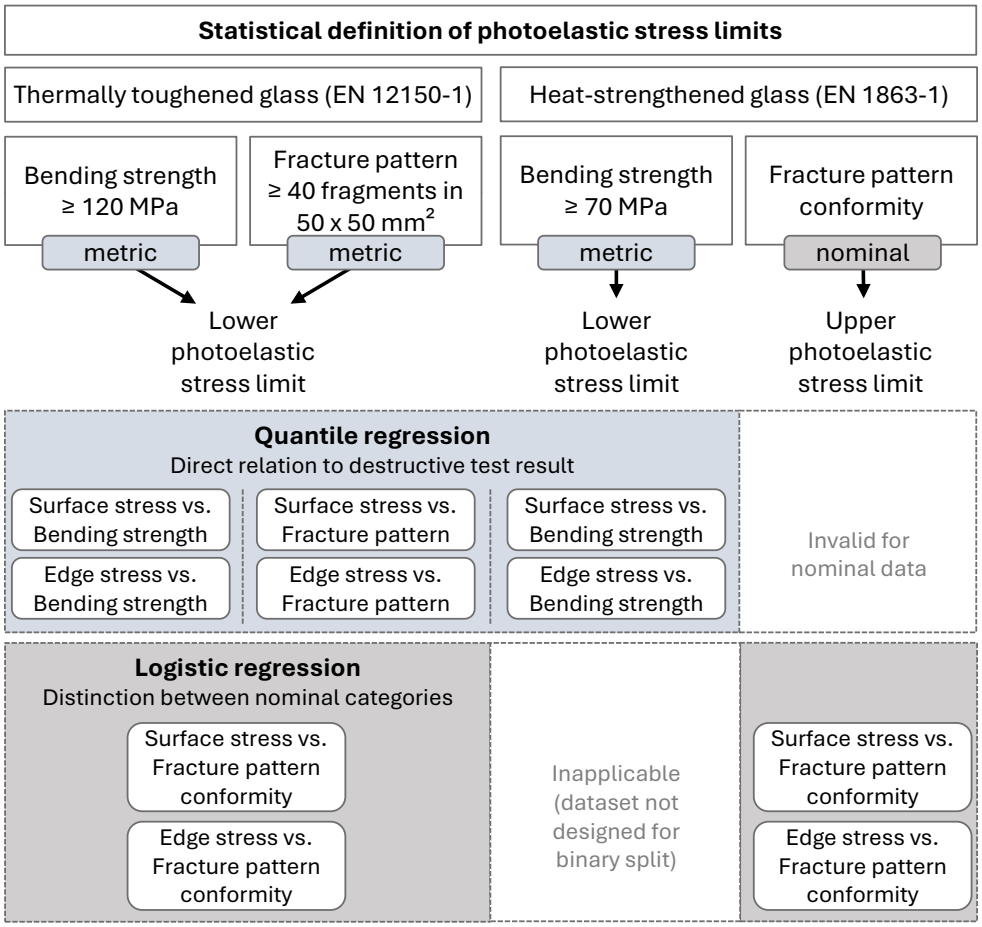

Figure 6.1: Flow chart of the statistical definition of photoelastic stress limits based on destructive tests of bending strength and fracture pattern with differentiation between thermally toughened glass and heat-strengthened glass

The logistic regression models for TTG did not distinguish between bending strength and fracture pattern. Therefore, the dataset was larger due to the integration of both destructive test results into a single predicted variable, which differentiates conformity. For TTG, two quantile (bending stress and fragments) and one logistic (conformity) regression models were analyzed and compared to ascertain lower limit values for each of the photoelastic measurements.

For ascertaining photoelastic limit values for HSG, it is important to note that a single model was applicable to each lower and upper limit for edge and surface stress, respectively. The reason for this is, on the one hand, that logistic regression could not be applied for ascertaining the lower photoelastic limit, as the database was not designed for this purpose: the database contained no specimens that fell below the 70 MPa bending strength criterion. Therefore, it was not possible to divide the data into two binary categories of too low pre-stressed specimens and conforming HSG specimens. On the other hand, quantile regression is not applicable for determining the upper photoelastic stress limit for HSG, because the predicted variable from the destructive test is not metric but nominal.

In the determination of general limit values, a possible influence of the manufacturer was deliberately not included in the analysis. This omission is statistically justified, as

incorporating manufacturer-specific effects would implicitly assume a stable and identifiable manufacturer-related structure in the data. Such a structure, however, was not desirable for the intended purpose. The objective of the limit determination was to derive universally applicable limits that remain valid across different production environments. When the regression models were calculated using the entire database, this could result in overfitting. To validate the model, a k-fold validation, see Section 6.4, was carried out. The results were then compared to the photoelastic stress limit values of the total database in the discussion sections for TTG in Section 6.8 as well as for HSG in Section 6.11.

6.2 Method of quantile regression

Quantile regression was applied to determine the photoelastic stress limits, by focusing on the lower 5% of the response distribution. This method was particularly suitable for determination of limit values, as it captures extreme values rather than relying on the mean, providing a reliable basis for quality and safety control in production. This section delineates the methodology for analyzing the quantile regression models, determining the photoelastic stress limits and investigating the influence of glass thickness using the confidence intervals of the intercept β_0 and predictor variable β_1 of the photoelastic measurement.

6.2.1 Basics

Quantile regression enables the modeling of conditional quantiles of the dependent variable without assuming normally distributed residuals or homoscedasticity (Koenker and Basset 1978, Koenker 2005). In the analysis of quantile regression performed here, the destructive test results of bending stress or number of fragments were the dependent metric variables, which were predicted by the photoelastic tests representing the independent variables of surface or edge stress. The principles of quantile regression are given in Section 2.3.7. In the quantile regression models presented below, the regression line in Equation (6.1) estimates the approximately linear relationship between photoelastic stress and destructive results for the selected quantile.

$$Y_{\text{destr}}\left(\tau = 0.05 \mid X\right) = \beta_0(0.05) + \beta_1(0.05)\, X_{\text{photo}} \tag{6.1}$$

Where as:

Y_{destr}	Prediction of dependent variable of destroying test of bending stress [MPa] or fracture pattern [fragments]
β_0	Coefficient of intercept of bending stress [MPa] or fracture pattern [fragments]
β_1	Coefficient of independent variable [MPa/MPa] or [fragments/MPa]
X_{photo}	Independent variable of photoelastic measurement of surface or edge stress [MPa]

Quantile regression offers distinct advantages over linear regression, particularly when the distributional properties of the response variable are of interest. By specifying a particular quantile level τ, the relationship between the independent and dependent variables could be

examined at a specified quantile τ of the conditional distribution of the response variable. The analysis in this research was conducted with a focus on the 5th percentile with $\tau = 5\%$ to capture the effects of the photoelastic measurement variables of surface stress and edge stress in the lower ranges of the distribution of the destructive measurement metric variable of number of fragments or bending stress. This corresponds to safety considerations in glass processing, where extreme values are of particular importance because EN 1990 (2021) regulates 95% and 5% quantiles for characteristic values. Selecting a higher quantile would shift the focus towards typical behavior rather than the most critical cases and would not represent a conservative approach to safety.

Quantile regression models impose fewer assumptions than OLS regression, making them particularly suitable for data that may exhibit heterogeneity or outliers. An underlying assumption is the independence of observations, which is fulfilled because each glass specimen was tested separately under controlled conditions. Furthermore, the tempering process, represented through edge and surface stress, was explicitly included in the regression model as a predictor to account for its direct influence on the measured mechanical properties.

Additionally, the assumption underlying quantile regression models is an approximately linear relationship between the utilized variables. The linearity between the photoelastic stress and the destructive test results can be visually assessed in the scatter diagrams provided in the respective sections of the quantile regression models. Previous studies, e.g., Anton et al. (2012), Mognato et al. (2019), Pourmoghaddam and Schneider (2018b), have also demonstrated an approximately linear relationship between surface stress and the number of fragments, as well as between surface stress and bending stress. Even in cases where linearity appeared imperfect visually, the use of linear quantile regression was justified, because this method focuses on estimation of limits. More complex non-linear models would complicate the interpretation and provide no substantial benefit in the relevant lower quantile range for determining photoelastic stress limits. Furthermore, the application of bootstrapping allowed for robust inference and the generation of confidence intervals for the regression coefficients, mitigating potential instability in the estimates (Buchinsky 1998).

The quantile regression analyses were carried out using the *rq()* function from the package *quantreg* (version 6.1) in R (R Core Team 2024).

6.2.2 Quantifying limit values via quantile regression

The quantile regression models allowed the calculation of lower limits for the photoelastic measured variables of edge stress and surface stress using the Equation (6.1) of the regression line. The visual procedure is exemplary shown in Fig. 6.2 where the datapoints of the photoelastic measurement with the corresponding destructive test results are plotted. In addition to the regression line derived from the quantile regression model, the required value for the destructive test (see Table 6.1) of bending strength (120 MPa for TTG or 70 MPa for HSG) or number of fragments (40 fragments for TTG) is also plotted as a horizontal red line in the diagram. The subsequent analysis examined the intersection of the quantile regression line and the horizontal destructive criterion, as illustrated in Fig. 6.2. The x-value corresponding to the intersection point was defined as the minimum threshold of the photoelastic variable required to pass the destructive test.

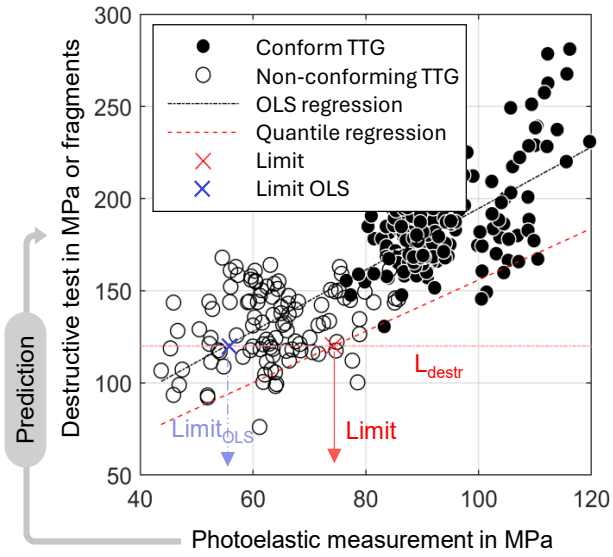

Figure 6.2: Visual determination of the photoelastic stress limit based on quantile regression analysis with comparison of ordinary least squares linear regression, from Efferz et al. (2025c)

After conversion of Equation (6.1), the photoelastic limit could be calculated in mathematical terms as shown in Equation (6.2).

$$Limit = \frac{L_{destr} - \beta_0}{\beta_1} \tag{6.2}$$

Where as:

L_{destr}	Limit of destructive test of bending strength [MPa] or fracture pattern [fragments], see Table 6.1
β_0	Coefficient of intercept of bending stress [MPa] or fracture pattern [fragments]
β_1	Coefficient of independent variable [MPa/MPa] or [fragments/MPa]

Table 6.1: Fragmentation and bending strength values for different glass types

	Number of fragments	Bending strength [MPa]
Thermally toughened glass EN 12150-1 (2020)	40	120
Heat-strengthened glass EN 1863-1 (2012)	Not metric	70

To accentuate the difference, the linear regression line derived from the OLS model is presented in Fig. 6.2 for comparison. The intersection of the linear regression line with the limit value of the destructive test resulted in a value that is exceptionally low, falling far below the measured photoelastic outcomes for TTG in the range of HSG. Consequently, this value is not suitable for use as a safe quality control criterion.

6.2.3 Thickness-specific considerations in the definition of limit values

To validate the results and investigate the influence of glass thickness, bootstrap standard errors based on 2000 resamples were calculated using the *summary()* function in R (R Core Team 2024) and used to determine the confidence intervals of the estimated regression coefficients. The theoretical approach for bootstrapping was described in Section 2.3.9. The resulting coefficients were aggregated to create confidence intervals with a confidence level of 95% and to enable a robust estimation of the model parameters. These intervals are based on the normal distribution and are employed to assess the statistical significance of the estimated regression coefficients. Moreover, the 95% confidence intervals of β_1 demonstrated the extent to which the predictor contributed significantly to the model's prediction. If the β_1 confidence interval exhibited a zero crossing, as is exemplary shown in Fig. 6.3 for the glass thickness of 10 mm, it could be deduced that the p-value of the estimate was not significant. Consequently, the model was not applicable for the purpose of describing the relationship between the photoelastic and destructive test results, nor for the determination of a reliable limit value.

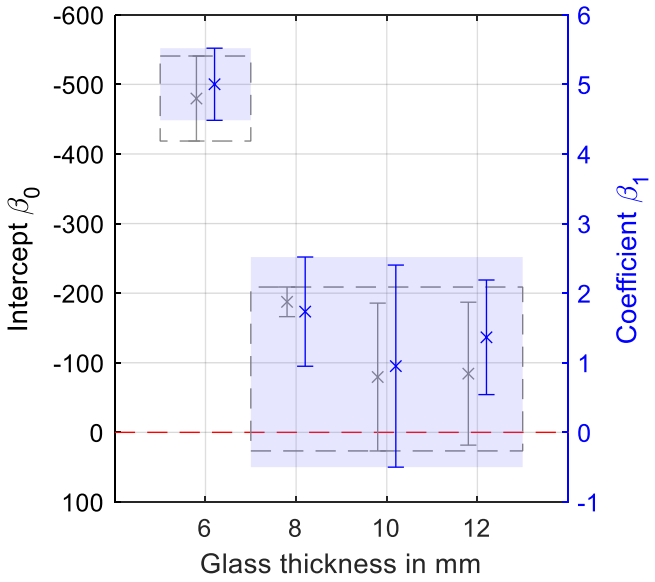

Figure 6.3: Comparison of 95% confidence intervals of intercept β_0 and estimate β_1 of quantile regression models for thickness-specific considerations

To investigate potential discrepancies between different glass thicknesses, quantile regression models were generated for each glass thickness. For each quantile regression sub-model, the 95% confidence intervals of β_0 and β_1, determined by bootstrapping were analyzed to assess whether glass thickness has a statistically significant effect. Fig. 6.3 presents the 95% confidence intervals of the intercept β_0 and the slope β_1. The intervals for the intercept β_0 are shown in grey on the left y-axis, while the 95% confidence intervals of β_1, representing the photoelastic estimate, are displayed in blue on the right y-axis and evaluated as follows: non-overlapping intervals of the estimated intercept β_0 and coefficient β_1 suggested statistically significant differences in the effects of the glass thicknesses on the target variable. To determine whether a dedicated limit is required for a specific thickness, both the slope β_1 and the intercept β_0 were considered, as both parameters enter the limit calculation in Equation (6.2). If both estimates for a given glass thickness differed

significantly from the coefficients of the other thicknesses, this supports the hypothesis that thickness influenced the observed relationship. In this case, a separate limit was derived for that particular thickness.

In Fig. 6.3, the 6 mm dataset yields significantly different β_0 and β_1 estimates compared to the datasets of glass thicknesses 8 mm, 10 mm and 12 mm. The finding suggests that it is necessary to formulate a distinct photoelastic limit for this glass thickness. Conversely, overlapping confidence intervals of β_0 and β_1 indicate that the effect of glass thickness may not be statistically distinguishable. In Fig. 6.3, the regression models of glass thicknesses of 8 mm, 10 mm and 12 mm exhibit overlapping β_0 and β_1 estimates, suggesting that a unified model across these thicknesses might be appropriate for obtaining a common photoelastic limit.

For the thickness-specific considerations in the definition of limit values, the quantile regression models of each glass thickness were investigated. In addition to evaluating the confidence intervals of β_0 and β_1 estimates, the comparison of the performance of the sub models and the individual limit values for each glass thickness was made. Furthermore, the metrics of recall and precision (see Section 2.3.4) will be determined from the photoelastic limits. Note that these limits were evaluated using all available photoelastic measurements, not only those included in the respective regression model. Within each section for quantile regression models, comparative analyses assessed whether distinct limit values are required for different glass thicknesses or whether a common photoelastic limit can be applied.

6.3 Method of logistic regression

In this section, the application of binary logistic regression for evaluating the conformity of TTG and HSG is described as well as different approaches for determining photoelastic stress limits.

6.3.1 Basics

Binary logistic regression predicts nominal values, not metric values. It is used for dependent variables classified into two categories. In this research, the dependent variable was the conformity of the glass type under consideration, divided into conforming (=1) and non-conforming (=0). The predictor variable was the photoelastic test results of edge and surface stress. As previously delineated in Section 2.3.8, the establishment of a continuous regression line was not feasible. The regression model was employed to predict the probability of conformity of the glass type at a particular photoelastic value. The curve displayed in Fig. 6.4 can be described as an S-shaped curve according to Equation (6.3).

$$P = \frac{1}{1 + e^{-(\beta_0 + \beta_1 x_{\text{photo}})}} \tag{6.3}$$

The assumptions of logistic regression are listed in Section 2.3.8.4. The models analyzed in this chapter included only one continuous predictor derived from the photoelastic measurement. As was previously demonstrated for quantile regression, the assumption of independence of observations is fulfilled. However, the assumption of linearity in the logit

was not fully met for some models. In large datasets such as the present ones, hypothesis tests tend to be overly sensitive, leading to frequent rejection of the null hypothesis even for minor deviations. Transformations of the predictor were tested but did not improve model performance given the empirical distribution of the data. The models were therefore estimated in their original form. The detailed verification of the model assumptions with the detection of outliers as well as the corresponding statistical goodness-of-fit measures, Nagelkerke's R^2, AUC, and OR are documented in Appendix Table A.10.15 to Table A.10.20.

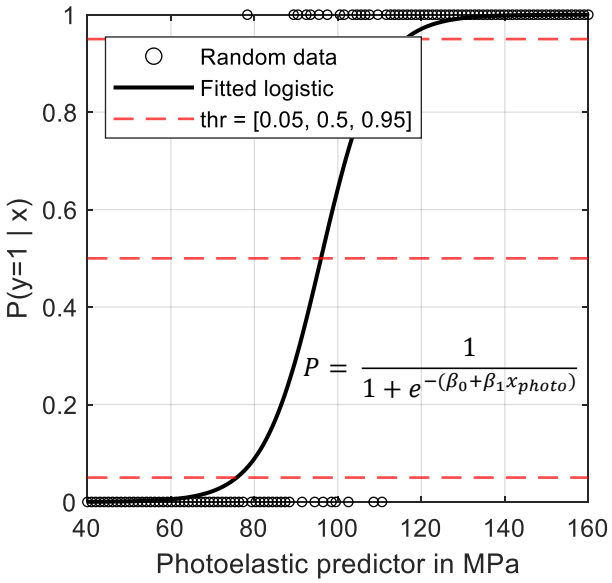

Figure 6.4: Logistic regression with photoelastic predictor as fitted sigmoid curve with 0.05, 0.5, and 0.95 probability thresholds

To illustrate the principle of logistic regression used in this chapter, exemplary data displayed in Fig. 6.4 model the relationship between the predictor variable of photoelastic stress and the binary response variable as conformity of TTG.

The logistic regression analyses were conducted using the *glmfit(), glmval(),* and *perfcurve()* functions in MATLAB (The MathWorks, Inc. 2024a), employing a binomial family with a logit link.

6.3.2 Quantifying photoelastic stress limits via logistic regression

Logistic regression provides a wider range of options for determining photoelastic stress limits. It is standard practice to select a threshold with a probability of 0.5, since this calculation yields the precise midpoint between the two classes. The corresponding x-value of this probability could then be determined as photoelastic stress limit. To enhance the reliability of the evaluation, alternative fixed threshold probability values of 0.05 and 0.95 can be employed. The three fixed probabilities are illustrated as lines for the logistic regression model with the random database in Fig. 6.4.

Additionally, various methods can be applied to adjust the probability threshold more precisely to the specific requirements of the application. The selection of the probability

threshold and the resulting photoelastic stress limit divided the data into predicted classes non-conforming and conforming as illustrated exemplary in Fig. 6.5. This classification did not necessarily correspond to the actual conformity assessment, meaning that real non-conforming samples may appear among the predicted positives and conversely, real conforming samples may be falsely classified as predicted non-conforming.

For each data point on the S-curve, a threshold evaluation could be performed, using the *perfcurve()* function in MATLAB (The MathWorks, Inc. 2024a) which determines TPR according to Equation (2.17) and FPR according to Equation (2.19). In addition to these two measures, recall according to Equation (2.17) and precision according to Equation (2.16) could be employed to evaluate how well the selected photoelastic stress limit distinguishes between conforming and non-conforming samples.

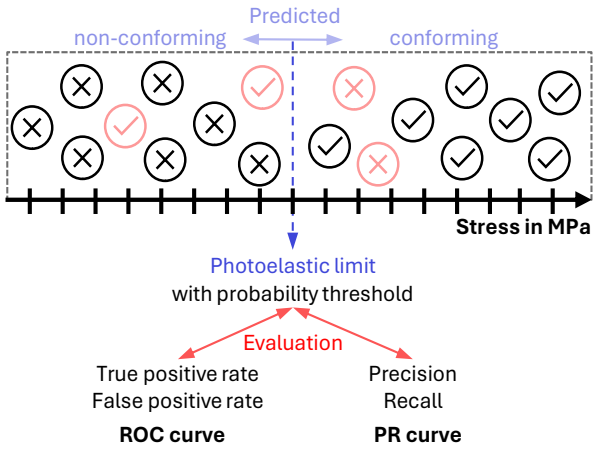

Figure 6.5: Logistic regression method: Classification by the photoelastic stress limit into predicted non-conforming and conforming and threshold evaluation by receiver operating characteristic curve and precision-recall curve

Logistic regression allows for the creation of ROC curves that compare the true positive rate and the false positive rate (see Fig. 6.6). The curve is plotted based on the predicted values for each model. Typically, a diagonal line from (0,0) to (1,1) is included in the diagram to represent random chance. A model performs better when the ROC curve is situated well above this diagonal line. As a complementary metric, AUC can be calculated. The closer this value is to 1, the more effective the logistic model is considered.

The ROC curve served as a useful tool for identifying specific probability thresholds. One approach for identifying an appropriate threshold was Youden's Index, which determined the decision point at which the difference between true positive and false positive rate reaches its maximum. An alternative criterion was the distance-based method, denoted here as Distance, which selected the point on the ROC curve with the minimal distance to the ideal classification point, representing optimal discrimination ability. Additionally, the present analysis considered a threshold where the false positive rate was kept below 0.1 (FPR < 0.1). For the random data, Fig. 6.6a shows the evaluation of true positive rate and the false positive rate described in Sections 2.3.4 and 2.3.8.3 and specifies the threshold values for Youden, Distance, and FPR < 0.1. In addition to ROC curves, precision-recall curves (PR curves) were also generated. In the ensuing analysis, the value for precision was determined to be higher than 0.9 (Prec > 0.9). This threshold is illustrated in Fig. 6.6b for the random data.

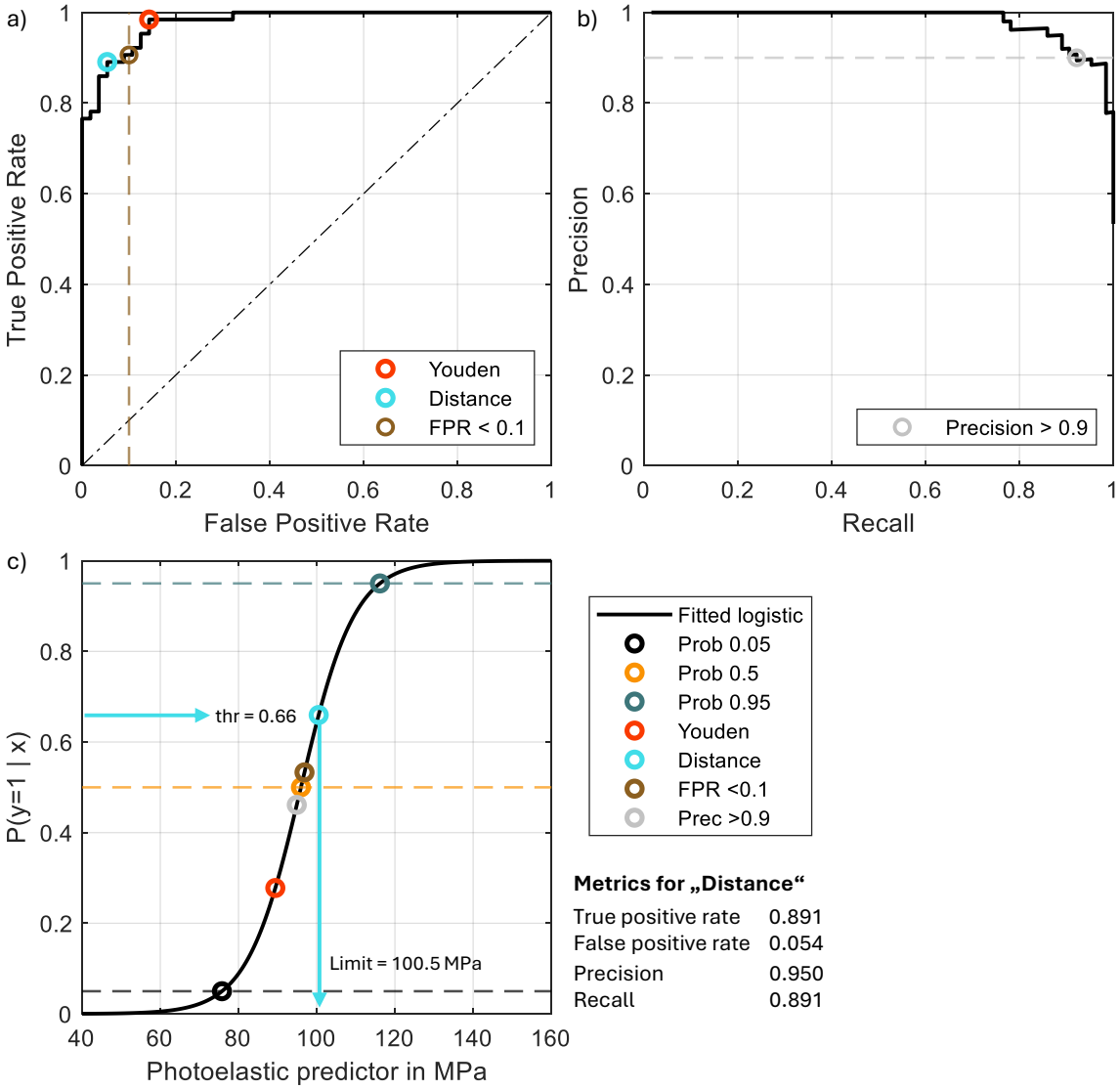

Figure 6.6: a) Exemplary receiver operating characteristic curve with probability thresholds according to Youden's Index, Distance, and false positive rate < 0.1, b) exemplary precision-recall curve with precision > 0.9, and c) threshold distribution of seven probability thresholds on the fitted logistic S-shaped curve of random data with corresponding photoelastic stress limit, exemplary shown for Distance

Employing these methods allowed for the refinement of the probability threshold, thereby enhancing the predictive accuracy and performance of logistic regression models. For each model, seven probability thresholds were available for comparison. These thresholds are illustrated in Fig. 6.6c on the fitted logistic S-shaped curve derived from the simulated data. The corresponding photoelastic stress limits can be read from the x-axis, as exemplified by the probability threshold determined according to the distance criterion. In addition, the associated performance metrics for this limit are given in Fig. 6.6c.

To calculate the photoelastic stress limit, Equation (6.4) was used, derived from the transformation of Equation (6.3). The calculation incorporates the selected probability threshold *thr* as well as the estimated coefficients β_0 and β_1 of the fitted logistic function.

$$\text{Limit} = -\frac{\ln\left(\frac{1}{\text{thr}} - 1\right) + \beta_0}{\beta_1} \tag{6.4}$$

6.3.3 Thickness-specific considerations in the definition of limit values

In the context of logistic regression, thickness-specific considerations were executed through qualitative analysis. A particular emphasis was placed on the statistical significance of the thickness-specific regression model, that was the question of whether the determination of the limit value was based on a reliable model. The thickness-specific limit values were then compared with each other and with the limit value derived from the model including all glass thicknesses. The analysis focused on the location and distribution of the measured values to assess their effect on the glass thickness.

6.4 Validation method

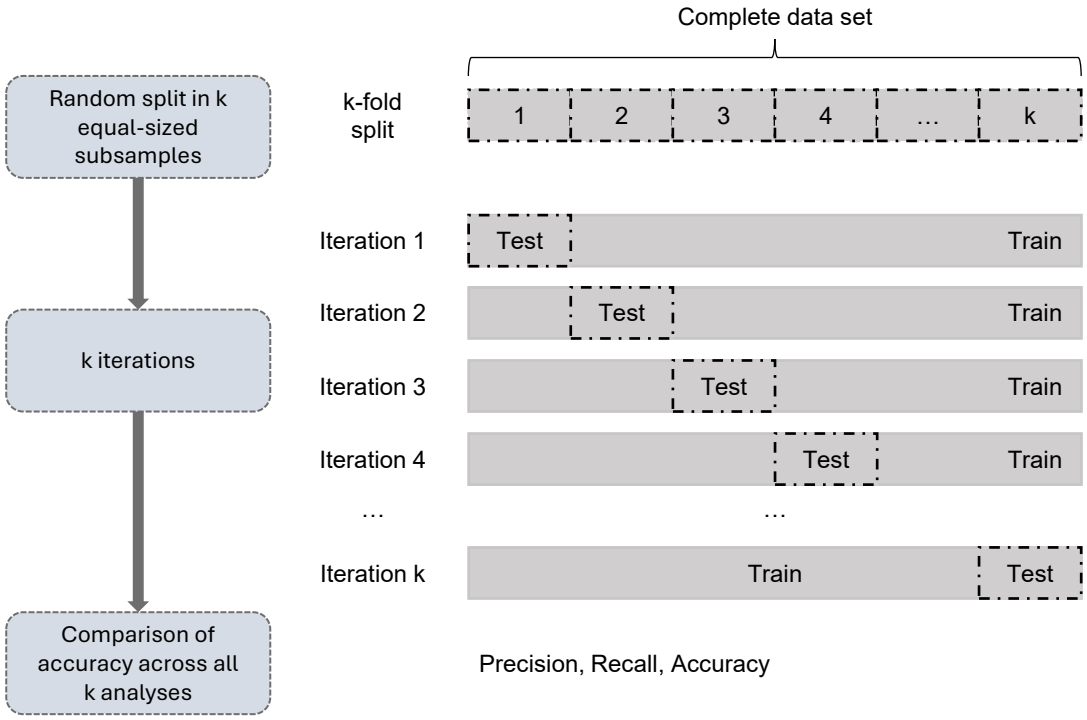

Figure 6.7: Procedure for k-fold validation of the regression models

To ensure a more reliable evaluation of the quantile and logistic regression models, validation was required. After identifying the main models, which determined the limit values while accounting for the influence of glass thickness, a k-fold cross-validation was performed and discussed in the Sections 6.8 and 6.11. The key advantage of k-fold cross-validation is that the model is repeatedly trained on slightly different training subsets of the data, rather than on the complete dataset at once. This iterative approach yields more stable performance estimates and reduces the risk of overfitting. In k-fold cross-validation, the complete dataset was divided into k equally sized folds. During each iteration, a single

fold was reserved for model evaluation, whereas the remaining $k-1$ folds are utilized for model fitting. Repeating this procedure k times ensured that every fold served once as the controlling test set. Fig. 6.7 illustrates this procedure. The choice of k was made in advance. In practice, values between 5 and 10 are most common (Verma et al. 2024). In this study, the final choice of k = 5 was made because it provides a larger training set in each iteration compared to k = 10, thereby allowing for a more diverse and representative selection of data while maintaining computational efficiency.

In addition to the k-fold cross-validation, each chapter also evaluates the limit values for the individual and summarized glass thicknesses testing on all available photoelastic results. This was particularly relevant for quantile regression, where only a subset of the photoelastic results could be used for destructive testing to build the predictive model. In such cases, this type of validation served as an effective method to verify whether the remaining photoelastic results were consistent with the determined limits.

6.5 Database for regression analysis

The test specimens for the following regression models are known from the previous chapter and were made of uncoated soda-lime silicate float glass in the standardized format 360 mm x 1100 mm with differing pre-stress levels. The glass thickness of the specimens ranged from 4 mm to 12 mm depending on the availability of the photoelastic measurements.

On the one hand, the regression models encompassed the dependent variable of the destructive test results: the bending stress determined of four-point bending test using the breaking force, the number of fragments automatically counted with the CulletScanner by Softsolution GmbH (2023a) in a square of 50 mm x 50 mm counting mask in the area of the coarsest fracture pattern of TTG and, in the case of HSG, the visual evaluation of the fracture pattern.

On the other hand, the regression models were predicted by the photoelastic values of surface and edge stress. The surface stress was the mean value of σ_1 of three measurement points (see Section 5.3.1) per sample measured with the SCALP-05 by GlasStress Ltd. (2013). The edge stress was measured with both methods of MWP and PST. The number of specimens differed for these methods: while 515 of the samples, produced by three different manufacturers, were investigated with MWP using the LineScanner by Softsolution GmbH (2023b), the edge stress values determined by PST using the StrainScope flex by ilis gmbh (2023) came from 114 specimens of only one manufacturer. For both methods, the edge stress value used in the regression models was the mean value of the six measurement areas per sample.

The subsequent three tables delineate the aggregate number of specimens investigated. Depending on the glass thickness, the specimens were categorized according to their conformity with TTG as defined in EN 12150-1 (2020) and HSG as defined in EN 1863-1 (2012). It was evident that destructive tests could only be conducted on a single specimen, either for the bending strength or for the fracture pattern test. Therefore, conformity assessment was carried out for the entire test series. Samples in a test series must fulfill both the fracture pattern and bending strength requirements specified in EN 12150-1 (2020) or EN 1863-1 (2012) to meet the product definition of the respective tempered glass. In cases where the test series failed to exhibit the required fracture pattern, the

non-conformity was assigned to the specimens within the test series that were tested for strength.

Table 6.2 lists the number of specimens on which surface stress values were measured and used for regression analysis. These specimens were tested for bending strength or fracture pattern.

Table 6.2: Number of specimens 360 mm x 1100 mm for regression analysis investigated for surface stress, divided by glass thickness and listed by conformity of thermally toughened glass (TTG) according to EN 12150-1 (2020) and heat-strengthened glass (HSG) according to EN 1863-1 (2012)

	4 mm	6 mm	8 mm	10 mm	12 mm
Conforming TTG according to EN 12150-1 (2020)	71	81	83	43	42
Conforming HSG according to EN 1863-1 (2012)	83	84	53	28	21
Non-conforming samples	12	0	25	14	21
Total	166	165	161	85	84

Table 6.3 shows the number of specimens whose edge stress values were determined by MWP and were tested for bending strength or fracture pattern. The edge stress values corresponding to the number of fragments were obtained from the CulletScanner (Softsolution GmbH 2023a) device equipped with two wavelengths, while edge stress values corresponding to bending stress were obtained from the LineScanner (Softsolution GmbH 2023b) using three wavelengths. As described in Section 4.3.5, the evaluation of samples with a glass thickness of 4 mm (TTG and HSG) and 6 mm (HSG) is not reliable when using MWP measurement. Therefore, these samples were excluded from these regression analysis models for determining the edge stress limit.

Table 6.3: Number of specimens 360 mm x 1100 mm investigated for edge stress with multiple-wavelength photoelasticity for regression analysis, divided by glass thickness and listed by conformity of thermally toughened glass (TTG) according to EN 12150-1 (2020) or heat-strengthened glass (HSG) according to EN 1863-1 (2012)

	4 mm	6 mm	8 mm	10 mm	12 mm
Conforming TTG according to EN 12150-1 (2020)	-	87	112	59	58
Conforming HSG according to EN 1863-1 (2012)	-	-	59	35	27
Non-conforming samples	-	-	34	20	24
Total	-	87	205	114	109

Table 6.4 shows the reduced database of specimens which were investigated by PST and produced by one manufacturer. Furthermore, these test specimens were only subjected to the bending test, so that regression was only possible with bending stress as dependent variable. The PST method is also not reliable for measuring edge stress in 4 mm TTG and HSG specimens, but the edge stress measurements for 6 mm HSG samples were included in the analysis.

Table 6.4: Number of specimens 360 mm x 1100 mm investigated for edge stress with phase-shifting technique for regression analysis, divided by glass thickness and listed by conformity of thermally toughened glass (TTG) according to EN 12150-1 (2020) or heat-strengthened glass (HSG) according to EN 1863-1 (2012)

	4 mm	6 mm	8 mm	10 mm	12 mm
Conforming TTG according to EN 12150-1 (2020)	-	20	20	9	10
Conforming HSG according to EN 1863-1 (2012)	-	19	10	5	5
Non-conforming samples	-	0	6	5	5
Total	-	39	36	19	20

Due to the limitation that only one destructive test could be conducted on a single specimen, the number of specimens differed in the subsequent regression analysis between the photoelastic and destructive variables.

Table 6.5 indicates the order of the investigated regression models. The limit determination for surface and edge stress was divided into the glass products of TTG and HSG. After the regression analysis of each glass product, a discussion section for each glass type follows. Here, the k-fold validation of the regression models was carried out. Following a comparative and evaluative analysis of the limit values of surface and edge stress, a specific value was designated for them.

Table 6.5: Investigation of regression models in the order of the following sections

Section	Glass product	Regression model	Photoelastic measurement	Dependent variable	Limit value
6.6.1.1	TTG	QuanReg	Surface stress	Number of fragments	Lower limit
6.6.1.2	TTG	QuanReg	Surface stress	Bending strength	Lower limit
6.6.2	TTG	LogReg	Surface stress	Conformity TTG	Lower limit
6.7.1.1	TTG	QuanReg	Edge stress (MWP)	Number of fragments	Lower limit
6.7.1.2	TTG	QuanReg	Edge stress (MWP)	Bending strength	Lower limit
6.7.1.3	TTG	QuanReg	Edge stress (PST)	Bending strength	Lower limit
6.7.2.1	TTG	LogReg	Edge stress (MWP)	Conformity TTG	Lower limit
6.7.2.2	TTG	LogReg	Edge stress (PST)	Conformity TTG	Lower limit
6.9.1	HSG	QuanReg	Surface stress	Bending strength	Lower limit
6.9.2	HSG	LogReg	Surface stress	Conformity HSG	Upper limit
6.10.1.1	HSG	QuanReg	Edge stress (MWP)	Bending strength	Lower limit
6.10.1.2	HSG	QuanReg	Edge stress (PST)	Bending strength	Lower limit
6.10.2.1	HSG	LogReg	Edge stress (MWP)	Conformity HSG	Upper limit
6.10.2.2	HSG	LogReg	Edge stress (PST)	Conformity HSG	Upper limit

6.6 Surface stress threshold analysis for thermally toughened glass

The regression models with surface stress as the predictor variable and the determination of limit values for the TTG were carried out with a database of glass thicknesses ranging from 4 mm to 12 mm. Appendix Table A.9, Table A.10 and Table A.15 contain statistical data and the investigated number of the specimens.

6.6.1 Quantile regression

This chapter employs quantile regression analysis with surface stress. The limit values for TTG were determined according to the intersection point of the regression line with the required fragments number of 40 or the characteristic bending strength of 120 MPa.

6.6.1.1 Surface stress vs. Number of fragments

To compare limit values derived from thickness-specific models with those obtained from the complete dataset, quantile regression was applied to the relationship between surface stress and the number of fragments. For this purpose, the database was divided into subsets according to glass thickness, and an individual regression model was fitted for each subset. In addition, a quantile regression model was derived from the complete dataset comprising all glass thicknesses. Table 6.6 lists the limit values determined for each individual glass thickness as well as for aggregated datasets comprising multiple glass thicknesses. The precision and recall metrics reported in the table were not calculated exclusively using the subset underlying the respective quantile regression model. Instead, they were evaluated based on the complete set of available surface stress data. The number of samples used for this evaluation is also reported in Table 6.6.

Table 6.6: Limit values for surface stress vs. number of fragments for thermally toughened glass, including classification metrics (precision and recall) for each glass thickness

t [mm]	n	Limit [MPa]	Precision [%]	Recall [%]
4 *	166	114.1	100.0	56.3
6 *	165	103.9	100.0	91.4
8 *	161	96.9	100.0	100.0
10 *	85	84.3	100.0	100.0
12 *	84	91.0	100.0	100.0
4–6 *	330	112.3	99.0	62.5
8–12 *	331	96.2	100.0	98.2
4–12 *	661	109.1	99.6	78.4

* Statistically significant based on bootstrap confidence intervals

Fig. 6.8a illustrates the 95% confidence intervals of the intercept β_0 and the coefficient β_1 associated with the independent variable surface stress for the five investigated glass thicknesses. The confidence intervals of β_0 and β_1 for the 4 mm and 6 mm glass thickness differed markedly from those of the remaining thicknesses. As the confidence intervals overlapped for β_1 for the 8 mm, 10 mm, and 12 mm glass thicknesses, these thicknesses were combined into an aggregated model.

The 4 mm and 6 mm glass thicknesses also exhibited overlapping confidence intervals, which would, in principle, justify their combination into a single model. However, evaluation of the resulting combined limit value of 112.3 MPa for the 4–6 mm model, based on the performance metrics presented in Table 6.6, revealed a low recall of 62%. This would lead to a high number of unnecessary rejections. A more favorable performance was achieved by maintaining separate models for the 4 mm and 6 mm glass thicknesses, as demonstrated by the corresponding rows in Table 6.6 and the resulting individual limit values.

Fig. 6.8b shows the scatter plot of *Surface stress vs. Number of fragments* together with the corresponding quantile regression lines for the datasets of 4 mm, 6 mm, and 8–12 mm glass thicknesses. The regression lines for the 4 mm and 6 mm models exhibited a steeper slope than that of the 8–12 mm glass thickness dataset, a difference that is clearly visible in Fig. 6.8b. In addition, the regression line for the 4 mm glass appeared to be shifted relative to that of the 6 mm glass.

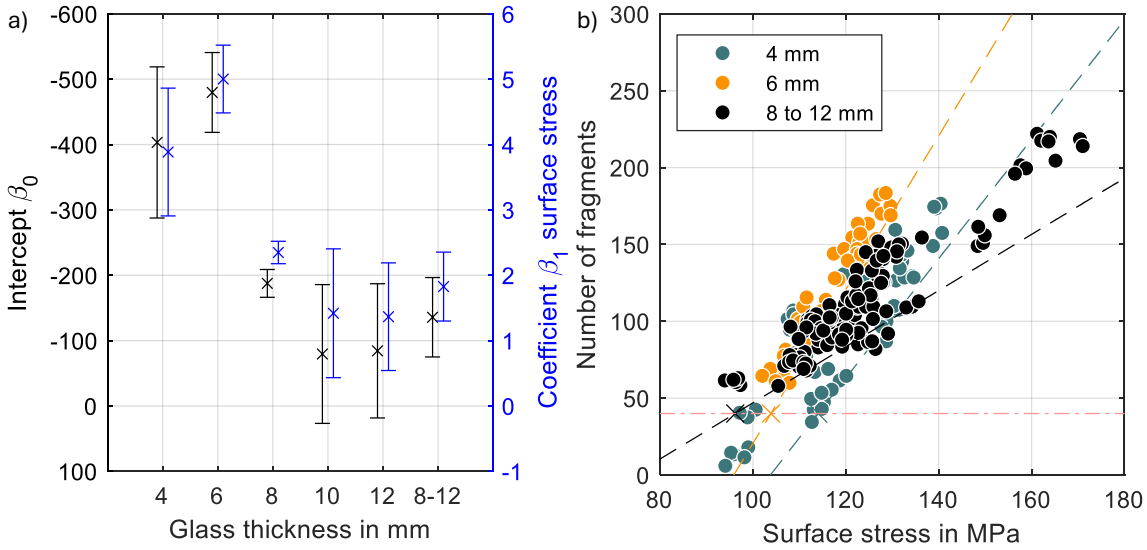

Figure 6.8: Quantile regression (5%) Surface stress vs. Number of fragments for thermally toughened glass with a) confidence intervals for the intercept β_0 and the coefficient β_1 of the independent variable surface stress depending on glass thicknesses and b) scatter plot with regression lines

For the aggregated 8–12 mm glass thickness dataset, the resulting surface stress limit value was 96.2 MPa. In contrast, the 6 mm model intersected the 40-fragment line at 103.9 MPa, while the 4 mm model yielded a higher limit value of 112.3 MPa. All three limit values achieved a precision of 100%, indicating a complete separation between conforming and non-conforming TTG.

The 4 mm dataset investigated in this regression model was the only one that included non-conforming TTG specimens. Using the higher limit value of 114.1 MPa, all non-conforming specimens would be reliably excluded. However, the corresponding recall was low, amounting to only 56.3%. As discussed in Section 5.5.5.2, a pronounced manufacturer dependence was observed for the 4 mm specimens. Consequently, individual limit values were determined and compared for each manufacturer.

Fig. 6.9a illustrates this manufacturer dependence by means of a scatter plot with color-coding and the corresponding quantile regression lines. The resulting limit values and performance metrics for each manufacturer as well as for the combined dataset including all 4 mm surface stress values are summarized in Table 6.7. The resulting limit values differed considerably between manufacturers. Each manufacturer-specific limit achieved a precision of 100%, while the corresponding recall values were substantially lower. The underlying reason becomes apparent in Fig. 6.9b, which illustrates the distribution of all surface stress values of the 4 mm specimens, separated by manufacturer.

Table 6.7: Limit values for surface stress vs. number of fragments for 4 mm thermally toughened glass depending on manufacturer, including classification metrics for manufacturer-specific and combined test sets

Manufacturer	Limit [MPa]	n (QuanReg)	n_{mfr}	Precision [%]	Recall [%]	n_{tested}	Precision [%]	Recall [%]
A	120.7	20	54	100.0	71.4	166	100.0	40.8
B	106.0	19	55	100.0	62.5	166	98.4	85.9
C	114.1	20	57	100.0	63.0	166	100.0	56.3

For manufacturer A, several conforming TTG data points were found to be below the statistically determined limit. These values were obtained from specimens tested for bending stress. Consequently, they were not included in Fig. 6.9a, which resulted in a comparatively high limit value of 120.7 MPa. When this limit was applied to the complete set of 4 mm surface stress data, the recall decreased to 40.8%.

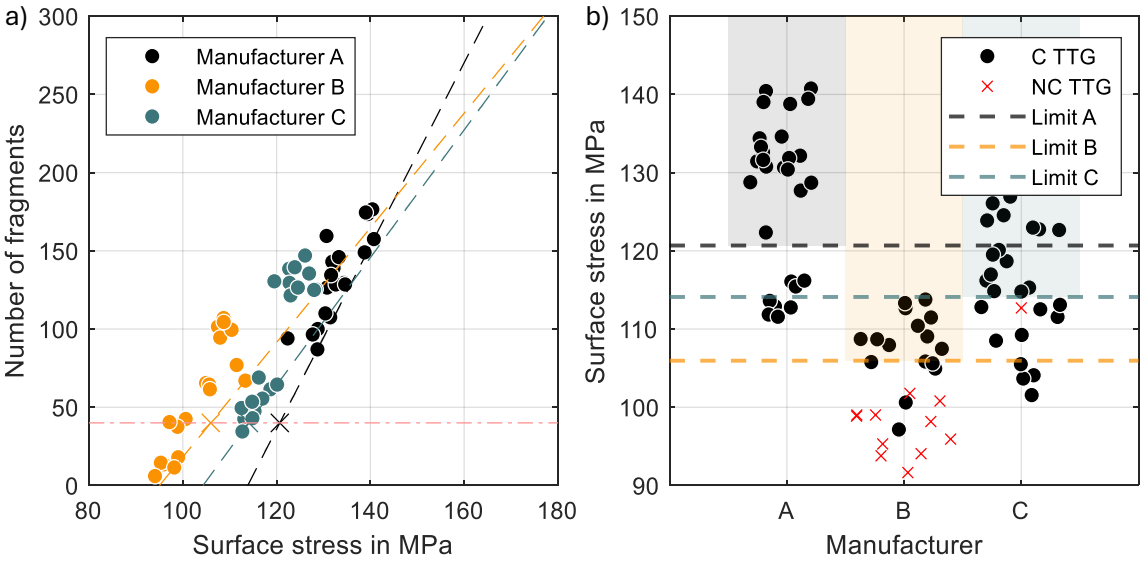

Figure 6.9: a) Quantile regression (5%) Surface stress vs. Number of fragments for 4 mm thermally toughened glass shown as scatter plot with regression lines separated by manufacturer and b) distribution of all 4 mm surface stress values grouped by manufacturer with corresponding limit lines

For manufacturer C, only a single specimen narrowly failed to reach the required threshold of 40 fragments at a surface stress of 112.7 MPa, as shown in Fig. 6.9b. In contrast, the non-conforming TTG specimens from manufacturer B were predominantly associated with surface stress values of up to approximately 102 MPa. When evaluating the performance metrics based on all 4 mm specimens, the limit determined for manufacturer B at 106.0 MPa provided the best overall performance among the three manufacturers, achieving a precision of 98.4% and a recall of 85.9%.

6.6.1.2 Surface stress vs. Bending stress

A comparison of the confidence intervals of β_1 obtained from the regression models *Surface stress vs. Bending stress* for individual glass thicknesses indicated that differentiation based on glass thickness was not necessary. This is illustrated in Fig. 6.10a: on the one hand, most 95% confidence intervals of both β_0 and β_1 overlapped. On the other hand, even in cases where the confidence intervals did not overlap, such as for the models of 4 mm and 8 mm glass thicknesses, no consistent trend with respect to glass thickness could be identified. Consequently, a single regression model was derived using the combined dataset comprising all investigated glass thicknesses.

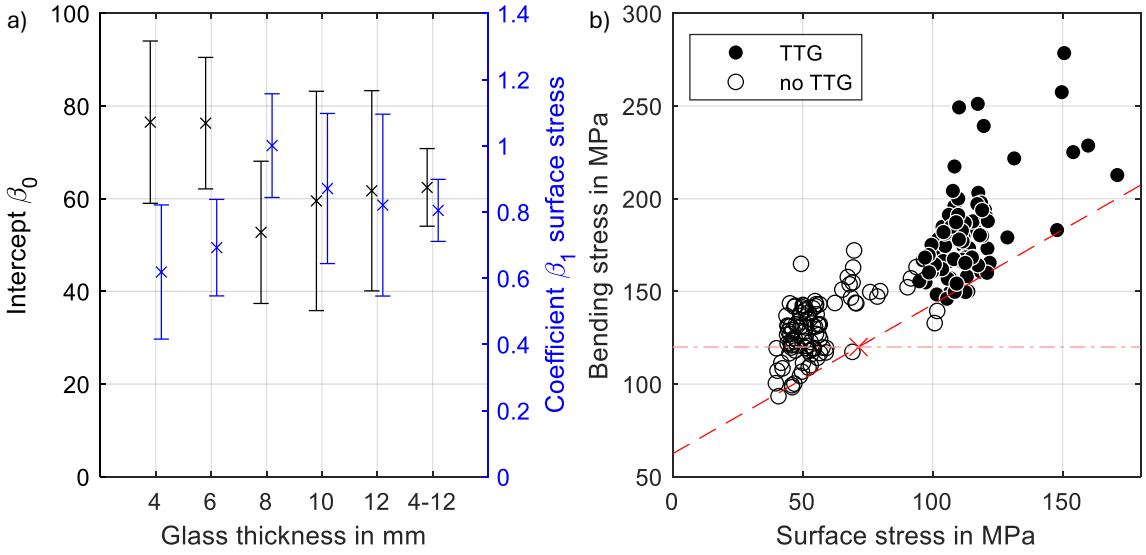

Figure 6.10: Quantile regression (5%) Surface stress vs. Bending stress for thermally toughened glass with a) confidence intervals for the intercept β_0 and the coefficient β_1 of the independent variable surface stress depending on glass thicknesses and b) scatter plot with regression line

Fig. 6.10b presents the scatter plot of *Surface stress vs. Bending stress* together with the corresponding regression line. The intersection of this regression line with the characteristic bending stress value of 120 MPa yielded a surface stress limit of 71.5 MPa for the model including glass thicknesses of 4–12 mm.

Table 6.8: Limit values for surface stress vs. bending stress for thermally toughened glass, including classification metrics for each glass thickness

t [mm]	n	Limit [MPa]	Precision [%]	Recall [%]
4 *	166	70.3	85.5	100.0
6 *	165	63.1	94.2	100.0
8 *	161	67.2	76.9	100.0
10 *	85	69.4	78.2	100.0
12 *	84	71.0	89.4	100.0
4–12 *	661	71.5	87.7	100.0

* Statistically significant based on bootstrap confidence intervals

Table 6.8 lists the limit values obtained for the individual thickness-specific subsets as well

as for the aggregated dataset, together with the corresponding performance metrics. It is evident that the limit value of the model including glass thicknesses of 4–12 mm exceeded all limit values determined for the individual subsets. Furthermore, while a recall of 100% was achieved in all cases, none of the evaluated limit values with a precision below 100% allowed for a fully reliable discrimination between conforming and non-conforming TTG.

6.6.2 Logistic regression

In the context of the logistic regression model with surface stress as the predictor variable, the metric destructive test results were categorized into conforming (1) and non-conforming (0) TTG. Fig. 6.11 shows the distribution of conformity depending on the surface stress displayed for the complete dataset, comprising all glass thicknesses as well as for the datasets separated according to the five investigated glass thicknesses. The specimens classified as non-conforming (0) comprise both non-conforming TTG and all HSG specimens. For glass thicknesses ranging from 6 mm to 12 mm, the thickness-specific datasets shown in Fig. 6.11 clearly distinguished between HSG and TTG based on the surface stress values. The dataset for the 4 mm glass thickness constituted an exception, as it also contained non-conforming TTG. In addition, the 4 mm dataset was the only dataset in which an overlap between the two categories was observed.

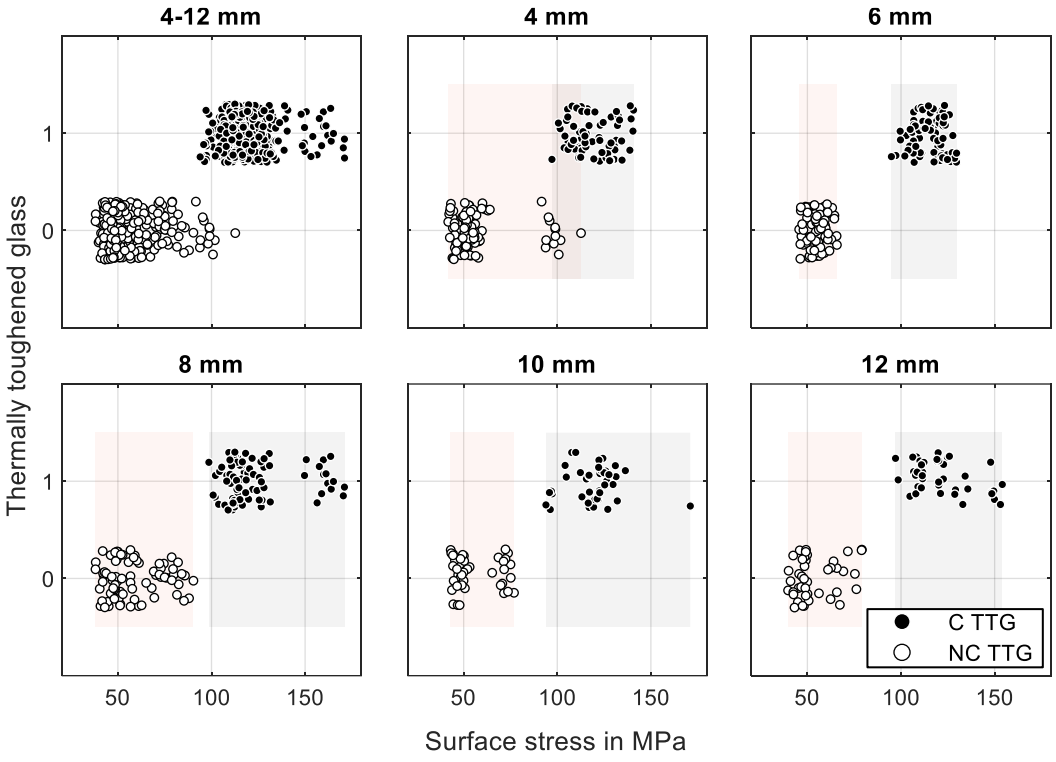

Figure 6.11: Distribution of conforming and non-conforming thermally toughened glass depending on surface stress split into glass thicknesses from 4 mm to 12 mm

In the context of the preceding quantile regression models, logistic regression models were calculated and compared for the individual glass thicknesses as well as for the aggregated dataset comprising glass thicknesses of 8–12 mm. The relevant statistical information can be found in Appendix Table A.15.

Due to the pronounced separation between conforming and non-conforming specimens, the logistic regression models for the 6 mm and 8–12 mm glass thicknesses did not converge, indicating that the model parameters could not be meaningfully estimated. This clear separation is also evident in Fig. 6.12a, which shows S-shaped curves with a very steep transition. As a result, the limit values determined for different probability levels laid in close proximity. As illustrated in Fig. 6.12b, the limit values were derived for probability levels of 0.5 and 0.95. For the individual glass thicknesses from 6 mm to 12 mm as well as for the aggregated 8–12 mm model, the corresponding limit values exhibited only minor variation. In contrast, the limit values obtained for the 4 mm subset showed a substantially larger separation.

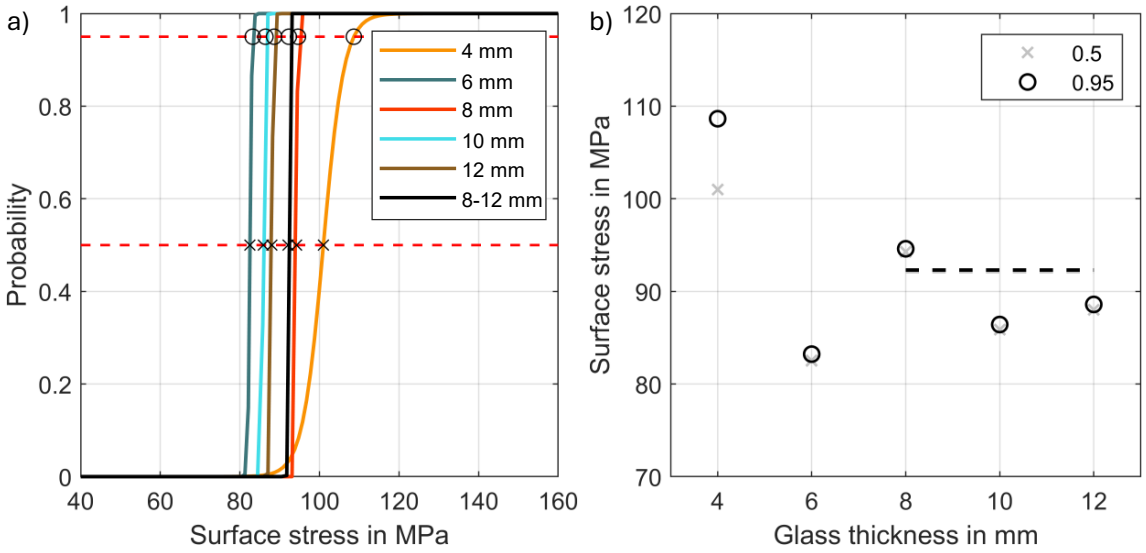

Figure 6.12: Logistic regression analysis of surface stress for thermally toughened glass: a) fitted sigmoid curves depending glass thickness and b) thickness-specific limit values derived from probability thresholds of 0.5 and 0.95

As summarized in Table 6.9, the limit values as well as the corresponding precision and recall metrics are reported for the individual glass thicknesses. Apart from the 4 mm glass thickness, all thickness-specific limits exhibited perfect precision and recall. An examination of the limit values in conjunction with the distribution shown in in Fig. 6.11 indicated that the limits were located near the midpoint between the clearly separated categories of conforming and non-conforming TTG. The comparatively low limit value of 82.5 MPa obtained for the 6 mm glass thickness could be attributed to the pronounced separation between classes 0 and 1. Given this clear distinction between the categories, the glass thicknesses of 4 mm, 6 mm, and 8–12 mm were selected for the determination of limit values at a probability level of 0.95. Accordingly, the surface stress limits for TTG derived from logistic regression were 108.6 MPa for 4 mm, 83.2 MPa for 6 mm, and 92.3 MPa for the 8–12 mm glass thickness group.

6.7 Edge stress threshold analysis for thermally toughened glass

The regression models with edge stress as the predictor variable and the determination of limit values for TTG were carried out with a database of TTG specimens with glass

Table 6.9: Limit values for surface stress for thermally toughened glass determined for probabilities 0.5 and 0.95, including classification metrics for each glass thickness

t [mm]	n	Probability = 0.5			Probability = 0.95		
		Limit [MPa]	Precision [%]	Recall [%]	Limit [MPa]	Precision [%]	Recall [%]
4 *	166	101.0	97.2	97.2	108.6	98.3	81.7
6	165	82.5	100.0	100.0	83.2	100.0	100.0
8	161	94.3	100.0	100.0	94.6	100.0	100.0
10	85	85.9	100.0	100.0	86.4	100.0	100.0
12	84	88.0	100.0	100.0	88.6	100.0	100.0
8–12 *	330	92.1	100.0	100.0	92.3	100.0	100.0

* Model fit significant by likelihood-ratio χ^2 test

thicknesses ranging from 6 mm to 12 mm and HSG specimens with glass thicknesses ranging from 8 mm to 12 mm. The statistical data and the precise number of specimens are presented in Appendix Table A.11, Table A.12, Table A.13, Table A.16, and Table A.17.

6.7.1 Quantile regression

This section applies quantile regression with edge stress as the predictor variable. The limit values for TTG were determined based on the intersection of the corresponding regression line either with the required minimum number of 40 fragments or with the characteristic bending strength of 120 MPa.

6.7.1.1 Edge stress (MWP) vs. Number of fragments

The analysis of the 95% confidence intervals of the intercept β_0 and the coefficient β_1 obtained from the thickness-specific quantile regression models between edge stress determined by MWP and number of fragments indicated no statistically significant differences with respect to glass thickness. This is illustrated in Fig. 6.13a, which shows that confidence intervals of both β_0 and β_1 overlap for all individual glass thicknesses. When the glass thicknesses were examined individually, the quantile regression models for the 10 mm and 12 mm glass thicknesses were found to be not statistically significant, as the corresponding 95% confidence intervals of β_1 included zero. In addition, for the 10 mm glass thickness, the mean of the 95% confidence interval of β_1 laid in the negative range, as illustrated in Fig. 6.13a, indicating a negative slope of the regression line. Consequently, the limit value determined for the 10 mm glass thickness as well as the other limit values obtained from the thickness-specific models listed in Table 6.10 could not be considered reliable.

In contrast, the quantile regression model derived from the complete dataset yielded a statistically significant result. Fig. 6.13b shows the scatter plot of *Edge stress vs. Number of fragments* together with the corresponding regression line. The intersection of this regression line with the required threshold of 40 fragments resulted in an edge stress limit of 67.2 MPa. In contrast, the quantile regression model derived from the complete dataset yielded a statistically significant result. Fig. 6.13b shows the scatter plot of *Edge stress vs.*

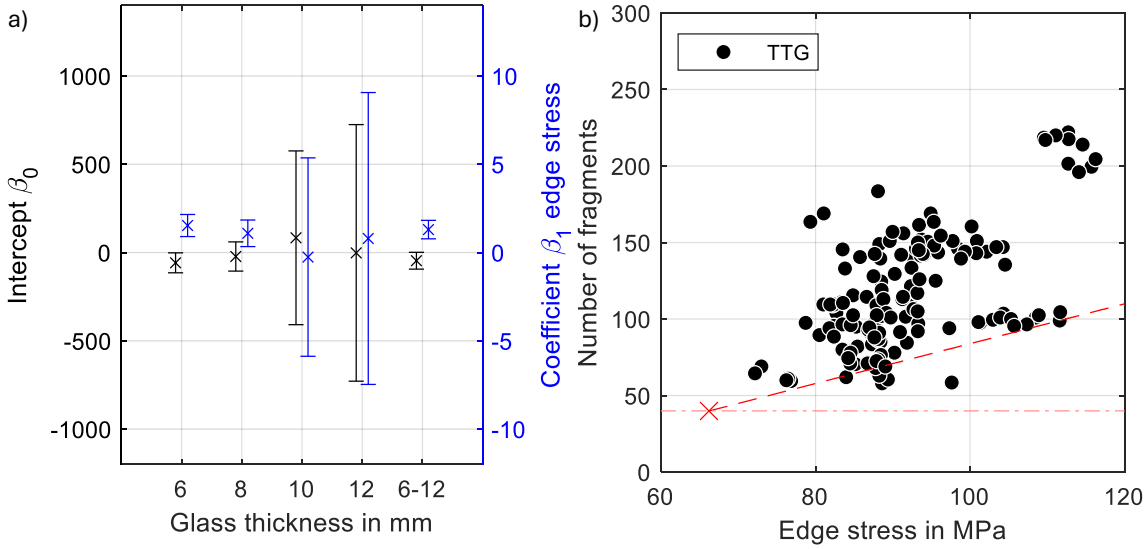

Figure 6.13: Quantile regression (5%) Edge stress (determined by multiple-wavelength photoelasticity) vs. Number of fragments for thermally toughened glass with a) confidence intervals for the intercept β_0 and the coefficient β_1 of the independent variable edge stress depending on glass thicknesses and b) scatter plot with regression line

Number of fragments together with the corresponding regression line. The intersection of this regression line with the required threshold of 40 fragments resulted in an edge stress limit of 67.2 MPa.

Table 6.10 summarizes the performance metrics associated with the limit values derived for the different glass thicknesses as well as for the aggregated model including specimens with glass thicknesses from 6 to 12 mm. These metrics were evaluated using all edge stress values determined by MWP, including both TTG and HSG. The number of specimens considered for each limit value is also reported. As the precision values were below 100% for all evaluated models, none of the derived limit values enabled a clear discrimination between conforming and non-conforming TTG. This indicates that the limit values obtained from the quantile regression models based on edge stress were not sufficient for reliable classification.

Table 6.10: Limit values for edge stress (determined by multiple-wavelength photoelasticity) vs. number of fragments for thermally toughened glass, including classification metrics for each glass thickness

t [mm]	n	Limit [MPa]	Precision [%]	Recall [%]
6 *	87	64.1	-	100.0
8 *	210	57.1	65.2	100.0
10	111	169.8	-	0.0
12	108	52.6	53.7	100.0
6–12 *	516	67.2	84.4	100.0

* Statistically significant based on bootstrap confidence intervals

6.7.1.2 Edge stress (MWP) vs. Bending stress

As demonstrated in Fig. 6.14a, the 95% confidence intervals of the intercept β_0 and slope coefficient β_1 of the regression models between edge stress determined by MWP and bending stress were in general overlapping for the individual glass thicknesses. Table 6.11 summarizes the limit values obtained for each glass thickness. The aggregated model covering glass thicknesses from 6 to 12 mm encompassed almost all limit values derived from the individual subsets, with the exception of the 12 mm model which exhibited a slightly higher limit value.

Table 6.11: Limit values for edge stress (determined by multiple-wavelength photoelasticity) vs. bending stress for thermally toughened glass, including classification metrics (precision and recall) for each glass thickness

t [mm]	n	Limit [MPa]	Precision [%]	Recall [%]
6	57	30.4	-	100.0
8 *	210	65.5	86.6	100.0
10 *	111	74.1	82.6	100.0
12 *	108	75.2	98.3	100.0
6–12 *	486	74.2	95.0	100.0

* Statistically significant based on bootstrap confidence intervals

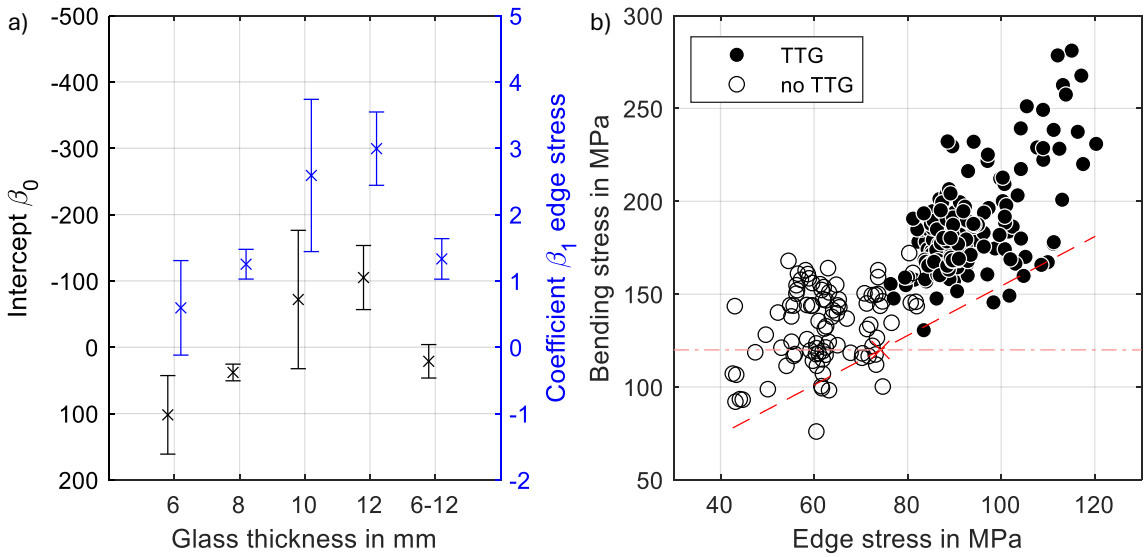

Figure 6.14: Quantile regression (5%) Edge stress (determined by multiple-wavelength photoelasticity) vs. Bending stress for thermally toughened glass with a) confidence intervals for the intercept β_0 and the coefficient β_1 of the independent variable edge stress depending on glass thicknesses and b) scatter plot with regression line

As shown in Fig. 6.14a, the confidence interval of coefficient β_1 for the 6 mm dataset included both positive and negative values, indicating that the corresponding regression model was not statistically significant. This result may be attributed to limitations of the underlying dataset, as edge stress values for 6 mm HSG specimens were not included in the evaluation. Consequently, the unusually low limit value of 30.4 MPa obtained for

the 6 mm glass thickness could be explained by the lack of statistical significance of the corresponding model, thereby calling the reliability of this value into question. Nevertheless, the aggregated regression model encompassing all evaluated glass thicknesses including 6 mm specimens remained statistically significant.

Fig. 6.14b shows the scatter plot of *Edge stress vs. Bending stress* together with the corresponding quantile regression line. The intersection of this regression line with the required bending stress threshold of 120 MPa yielded an edge stress limit of 74.2 MPa for the complete database with glass thicknesses of 6–12 mm. The performance metrics reported in Table 6.11 and tested on all available edge stress values measured by MWP indicated a precision below 100%, implying that within the derived limits a clear distinction between conforming glass and non-conforming TTG.

6.7.1.3 Edge stress (PST) vs. Bending stress

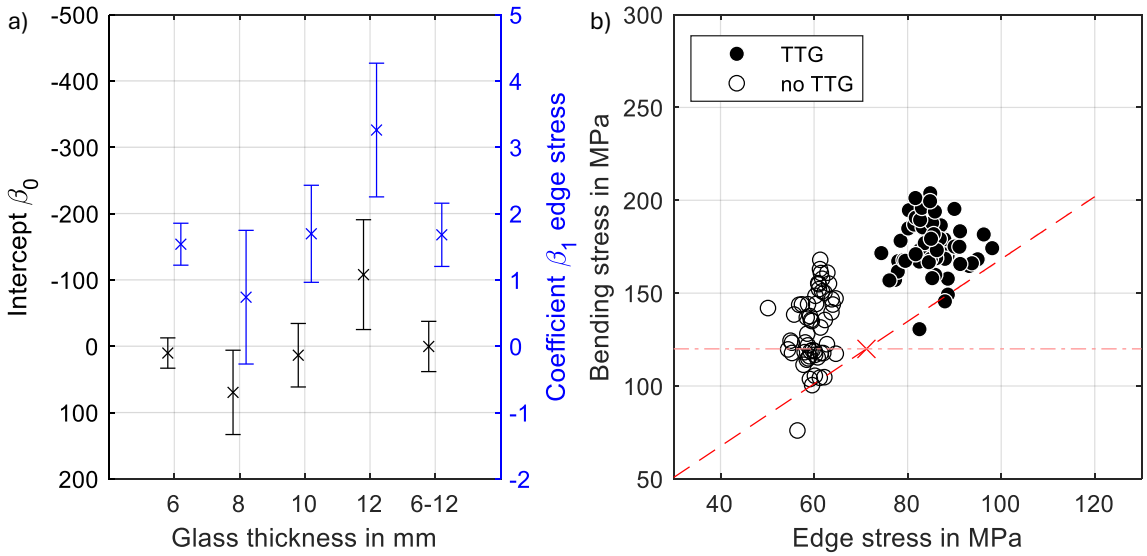

Figure 6.15: Quantile regression (5%) Edge stress (determined by phase-shifting technique) vs. Bending stress for thermally toughened glass with a) confidence intervals for the intercept β_0 and the coefficient β_1 of the independent variable edge stress depending on glass thicknesses and b) scatter plot with regression line

The quantile regression model with bending stress as the dependent variable was also evaluated using edge stress values measured by PST as the predictor variable. To investigate the potential influence of glass thickness, thickness-specific subsets for glass thicknesses ranging from 6 mm to 12 mm were analyzed. Fig. 6.15a presents the 95% confidence intervals of the intercept β_0 and regression coefficients β_1 associated with edge stress for each glass thickness. The diagram indicates that the 95% confidence intervals of both β_0 and β_1 largely overlapped across the different thickness groups, suggesting that no specific glass thickness exhibited a statistically significant difference. The corresponding scatter plot of the complete dataset is shown in Fig. 6.15b. Nevertheless, more subtle tendencies could be identified. In particular, the 12 mm model showed slight deviations compared to the 6 mm and 8 mm models, indicating a possible thickness-related influence. At the

same time, the model for the 8 mm glass thickness was not statistically significant, as the corresponding confidence interval of β_1 included both positive and negative values.

A comparison of the limit values for the individual glass thicknesses reported in Table 6.12 revealed that the limits for the 6 mm and 12 mm subsets did not differ substantially. In contrast, the limit value obtained for the 10 mm subset, amounting to 62.8 MPa, was considerably lower than those of the other thicknesses. However, this case was also associated with the lowest precision at 69.2%. The selection of an aggregated model comprising glass thicknesses from 6 mm to 12 mm was therefore appropriate, as the resulting overall limit value of 71.2 MPa encompassed the rounded limit values of the individual glass thicknesses. Using this limit, a clear distinction between TTG and HSG could be achieved when edge stress was measured using the PST method. At the same time, the corresponding recall reached 100%.

Table 6.12: Limit values for edge stress (determined by phase-shifting technique) vs. bending stress for thermally toughened glass, including classification metrics for each glass thickness

t [mm]	n	Limit [MPa]	Precision [%]	Recall [%]
6 *	39	71.3	100.0	100.0
8	37	68.2	100.0	100.0
10 *	19	62.8	69.2	100.0
12 *	20	69.9	100.0	100.0
6–12 *	115	71.2	100.0	100.0

* Not statistically significant based on bootstrap confidence intervals

6.7.2 Logistic regression

For logistic regression with edge stress as predictor, the specimens were categorized as conforming and non-conforming TTG depending on the destructive test results according to the fracture pattern and bending strength required in EN 12150-1 (2020).

6.7.2.1 Logistic regression with edge stress (MWP)

As illustrated in Fig. 6.16a, the edge stress values determined by MWP were classified into two categories: conforming (=1) and non-conforming (=0) TTG for all glass thicknesses. Fig. 6.16b presents the corresponding categorization for the individual glass thicknesses ranging from 6 mm to 12 mm. A clear distinction between TTG and HSG was evident for glass thicknesses of 8 mm and 12 mm. The 10 mm specimens exhibited an overlap in the edge stress range from approximately 80 MPa to 82 MPa. For the 6 mm glass thickness, the dataset did not contain any HSG specimens, as edge stress measurements obtained by MWP were not reliable for this glass type. As a result, it was not feasible to construct a regression model for the 6 mm specimens.

The statistical data of the model is given in Appendix Table A.16. The S-shaped curves of the individual glass thicknesses as well as the complete model including all glass thicknesses are displayed in Fig. 6.17a. The curves of the thickness-specific models were very steep and laid close to each other. Accordingly, the limit values for probabilities of 0.5 and 0.95 were

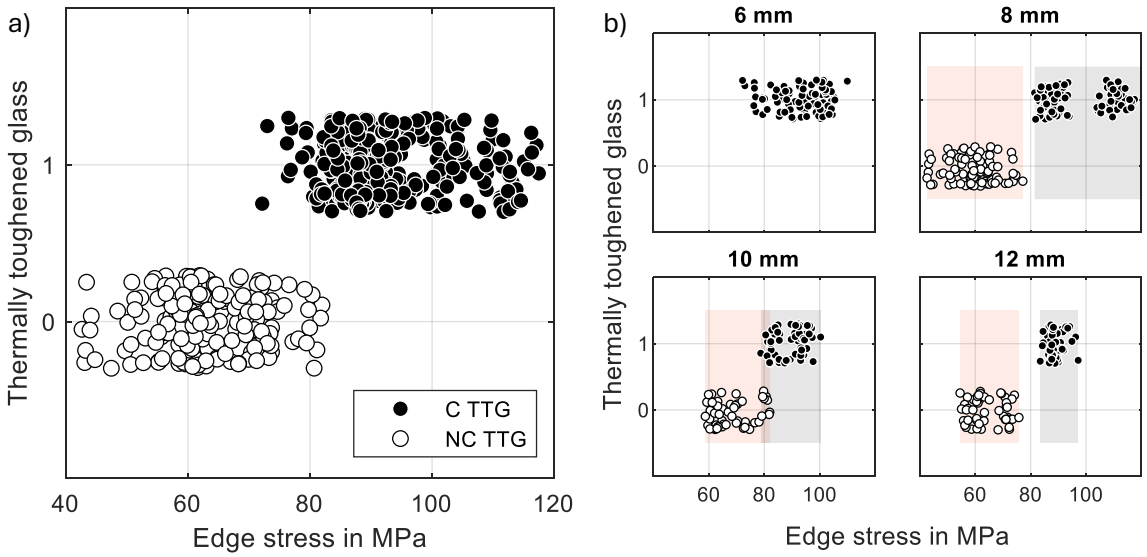

Figure 6.16: Distribution of conforming and non-conforming thermally toughened glass depending on edge stress (determined by multiple-wavelength photoelasticity) a) for all glass thicknesses 6–12 mm and b) split into glass thicknesses from 6 mm to 12 mm

almost identical, as illustrated in Fig. 6.17b. Only the complete model of glass thicknesses 6–12 mm yielded a statistically significant regression model. Therefore, the limit values derived for the individual glass thicknesses (reported in Table 6.13) together with their corresponding performance metrics should be interpreted with caution.

Table 6.13: Limit values for edge stress (determined by multiple-wavelength photoelasticity) for thermally toughened glass determined for probabilities 0.5 and 0.95, including classification metrics

t [mm]	n	Probability = 0.5			Probability = 0.95		
		Limit [MPa]	Precision [%]	Recall [%]	Limit [MPa]	Precision [%]	Recall [%]
8	210	79.2	100.0	100.0	79.4	100.0	100.0
10 *	111	80.9	94.8	96.5	83.5	100.0	80.7
12	108	78.6	100.0	100.0	78.9	100.0	100.0
6–12 *	516	77.9	96.9	97.8	83.4	100.0	90.9

* Model fit significant by likelihood-ratio χ^2 test

For the determination of the limit values, the analysis was restricted to probability levels of 0.5 and 0.95 due to the steep slope of the corresponding logistic curve. The limit value obtained for the aggregated model at a probability level of 0.95, amounting to 83.4 MPa, was comparatively high and resulted in a rejection rate of 9% while maintaining a precision of 100%. This indicated a clear separation between conforming and non-conforming TTG specimens. In contrast, the limit value of 77.9 MPa derived at a probability level of 0.5 represented a more balanced trade-off between precision and recall. Both limit values were subsequently compared and discussed in Section 6.8.

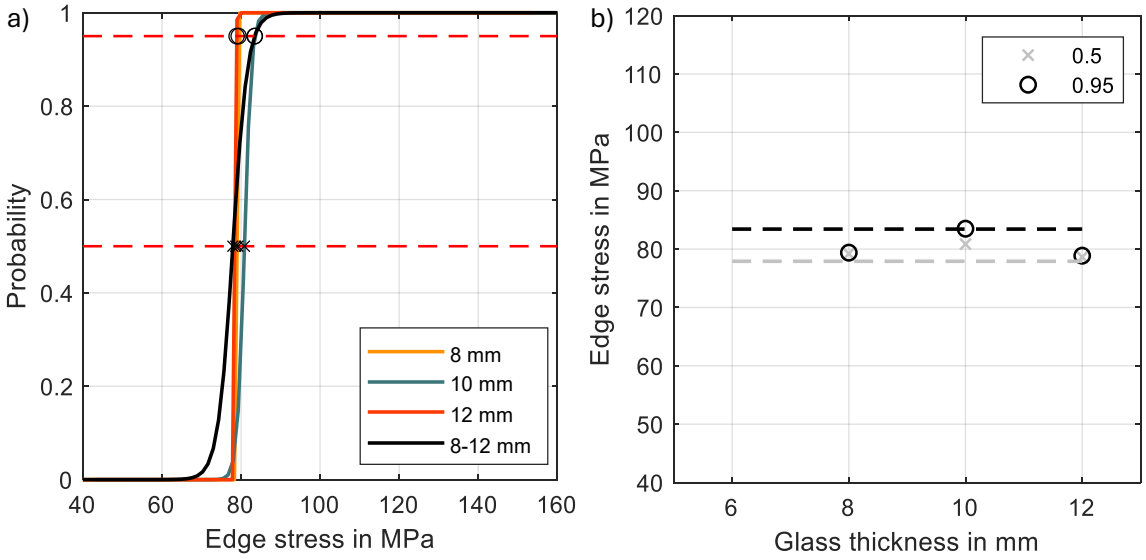

Figure 6.17: Logistic regression analysis of edge stress (determined by multiple-wavelength photoelasticity) for thermally toughened glass: a) fitted sigmoid curves depending glass thickness; b) thickness-specific limit values derived from probability thresholds of 0.5 and 0.95

6.7.2.2 Logistic regression with edge stress (PST)

In contrast to the edge stress values determined using MWP, the edge stress measured by PST allowed a clear distinction between the two conformity categories, as illustrated in Fig. 6.18 for both the aggregated model comprising (a) all glass thicknesses and (b) the models for the individual glass thicknesses. In addition, the PST method provided reliable measurements for 6 mm HSG, enabling the derivation of four thickness-specific models for glass thicknesses ranging from 6 mm to 12 mm.

Due to the pronounced separation between the two categories, the resulting logistic regression models were not statistically significant. The corresponding statistical parameters are reported in Appendix Table A.17. The associated S-shaped curves shown in Fig. 6.19a exhibited a very steep transition. Consequently, only probability thresholds of 0.5 and 0.95 were considered for the determination of the limit values, as the corresponding limits laid in close proximity.

The aggregated model including glass thicknesses from 6–12 mm yielded lower limit values than the thickness-specific models for 10 mm and 12 mm glass. Although Table 6.14 shows that the aggregated model also achieved perfect performance metrics, with both precision and recall reaching 100%, the highest rounded limit value of 72 MPa, corresponding to the limits obtained for the 10 mm and 12 mm glass thicknesses, was selected for further comparison. This choice ensured a conservative and robust assessment of TTG.

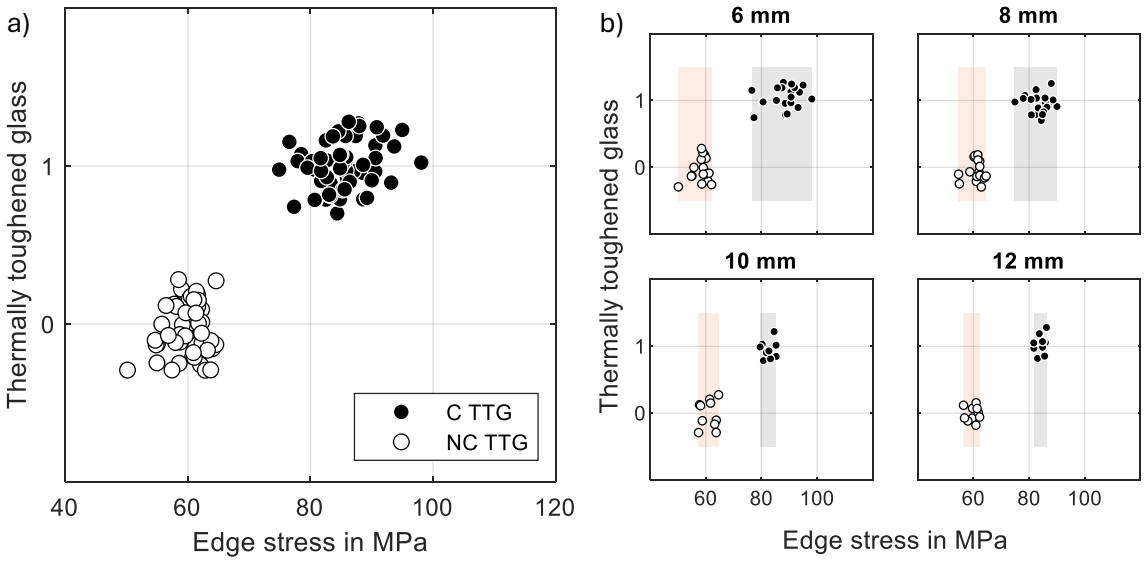

Figure 6.18: Distribution of conforming and non-conforming thermally toughened glass depending on edge stress (determined by phase-shifting technique) a) for all glass thicknesses and b) split into glass thicknesses from 6 mm to 12 mm

Table 6.14: Limit values for edge stress (determined by phase-shifting technique) for thermally toughened glass determined for probabilities 0.5 and 0.95 for each glass thickness, including classification metrics

t [mm]	n	Probability = 0.5			Probability = 0.95		
		Limit [MPa]	Precision [%]	Recall [%]	Limit [MPa]	Precision [%]	Recall [%]
6	39	71.1	100.0	100.0	71.5	100.0	100.0
8	36	70.8	100.0	100.0	71.1	100.0	100.0
10	19	71.9	100.0	100.0	72.2	100.0	100.0
12	20	72.0	100.0	100.0	72.3	100.0	100.0
6–12 *	114	70.9	100.0	100.0	71.1	100.0	100.0

* Model fit significant by likelihood-ratio χ^2 test

6.8 Discussion of limit values for thermally toughened glass

To investigate the reliability of the determined limit values for TTG, the models selected from the previous chapters were validated. A k-fold validation with five subsets (k = 5) was utilized for this purpose. The validation was performed on quantile and logistic regression model for both photoelastic measurements of MWP and PST. Within the iterations, limit values were formed, which could be compared to the main model with the complete dataset without test set as a range with minimum and maximum values.

6.8.1 Evaluating TTG with surface stress

The surface stress limit values derived from quantile regression based on fracture pattern and from logistic regression for TTG were dependent on glass thickness, with distinct

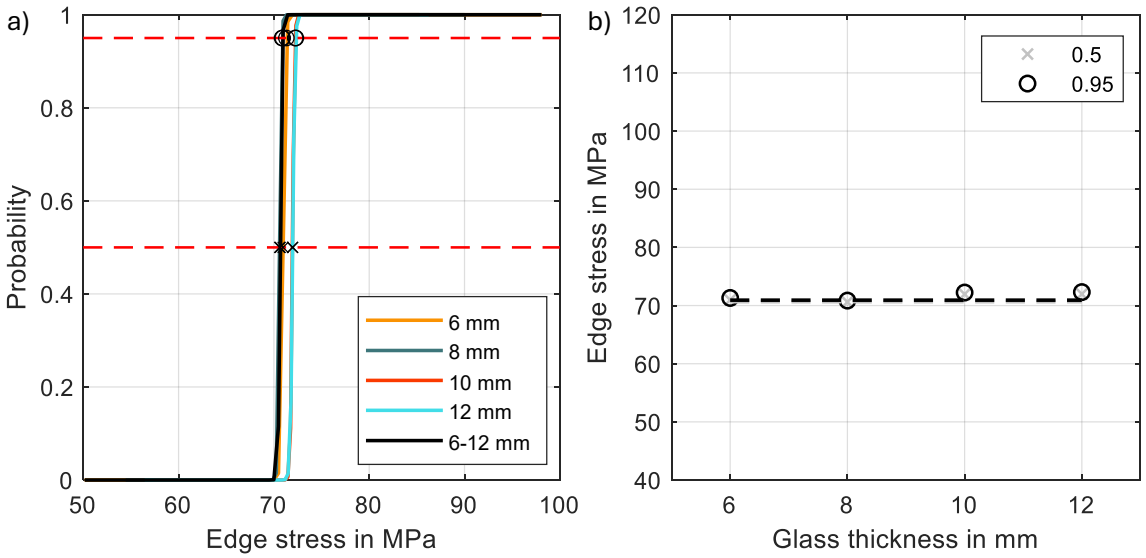

Figure 6.19: Logistic regression analysis of edge stress (determined by phase-shifting technique) for thermally toughened glass: a) fitted sigmoid curves depending glass thickness and b) thickness-specific limit values derived from probability thresholds of 0.5 and 0.95

ranges observed for thicknesses of 4 mm, 6 mm, and 8–12 mm. Fig. 6.20 illustrates the limit values obtained using k-fold cross-validation as well as those derived from the complete dataset. Evaluation of Fig. 6.20 shows that meeting the fracture pattern criterion required higher surface stress values. This indicates that the fracture pattern constitutes the more critical conformity criterion for TTG with respect to surface stress, in comparison to strength-based evaluation. The statistical details of the individual k-fold validations can be found in Appendix from Table A.21 to Table A.27.

As illustrated in Fig. 6.20, the results of the logistic regression analysis yielded lower values in comparison to those of the quantile regression analysis. This occurrence could be attributed to the clear division of the surface stress for the test specimens with glass thicknesses of 6 mm and 8–12 mm into two categories 0 and 1. Logistic regression was a more suitable model for a database with categories that overlap. Given that logistic regression was not statistically significant because of this clear distinction, the limit value was determined by selecting approximately the midpoint between the classes. Therefore, the selection of probability was of negligible relevance, as the limit values were similar. The spacing between the surface stress values of HSG and TTG was pronounced for the 6 mm dataset and the aggregated 8–12 mm dataset investigated in this study. Therefore, the selection of the limit values determined by logistic regression would not be a safe option, as it cannot be guaranteed that the low limit values chosen in the middle between the categories would identify non-conforming TTG correctly. Consequently, for glass thicknesses of 6 mm and the aggregated 8–12 mm range, the limit values derived from quantile regression for predicting the fracture pattern of TTG were better suited for non-destructive quality control based on surface stress.

However, given the availability of non-conforming TTG specimens for 4 mm glass thickness, logistic regression was a suitable alternative to quantile regression. Given that the limit value of 114 MPa determined by quantile regression with all 4 mm specimens with a

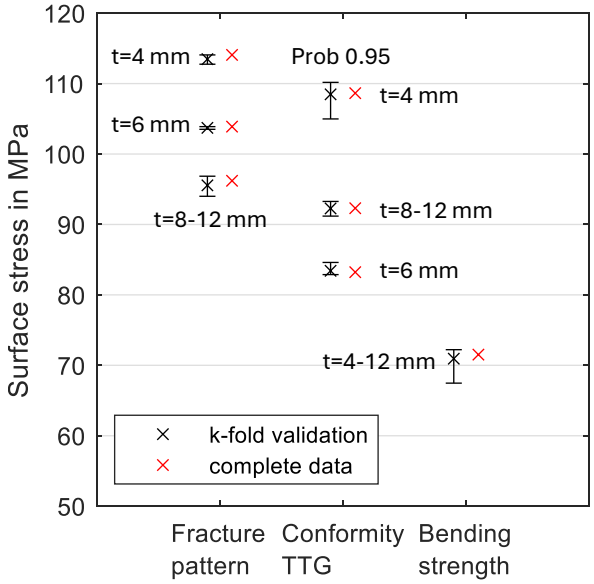

Figure 6.20: Surface stress limit values for thermally toughened glass determined by quantile regression for fracture pattern and bending strength and by logistic regression for assessing TTG conformity with min and max values of k-fold validation and values determined with complete data, specification of valid glass thickness

recall of 56.3% would result in the rejection of an excessive number of test specimens, the limit value of 109 MPa obtained by the logistic regression with a recall of 76.1% and a precision of 98.2% provided an acceptable compromise. However, the even lower limit of 106 MPa from the quantile regression, which was determined using only the data points from manufacturer B, showed a comparable precision of 98.4% when tested on all 4 mm surface stress values, but a higher recall of 85.9%. Therefore, the limit for the 4 mm glass was set at 106 MPa.

The limit values for surface stress, which are intended to ensure both TTG properties with a focus on the fracture pattern as a critical variable, are given in Table 6.15 for each glass thickness.

Table 6.15: Preliminary minimum surface stress limit values for thermally toughened glass statistically determined on standard-format specimens (360 mm x 1100 mm)

Glass thickness [mm]	4	6	8	10	12
Surface stress [MPa]	106	104	96	96	96

6.8.2 Evaluating TTG with edge stress

Fig. 6.21 shows the minimum and maximum limit values for edge stress from the k-fold validation compared to the calculation with the complete database, differentiated by regression model and edge stress measurement method of MWP and PST. The associated statistical details of the k-fold validation are provided in Appendix from Table A.28 to Table A.33.

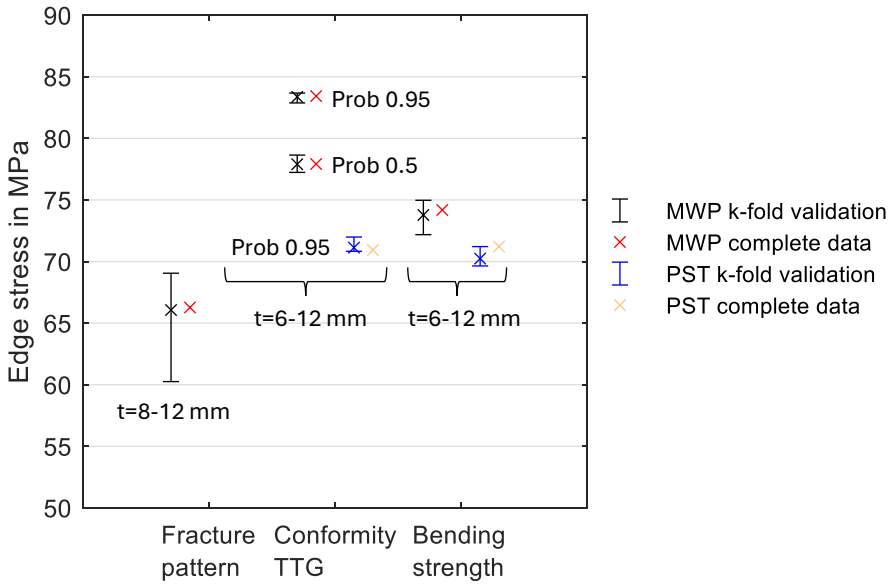

Figure 6.21: Edge stress limit values for thermally toughened glass determined by quantile regression for fracture pattern and bending strength and by logistic regression for assessing TTG conformity with min and max values of k-fold validation and values determined with complete data, edge stress measured with multiple-wavelength photoelasticity and phase-shifting technique, specification of valid glass thickness and probability threshold for logistic regression

The spread in the k-fold validation of logistic regression as well quantile regression with bending stress was low for glass thicknesses of 6–12 mm. In contrast, the scatter in the k-fold validation of the quantile regression model of edge stress measured by MWP with fracture pattern was higher. It is evident that the quantile regression model yielded higher limit values for bending strength than the fracture pattern model. On the one hand, this could be due to the fact that the edge stress has more of an influence on strength. On the other hand, it may also be that the statistical model of edge stress and fracture pattern was not strong, as the correlation analysis from Section 5.5.4 has already shown. The focus was therefore on the higher limits of the models of logistic regression and quantile regression with bending strength.

The statistical determination of limit values for edge stress was performed using PST as well as MWP. Although the regression analysis based on edge stress measured by PST used fewer specimens than by MWP, a more reliable evaluation of the 6 mm specimens was possible, as the HSG specimens could also be evaluated. As can be seen in Fig. 6.21, regression models employing PST edge stress values attained reduced limits in comparison to those derived from MWP values. A significant difference between MWP and PST was especially apparent in the case of logistic regression.

However, the limit values determined in this research and intended for use in production control should not be limited to a method or a measuring device for measuring edge stress. The limit value for edge stress should be set in such a way that it is neither too high and thus has a high reject rate, nor is it too low to pose a safety risk in quality control. Consequently, limits of various regression models from both edge stress measurement methods MWP and PST are compared in Table 6.16. The limit values were chosen on

the basis of the maximum limit value of the k-fold validation and are ordered by size. In addition, the metric values are listed, which were tested separately on edge stress values measured with one method or on all available values together.

Table 6.16: Comparison of edge stress limit values determined by multiple-wavelength photoelasticity and phase-shifting technique for thermally toughened glass, tested on all small-format specimens

			Database including all edge stress values		Edge stress values by MWP		Edge stress values by PST	
Modell	Method	Limit [MPa]	Precision [%]	Recall [%]	Precision [%]	Recall [%]	Precision [%]	Recall [%]
LogReg (0.95)	PST	71	91.3	100.0	89.8	100.0	100.0	100.0
QuanReg	PST	72	92.6	100.0	91.4	100.0	100.0	100.0
QuanReg	MWP	75	96.6	99.2	96.0	99.4	100.0	98.3
LogReg (0.5)	MWP	78	97.3	96.8	96.9	97.8	100.0	91.5
LogReg (0.95)	MWP	84	100.0	82.76	100.0	86.8	100.0	61.0

The tested models showed different levels of precision and recall. In this section, the precision rate was utilized as a metric for distinguishing TTG and NC HSG, given that no non-conforming TTG was present in the database of edge stress. While the lower limits of 71 and 72 MPa led to a recall of 100%, the precision in this range diminished to approximately 90–93%. Consequently, insufficiently tempered glass was incorrectly classified as TTG and the probability of false positives increases.

It is noticeable that the differentiation of the glass types regarding edge stress measured by PST could be achieved with a precision of 100% for all limit values. At the same time, the recall rate increased with increasing limit values up to 61% at 84 MPa. Especially when measuring edge stress using PST, too many test specimens would be sorted out unnecessarily.

Finally, at a limit value of 78 MPa, the model achieves the highest precision (97–100%), while the recall is moderately reduced (approx. 92–97%). This minimizes the risk of false positives to a minimum. In the context of quality control for TTG, it is imperative to ensure the safety of the process, particularly in instances where glass is declared as conforming by photoelastic measurement despite not meeting the requisite tempering standards. Therefore, it is reasonable to accept a small percentage of false negatives to achieve maximum discrimination between conforming and non-conforming TTG.

The choice of the limit of 78 MPa for edge stress to ensure both the properties of fracture pattern and bending strength of TTG for glass thicknesses of 6–12 mm proved to be a good compromise. Although the value did not allow a clear distinction between non-conforming HSG and conforming TTG for MWP values, a distinction between conforming HSG and TTG was at least possible. Therefore, in production control, this limit value should ideally be applied primarily to specimens pre-stressed as TTG to check if the conformity according to EN 12150-1 (2020) is fulfilled. Should the edge stress measured with MWP be utilized as a differentiating criterion, a measured value of over 84 MPa would reliably indicate conforming TTG.

The limit values for edge stress, which are to be used to evaluate the tempering quality of TTG including the fracture pattern and bending strength, are given in Table 6.17

depending on the glass thickness.

Table 6.17: Preliminary minimum edge stress limit values for thermally toughened glass statistically determined on standard-format specimens (360 × 1100 mm^2)

Glass thickness [mm]	4	6	8	10	12
Edge stress [MPa]	–	78	78	78	78

6.9 Surface stress threshold analysis for heat-strengthened glass

A photoelastic limit range was required to characterize HSG with surface stress measurements. The lower limit ensures a strength of 70 MPa and was determined using quantile regression. The upper limit restricts the coarse fracture pattern of HSG according to EN 1863-1 (2012) and was determined using logistic regression. The database used to determine the surface stress limits consisted of glass thicknesses ranging from 4 to 12 mm. Appendix Table A.14 and Table A.18 shows the statistical information and the exact number of specimens.

6.9.1 Quantile regression for the lower limit

The analysis of quantile regression, with surface stress as the predictor and bending stress as the predicted metric variable, was a suitable method for determining the lower limit value for classifying HSG regarding the minimum strength of 70 MPa. If the regression model were calculated based on the complete database compromising TTG and HSG specimens, a limit value of 9.4 MPa would be obtained, as illustrated as the grey regression line with intersection point in Fig. 6.22b. It is evident that, in view of the available experience, the specified value was inadequate to guarantee the requisite strength for HSG. In the subsequent stage of the investigation, the variation was analyzed by removing TTG specimens from the database. After reducing the complete dataset to specimens tempered using cooling parameters for HSG, the regression line exhibited a steeper slope, as evidenced by the red curve in Fig. 6.22b. The intersection point of this regression line with the strength criterion of 70 MPa resulted in a corresponding surface stress limit of 20.9 MPa. An analysis of the 95% confidence intervals of the intercept β_0 and the slope coefficient β_1 obtained from the thickness-specific models shown in Fig. 6.22a revealed complete overlap of both coefficients. This indicated that a differentiation based on glass thickness was not required. Furthermore, the diagram shows that the models for the 4 mm, 6 mm, and 10 mm glass thicknesses were not statistically significant, as the corresponding confidence intervals of β_1 included zero. This suggested that the associated limit values were of limited reliability and should therefore be interpreted with caution.

Table 6.18 presents the surface stress limits for each glass thickness, which exhibited significant differences. Nevertheless, no systematic trend attributable to glass thickness could be identified. Therefore, the limit of 20.9 MPa was determined from the complete dataset including all HSG specimens with glass thicknesses from 4 to 12 mm. In this case, an assessment of the precision metric was not meaningful, as no specimens with insufficient

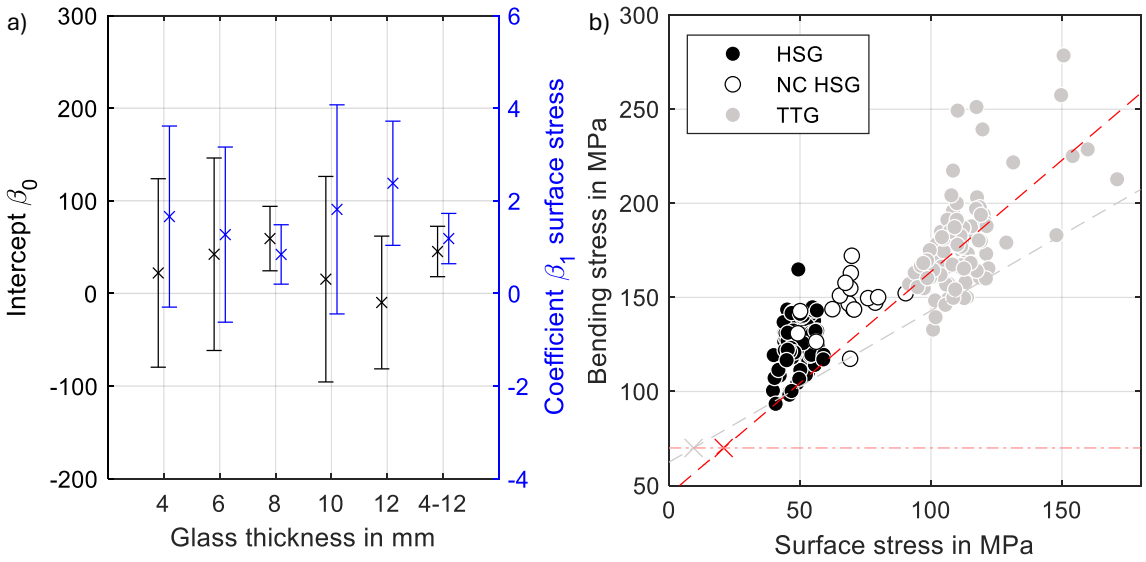

Figure 6.22: Quantile regression (5%) Surface stress vs. Bending stress for heat-strengthened glass with a) confidence intervals for the intercept β_0 and the coefficient β_1 of the independent variable surface stress depending on glass thicknesses and b) scatter plot with regression lines

Table 6.18: Limit values for surface stress vs. bending stress for heat-strengthened glass, including classification metrics for each glass thickness

t [mm]	n	Limit [MPa]	Precision [%]	Recall [%]
4	166	28.9	-	100.0
6	165	21.8	-	100.0
8 *	161	12.8	-	100.0
10	85	30.1	-	100.0
12 *	84	33.5	-	100.0
4–12 *	661	20.9	-	100.0

* Statistically significant based on bootstrap confidence intervals

pre-stress were present in the dataset. Since the recall reaches 100% for all evaluated limit values, it was plausible that the currently applied limit value may be underestimated.

6.9.2 Logistic regression for the upper limit

The upper limit for HSG depends on the fracture pattern, which was evaluated in accordance with EN 1863-1 (2012). The evaluation of this variable was classified as either conforming or non-conforming, and a logistic regression was a suitable analysis method in this case. As illustrated in Fig. 6.23, the division into the two categories conforming (=1) and non-conforming (=0) is shown for all glass thicknesses as well as for each individual glass thickness. The diagram showing the complete database with all glass thicknesses demonstrated an overlap of the classes. Conversely, the glass thicknesses of 4 mm and 6 mm demonstrated a substantial gap between the non-conforming and conforming HSG, while the glass thicknesses of 8 mm and 10 mm exhibited a discernible distinction between

the two classes, albeit with a reduced gap. It was notable that only the 12 mm thick glass model displayed a minimal overlapping area.

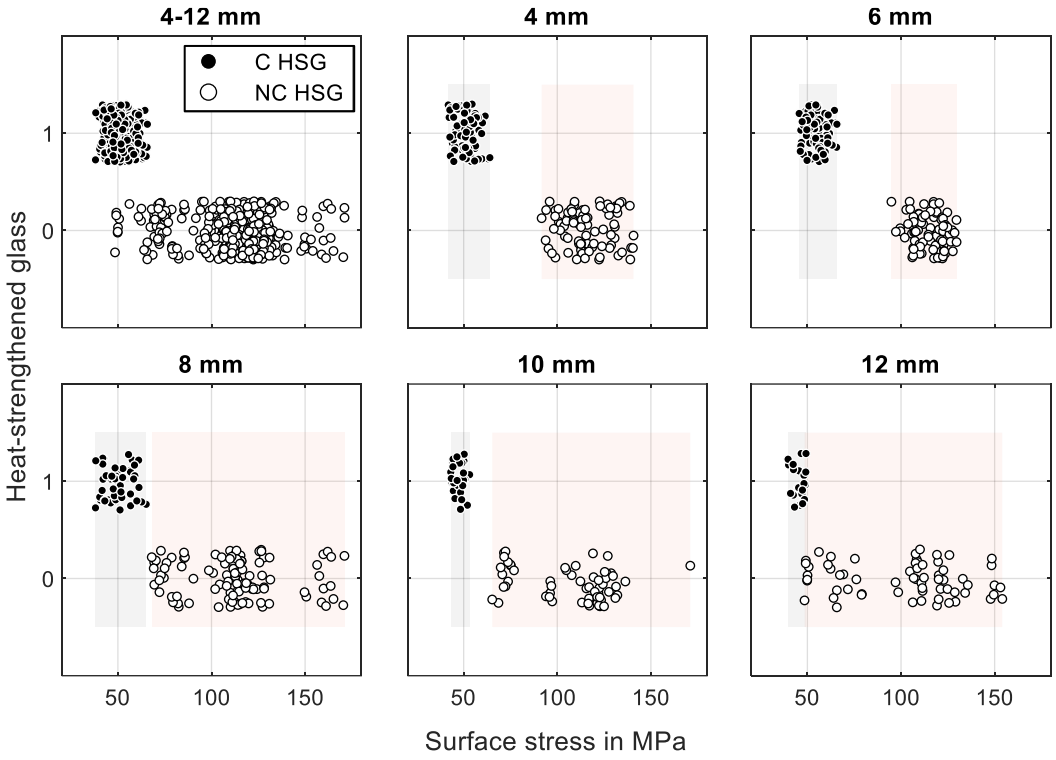

Figure 6.23: Distribution of conforming and non-conforming heat-strengthened glass depending on surface stress split into glass thicknesses from 4 mm to 12 mm

As shown in Fig. 6.23, the categories were imbalanced with a higher number of specimens classified as non-conforming HSG. This was because the non-conforming category included not only HSG specimens exhibiting an insufficient tempering level but also TTG specimens. To better understand the distribution of categories, Fig. 6.24 presents the surface stress values per glass thickness distinguishing between glass types of conform/non-conforming HSG and TTG. It can be seen here that there were no non-conforming HSG test specimens in the range of 66 MPa to 91 MPa for glass thicknesses of 4 mm and 6 mm. As previously observed for the logistic regression based on surface stress for TTG, a pronounced separation between the categories was also evident in the present case. For glass thicknesses ranging from 8 mm to 12 mm, a decreasing trend in surface stress with increasing glass thickness was observed for both non-conforming and conforming HSG specimens. This observation was highlighted in color in Fig. 6.24. Given the finding that the surface stress measurements for glass thicknesses of 4 mm, 6 mm, and 8 mm were approximately equivalent, these thicknesses were grouped and assessed within a single logistic model. The glass thicknesses of 10 mm and 12 mm formed two separate logistic models.

The S-shaped curves for the thickness-specific models as well as for the aggregated 4–8 mm model are shown in Fig. 6.25. The 8 mm curve is obscured by the 4–8 mm curve. Depending on the glass thickness, a decreasing trend in surface stress could be observed: while the curves for glass thicknesses of 4 mm and 6 mm were located in the higher range of the surface stress scale, the curves for thicker glass laid in the lower range of values. All curves were very steep, which could be attributed to the clear separation between the classes. As

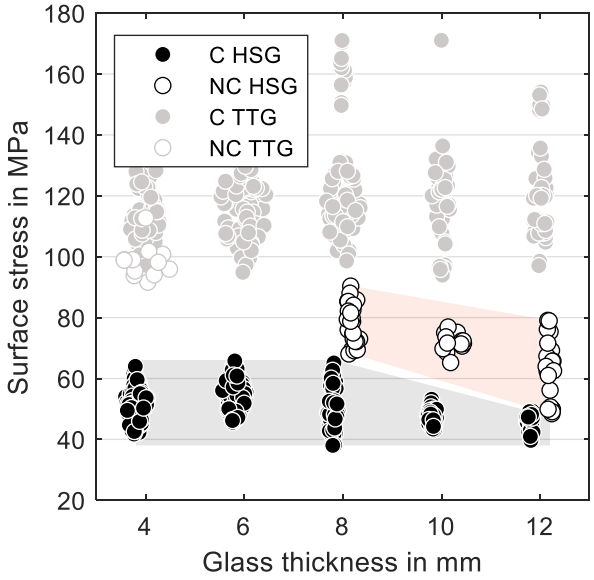

Figure 6.24: Surface stress values distinguished by color for conforming heat-strengthened glass, non-conforming heat-strengthened glass, and thermally toughened glass

illustrated in Fig. 6.25b, the limit values of the probabilities 0.5 and 0.95 were once again in close proximity. In addition to these two fixed probabilities, the Youden method was employed to determine the optimal threshold. The probability threshold, as determined through this methodology, is presented in Table 6.19, along with the associated limit value and metrics.

Table 6.19: Limit values for surface stress for thermally toughened glass determined for probability 0.95 and the Youden's method with probability threshold for each glass thickness, including classification metrics

t [mm]	n	Probability = 0.95			Youden			
		Limit [MPa]	Precision [%]	Recall [%]	thr	Limit [MPa]	Precision [%]	Recall [%]
4	166	79.6	100.0	100.0	1.00	71.5	100.0	100.0
6	165	81.8	100.0	100.0	1.00	74.0	100.0	100.0
8	161	66.4	100.0	100.0	1.00	65.1	100.0	100.0
10	85	59.5	100.0	100.0	1.00	54.3	100.0	100.0
12	84	50.3	100.0	100.0	1.00	50.1	100.0	100.0
4–8 *	492	66.8	100.0	100.0	1.00	65.8	100.0	100.0

* Model fit significant by likelihood-ratio χ^2 test

Based on the available test specimens, it was reasonable to combine the specimens in the 4–8 mm glass thickness range. The 4 mm and 6 mm thicknesses could not be reliably evaluated individually, as no non-conforming HSG specimens were available in the database, as can be seen in Fig. 6.24. This would otherwise shift the limit value to a midpoint between the two categories. This would not be a good approach in terms of safety guarantees, as it would result in a too wide range, which the HSG may not be able to verify reliably: as shown in Fig. 6.24, the maximum measured surface stress values for conforming HSG in glass thicknesses from 4 to 8 mm indicated that such high limit values were not on the safe

side. Nevertheless, the combined model was also not statistically significant due to the pronounced separation between the two classes. However, the determined limit value of 65.8 MPa appeared to be a suitable compromise, as it approximately matched the limit value of the single 8 mm model while also constraining the 4 mm and 6 mm values.

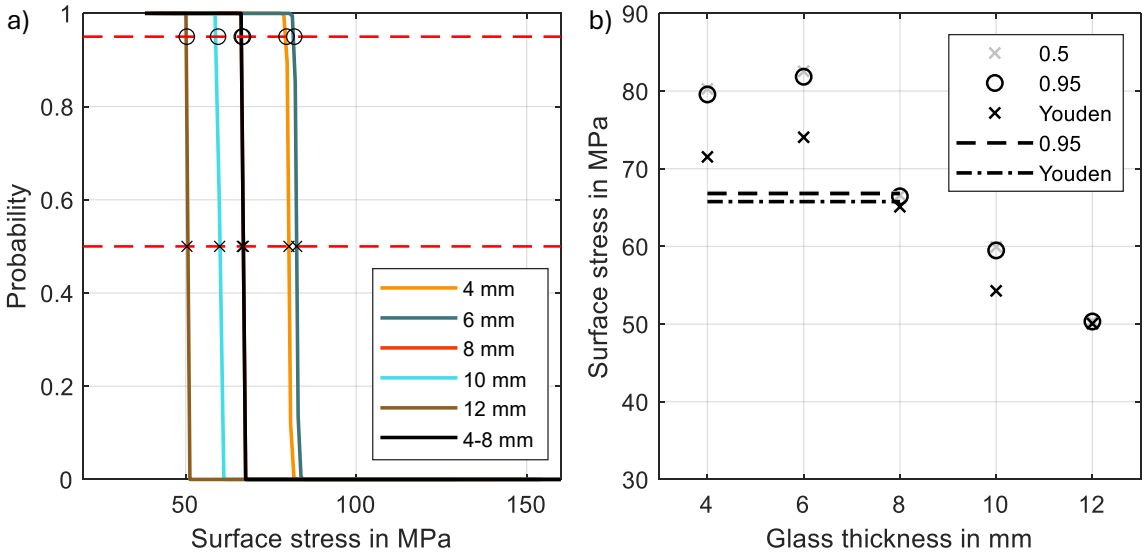

Figure 6.25: Logistic regression analysis of surface stress for heat-strengthened glass: a) sigmoid fitted curves depending glass thickness and b) thickness-specific limit values derived from probability thresholds of 0.5 and 0.95 and the Youden's Index

The dataset for 10 mm glass thicknesses also demonstrated a clear distinction between non-conforming and conforming HSG. Consequently, the statistical model was not significant. However, the limit value of 54.3 MPa, as determined by Youden threshold, was deemed an acceptable value. This determination was supported by the surface stress values measured and presented in Fig. 6.24. The individual model for 12 mm demonstrated an overlap between non-conforming and conforming HSG, thereby indicating its statistical significance. According to Youden's methodology, the limit value was thus established at 50.1 MPa.

6.10 Edge stress threshold analysis for heat-strengthened glass

Two limit values were required to characterize HSG with edge stress. The lower strength limit of 70 MPa was determined using quantile regression. The upper limit value, which regulates the fracture pattern of HSG, was determined using logistic regression. The database used to determine the edge stress limits consists of glass thicknesses ranging from 8 to 12 mm. The evaluation also included TTG specimens with a glass thickness of 6 mm. Statistical information and the exact number of specimens are displayed in Appendix Table A.11, Table A.13, Table A.19 and Table A.20.

6.10.1 Quantile regression for the lower limit

The quantile regression analysis was conducted with edge stress values determined by MWP as well as by PST to obtain a lower limit value for evaluating the strength requirement of

HSG. The different measurement methods were compared in Section 6.11.

6.10.1.1 Edge stress (MWP) vs. Bending stress

The quantile regression analysis between edge stress measured by MWP and bending stress employed the same database for determining limit values for HSG as for TTG. Table 6.20 presents the thickness-specific lower limits. It is evident that the glass thicknesses of 10 mm and 12 mm exhibited higher limits that diverge from the 8 mm limit. The established limit value for glass thickness of 12 mm, was deemed inadequate, as evidenced by the recall rate of 90%.

Table 6.20: Limit values for edge stress (determined by multiple-wavelength photoelasticity) vs. bending stress for heat-strengthened glass, including classification metrics for each glass thickness

t [mm]	n	Limit [MPa]	Precision [%]	Recall [%]
6	87	-53.8	-	-
8 *	210	25.5	-	100.0
10 *	111	54.8	-	100.0
12 *	108	58.5	-	90.0
6–12 *	516	36.6	-	100.0

* Statistically significant based on bootstrap confidence intervals

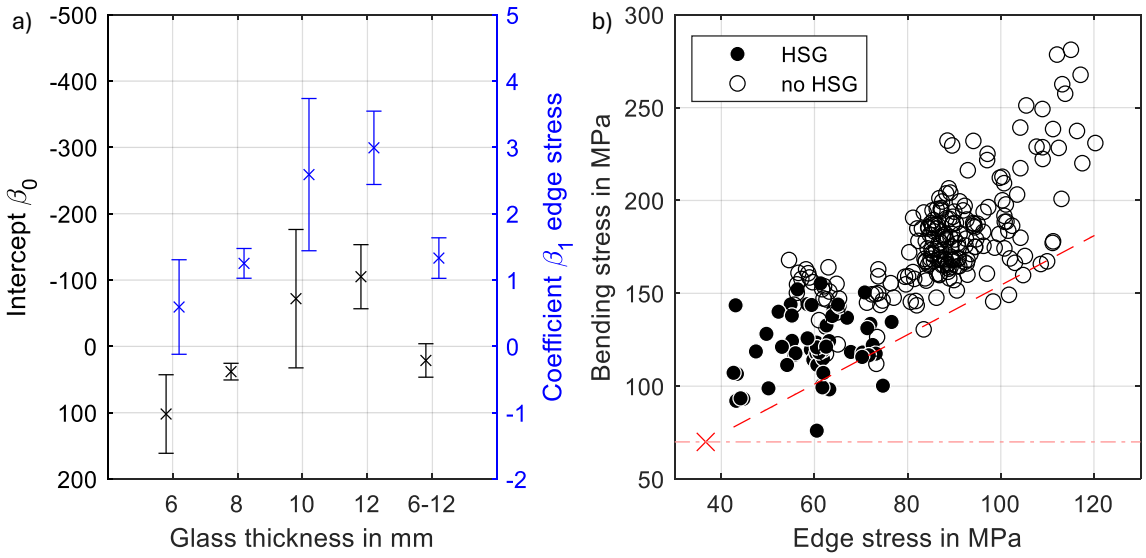

Figure 6.26: Quantile regression (5%) Edge stress vs. Bending stress for heat-strengthened glass with a) confidence intervals for the intercept β_0 and the coefficient β_1 of the independent variable surface stress depending on glass thicknesses and b) scatter plot with regression lines

A closer look at Fig. 6.26a, analogue to the TTG evaluation, revealed that the 6 mm model was not significant, as the 95% confidence interval of β_1 included zero. This outcome could be attributed to the limited dataset, which consisted solely of 6 mm TTG specimens and therefore lacked sufficient variability to produce a robust model. The inadequacy of this

subset for determining a meaningful limit value for HSG became evident in the implausible negative limit value of -53.8 MPa reported in Table 6.20.

Fig. 6.26a displays that the thickness-specific 95% confidence intervals of intercept β_0 and coefficient β_1 for the predictor edge stress were overlapping, see Fig. 6.26a. Therefore, the determination of the lower limit value for HSG was conducted on the entire dataset including specimens with glass thicknesses ranging from 6–12 mm. The regression line exhibited a point of intersection with the required 70 MPa bending strength at a point of 36.6 MPa edge stress, as illustrated in Fig. 6.26b.

6.10.1.2 Edge stress (PST) vs. Bending stress

In contrast to the edge stress values of MWP, an assessment of 6 mm specimens measured using PST, as this method was applicable when measuring 6 mm HSG specimens. This enabled the derivation of four thickness-specific models to assess the influence of glass thickness. Table 6.21 presents the limit values of the thickness-specific models as well as of the aggregated model of 6–12 mm glass thicknesses.

The same dataset as used for the determination of the limit values of TTG was applied, so that the evaluation of the 95% confidence intervals of β_0 and β_1 in Fig. 6.27a remained identical: the intervals overlapped for certain glass thicknesses, with a difference observable between 6 mm/8 mm and 12 mm. However, a clear separation across all glass thicknesses as well as a consistent trend regarding glass thickness could not be identified in this work.

Table 6.21: Limit values for edge stress (determined by phase-shifting technique) vs. bending stress for heat-strengthened glass, including classification metrics for each glass thickness

t [mm]	n	Limit [MPa]	Precision [%]	Recall [%]
6 *	39	38.8	-	100.0
8	37	0.5	-	100.0
10 *	19	33.3	-	100.0
12 *	20	54.6	-	100.0
6–12 *	115	41.4	-	100.0

* Statistically significant based on bootstrap confidence intervals

For the 8 mm model, Fig. 6.27a shows a zero crossing of the 95% confidence interval for the estimate β_1. This finding indicated that the edge stress of this glass thickness did not provide a significant contribution to the description of the regression model. This was further supported by the resulting limit value of 0.53 MPa shown in Table 6.21, which was implausible from a practical standpoint.

The difference between the confidence intervals of 6 mm and 12 mm models observed in Fig. 6.27a was also evident in the corresponding limit values, which differed by 16 MPa. However, the selection of the limit of 54.6 MPa from the 12 mm model as the lower limit for HSG was not considered meaningful. The limit obtained from the 6–12 mm model yielded a more appropriate and practically applicable value of 41.4 MPa, as it was sufficiently high to reliably capture the measurements across thicknesses. The scatter plot and the quantile regression line of the aggregated model without differentiation by glass thickness is shown in Fig. 6.27b.

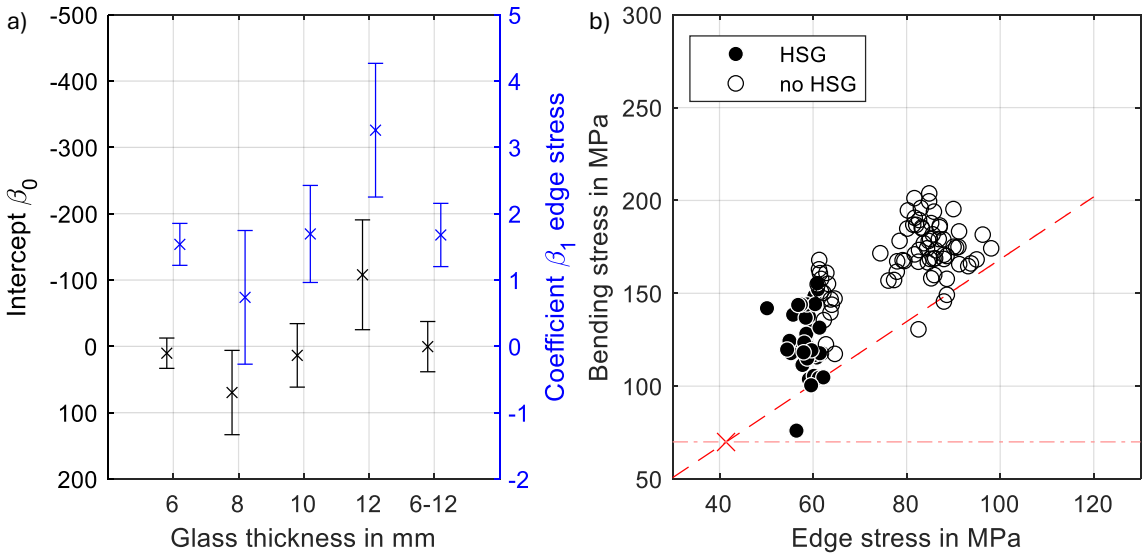

Figure 6.27: Quantile regression (5%) Edge stress (determined by phase-shifting technique) vs. Bending stress for heat-strengthened glass with a) confidence intervals for the intercept β_0 and the coefficient β_1 of the independent variable surface stress depending on glass thicknesses and b) scatter plot with regression lines

6.10.2 Logistic regression for the upper limit

For HSG, logistic regression models were calculated to determine the upper limit of edge stress using values measured by MWP and PST.

6.10.2.1 Logistic regression with edge stress (MWP)

Fig. 6.28 illustrates the division of the edge stress values determined by MWP into two categories: conforming (1) and non-conforming (0) HSG summarized for the glass thicknesses of 8–12 mm (Fig. 6.28a) as well for each individual glass thickness from 6 to 12 mm (Fig. 6.28b). Classification in both classes was based on the evaluation of the fracture pattern in accordance with EN 1863-1 (2012). As could be seen in Fig. 6.28b, the 6 mm dataset consisted exclusively of TTG. Given the fact that the 0 category already comprised a greater number of data points, the aggregated model was calculated without the 6 mm TTG specimens to avoid further imbalance in the distribution of the categories. The complete dataset as well as the group of individual glass thicknesses demonstrated evident overlaps between the two categories.

To gain a more profound insight into the distribution of the 0 category in this logistic regression, Fig. 6.29 demonstrates the pre-stress levels of non-conforming HSG and conforming TTG, divided into glass thickness. For the 8 mm and 12 mm specimens, a clear distinction between TTG and HSG, as well as between TTG and NC HSG could be made. However, the specimens with a glass thickness of 10 mm demonstrated an overlap between TTG and NC HSG. This diagram also demonstrates that the non-conforming HSG specimens of 10 mm and 12 mm glass thicknesses were at the lower end of the conforming HSG. The 10 mm NC HSG specimens appeared to be divided into two parts, a phenomenon that could be explained by the different manufacturers involved.

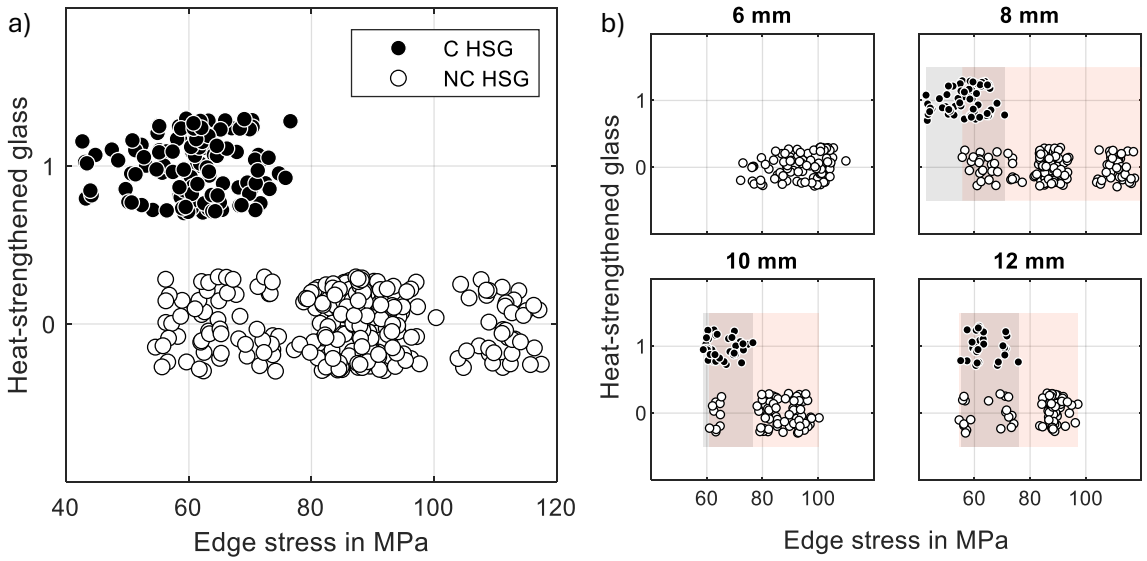

Figure 6.28: Distribution of conforming and non-conforming heat-strengthened glass depending on edge stress (determined by multiple-wavelength photoelasticity) a) summarized for glass thicknesses 8–12 mm and b) split into glass thicknesses from 6 mm to 12 mm

For each glass thickness, a logistic regression model was calculated. The results of the model information are listed in Appendix Table A.19. Fig. 6.30a illustrates the S-shaped curves of the three distinct glass thicknesses. The position of these curves did not differ greatly. Moreover, no uniform trend could be identified regarding glass thickness, so the glass thicknesses were aggregated in one model for determining the limit value.

Table 6.22: Limit values for the 8–12 mm database determined by different evaluation methods and probability thresholds, including classification metrics

Evaluation method	thr	Limit [MPa]	Precision [%]	Recall [%]
Fix threshold	0.95	50.6	100.0	8.6
Precision > 0.9	0.88	55.9	90.6	22.7
False positive rate < 0.1	0.59	64.8	76.2	75.0
Fix threshold	0.50	66.8	72.9	79.7
Distance	0.28	72.0	72.2	95.3
Youden's index	0.24	73.2	71.0	97.7
Fix threshold	0.05	83.0	60.4	100.0

As some of the measured values of NC HSG specimens laid in the range of the conforming HSG specimens, various approaches were tested and compared for ascertaining the opportune probability threshold of the regression model to determine the edge stress limit values for HSG. On the one hand, the evaluation approaches consisted of fixed thresholds of 0.05, 0.5, and 0.95 probability. On the other hand, probability thresholds derived from the ROC curve, such as Youden's Index and Distance, as well as thresholds for the precision of minimum 0.95 probability for HSG and a maximal false negative rate of 0.1 were determined. These thresholds and limit values of the various evaluation methods with metrics are listed in Table 6.22, sorted in ascending order by limit.

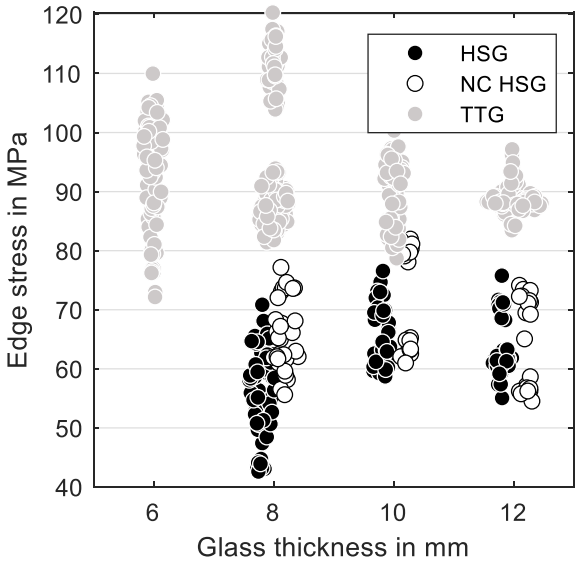

Figure 6.29: Edge stress values (determined by multiple-wavelength photoelasticity) distinguished by color for conforming heat-strengthened glass, non-conforming heat-strengthened glass, and thermally toughened glass

In addition, the position of the limit values determined by the different threshold methods are displayed in the diagrams of the ROC and Precision-Recall curves in Fig. 6.31a und b. The ROC curve had an AUC of 0.9332. The false positive rate increased even at a low true positive rate. This could also be seen in the diagrams in Fig. 6.28 and Fig. 6.29, where the overlap area of the two categories began already at the lowest edge stress values of the conforming HSG.

The automatic calculation to find the optimal threshold according to the method of Distance and Youden's Index as well as the fixed thresholds of 0.5 and 0.05 probability resulted in high limit values of 66.8 MPa to 83.0 MPa. Their recall rates were high, but the precision rates were with 60.4% to 72.9% not sufficiently reliable for ensuring the fracture pattern of HSG. Conversely, the other fixed probability threshold of 0.95 yielded in a limit value of 50.6 MPa which achieved a 100% precision rate. However, the recall rate was found to be low at 8.6%, resulting in an excessive number of rejections.

Therefore, the limit values based on a false positive rate of less than 0.1 and a precision of at least 90% were now under review. Between the values derived from FPR < 0.1 and Prec > 0.9, a considerable gap could be observed in Fig. 6.31a, particularly with respect to the true positive rate. This effect, when expressed as recall, is also evident in Fig. 6.31b. The key question, therefore, was which threshold should be considered as more appropriate. The threshold based on FPR < 0.1 at 64.8 MPa resulted in a precision of 76.2% but achieved a recall of 75.0%. In contrast, the threshold determined by Prec > 0.9 laid at 55.9 MPa, yielding a recall of only 22.7%, which means that approximately 77% of the specimens were falsely rejected. However, with a precision of 90.6%, this threshold would ensure a more conservative and safety-oriented assessment.

Fig. 6.31c shows the S-shaped curve of the logistic regression model including all thicknesses from 8–12 mm. In addition, the conforming and non-conforming HSG specimens are shown, and the corresponding limit values are color-coded according to the threshold method.

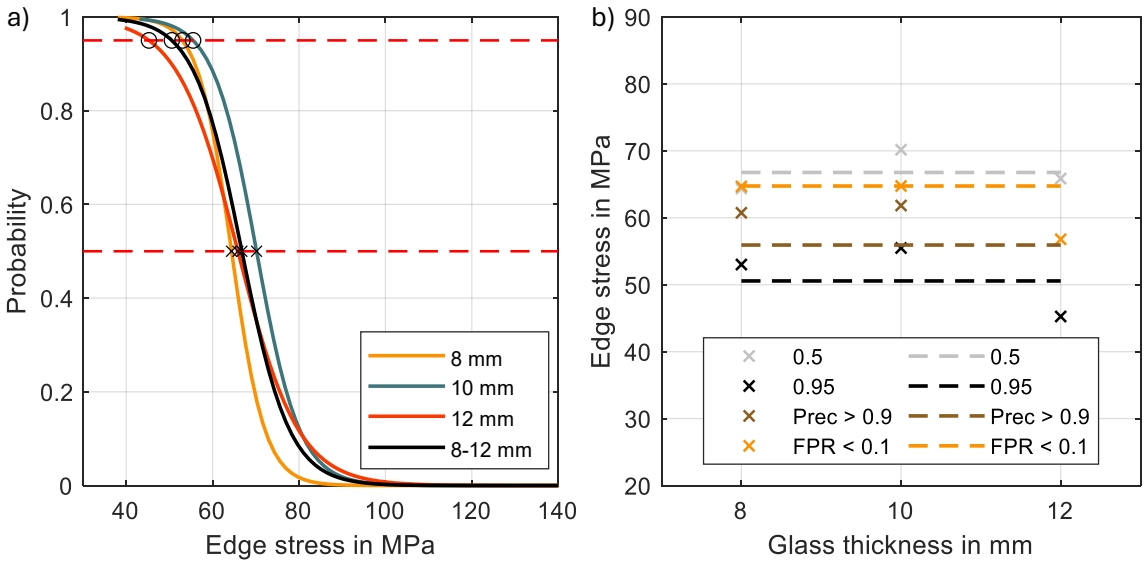

Figure 6.30: Logistic regression analysis of edge stress (determined by multiple-wavelength photoelasticity) for heat-strengthened glass: a) sigmoid fitted curves depending glass thickness and b) thickness-specific limit values derived from probability thresholds of 0.5, 0.95, precision $>$ 0.9, and false positive rate $<$ 0.1

Based on the explanations above, the minimum precision of 90% and the maximum false positive rate of 10% represented a good compromise, so those threshold methods were selected for the further analysis. The resulting limit values of rounded 64 MPa and 56 MPa were compared with the limit values derived from the regression model, which was based on measured values determined by PST edge stress values.

Conclusively, to investigate the influence of glass thickness, Fig. 6.30b shows the limit values for each glass thickness as well as for the complete database, determined by the fixed probabilities of 0.5 and 0.95 as well as by the minimum precision of 90% and the maximum false positive rate of 10%. In addition, the limit values of Prec $>$ 0.9 and FPR $<$ 0.1 including the metrics are shown in Table 6.23.

Table 6.23: Limit values of edge stress (determined by multiple-wavelength photoelasticity) for heat-strengthened glass for each glass thickness determined for precision $>$ 0.9 and false positive rate $<$ 0.1, including classification metrics

t [mm]	n	Precision $\geq$ 90%			False positive rate $\leq$ 10%		
		Limit [MPa]	Precision [%]	Recall [%]	Limit [MPa]	Precision [%]	Recall [%]
8	210	60.7	90.0	70.3	64.7	80.3	89.1
10	111	61.8	91.7	32.35	64.7	72.0	52.9
12	108	–	–	–	56.8	12.5	3.3
8–12 *	486	55.9	90.6	22.7	64.7	76.2	75.0

* Model fit significant by likelihood-ratio χ^2 test

For the 12 mm model, it could be observed that no limit value for a minimum precision of 90% could be determined, since the required precision value was not reached. Furthermore,

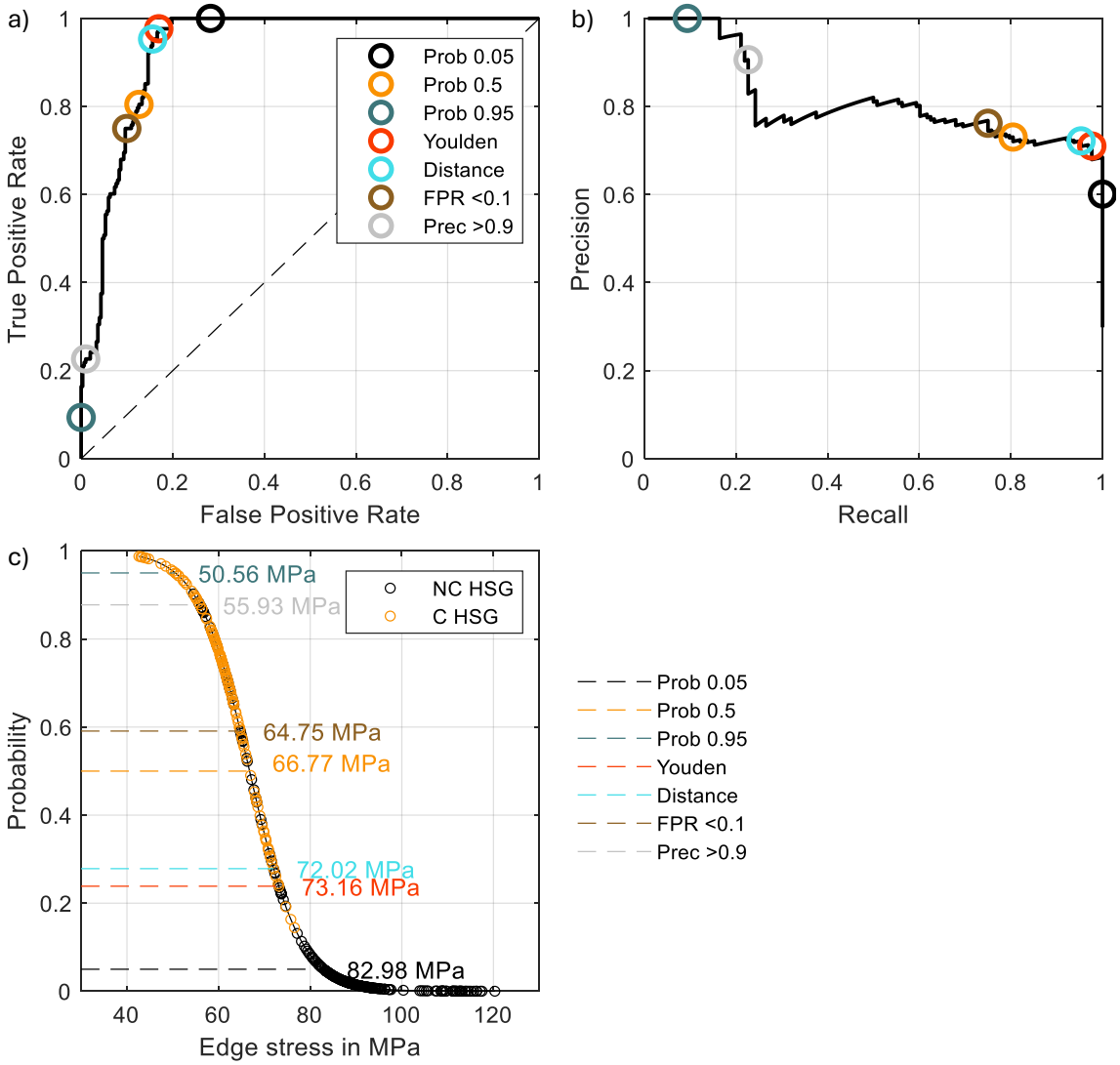

Figure 6.31: Evaluation of classification performance of logistic regression analysis of heat-strengthened glass with edge stress (determined by multiple-wavelength photoelasticity): a) receiver operating characteristic curve, b) precision-recall curve and c) sigmoid curve with marked non-conforming and conforming HSG and method-specific limit values

it could be noted that the limit values for 8 mm and 10 mm models given the criterion Prec > 0.9 were higher than the limit values obtained from the overall model including all glass thicknesses. While the precision rates were comparable, the recall rates of the 8 mm and 10 mm models were superior to those of the complete model. This indicates that the 12 mm specimens exerted an unfavorable influence on the limit value of the overall database. In contrast, given the criterion FPR < 0.1, the limit values of the 8 mm and 10 mm models were similar to those of the complete database. Conversely, the low limit value for the 12 mm specimens based on FPR < 0.1 at 56.8 MPa showed low rates for both precision and recall.

6.10.2.2 Logistic regression with edge stress (PST)

Fig. 6.32 divides the edge stress values measured by PST into the two categories conforming (=1) and non-conforming (=0), both (a) for all glass thicknesses and (b) for each individual glass thickness from 6 to 12 mm. The classification into both categories was based on the evaluation of the fracture pattern according to EN 1863-1 (2012). For the edge stress values obtained by PST, analysis of 6 mm HSG specimens was also possible, even though no non-conforming HSG specimens were available in the dataset (see Fig. 6.33). In Fig. 6.32b, the clear distinction between HSG and TTG specimens of 6 mm glass thickness was visible, while at the same time the distance between the two categories was very wide. The logistic regression model was therefore not significant.

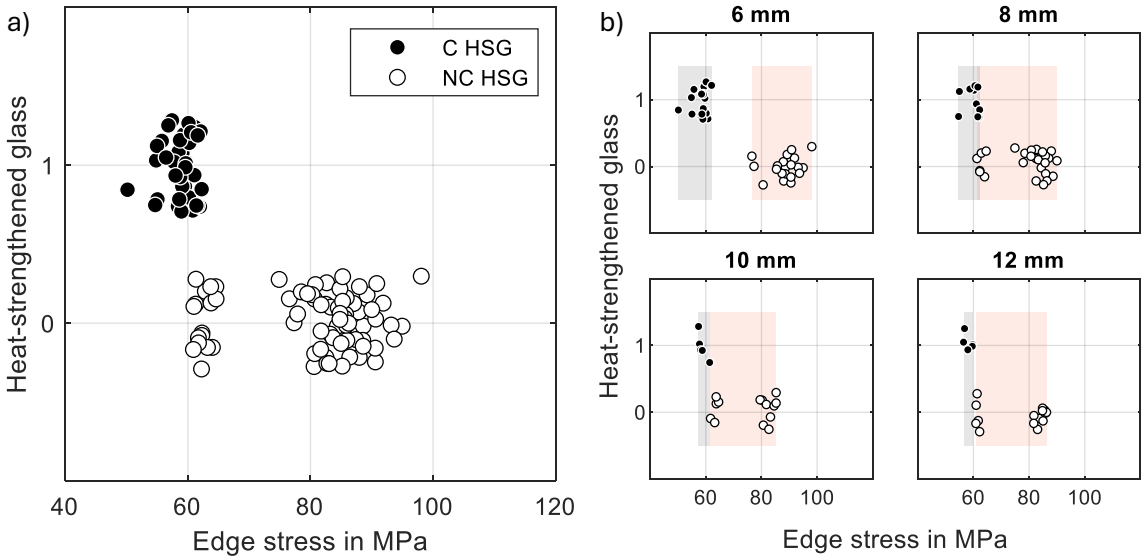

Figure 6.32: Distribution of conforming and non-conforming heat-strengthened glass depending on edge stress (determined by phase-shifting technique) a) for all glass thicknesses and b) split into glass thicknesses from 6 mm to 12 mm

The specimens of glass thicknesses of 10 mm and 12 mm also showed no overlap between categories 0 and 1. However, the distance between the two glass types was very small. This can also be seen in Fig. 6.33, where the categories appeared to almost touch. In contrast, the edge stress values of the complete dataset and the 8 mm dataset exhibited an overlap in the categories, which allowed the logistic regression models to identify a statistically significant relationship.

In Fig. 6.33, the comparison of the measurement values, displayed according to the conformity of the glass type, did not reveal a clear influence of glass thickness on the HSG values: as can be seen, the maximum values of the conforming HSG specimens did not differ substantially with respect to glass thickness. Possibly at 12 mm, a slightly decreasing trend could be identified, which was also reflected in the NC HSG specimens.

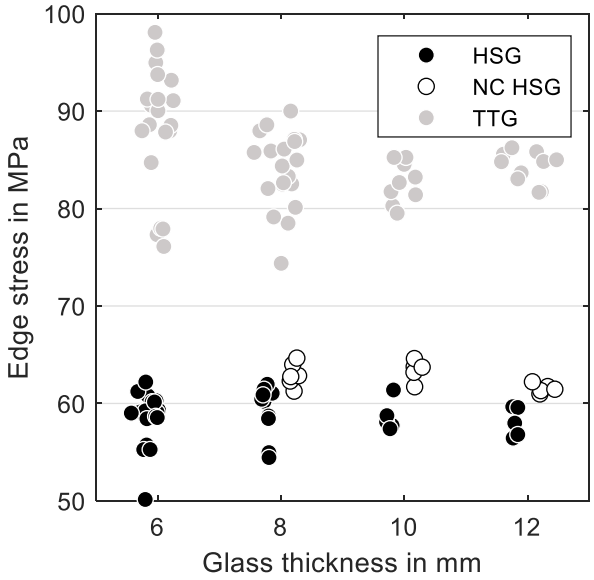

Figure 6.33: Edge stress values (determined by phase-shifting technique) distinguished by color for conforming heat-strengthened glass, non-conforming heat-strengthened glass, and thermally toughened glass

Fig. 6.34a shows the course of thickness-specific S-shaped curves of the logistic regression models. Since the dataset of the PST values resulted in almost distinguishable models, the probability thresholds were set at 0.5, 0.95, and at Prec > 0.9. The corresponding limit values are presented in Fig. 6.34b.

In the diagram in Fig. 6.34a, it could be observed that the 6 mm model showed a substantial difference compared to the other thickness-specific models. This was also reflected in the limit values in Fig. 6.34b, where the regression model of 6 mm glass thickness achieved a higher value, even exceeding the overall 6–12 mm model. Due to the clear and wide separation of the glass types for the 6 mm dataset, the limit value corresponded to the midpoint between the two categories. Since the 6 mm model did not contain any non-conforming HSG specimens, the limit value for the assessment of HSG could not, for safety reasons, be set too high. This means that the resulting limit value was not reliable.

Table 6.24 shows the limit values of the models of individual glass thicknesses as well as of the overall model for the probability thresholds of 0.95 and Prec > 0.9, together with the corresponding metrics precision and recall. It could be observed that, in determining the limit value, the edge stress values of the 8 mm specimens were decisive, as this model was the only one among the models of individual glass thicknesses that was statistically significant.

The 12 mm subset yielded the lowest limit value of 59.7 MPa. Since no clear glass-thickness-dependent behavior could be observed in Fig. 6.33, the model including specimens form 6–12 mm glass thicknesses was used for the determination of the limit value for HSG.

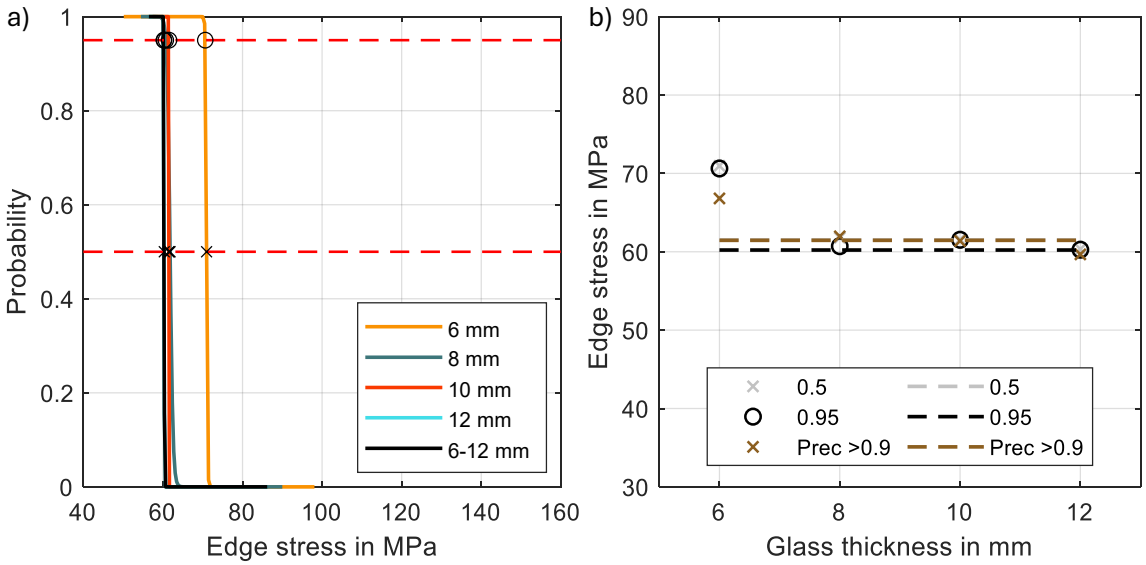

Figure 6.34: Logistic regression analysis of edge stress (determined by phase-shifting technique) for heat-strengthened glass: a) sigmoid fitted curves depending glass thickness and b) thickness-specific limit values derived from probability thresholds of 0.5, 0.95, and precision > 0.9

For a clear identification of non-conforming HSG, a limit value of 60.2 MPa determined by the probability threshold of 0.95 for glass thicknesses of 6–12 mm was recommended, when the edge stress values were measured with PST. However, this was associated with a recall rate of 71.8%. The limit value of 61.5 MPa for glass thicknesses of 6–12 mm achieved a higher recall of 94.9% with a simultaneously lower precision of 90.2%. A closer look at Fig. 6.33 shows that, although such a low limit value would lead to a rejection of some 6 mm specimens, several measured values nevertheless still fell within the limit. For the subsequent comparison with the limit values and edge stress values measured by MWP method, the rounded value of 60 MPa for glass thicknesses of 6–12 mm was selected. For the 12 mm specimens as well, the limit value of 60 MPa corresponded to a precision rate of 100%.

Table 6.24: Limit values of edge stress for heat-strengthened glass for each glass thickness determined for precision > 0.9 and false positive rate < 0.1, including classification metrics

t [mm]	n	Probability = 0.95			Precision ≥ 90%		
		Limit [MPa]	Precision [%]	Recall [%]	Limit [MPa]	Precision [%]	Recall [%]
6	39	70.6	100.0	100.0	66.8	100.0	100.0
8	36	60.7	100.0	60.0	62.0	90.9	100.0
10	19	61.5	100.0	100.0	61.4	100.0	100.0
12	20	60.3	100.0	100.0	59.7	100.0	100.0
6–12 *	114	60.2	100.0	71.8	61.5	90.2	94.9

* Model fit significant by likelihood-ratio χ^2 test

6.11 Discussion of limit values for heat-strengthened glass

The quantile and logistic regression models selected in the preceding chapters were validated using k-fold validation with five subsets (k = 5). To assess the variability of the limit values from the model, a photoelastic limit value was determined for each iteration.

6.11.1 Evaluating HSG with surface stress

The minimum, maximum, and mean values of the five surface stress limit values of the k-fold validation were compared with the limit value of the complete dataset in Fig. 6.35. The statistical details of the individual k-fold validations can be found in Appendix Table A.34 to Table A.37. The lower surface stress value for HSG, intended to evaluate the strength of 70 MPa, was valid for glass thicknesses ranging from 4 to 12 mm. As illustrated in Fig. 6.35, the k-fold validation of the quantile regression model demonstrated a dispersion range of 3.5 MPa, which marginally exceeded the value ascertained in the overall model. Due to the absence of test specimens that could be utilized for the assessment of inadequate pre-stressing, the maximum value of the k-fold validation of 23 MPa has been designated as the lower limit value of surface stress measurements for controlling HSG. This value is proximate to the thresholds delineated in ASTM C1048 (2025), which is 24 MPa, and ISO 22509 (2020), which is 25 MPa.

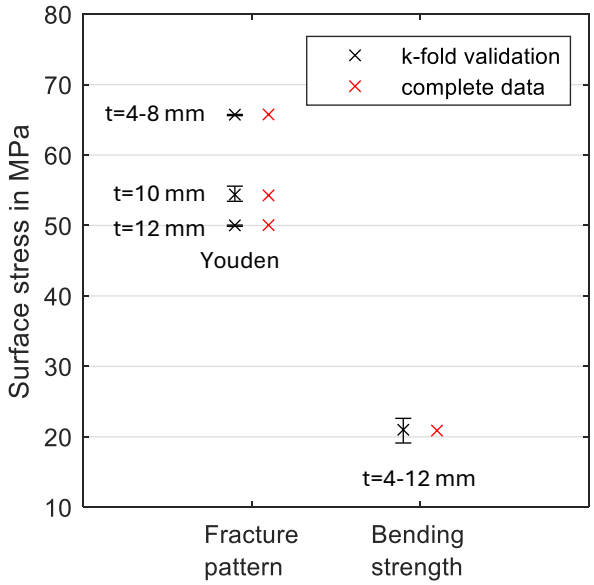

Figure 6.35: Surface stress limit values for heat-strengthened glass determined by quantile regression for bending strength and by logistic regression for fracture pattern with min and max values of k-fold validation and values determined with complete data, specification of valid glass thickness, determined on standard-format specimens

The upper limit values were established for the evaluation of the fracture pattern of HSG for glass thicknesses of 4–8 mm, 10 mm, and 12 mm. The scatter of the k-fold validation was very low for the 4–8 mm and 12 mm models. The 10 mm model also had minimal

scatter. The precision and recall were both 100% for all limit values. Depending on glass thickness, the upper limit values were defined as 66, 53, and 50 MPa.

ASTM C1048 (2025) specifies an upper limit of 52 MPa for surface stress to define HSG, for glass thicknesses $\leq$ 6 mm. When applied to the 4–6 mm specimens investigated in this work, this limit yielded a precision of 100% but low recall of 41.3%. ISO 22509 (2020) defines the same upper limit. However, it was applied uniformly across all glass thicknesses. When evaluated using the 4–12 mm specimens, this resulted in a precision of 99.4% and a recall of 57.8%.

The lower and upper limits of surface stress for classifying HSG are listed in Table 6.25.

Table 6.25: Preliminary surface stress limit values for thermally toughened glass statistically determined on standard-format specimens (360 mm $\times$ 1100 mm)

Glass thickness [mm]		4	6	8	10	12
Surface stress [MPa]	Min.	23	23	23	23	23
	Max.	66	66	66	53	50

6.11.2 Evaluating HSG with edge stress

The minimum and maximum edge stress values of the k-fold validation and the regression of the complete dataset for HSG are displayed in Fig. 6.36. The limits are divided into controlling the bending strength as a lower limit value which was determined via quantile regression and the fracture pattern as an upper limit which was determined via logistic regression. For each property of HSG, the limits were calculated using edge stress values measured by MWP as well as by PST. The limits determined by MWP are valid for glass thicknesses of 8–12 mm, while the limit values determined by PST are valid for 6–12 mm. The associated statistical details of the k-fold validation are provided in Appendix Table A.38 to Table A.42.

When considering the lower limit value for ensuring the strength of HSG, it is evident that the PST limit value was higher and exhibited less dispersion in the k-fold validation of the quantile regression analysis. For glass thicknesses of 6–12 mm for the MWP method, the k-fold validation resulted in a dispersion range of 9 MPa, with a mean value of 38.5 MPa, which was above the overall model value of 36.6 MPa. Table 6.26 shows a comparison of the performance of limit values of 42 and 44 MPa, corresponding to the maximum values from k-fold validation of PST and MWP values, respectively. The limit values were tested on the entire database of available edge stress values as well as on values obtained separately by the MWP and PST measurement methods. The higher value of 44 MPa showed a low recall value originating from the MWP database. Nevertheless, for safety reasons, the higher limit value of 44 MPa was set here for measuring edge stress for glass thicknesses of 6–12 mm for assessing HSG.

The edge stress limits for HSG that ensure the fracture pattern were determined by logistic regression. A comparison of the values revealed discrepancies between the results of the MWP and PST methods. As demonstrated in Fig. 6.36, MWP edge stress values led to limits of 55.9 MPa ascertained with a minimum precision of 0.9 and 64.7 MPa ascertained by a maximum false positive rate of 0.1 for a database of 8–12 mm glass thickness. The

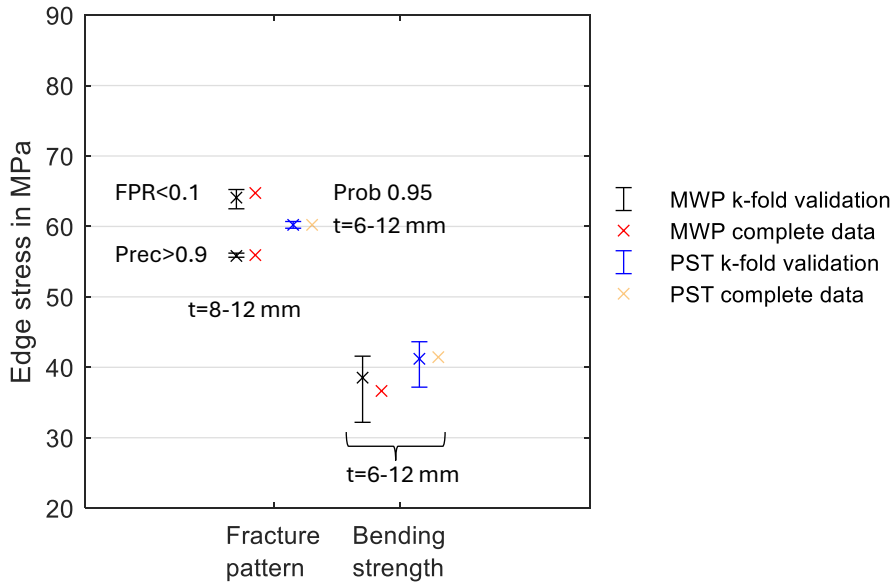

Figure 6.36: Edge stress limit values for heat-strengthened glass determined by quantile regression for bending strength and by logistic regression for fracture pattern with min and max values of k-fold validation and values determined with complete data, edge stress measured with multiple-wavelength photoelasticity and phase-shifting technique, specification of valid glass thickness, determined on standard-format specimens

scattering of the k-fold validation at threshold FPR < 0.1 was marginally larger than the scattering of Prec > 0.9. So, the limit values were selected as 64 MPa and 56 MPa for the subsequent testing in Table 6.27. The PST method yielded a limit value of 60.2 MPa, rounded to 60 MPa, determined by the threshold of 0.95 probability with a minimal dispersion.

The testing of the upper limit value was carried out using the database of glass thicknesses 6–12 mm for PST values and 8–12 mm for MWP values, as shown in Table 6.27. In addition to precision and recall, this table reports the specificity, which described the proportion of correctly identified non-conforming specimens relative to all non-conforming HSG specimens, see Equation (2.18). It should be noted that for calculating the performance metrics the

Table 6.26: Test of lower limit values (strength criterion) determined by quantile regression for heat-strengthened glass on edge stress values measured independently and dependently by multiple-wavelength photoelasticity and phase-shifting technique, tested on all small-format specimens

			Database including all HSG edge stress values		MWP		PST	
Model	Method	Limit [MPa]	Prec [%]	Rec [%]	Prec [%]	Rec [%]	Prec [%]	Rec [%]
QuanReg	MWP	42	–	100.0	–	100.0	–	100.0
QuanReg	PST	44	–	97.0	–	96.1	–	100.0

Table 6.27: Test of upper limit values (fracture pattern criterion) determined by logistic regression with different probability thresholds and methods for heat-strengthened glass on edge stress values measured independently and dependently by multiple-wavelength photoelasticity and phase-shifting technique, tested on all small-format specimens

			Database including all HSG edge stress values			MWP			PST		
Model	Method	Limit [MPa]	Prec [%]	Rec [%]	Spec [%]	Prec [%]	Rec [%]	Spec [%]	Prec [%]	Rec [%]	Spec [%]
LogReg (Prec > 0.9)	MWP	56	92.1	21.0	96.5	90.6	22.7	95.7	100.0	15.4	100.0
LogReg (0.95)	PST	60	84.8	46.7	83.7	78.8	40.6	80.0	100.0	66.7	100.0
LogReg (FPR < 0.1)	MWP	64	75.1	77.8	50.0	75.8	71.1	58.6	73.6	100.0	12.5

dataset was restricted to the intended HSG specimens. While this reduction of the database did not affect precision and recall, it increased the accuracy of the specificity estimate. Consequently, specificity was used to evaluate how effectively the upper limit value excluded non-conforming HSG specimens.

The objective was to ascertain a limit value that is suitable for both measurement methods for evaluating HSG with edge stress without compromising safety and residual load-bearing capacity. Concurrently, however, the number of specimens erroneously rejected should be minimized. As shown in Table 6.27, the metrics for PST and MWP values differed substantially for the limit values, providing no clear trend in favor of either limit value or measurement method.

For comparison purposes, Fig. 6.37 shows the distribution of edge stress measured by (a) MWP and (b) PST, divided by the conformity of HSG and TTG. For improved clarity, the figure is zoomed into the measurement range relevant for HSG. In addition, the potential limit values of 56 MPa, 60 MPa, and 64 MPa are indicated. A limit value of 64 MPa was not a suitable selection criterion for the PST method, as only a low specificity of 12.5% would result in correctly identifying non-conforming specimens. This can be seen in Fig. 6.37b, where 14 out of 16 non-conforming specimens measured by PST fell below the 64 MPa limit value, despite not exhibiting an HSG fracture pattern. For this reason, the 64 MPa limit was considered inadequate and is excluded from further comparisons.

Reducing the limit value from 64 MPa to 60 MPa changed the precision rate of the MWP values by only 3% but increased the specificity from 58.6% to 80%. For the PST values, the specificity ideally reached 100%, meaning that all non-conforming HSG specimens were correctly identified using the 60 MPa limit. Furthermore, edge stress values measured by PST achieved an ideal precision rate of 100% at both limits 56 MPa and 60 MPa. However, at the lower limit of 56 MPa, the recall dropped to only 15%. This implies that 85% of specimens would be unnecessarily rejected in quality control. In contrast, the 60 MPa limit would incorrectly exclude approximately one-third of all PST specimens. In Fig. 6.37b, this is visible in the black data points lying above the blue 60 MPa line.

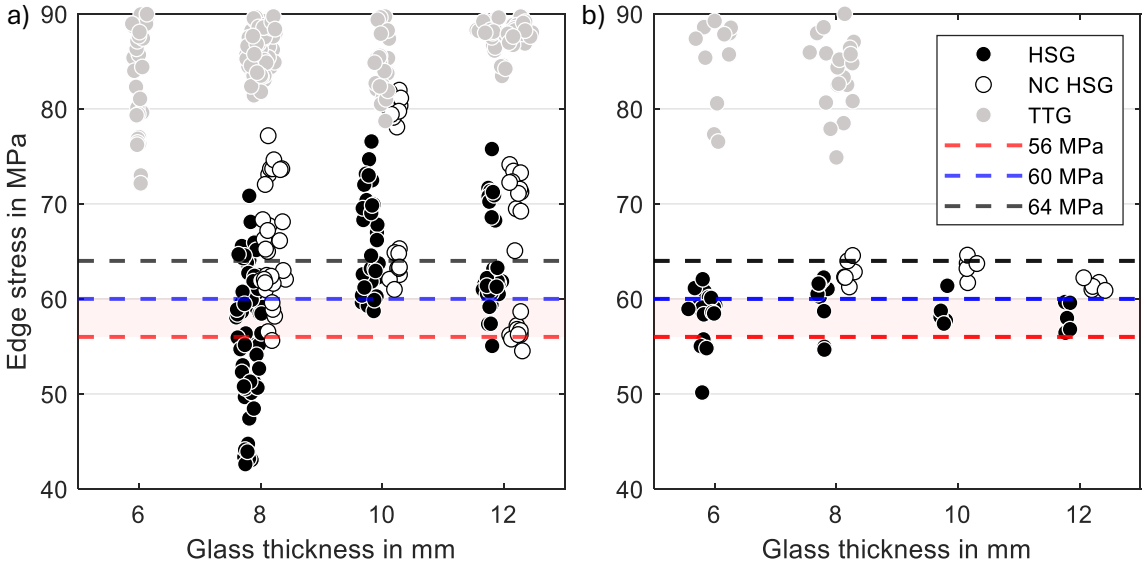

Figure 6.37: Edge stress values measured by a) multiple-wavelength photoelasticity and b) phase-shifting technique, for comparison of limit values 56 MPa, 60 MPa, and 64 MPa

For the MWP specimens, the recall at 56 MPa was 22.7% with a specificity of 95.7%. As shown in Fig. 6.37a, these metrics were primarily influenced by the 8 mm specimens, which were the only glass thickness that reaches values below 55 MPa. Since the 10 mm specimens exhibited edge stress values starting from 58.7 MPa, the 56 MPa limit had no discriminatory effect and failed to identify any HSG specimens.

Taken together, this comparison raised concerns regarding the reliability of the MWP method for classifying HSG specimens. Fig. 6.37a clearly illustrates that the non-conforming HSG specimens measured by MWP showed a wide spread, extending even into the range above 70 MPa. From a conservative perspective, an upper limit of 56 MPa should be applied for quality control of HSG, when using the MWP method. However, this choice inevitably led to a high unnecessary rejection rate of 77.3% of specimens that were, in fact, conforming HSG.

For the PST method, a limit value of 60 MPa was considered ideal. To establish a uniform limit value across measuring methods at 60 MPa, it may be useful to cross-check the edge stress values determined by MWP with surface stress measurements. To ensure increased safety, specimens with edge stress values between 56 and 60 MPa measured using MWP should be additionally verified using the surface stress limit values, provided in Table 6.25. This approach was tested on the MWP dataset used in Table 6.27. A total of 24 specimens fell within the 56–60 MPa range of edge, highlighted as the red zone in Fig. 6.37. Of these, 17 specimens complied with the corresponding surface stress limits depending on glass thickness, and could, therefore, be reliably classified as conforming HSG.

As a result, the specificity of the 60 MPa limit increased from 80% to 95.7%. The recall rate also improved from 22.7% to 36.7%, although it remained below the 40.6% recall achieved when applying the 60 MPa limit. Precision likewise increased, rising from 90.6% (at 56 MPa) and 78.8% (at 60 MPa) to 94%. The progression of the metrics for the MWP

data, tested on the limits of 56 MPa, 60 MPa, and the additional condition of 56–60 MPa verified by surface stress measurements, is illustrated in Fig. 6.38.

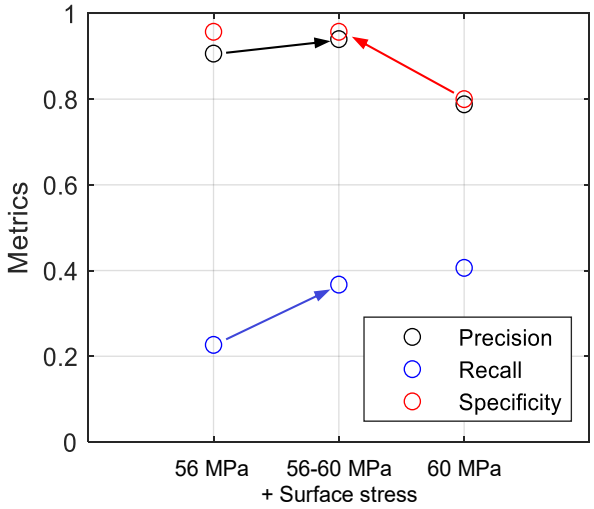

Figure 6.38: Comparison of performance metrics for edge stress limits of 56 MPa and 60 MPa, evaluating the additional condition of 56–60 MPa validated by surface stress measurements

In conclusion, it can be stated that the MWP method was only suitable to a limited extent for the quality control of HSG. Consequently, a conservative upper limit value of 56 MPa was applied for measurements obtained using MWP. The upper limit value for classifying HSG in edge stress measurements using PST was set to 60 MPa. MWP edge stress values falling between 56 and 60 MPa should be verified using surface stress measurements and their corresponding limit values from Table 6.25. The lower and upper limit values for edge stress, which are used to assess the tempering quality of HSG, are specified in Table 6.25. The limits are valid for glass thicknesses from 6 mm to 12 mm.

Table 6.28: Preliminary edge stress limit values for heat-strengthened glass (statistically determined on standard-format specimens 360 mm x 1100 mm)

Glass thickness [mm]		4	6	8	10	12
Edge stress [MPa]	Min.	–	44	44	44	44
	Max.	60 *	60 *	60 *	60 *	60 *

* MWP values between 56 and 60 MPa must be controlled via surface stress limits from Table 6.25.

6.12 Conclusions

In this chapter, limit values for photoelastic surface and edge stress measurements were established for classifying TTG and HSG using quantile regression and logistic regression analysis. The regression models were validated through k-fold cross-validation and the resulting limit values were compared across the different regression approaches and, in the case of edge stress, across different measurement methods, to find the most appropriate limit values. The selected surface and edge stress limits are illustrated as color-coded ranges in Fig. 6.39.

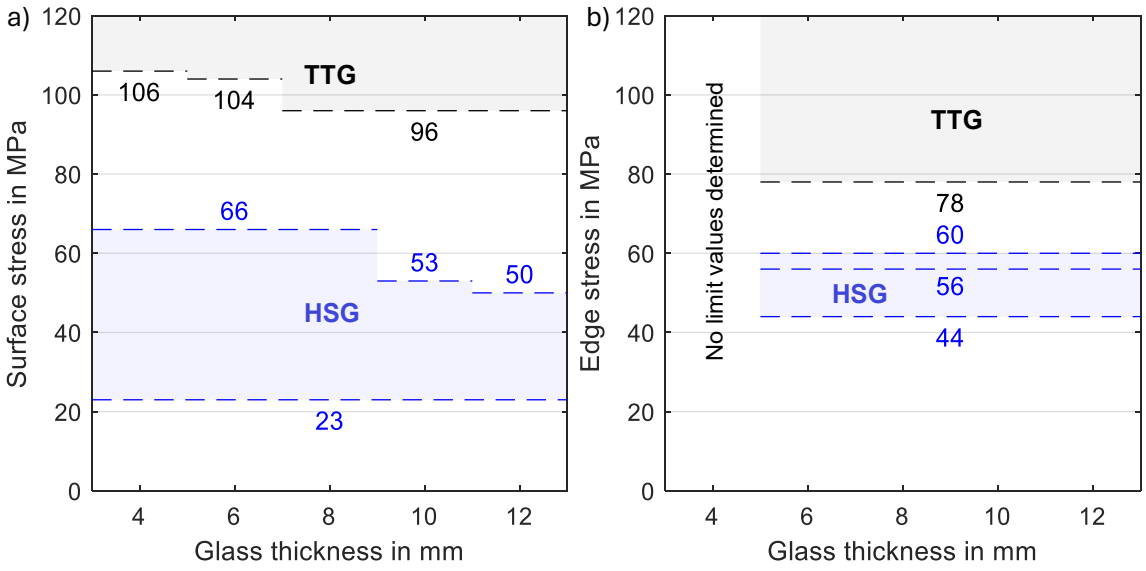

Figure 6.39: Preliminary photoelastic limits for measurement of a) surface stress and b) edge stress depending on the glass thickness for thermally toughened glass and heat-strengthened glass (statistically determined on standard-format specimens 360 mm x 1100 mm)

For TTG, only a lower limit value was defined, whereas HSG required both a lower and an upper limit to reliably control its tempering quality. While surface stress limits vary with glass thickness for both glass types, edge stress limits were consistent across thicknesses. However, this thickness separation for surface stress limits differed between the two glass types: for TTG, limits were distinguished for 4 mm, 6 mm, and 8–12 mm, whereas for HSG, specific ranges exist for 4–6 mm, 10 mm, and 12 mm. In both cases, thinner glasses required higher surface stress values to achieve conformity.

A direct comparison between the ranges of surface stress (Fig. 6.39a) and edge stress (Fig. 6.39b) highlights several important differences. Surface stress limits were spaced further apart, particularly for TTG, where higher values were required in contrast to edge stress. For HSG, the surface stress range was also broader, with lower minimum limits and higher maximum limits than from edge stress. For edge stress, the distance between TTG and HSG limits was relatively small at 18 MPa, whereas for surface stress the smallest distance between classes amounted to 30 MPa at 8 mm thickness. Furthermore, the HSG surface stress range spanned 27 MPa (t = 12 mm) to 43 MPa (t = 4–8 mm), in contrast to the comparatively narrow HSG edge stress range of only 16 MPa.

Finally, it should be emphasized that, based on the analysis presented in this chapter, the MWP method for edge stress determination did not demonstrate sufficient reliability for classifying HSG. For this reason, a conservative upper limit of 56 MPa was defined, ensuring a more robust and safety-oriented basis for quality control. To reduce the number of specimens that would be unnecessarily rejected based solely on MWP measurements, an additional verification step can be introduced. For MWP, edge stress values in the range of 56 to 60 MPa may be further assessed by performing surface stress measurements and comparing the results with the corresponding limit values. This supplementary check helps prevent false rejections and improves the reliability of the classification process for HSG.

7 Validation on large-format specimens

In the last chapter, photoelastic limit values were determined using statistical methods for evaluating the pre-stress quality of TTG and HSG. The aforementioned findings, in conjunction with other photoelastic investigations (Aben et al. 2010, Mognato et al. 2019, Pour-Moghaddam 2020), are predominantly based on small-format test specimens of 360 mm x 1100 mm. However, this standard format has no practical relevance. The transferability of photoelastic measurements to large-format glass components used in façades has not yet been sufficiently investigated. The objective of this chapter is to evaluate the applicability of photoelastic measurement techniques for the non-destructive quality control of large-format tempered glass of 1000 mm x 3000 mm. The specimens also originate from the research project NEMA (Efferz et al. 2025a) and were tempered by the same manufacturers as those investigated in the previous chapters. The experimental investigations were carried out at HM.

Specifically, it will be investigated if the limit values determined in this research can be transferred to larger glass formats, in comparison to the limit values of the standards of ASTM C1048 (2025), ISO 12540 (2017), and ISO 22509 (2020). On the one hand, it is assessed how accurately the limit values recognize the non-conforming tempered glass specimens and how many are erroneously identified as conforming. On the other hand, the percentage of conforming TTG and HSG samples that are unnecessarily rejected due to the photoelastic limit will also be analyzed.

In addition to an analysis of the test results, the focus is directed toward a direct comparison of the tempering process applied to the standard-size and large-format specimens. In one scenario, the test specimens were produced under the same cooling parameters of the quench as in the small format. In the other scenario, the cooling parameters were adapted to the larger glass format. The objective of this investigation is to identify disparities in fracture patterns as well as surface and edge stress outcomes in these two scenarios and to determine the influence of specimen format. Parts of this chapter were pre-published with a reduced database in Efferz et al. (2025b).

7.1 Test approach and database

The analyzed test specimens measured 1000 mm x 3000 mm, were uncoated, and had glass thicknesses of 6, 8, 10, and 12 mm. Each glass thickness was produced by two of the three participating manufacturers. All specimens had an edge processing of ground edges and were tempered to produce TTG in accordance with EN 12150-1 (2020) as well as HSG in accordance with EN 1863-1 (2012).

To investigate the potential effects of production parameters on photoelastic measurements and fracture pattern, two different pre-stress levels were generated within the glass type TTG by modifying the furnace process conditions. The classification of low and high

TTG was already established from previous experimental investigations conducted on standard-size specimens. The HSG specimens were divided into conforming and non-conforming HSG depending on the fracture pattern. Table 7.1 shows the number of test specimens depending on the thickness, pre-stress level of TTG, and conformity of HSG.

Table 7.1: Number of large-format test specimens measuring 1000 mm x 3000 mm depending on glass thickness, pre-stress level of thermally toughened glass, and conformity of heat-strengthened glass

	6 mm	8 mm	10 mm	12 mm
Low thermally toughened glass	6	9	6	6
High thermally toughened glass	6	9	6	6
Conforming heat-strengthened glass	12	15	6	6
Non-conforming heat-strengthened glass	0	3	0	6
Total	24	36	18	24

In total, 102 test specimens were analyzed as follows: the edge stress was determined using the MWP by scanning the specimens with the LineScanner from Softsolution GmbH (2023b). One part of the specimens was scanned at HM, whose measuring device generates three isochromatic images per specimen. The other part was scanned using the LineScanner as an in-line measuring device directly after production at the manufacturer. This device uses two wavelengths, so the evaluation was based on two isochromatic images per specimen. In this chapter, the 6 mm HSG specimens were nevertheless included in the evaluation of edge stress, although this thickness was explicitly excluded from the analysis in the previous chapters. The reason for their consideration was that these specimens were deliberately examined to obtain additional insights. However, the resulting values must be interpreted with caution, as their reliability is limited.

Fig. 7.1 illustrates the approach of the experimental investigations shown on an exemplary isochromatic image of a large-format 8 mm TTG. First, the edge stress was measured. Therefore, the edge isochromatics, indicated as lines of intensity minima and maxima on these images, were counted automatically, corresponding to the respective fringe order of the wavelength of the isochromatic image. This methodology enabled the determination of the retardation of the light at the points of the isochromatics. The maximum retardation at the edge was determined by extrapolation with a 3rd degree polynomial based on the positions of the isochromatics of all images of a specimen. The edge stress was then calculated from Equation (3.3). The edge stress of the large-format specimens was determined in nine evaluation regions along each longitudinal edge, as shown in Fig. 7.1. Each evaluation region in this investigation consisted of 16 cuts, where the intensity progression of the isochromatics were analyzed collectively. The mean value of the 18 evaluation regions was then calculated for each specimen, which was used as a control value for the evaluation with the photoelastic limit value.

In the second part of the photoelastic measurements, the surface stress was measured at three measurement points using the SCALP-05 from GlasStress Ltd. (2013). The measuring device was configured with a fit closeness parameter of 0.5, using a local approximation method based on a 3rd degree polynomial. Measurements were taken at one measurement point in three or four directions in 45° steps to obtain the principal stresses σ_1 and σ_2 at the surface using the equations according to the manual of GlasStress Ltd. (2013).

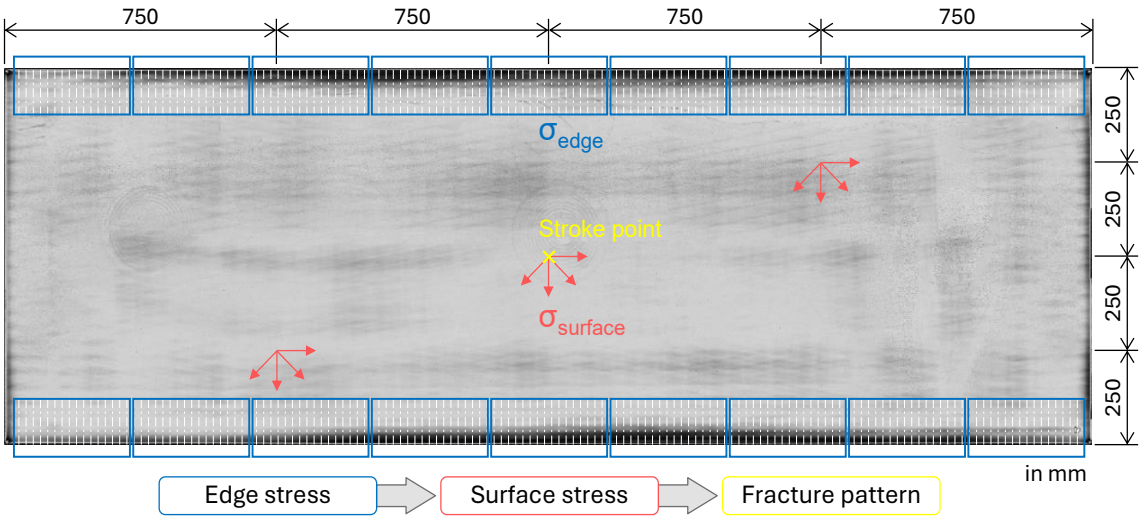

Figure 7.1: Position of measurement points of the edge stress, surface stress and fracture pattern test on an isochromatic image for experimental investigations on large-format specimens measuring 1000 mm x 3000 mm, dimensions in mm, from Efferz et al. (2025b)

Although several authors (Nielsen 2009, Zaccaria and Overend 2020) have investigated how the accuracy of measuring the surface stress depends on the photoelastic constant for glass, this study applied the value of 2.72 TPa^{-1}, based on recommendations in the SCALP-05 manual (GlasStress Ltd. 2013) and Ramakrishnan and Ramesh (2016) to ensure comparability with previous investigations. The mean value of the principal stress with the higher absolute magnitude, σ_1, was then calculated from the three measurement points and used as the evaluation criterion in conjunction with the photoelastic limit value.

For evaluation of the fracture pattern, the specimen was impacted with a center punch at the midpoint of the pane. For the TTG, the fragments in the area of the coarsest fracture pattern were manually counted in a 50 mm x 50 mm square. Thereby, the area around the stroke point with a radius of 100 mm and the edge area of 25 mm wide stripes were excluded from the evaluation. The number of fragments was utilized as an evaluation criterion to ascertain whether the test specimens conformed to the glass type TTG. The EN 12150-1 (2020) standard specifies a minimum of 40 fragments in the counted area for TTG for glass thickness of 4 mm to 12 mm.

The evaluation of the fracture pattern of HSG was based on the general building approval Z-70.3-55 (Deutsches Institut für Bautechnik 2016). This approval was valid from August 23, 2016, to April 14, 2020 and delineated the glass product HSG manufactured by AGC Interpane under the product name "Ipasafe TVG" (teilvorgespanntes Glas, German for heat-strengthened glass). Furthermore, the document delineates the requirements for the fracture pattern test on large-format specimens, with the objective of ensuring the residual load-bearing capacity of HSG in laminated glass. In this method, the specimen is fractured using a sharp steel tool in the middle of the pane. Subsequently, the fragments are examined using a disc with a diameter of 120 mm. Fig. 7.2a shows exemplary the differentiation between critical and non-critical fragments: fragments in which the disc can be placed are classified as non-critical. If the disc does not fit, the fragment is considered critical, marked, and weighed. For conformity with HSG requirements, the total mass of such small, critical

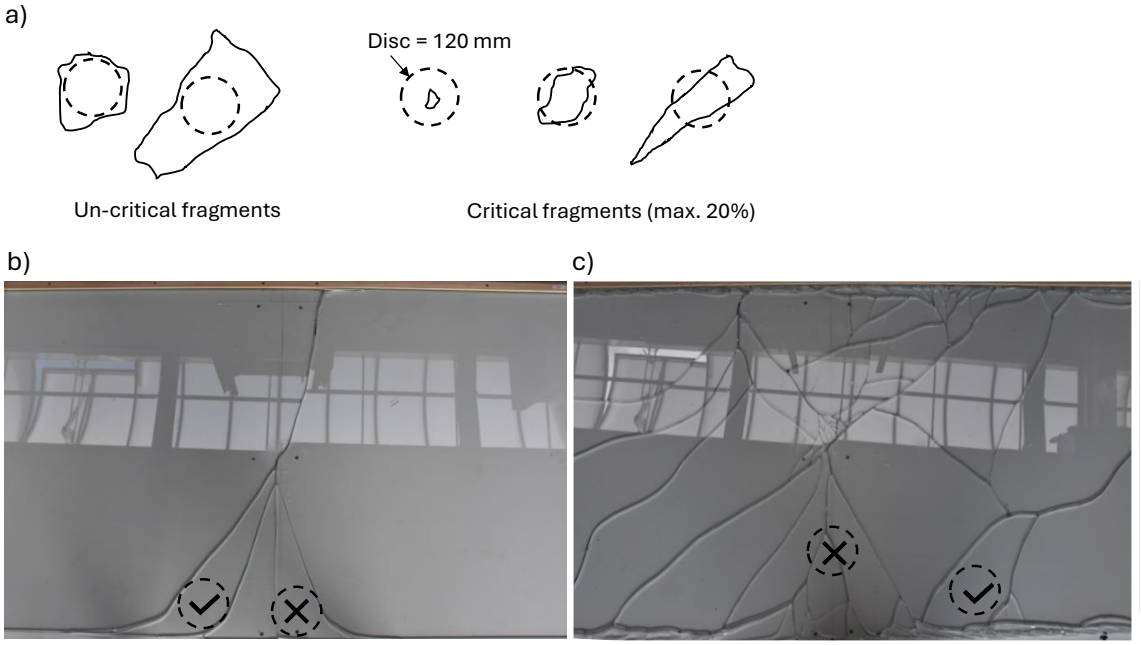

Figure 7.2: Evaluation of fracture pattern of large-format heat-strengthened glass according to the general building approval Z-70.3-55 (Deutsches Institut für Bautechnik 2016) using a 120 mm disc: a) evaluation of the fragments, differentiation of critical and non-critical fragments, b) exemplary fracture pattern of an overall conforming HSG, and c) exemplary fracture pattern of an overall non-conforming HSG

fragments must not exceed 20% of the overall pane mass. Fig. 7.2b presents a fracture pattern of a conforming HSG specimen, while (c) shows a non-conforming fracture pattern since the part of the critical fragments is higher than 20%.

To investigate how the different photoelastic limit values recognize the non-conforming tempered glass specimens correctly and how many specimens are unnecessarily rejected, contingency tables were used, since they provide a detailed overview of the potential of the various limit criteria for surface and edge stress. A contingency table shows the number of real positives and negatives depending on the fracture tests and the predicted positives and negatives based on the photoelastic measurements. Some limit values, which determined in this research, depend on glass thickness. To enable a more comprehensive analysis, the number of values was investigated for each glass thickness. Based on the contingency tables, the measures of precision, recall, and specificity was calculated. This enables a comparison and evaluation of the different photoelastic limit values specified in ASTM C1048 (2025), ISO 12540 (2017), ISO 22509 (2020) as well as those determined in the present work.

7.2 Experimental investigations on large-format specimens

This section investigates the destructive and photoelastic measurements on large-format specimens. First, destructive tests were used to assess the conformity of the specimens as TTG according to EN 12150-1 (2020) or as HSG according to EN 1863-1 (2012) based on their fracture pattern. Then it was controlled if the photoelastic limit values of edge

and surface stress measurements recognize the conformity of the tempered glass specimens and sort out non-conforming specimens correctly. Then, the relation between the fracture pattern and the photoelastic measurements was investigated. This was followed by the correlation between edge and surface stress.

7.2.1 Photoelastic and destructive results of large-format specimens

For TTG, Fig. 7.3a shows the number of fragments depending on glass thickness. Three specimens with a glass thickness of 6 mm fell below the limit of 40 fragments that TTG must reach in a square of 50 mm x 50 mm in the coarsest fracture pattern in accordance with EN 12150-1 (2020). The remaining 51 test specimens exhibited a sufficiently fine fracture pattern, thereby conforming to the requirements of TTG as specified in EN 12150-1 (2020). A comparison of the pre-stress levels shown in color revealed a clear difference between the low and high toughened specimens. As expected, the high toughened specimens exhibited a finer fracture pattern and resulted in a higher average number of fragments. This is in line with the expectation that a higher pre-stress level would lead to greater fragmentation at break. Nevertheless, there was an overlap between the categories of high and low pre-stressed TTG. Some specimens that were classified as high toughened exhibited number of fragments that were in the range of the low toughened specimens. This observation could be attributed to manufacturer-specific differences: within the test series of a single manufacturer, the pre-stress levels were consistent and clearly distinguishable. Only when comparing different manufacturers, variations in pre-stress levels could be observed.

Since it was not possible to quantitatively record the fracture pattern for HSG, Fig. 7.3b illustrates the distribution of conforming and non-conforming specimens based on glass thickness. Overall, 9 out of 48 HSG specimens did not exhibit a typical fracture pattern.

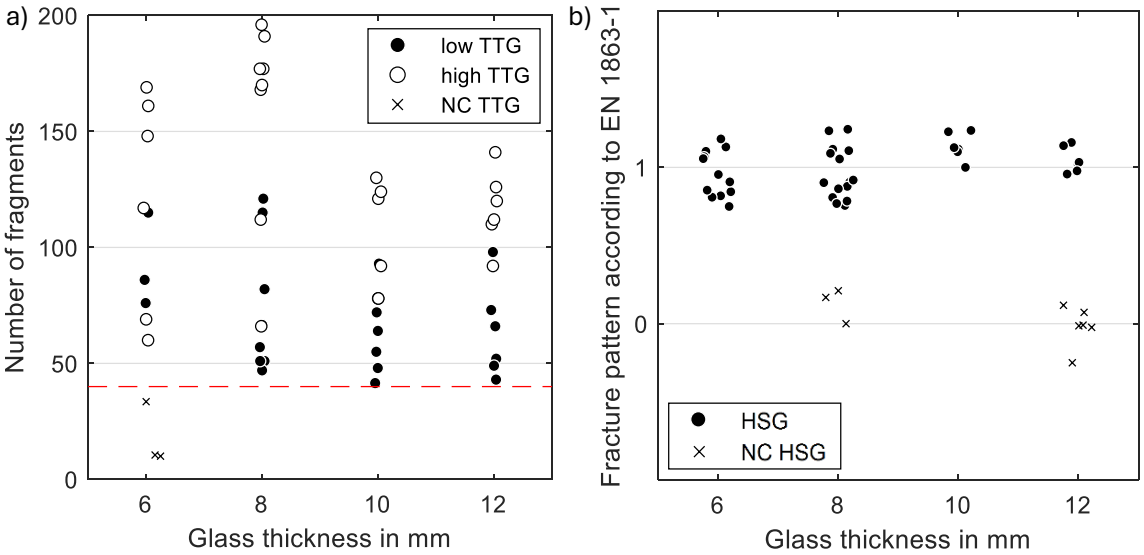

Figure 7.3: Analysis of fracture behavior for large-format specimens: a) number of fragments depending on the glass thickness and pre-stress level of the thermally toughened glass and b) assessment of fracture pattern conformity for heat-strengthened glass

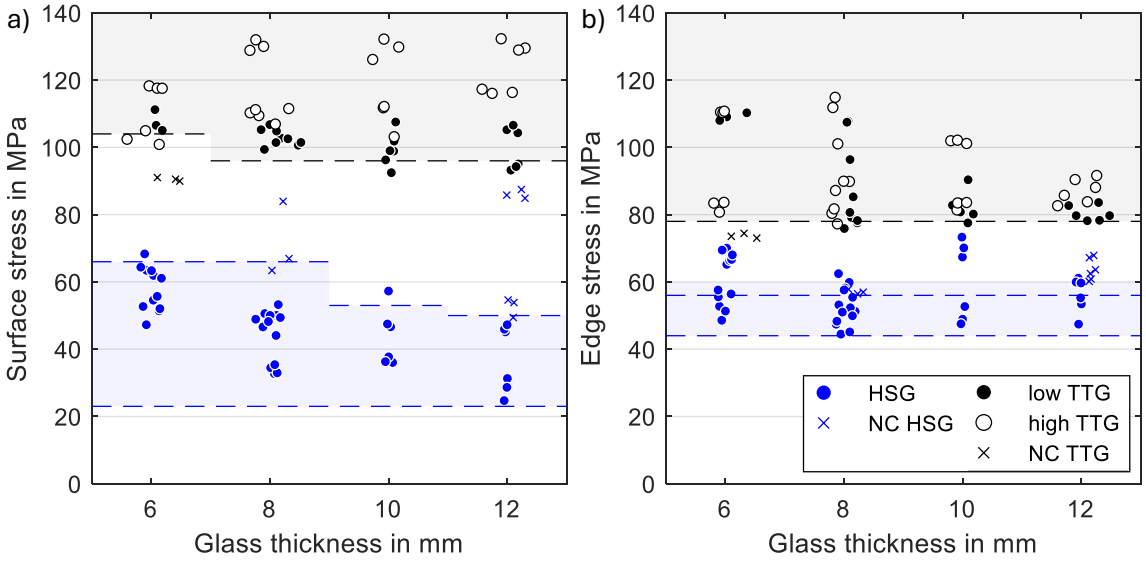

Figure 7.4: Photoelastic measurements on large-format specimens: a) surface stress and b) edge stress, depending on the glass thickness, conformity, and pre-stress level of the specimens, with photoelastic limits obtained in Section 6.12

Fig. 7.4 shows the results of the photoelastic measurements, i.e., the average values of the measurement points per specimens of (a) surface stress and (b) edge stress. In both diagrams, the limit values determined in this work are shown as shaded areas for TTG and HSG. The data points are color-coded according to their conformity status and pre-stress level. Surface stress values of TTG were measured in the range of 90 to 111 MPa on the conforming low toughened specimens and 101 to 132 MPa on the high toughened specimens. Edge stress measurements of TTG ranged from 76 to 111 MPa for the low toughened specimens and 80 to 115 MPa for the high toughened specimens. The noticeable overlap in these ranges could again be explained by manufacturer differences, but within the manufacturer, the pre-stress levels could be differentiated.

For conforming HSG, the surface stress measurements ranged from 24 MPa to 68 MPa. The non-conforming specimens exhibited values between 49 MPa and 87 MPa, in some cases extending into the range typically associated with TTG. Nevertheless, a clear separation between conforming HSG and TTG was still evident. A different pattern was observed for the edge stress measurements: even conforming HSG specimens showed values similar to those of TTG. However, these did not exceed the limit value of 78 MPa. The range of edge stress for conforming HSG specimens was 44 MPa to 73 MPa, while the non-conforming HSG specimens laid between 56 MPa and 68 MPa.

The 6 mm HSG edge stress values should be examined more closely, as the 6 mm HSG standard-size specimens were excluded from the previous evaluations due to unreliable values: here, the 6 mm HSG large-format specimens showed partially valid values. However, some measurements at approximately 70 MPa exceeded the defined limit range, even though the specimens were classified as conforming. This behavior could not be attributed solely to glass thickness, as similar deviations were also observed for conforming 10 mm HSG specimens.

7.2.2 Classification for large-format thermally toughened glass

For the evaluation of the conformity of large-format TTG using the limit values of surface stress and edge stress, the following two contingency tables showed the counts for the four categories TN, FP, FN, and TP as well as the corresponding metrics of precision, recall, and specificity. The classification was limited to specimens that were pre-stressed as TTG. Table 7.2 presents the evaluation of the surface stress limits. As shown, the standards do not differentiate the limit values with respect to glass thickness. None of the three non-conforming TTG specimens with a thickness of 6 mm were detected by the limit value specified in ASTM C1048 (2025): their measured surface stress values of approximately 90 MPa laid well above the minimum value of 69 MPa defined by ASTM C1048 (2025). Consequently, a precision of 94.3% was obtained, while the recall reached 100%. Given the comparatively low limit value, this result was expected, as all measured surface stress values exceeded this value. However, the specificity rate was 0%, indicating that all actual non-conforming specimens were incorrectly classified as conforming due to the low limit value of 69 MPa. Since ASTM C1048 (2025) regulates the strength of glass but not the fracture pattern, these findings confirmed that the limit value of 69 MPa is not suitable for verifying the fracture pattern of TTG. The limit value of ISO 12540 (2017) of 90 MPa correctly identified only 1 specimen as non-conforming. This resulted in a precision of 96.2%. No specimen was unnecessarily rejected, resulting in a recall rate of 100%. Its specificity was deemed inadequate, with a rate of 33.3% for identifying non-conforming specimens. In the context of quality control for TTG, insufficient specificity can have serious consequences if glass is accepted based on photoelastic measurements, despite exhibiting an inadequately fine fracture pattern.

Table 7.2: Contingency tables of different limit values of surface stress with metrics precision, recall and specificity for large-format thermally toughened glass

Reference	Limit [MPa]	t [mm]	TN	FP	FN	TP	Prec [%]	Rec [%]	Spec [%]
ASTM C1048 (2025)	69	6–12	0	3	0	50	94.3	100.0	0.0
ISO 12540 (2017)	90	6–12	1	2	0	50	96.2	100.0	33.3
Section 6.12	104	6	3	0	2	7	100.0	77.8	100.0
	96	8–12	0	0	4	37	100.0	90.2	-

The surface stress limit value of 104 MPa for a glass thickness of 6 mm, correctly identified all three non-conforming specimens. These specimens did not reach the defined limit value, resulting in the correct classification of all true negative cases. Consequently, the classification based on the 104 MPa limit achieved a specificity of 100%. In contrast, the limit value of 96 MPa determined for glass thicknesses ranging from 6 mm to 12 mm could not be evaluated with respect to specificity, as no non-conforming specimens were present within this thickness range. Moreover, Fig. 7.4a reveals that specific specimens of varying glass thicknesses demonstrated surface stress values that fell below the established limits for surface stress. These specimens, however, demonstrated the fracture pattern characteristic of TTG. The quantity of the false negatives was listed in the corresponding column. The results revealed a recall rate of 77.8% for 6 mm and 90.2% for 8–12 mm specimens, thereby suggesting that not all real conforming TTG is recognized as such. Considering both limits of the glass thicknesses means that in total 12% of specimens would erroneously be

disqualified in quality control due to surface stress measurement, although fulfilling the fracture pattern of TTG.

The classification based on edge stress for TTG is shown in Table 7.3. The ASTM C1048 (2025) limit value of 67 MPa failed to identify the three non-conforming specimens, which exhibited values between 73 and 74 MPa. As a result, both recall and precision were identical to those obtained for surface stress. This demonstrated that the 67 MPa limit value was not suitable for reliably detecting non-conforming specimens, as it erroneously classified all specimens as conforming TTG. In contrast, the limit value of 78 MPa determined in this research correctly identified the three non-conforming specimens, leading to precision and specificity rates of 100%. However, four specimens were incorrectly rejected, resulting in a recall rate of 92.2%.

Table 7.3: Contingency tables of different limit values of edge stress with metrics precision, recall and specificity for large-format thermally toughened glass

Reference	Limit [MPa]	t [mm]	TN	FP	FN	TP	Prec [%]	Rec [%]	Spec [%]
ASTM C1048 (2025)	67	6–12	0	3	0	51	94.4	100.0	0.0
Section 6.12	78	6–12	3	0	4	47	100.0	92.2	100.0

7.2.3 Classification for large-format heat-strengthened glass

As in the previous chapter, the following contingency tables were used to evaluate the conformity of large-format HSG specimens by means of the limit values for surface stress and edge stress. The tables provide the counts for the four categories four categories TN, FP, FN, and TP as well as the metrics derived precision, recall, and specificity. The classification in this section was restricted to specimens that were pre-stressed as HSG. It should be noted that the measurements were primarily defined by the upper boundary of the limit range, which corresponds to the fracture pattern, since bending strength could not be tested on the large-format specimens. Table 7.4 shows the evaluation of the classification of the different limit ranges for surface stress: the surface stress limit range of 24–52 MPa specified in ASTM C1048 (2025) was only applicable to HSG specimens with a glass thickness of ≤ 6 mm. Within the dataset of 6 mm HSG specimens, no non-conforming HSG samples were present. Consequently, the applicability of this limit range could only be assessed with respect to false-negative classifications. In this case, 10 specimens were falsely rejected, resulting in a recall of 16.7%. The surface stress range defined in ISO 22509 (2020) was very similar to that of ASTM C1048 (2025), spanning 25–52 MPa, but could be applied to specimens with glass thicknesses ranging from 6 to 12 mm. Since both standards define the same upper limit of 52 MPa, the performance metrics obtained by applying the ASTM C1048 (2025) limit range without considering the thickness restriction would be identical to those derived from ISO 22509 (2020). The limit range specified in ISO 22509 (2020) misclassified one specimen as conforming HSG, resulting in a specificity rate of 88.9%. In addition, 12 specimens were incorrectly rejected by the upper limit of 52 MPa, corresponding to a recall rate of 67.6%.

Subsequently, the limit ranges determined in this research, differentiated by glass thicknesses of 6–8 mm, 10 mm, and 12 mm, were evaluated. For the 6–8 mm samples, 1 of the 3

Table 7.4: Contingency tables of different limit values of surface stress with metrics precision, recall and specificity for large-format heat-strengthened glass

Reference	Limit [MPa]	t [mm]	TN	FP	FN	TP	Prec [%]	Rec [%]	Spec [%]
ASTM C1048 (2025)	24–52	6	0	0	10	2	100.0	16.7	-
ISO 22509 (2020)	25–52	6–12	8	1	12	25	96.2	67.6	88.9
Section 6.12	23–66	6–8	2	1	1	24	96.0	96.0	66.7
Section 6.12	23–53	10	0	0	1	5	100.0	83.3	-
Section 6.12	23–50	12	5	1	0	6	85.7	100.0	83.3

non-conforming specimens was incorrectly classified as conforming at the limit value of 66 MPa, yielding a specificity rate of 66.7%. All the other specimens of this thickness were correctly identified, except for 1 that was rejected unnecessarily, resulting in a recall of 96.0%. For the 10 mm thickness, all tested specimens were conforming HSG and correctly classified except for 1 specimen, resulting in a recall rate of 83.3%. Due to the absence of non-conforming specimens in this category, specificity could not be evaluated. In the case of the 12 mm specimens, half of the specimens were non-conforming HSG. Of these, 1 specimen was incorrectly identified as conforming at the limit value of 50 MPa, leading to a specificity rate of 83.3%. All of the conforming specimens were correctly identified.

Summarizing the performance of the three upper limit values from this research, the result was a recall of 94.6% and a specificity rate of 77.8% across all glass thickness. For the standards, the evaluation of the surface stress limits for HSG was as follows: according to the ASTM C1048 (2025) standard, 10 of the 6 mm HSG specimens would be unnecessarily rejected. Furthermore, a lower recall rate was demonstrated by ISO 22509 (2020), resulting in 12 FN specimens. In contrast, the limit values determined in Chapter 6 incorrectly rejected only 2 specimens. This finding indicates the necessity of differentiating the upper limit values for HSG based on variations in glass thickness. In terms of specificity, it was found that ISO 22509 (2020) incorrectly classified a single non-conforming HSG specimen measuring 12 mm. The limit values proposed in 6 produced a total of 2 FP: 1 of these was the same 12 mm specimen, while the other was an 8 mm specimen.

As outlined in Sections 6.11.2 and 6.12, the conservative limit value for edge stress, when evaluating the HSG tempering quality using the MWP method, is 56 MPa for glass thicknesses ranging from 6–12 mm. This is since the higher limit value of 60 MPa resulted in an unreliable assessment of the utilized database of standard-format glass. The potential for extending these findings to large-format specimens will be analyzed in the subsequent investigations. The contingency tables and the classification metrics of edge stress limit ranges for HSG are listed in Table 7.5. Since the ASTM C1048 (2025) does not specify limits for edge stress measurements for HSG, this section focuses exclusively on testing the limit values determined in this research on the 46 large-format HSG specimens.

The limit range of 44–56 MPa correctly identified all non-conforming HSG specimens with a 100% specificity and precision rate. However, given the low limit value of 56 MPa, the classification of only half of the specimens was accurate, while the remaining half were erroneously rejected, resulting in a recall rate of 53%. Conversely, the 44–60 MPa limit range improved the recall rate to 71.1%, but at the expense of specificity, which decreased to 66.7%, resulting in 3 FP specimens. The special regulation, delineated in Sections 7.11.2

and 7.12, governed the intermediate MWP edge stress value range of 56–60 MPa through the implementation of validating surface stress measurements including the control of corresponding established limits. This approach will be investigated in Section 7.2.6

Table 7.5: Contingency tables of different limit values of edge stress with metrics precision, recall and specificity for large-format heat-strengthened glass

Reference	Limit [MPa]	t [mm]	TN	FP	FN	TP	Prec [%]	Rec [%]	Spec [%]
Section 6.12	44–56	6–12	9	0	18	20	100.0	52.6	100.0
	44–60	6–12	6	3	11	27	90.0	71.1	66.7

7.2.4 Homogeneity of pre-stress at the surface and edge

As previously performed for the standard-size specimens in Sections 5.3.2.2 and 5.4.3.2, the homogeneity of the pre-stressing was also investigated for the large-format specimens. Regarding the surface stress, two parameters were evaluated: first, the standard deviation derived from the three measurement points, and second, the principal stress difference given by $(\sigma_1 - \sigma_2)$. Fig. 7.5a shows the standard deviation of the surface stress obtained from the three measurement points. It could be observed that only 1 specimen of 6 mm HSG exceeded a value of 10 MPa, while all remaining specimens exhibited standard deviation below 6.6 MPa. This behavior, characterized by generally low standard deviation, was consistent with the results obtained for the standard-size specimens.

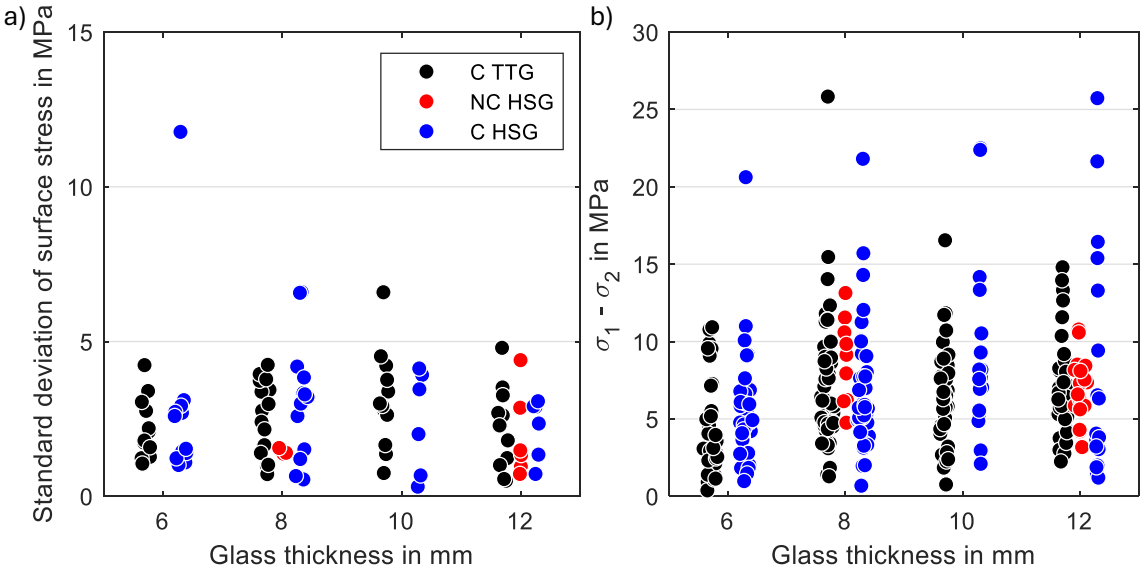

Figure 7.5: a) Standard deviation of the three individual surface stress measurement locations per large-format specimen and b) principal stress difference σ_1–σ_2 of the three individual surface stress measurement locations of the large-format specimens depending on glass thickness and conformity

Fig. 7.5b presents the principal stress difference σ_1–σ_2 for each measurement point of the large-format specimens. The maximum difference, approximately 26 MPa, occurred at one

measurement point of an 8 mm TTG specimen. The majority of the measured differences remained below 15 MPa, with a few isolated outliers exceeding 20 MPa. Compared to the standard-size specimens, slightly higher deviations between σ_1 and σ_2 were observed. In both diagrams shown in Fig. 7.5, the conformity classification, similar to the findings for the standard-size specimens, did not appear to have a discernible influence on the variability of the surface stress measurement points.

Fig. 7.6 shows the standard deviation of the edge stress evaluated over 18 measurement points. With increasing glass thickness, the standard deviation decreased, an effect that was particularly pronounced for TTG specimens. The maximum standard deviation of 17.5 MPa was observed for a 6 mm TTG specimen. For HSG, the highest deviation amounted to 10.6 MPa and occurred for an 8 mm specimen. Comparable magnitudes of standard deviation, likewise, decreasing with increasing glass thickness, were already observed for the standard-size specimens. It is noteworthy that all 6 specimens with a glass thickness of 6 mm exhibiting relatively high standard deviation originated from the same manufacturer, whereas the 8 mm specimens with standard deviation exceeding 10 MPa were produced by the other manufacturer.

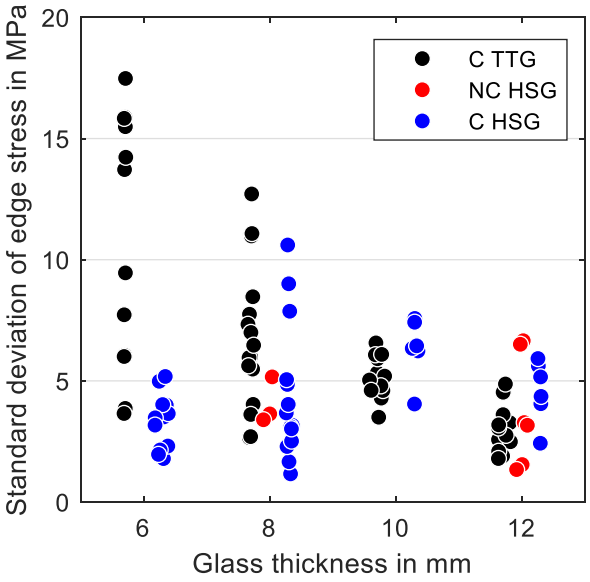

Figure 7.6: Standard deviation of the 18 individual edge stress measurement areas per large-format specimen determined by MWP depending on glass thickness and conformity

7.2.5 Relations between photoelastic and destroying test results

The relation between the photoelastic measurements and the destructive test results could only be visualized for the TTG specimens, as the number of fragments represented a metric variable, in contrast to the binary classification of fracture pattern used for HSG. Fig. 7.7 illustrates this relationship by plotting the surface stress against the number of fragments (a) and the edge stress against the number of fragments (b). In both diagrams, the photoelastic limit values determined in this research as well as the required number of 40 fragments according to EN 12150-1 (2020) are indicated.

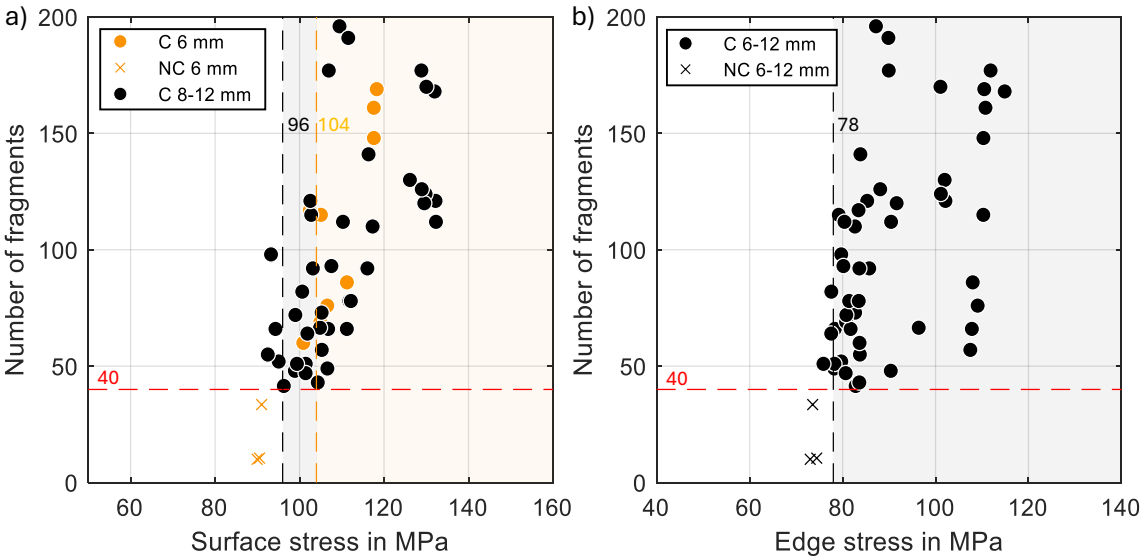

Figure 7.7: Relation between number of fragments and a) surface stress and b) edge stress on large-format specimens of thermally toughened glass with photoelastic limits obtained in Section 6.12

The limits of surface stress determined in Section 6.12 were dependent on glass thickness. Accordingly, Fig. 7.7a distinguishes samples with a thickness of 6 mm from those with thicknesses ranging from 8 mm to 12 mm by using different colors. However, the higher limit value of 104 MPa determined for the 6 mm glass thickness, was not strictly required for the present evaluation. As illustrated in Fig. 7.7a, all 3 non-conforming 6 mm specimens laid below both the thickness-specific limit of 104 MPa, and the lower limit value of 96 MPa defined for the 8–12 mm glass thickness range. Overall, the relation between surface stress and the number of fragments could be described as approximately linear. The correlation analysis confirmed this with a Pearson correlation coefficient r = 0.685 with confidence interval of [0.548, 0.804] (n = 53, bootstrapped in R (R Core Team 2024) with 2000 resamples), indicating a significant, strong positive relationship between the two variables.

By contrast, the relationship between edge stress and the number of fragments in Fig. 7.7b exhibited greater variability. Here, the data points were more widely scattered, and the trend was less clearly defined. The correlation analysis resulted in a lower Pearson correlation coefficient of r = 0.545 [0.335, 0.711] (n = 53, bootstrapped in R (R Core Team 2024) with 2000 resamples), which still indicated a significant, moderate positive relationship, but with considerably more dispersion compared to surface stress and number of fragments. Statistical data for the correlation analysis can be found in Appendix Fig. A.6, Fig. A.7 and Table A.3.

In Section 5.5.4, the 95% confidence intervals of r were examined to ascertain which photoelastic measurement exhibited a significantly higher correlation with the destructive test. For the large-format specimens, the overlapping behavior of confidence intervals differed from that observed in the standard-format specimens. For the standard-format specimens, the investigations with 95% confidence intervals demonstrated that the correlation between the number of fragments and surface stress was significantly higher than with edge stress. For the large-format specimens, the correlation analysis revealed that the relationships

between the number of fragments and surface stress, as well as the number of fragments and edge stress, were statistically indistinguishable due to the overlapping of the confidence intervals. In general, the Pearson correlation coefficients for the large-format specimens were lower than for the standard-format specimens.

7.2.6 Relation between edge stress and surface stress

The overall correlation analysis between edge stress and surface stress across all thicknesses resulted in a Pearson correlation coefficient of 0.877 (n = 98, bootstrapped in R (R Core Team 2024) with 2000 resamples), which indicated a significant, strong positive association between the two photoelastic measurements. This value was nearly identical to the correlation found in the standard-format specimens, suggesting that the relationship between surface and edge stress was consistent across specimen size and scale. Detailed statistical results of the correlation analysis are provided in Appendix Fig. A.8 and Table A.3.

To provide a clearer understanding of the relation between edge stress and surface stress, Fig. 7.8 presents scatter plots separated by glass thickness. From a thickness of 8 mm onwards, a general trend can be identified: conforming HSG specimens were consistently located below the reference line with a slope of 1, whereas both conforming and non-conforming TTG specimens were predominantly situated above this line. This finding was also evident in the non-conforming HSG specimens, which were positioned above the reference line, with only a few exceptions for 12 mm samples.

The distribution also suggests differences in the slopes between HSG and TTG depending on the thickness. For 10 mm and 12 mm specimens, the separation between HSG and TTG appeared steeper than the reference line, while the 6 mm specimens tended to align more closely with the one-to-one relation. This observation indicated that the ratio between surface stress and edge stress may vary systematically with thickness and that thinner specimens of 6 mm follow a different proportional relationship compared to thicker ones.

Additionally, Fig. 7.8 illustrates shaded colorful regions, which result from the applied photoelastic limit values and are shown for each glass thickness and glass type. Data points located within the grey and blue shaded regions indicate specimens that are classified as conforming TTG or HSG by both edge stress and surface stress criteria. This region is denoted as σ_e & σ_s. However, as can be seen in Fig. 7.8, a small number of specimens are located outside these darker boundary regions but still within the yellow or red shaded areas. Specimens in a yellow area were classified as conforming solely based on the surface stress limit and are assigned to the region σ_s, whereas data points located in the red region σ_e represented specimens that were identified as conforming exclusively by the edge stress criterion. This indicates that, for these specimens, edge stress and surface stress measurements did not lead to identical conformity classifications. For clarity, the region labels are shown only for the 6 mm specimens in the diagram but apply equally to all other glass thicknesses.

To further assess which of the two photoelastic measurements provides more reliable information in cases of disagreement, Fig. 7.9 presents stacked bar charts for (a) TTG and (b) HSG. The diagrams illustrate the classification results as a function of glass thickness based on surface stress (σ_s) and edge stress (σ_e). For each glass thickness, two stacked bars are shown: the left bar represents conforming specimens (C), while the right

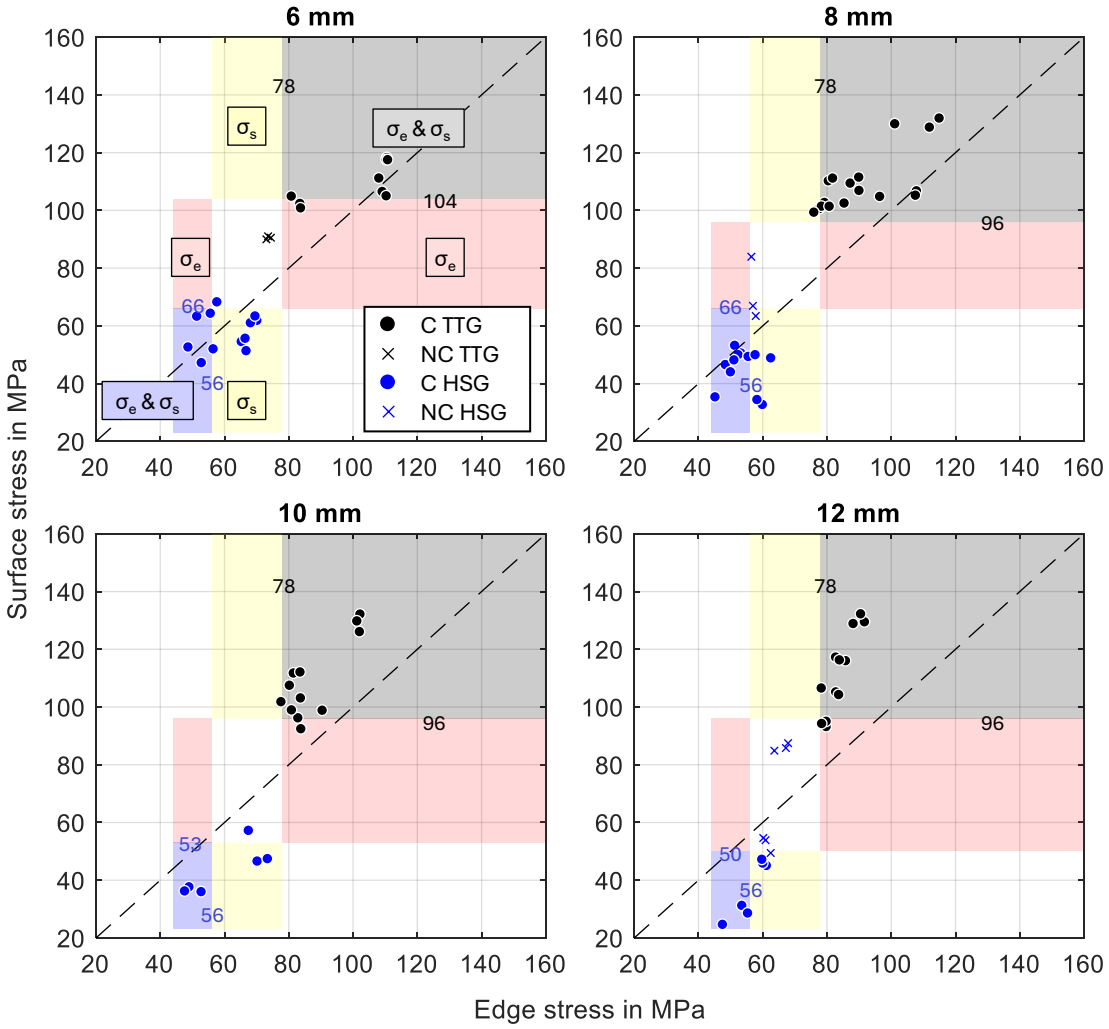

Figure 7.8: Relation between surface and edge stress of large-format specimens divided by glass thickness with photoelastic limits obtained in Section 6.12

bar represents non-conforming specimens (NC). The height of each bar corresponds to the number of specimens investigated. Each bar can be subdivided into four segments, representing different classification outcomes: specimens correctly classified by both σ_s & σ_e, specimens correctly classified exclusively by σ_e or exclusively by σ_s, and specimens for which neither stress parameter enabled a correct classification. The color-coding of these segments corresponds to the regions shown in Fig. 7.8.

Within the context of quality control, the identification of non-conforming specimens constitutes the primary evaluation criterion. Ideally, both photoelastic measurements of surface stress and edge stress lead to the same classification decision. For the NC bars, specimens consistently identified as non-conforming by both measurements represent the most reliable exclusion from the production process, whereas discrepancies between the two parameters indicate increased classification uncertainty. For the C bars, it should be noted that classifications based on only one of the two measurements imply the potential unnecessary rejection of conforming specimens. While such cases are less critical from a safety perspective than overlooking non-conforming specimens, they result in increased

abandon rates and thus entail economic disadvantages.

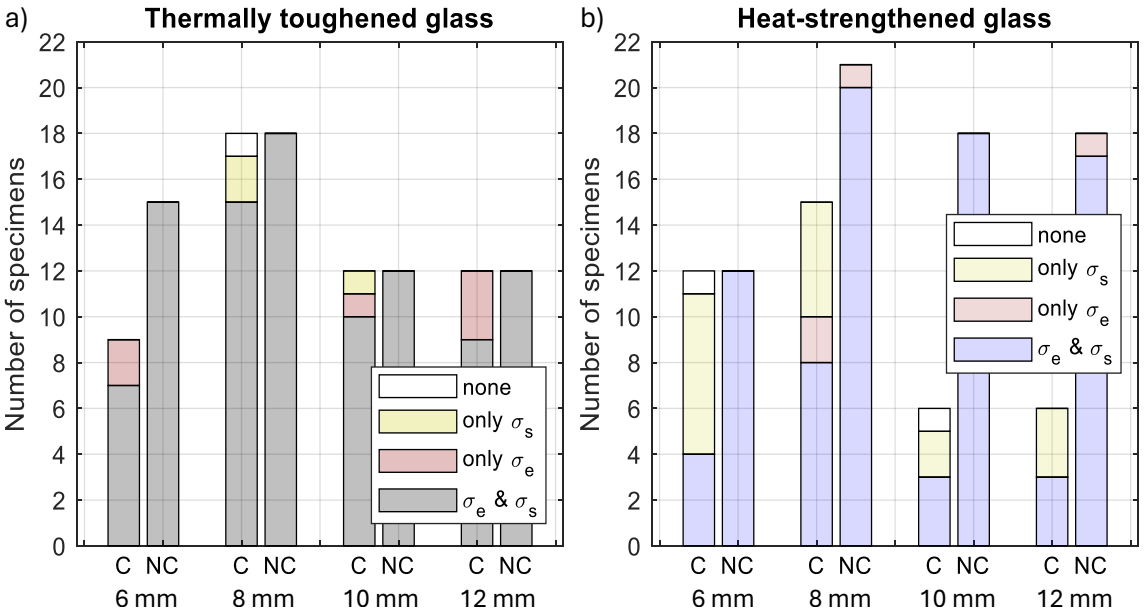

Figure 7.9: Correct classification of conforming (C) and non-conforming (NC) large-format a) thermally toughened glass and b) heat-strengthened glass, based on surface stress (σ_s) and edge stress (σ_e), including classifications using both, either or neither method, as a function of glass thickness

For TTG, the analysis in Fig. 7.9a revealed that all non-conforming specimens across all investigated glass thicknesses were correctly identified by both photoelastic limit values. Considering the C bars, a total of six specimens across all thicknesses were correctly classified solely based on edge stress, whereas only 3 specimens of 8 mm and 10 mm thickness were exclusively identified by surface stress. Furthermore, 1 actually conforming 8 mm specimen could not be correctly classified as conforming by either measurement.

In contrast, the classification of HSG specimens exhibited a different pattern, as shown in Fig. 7.9b. Almost all non-conforming specimens were successfully identified. In particular, the edge stress limit of 56 MPa proved advantageous, as it enabled the detection of 2 non-conforming 8 mm and 12 mm HSG specimens that were not identified by the surface stress criterion. However, correct identification of 17 conforming specimens distributed across all glass thicknesses was only possible through surface stress measurement. This means that the 56 MPa edge stress limit unnecessarily excluded 17 specimens. Nevertheless, 2 conforming 6 mm and 10 mm HSG specimens were not detected by any of the photoelastic measurements. As previously described, the recall rate of the edge stress limit of 56 MPa was notably low. However, when evaluating the specimens with an edge stress limit of 60 MPa, these 2 non-conforming specimens would not be detected. The result was a reduction in specificity of 66.7%, as illustrated in Table 7.5 and demonstrated in Fig. 7.10b in the right column.

Consequently, the validation of HSG specimens with edge stress values between 56 and 60 MPa will be conducted using surface stress measurements and the evaluation by limits depending on glass thickness. Fig. 7.10a presents this range with the corresponding values in color depending on glass thickness, while the other values, which were below 56 MPa

and above 60 MPa, are displayed in grey. A total of 10 specimens yielded edge stress values from 56 MPa and 60 MPa, of which 2 were non-conforming HSG specimens. The surface stress measurement correctly identified one of them as non-conforming, but the other one was classified incorrectly. The consequences are shown in Fig. 7.10b: the recall rate of formerly 52.6% for the limit of 56 MPa increased to 68.4% for the additional validation, while the specificity decreased to 88.9% in comparison to the evaluation with the 56 MPa edge stress limit. Conducting the quality control exclusively with an edge stress limit of 60 MPa without comparing surface stress measurements would result in a subsequent decrease in specificity of 66.7%, while the recall would remain at a comparable level.

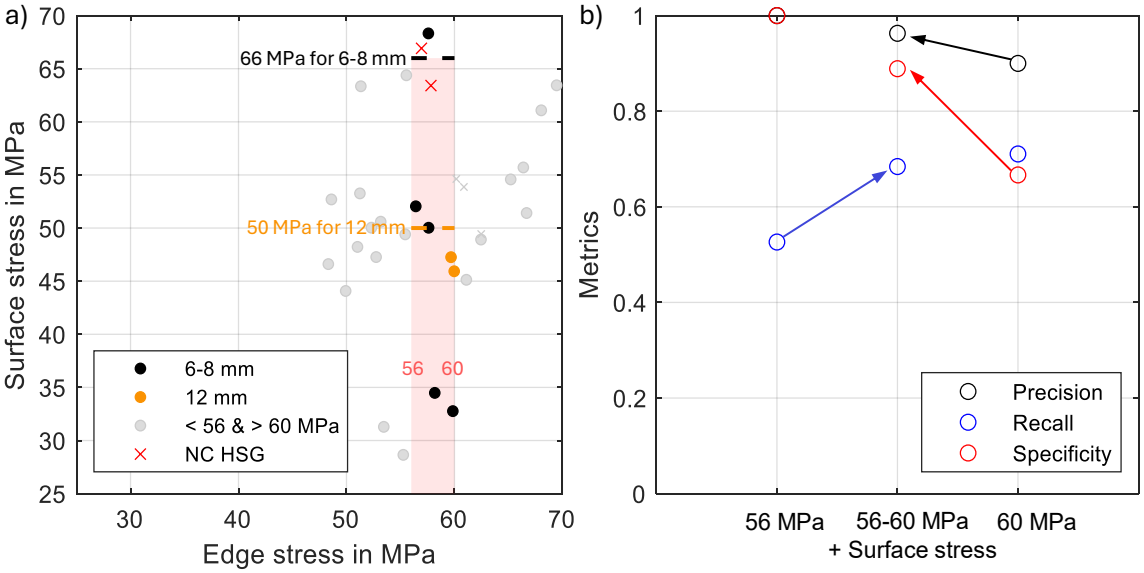

Figure 7.10: a) Relation between edge stress and surface stress values of large-format HSG, highlighting the area between 56–60 MPa edge stress, b) comparing metrics of precision, recall, and specificity for evaluation with 56 MPa and 60 MPa edge stress limit and inter area validating with surface stress values

It is noteworthy that the close clustering of edge stress values within the range of 56–60 MPa was not reflected in the distribution of surface stress. In contrast, the surface stress values exhibited a substantially wider spread, covering a range of 36 MPa.

Taken together, these findings suggest that edge stress measurements are more reliable for TTG, as surface stress tends to result in a higher rate of false rejections. On the other hand, surface stress measurement tends to reduce the erroneous exclusion of conforming HSG, but at the expense of accuracy in detecting non-conforming cases. In general, the simultaneous application of both methods in production quality control does not appear to be necessary. However, especially for the product type HSG, the use of surface stress measurements for the validation of edge stress values between 56 and 60 MPa has been demonstrated to reduce erroneous rejection.

7.3 Comparison between standard-format and large-format

This section explores the influence of the dimensions of the specimens, specifically the small-format, standard size (360 mm x 1100 mm) and large-format (1000 mm x 3000 mm)

specimens which were produced by the same manufacturers. The subsequent analysis distinguished between two scenarios regarding the tempering process, to evaluate the relationship between standard-size and large-format tests:

- Scenario I: Same cooling parameters
- Scenario II: Adapted cooling parameters

In scenario I, the manufacturer tempered the specimens of the standard-size and large format in different time periods, but with the same cooling setting parameters for the air pressure in the quench for their respective glass thickness and pre-stress level of low and high TTG as well as HSG. Only the heating time was adjusted to the glass size and mass. In scenario II, the manufacturer adapted the tempering settings specifically to the large-format specimens, so that the furnace settings differed from those of the standard-size specimens. This differentiation enables a systematic analysis of the effects of the sample size on the tempering process under controlled conditions.

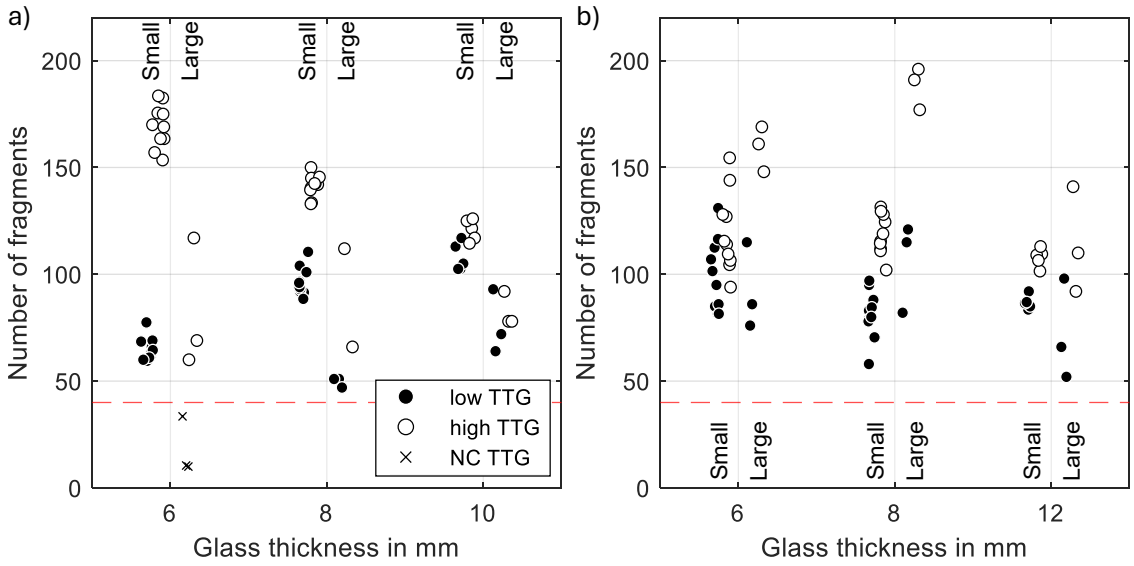

Figure 7.11: Results of number of fragments of low and high thermally toughened for a) same (scenario I) and b) adapted (scenario II) cooling parameters of the standard-size and large-format specimens

The following comparison presents the destructive and photoelastic results of the standard-size specimens versus the large-format specimens, separated by glass thickness. In the subsequent figures, data points located to the left of the light reference line represent the small-format samples, while those on the right correspond to the large-format specimens. Fig. 7.11 shows the number of fragments for the (a) same and (b) the adapted cooling parameters of the standard-size and large-format specimens depending on the pre-stress level of low and high TTG. For scenario I, it can be seen in Fig. 7.11a that the number of fragments decreased for the same cooling parameters for the 1000 mm x 3000 mm specimens at both pre-stress levels. The 6 mm low toughened specimens even fell below the limit of 40 fragments, although the standard-size specimens still exhibited the fracture pattern required for TTG. For the specimens in scenario II in Fig. 7.11b, which were produced with adapted cooling parameters, no uniform trend could be observed in the comparison of standard size to large format. In scenario II, all specimens were in accordance with the

properties of TTG. A metric evaluation of the HSG specimens with respect to the fracture pattern was not possible and could not be displayed as for TTG in Fig. 7.11. However, conformity could be assessed in Fig. 7.12 for surface stress and Fig. 7.13 for edge stress.

Fig. 7.12 shows the results of surface stress for the (a) same and (b) the adapted cooling parameters including the limit ranges for TTG and HSG. The decreasing trend in the number of fragments, observed in scenario I for the larger specimen size in Fig. 7.11a, was also reflected in the surface stress behavior of glass type TTG shown in Fig. 7.12a. For the 6 mm HSG specimens, the surface stress values remained largely constant, showing only a slight tendency toward higher values. All 6 mm HSG specimens exhibited a conforming HSG fracture pattern. In contrast, a different pattern emerged for the 8 mm specimens: half of the small-format specimens did not exhibit a conforming HSG fracture pattern. The large-format specimens, however, all showed a conforming HSG fracture pattern and fell within the HSG surface stress limit range of 23 to 66 MPa.

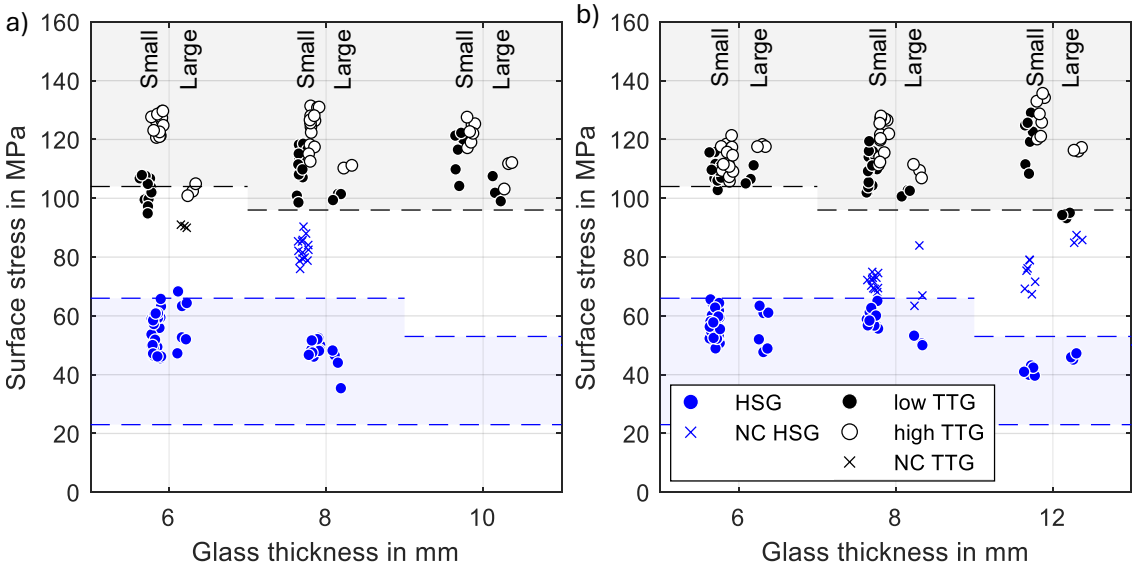

Figure 7.12: Results of surface stress of low and high thermally toughened and heat-strengthened glass for a) same (scenario I) and b) adapted (scenario II) cooling parameters of the standard-size and large-format specimens, with photoelastic limits obtained in Section 6.12

In scenario II, the higher number of fragments observed for the high TTG large-format specimens in Fig. 7.11b, especially for glass thicknesses of 6 mm and 8 mm, compared to the corresponding high TTG small-format specimens was not consistent with the results of the surface stress analysis in Fig. 7.12b: the high TTG large-format specimens had lower surface stress values compared to the standard-format. The conformity of the HSG specimens remained unchanged with the change in format size.

Fig. 7.13 presents the results of edge stress measured on standard-size and large-format specimens. Additionally, the limit ranges for TTG are indicated in gray and for HSG in blue. Fig. 7.13a also demonstrates the decreasing trend of the number of fragments regarding the specimen size in the edge stress measurements in scenario I for TTG. For the 6 mm and 8 mm high toughened TTG specimens, the large-format specimens exhibited higher edge stress compared to the standard-size specimens in scenario II (Fig. 7.13b). This observation

was consistent with the number of fragments shown in Fig. 7.11b. Across both scenarios, the difference in edge stress values between high- and low-toughened specimens fell within a comparatively narrow range than in the surface stress values. For the 6 mm specimens, the measured values were in a similar range for small- and large-format specimens. Compared to the surface stress values, the edge stress values fell within a narrower range. In contrast to the small-format 8 mm and 12 mm specimens, a clearer separation between C and NC HSG could be achieved for the large-format glass panes. The 8 mm large-format specimens exhibited lower edge stress values than their small-format counterparts. This trend was also observed in the surface stress measurements.

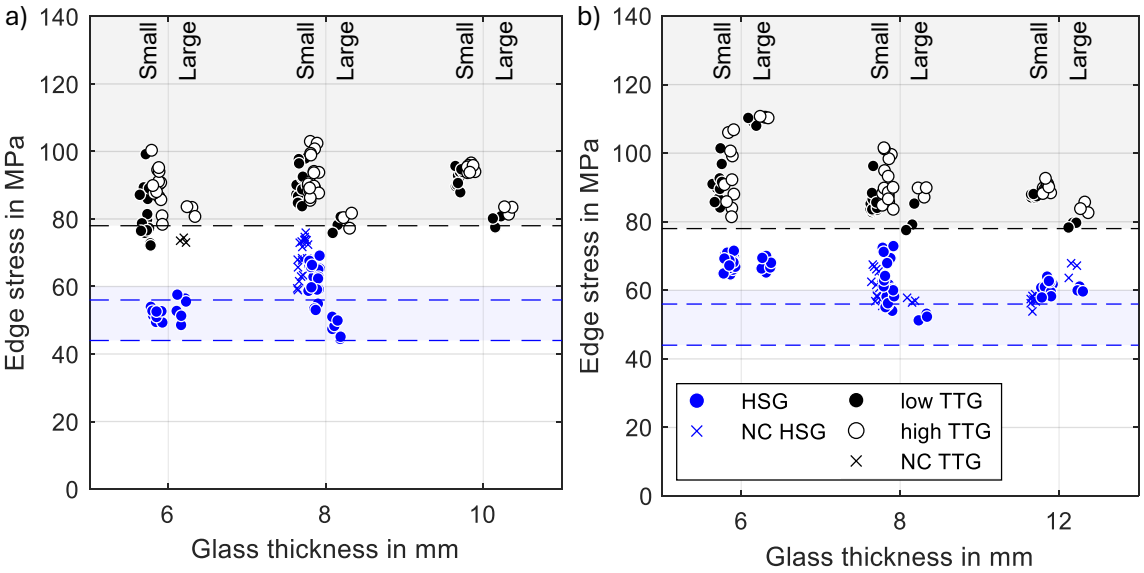

Figure 7.13: Results of edge stress of low and high thermally toughened and heat-strengthened glass for a) same (scenario I) and b) adapted (scenario II) cooling parameters of the standard-size and large-format specimens, with photoelastic limits obtained in Section 6.12

To analyze the changing effects of sample size on the test results in scenario I with greater clarity, the mean value for the test results of large-format and standard-size was calculated for each test series, separately for glass thickness and pre-stress level. As the ratio of small format to large format was less than 1 for all measurement methods, the *reduction factor* was calculated using the *mean* values, as shown in Equation (7.1).

$$\text{Reduction factor} = 1 - \frac{\text{mean}_{\text{large format}}}{\text{mean}_{\text{standard size}}} \tag{7.1}$$

Divided by glass type, Fig. 7.14 and Fig. 7.15 show the reduction factors of the large-format compared to the standard-format specimens, which were produced under the same cooling parameters (scenario I). It was not possible to calculate the factor of individual samples, as there was no direct pairing between specific large-format and standard-size specimens. However, to reflect the variability within the changing effects, error bars indicating the minimum and maximum possible reduction factors are included in Fig. 7.14 and Fig. 7.15. The diagrams illustrate the distinction in color between the measurement method and pre-stress level. Fig. 7.14 shows the evaluation of reduction factors for TTG. Here, the different transparency of the bars represents the test series of high and low toughened

glass. The influence of glass format has been demonstrated to be particularly apparent in fracture pattern tests: the number of fragments from the large-format glass decreased by 73% in the 6 mm low toughened series. With increasing glass thickness, the reduction in the number of fragments diminished to 31% for the 10 mm high toughened specimens. The strong reduction in the number of fragments in the large-format specimens in comparison to the standard-size specimens did not correspond to the same extent with the photoelastic measurements. A maximum mean reduction factor of 18% in surface stress and up to 14% in edge stress has been observed. Furthermore, no consistent trend was apparent in the photoelastic measurements in relation to the glass thickness. However, the 6 mm TTG specimens showed a minor reduction in edge stress values in comparison to the reduction factor of number of fragments as well as in comparison to other glass thicknesses. Nevertheless, the photoelastic limits obtained were sufficient to identify the non-conforming specimens.

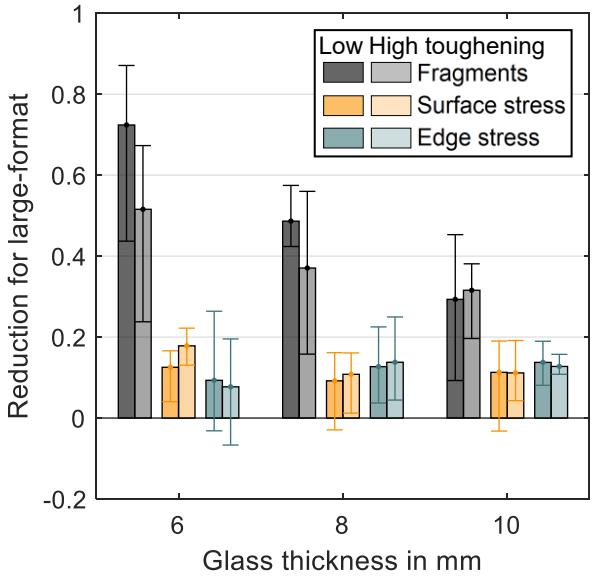

Figure 7.14: Reduction for large-format compared to the standard-size series with the same cooling parameters, depending on pre-stress level and measurement method with deviations as error bars for thermally toughened glass

The evaluation of HSG could only be analyzed metrically for edge and surface stress measurements, as the fracture pattern of HSG must be assessed qualitatively. Consequently, the impact of the glass format on the fracture pattern of HSG is delineated in the following text: the 6 mm standard-size specimens exhibited a conforming fracture pattern characteristic of HSG, and the corresponding large-format specimens likewise demonstrated conformity. This phenomenon is illustrated by a black dot in Fig. 7.15. This behavior was also evident in the residual stresses, as indicated by the variability of edge and surface stress values around the 0 line of reduction but with large deviations.

Conversely, a few standard-size specimens with a glass thickness of 8 mm did not demonstrate a HSG fracture pattern. Using the same cooling parameters, the 3000 mm x 1000 mm large-format specimens exhibited a lower pre-stress level compared to smaller specimens due to their increased format size. As a result, the fracture pattern characteristic of HSG was maintained, and all 8 mm large-format specimens could be classified as conforming HSG. This was further evidenced by the significant reduction in residual stress, reaching

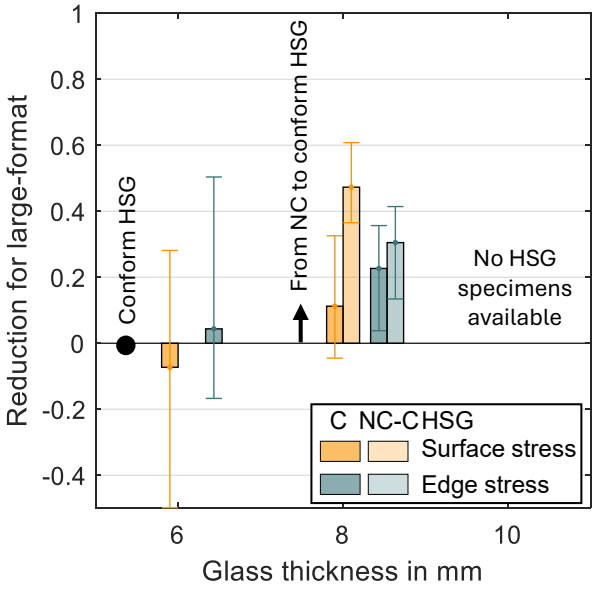

Figure 7.15: Reduction for large-format compared to the standard-size series with the same cooling parameters, depending on pre-stress level and measurement method with deviations as error bars for heat-strengthened glass

max. 47% in surface and 31% in edge stress shown as transparent bars. However, a similar trend of decreasing photoelastic measurements has also been observed in the conforming standard-size HSG specimens, where the edge stress values were reduced by 23% and the surface stress values were reduced by 11%. This phenomenon could be attributed to the observation that the standard-size HSG specimens exhibited higher edge stress values, which, however, exceeded the established limit of 56 MPa and were consequently falsely rejected. Due to the larger format, lower edge stress values were measured, thereby ensuring the accurate classification of the larger format as conforming HSG.

The reduction in residual stress detected for TTG from small to large format could thus be confirmed for the 8 mm HSG specimens. In contrast, the 6 mm HSG large-format specimens exhibited comparable residual stresses to those of the standard-size specimens when pre-stressed with same cooling parameters. This finding stood in contrast to the results observed in TTG, where a substantial decrease in fragment number was noted for the 6 mm specimens. The examination of HSG specimens in large components with a glass thickness of 10 mm was not possible due to the lack of such samples.

EN 12150-1 (2020) and EN 1863-1 (2012) specify destructive tests on standard-size specimens measuring 360 mm x 1100 mm, which must be tempered simultaneously with the real-sized panes of the same glass thickness used for installation. These tested specimens are assumed to be representative of all other formats in the production batch with the same thickness and to comply with the finely crumbled fracture pattern specified for TTG or the fracture pattern of HSG which ensures post-fracture behavior. However, evaluations in this research suggest that the residual stress state of these standard-size specimens is higher than that of the larger panes. While small-format panes with a higher stress state are assessed as part of quality control, they may not accurately represent the actual tempering quality of full-size panes. This could lead to an overestimation of their residual stress state. Therefore, it is generally recommended to confirm the fragmentation pattern

and adapt the tempering setting parameters when scaling up. Conversely, that indicates that the photoelastic limits determined in Section 6.12 are on the safe side because the determination of the limits is based on higher values measured on standard-size specimens, and therefore more conservative limits were achieved.

7.4 Summary and conclusions

To validate the photoelastic limit values obtained in Chapter 6, this chapter investigated 102 large-format specimens with dimensions of 3000 mm x 1000 mm measuring edge and surface stress, followed by a fracture pattern test to check the conformity of thermally toughened and HSG.

The limit values for photoelastic measurements obtained for TTG proved to be effective on the large-format specimens. Notably, the 3 TTG specimens in glass thickness of 6 mm, which did not conform to the fracture pattern characteristic of TTG, were accurately classified as non-conforming, exhibiting a specificity ratio of 100%. Conversely, it should be noted that the low limit values specified by ASTM C1048 (2025) for surface and edge stress are not adequate for the purpose of checking the fracture pattern of TTG. Furthermore, the classification method showed that the limit value of the ISO 12540 (2017) for the surface stress cannot recognize all the non-conforming specimens.

Evaluating large-format specimens of the glass type HSG is less straightforward. For surface stress measurements, it is reasonable to define the upper limit value depending on glass thickness. This is supported by the comparison with the ISO 22509 (2020) limit, which does not take thickness into account and consequently results in a lower recall rate compared to the thickness-dependent limits obtained in this research. Furthermore, the ASTM C1048 (2025) limit range for 6 mm HSG demonstrated a high percentage of rejections. Nevertheless, the previous surface stress limit value for 8 mm glass is not capable of identifying all non-conforming HSG specimens with full precision. The limit value for 8 mm is therefore reduced from 66 MPa to 60 MPa.

The assessment of HSG by edge stress measurements was carried out independently of glass thickness but with two different upper limit values of 56 MPa and 60 MPa. While the conservative limit of 56 MPa achieves a 100% detection rate of non-conforming HSG specimens, it incorrectly rejects almost half of the conforming specimens. Raising the upper limit to 60 MPa reduces these rejections but also causes a decrease in precision and specificity. For evaluating TTG, the combined routine application of both methods does not appear necessary. However, for HSG, specifically as measured by the MWP method, the additional validation of edge stress values in the intermediate range of 56–60 MPa through surface stress limits has been proven useful, as it significantly improves the precision in comparison of the higher limit value of 60 MPa and reduces unnecessary rejections in case of the conservative limit value of 56 MPa.

Furthermore, a one-to-one relation between edge and surface stress is not evident in large-format specimens. It has been observed that, particularly in thicker specimens, non-conforming HSG specimens attain higher surface stress values, while conforming specimens exhibit higher edge stress values. In accordance with the findings observed for the standard-size specimens, a higher correlation coefficient is demonstrated by the

relationship between the number of fragments and surface stress than by the relationship with edge stress.

In the comparison between small- and large-format test specimens, two different tempering scenarios were considered: in scenario I, same and in scenario II, adapted cooling settings during the tempering process were applied to the specimens. In scenario II, the standard-size and large-format specimens attained comparable pre-stress states, as the tempering conditions were adapted to the respective format. The investigation of the format of the specimens demonstrated that the TTG large-format specimens from scenario I, which were produced with the same cooling parameters, exhibited a lower pre-stress state. The reduction in fragments in the large-format specimens was also confirmed by the two photoelastic measurement methods of surface and edge stress. For the 6 mm large-format TTG specimens, the number of fragments was reduced by up to 73% compared to the standard format. While the standard-format specimens still exhibit the required fracture pattern in accordance with EN 12150-1 (2020) under the same cooling settings, the large-format specimens no longer achieve the minimum number of 40 fragments.

The behavior of the scenario I looked different for HSG: only for the 8 mm, a reduction for the residual stresses could be detected. The magnitude of the decrease was so significant that a change in the conformity was observed. The preceding standard-size test series were non-conforming HSG specimens with a too fine fracture pattern. The large-format specimens with the same cooling parameter are now conforming HSG specimens. Conversely, the 6 mm HSG large-format specimens show residual stress levels comparable to those of the standard-size specimens when subjected to the same cooling parameter.

In general, the reduction in pre-stress expressed through fracture behavior from standard format to large format is less pronounced in photoelastic measurements. This emphasizes the necessity to adapt production parameters specifically for large-format glass to achieve the safety-relevant properties. At the same time, this also means that the reference panes, which are tempered alongside the large-format panes, exhibit a higher stress state. While this higher stress state is currently tested as part of quality control, it does not accurately reflect the actual tempering quality of the full-size panes.

It can be concluded that the photoelastic limits obtained in this study are suitable for assessing the pre-stress quality of large-format TTG, both for edge and surface stress measurements. In contrast, the evaluation of HSG is more complex. After adapting the surface stress limit of 8 mm glass to 60 MPa, the limits are able to reliably detect all non-conforming specimens. For HSG, the edge stress measurements using the MWP method proved particularly challenging. Here, the large scatter of results and the wide divergence between precision and recall metrics highlight the limitations of the method. Consequently, the assessment of HSG using photoelastic measurements must be interpreted with caution and cannot be considered fully reliable. However, evaluation employing edge stress measurement is more efficacious in the case of large-format specimens than standard-size specimens.

8 Recommendations for non-destructive evaluation criteria

To enable a non-destructive quality control of tempered glass, this chapter defines the requirements, prerequisites, and limitations of photoelastic measurements of surface stress and edge stress. Furthermore, it specifies whether and which limit values are suitable for the two glass products TTG according to EN 12150-1 (2020) and HSG according to EN 1863-1 (2012) as a function of glass thickness and describes how and at which positions these stresses shall be measured.

8.1 Measurement of surface stress

As part of the parabolic stress distribution in the undisturbed surface area of a glass pane, the surface stress can be measured as compressive stress. In this work, the scattered light method was applied using the SCALP-05 (GlasStress Ltd. 2013) measuring device in its standard configuration. The photoelastic constant C was set to 2.72 TPa^{-1}. Other measuring devices may also be used, provided they fulfill the requirements specified in this chapter. The measurement method for surface stress is comparatively demanding and should only be applied by trained and experienced users. In particular, the operator must be aware of the conditions under which the device yields reliable results. Special attention shall be paid to ensuring a clean glass surface and a dark measurement environment free from disturbing light sources.

The investigations presented in Chapters 5, 6, and 7 demonstrated that surface stress exhibits a strong correlation with both the fracture pattern and the bending tensile strength. For TTG, the fracture pattern represents the critical conformity criterion and requires comparatively higher surface stress levels to be fulfilled. In contrast, the bending tensile strength criterion is already satisfied at lower surface stress values.

The following recommendation concerning the procedure are given: since the direction of the principal stress $\sigma_{1,\mathrm{MPi}}$ is generally unknown, measurements shall be performed at each measurement point in the three or four orientations of 0°, 45°, 90°, and 135° (see Fig. 8.1a). Using the equations given in Section 3.2, these measurements shall be transformed into the two principal stresses $\sigma_{1,\mathrm{MPi}}$ and $\sigma_{2,\mathrm{MPi}}$, where i denotes the index of the measurement point.

Based on an initial assessment of the polarization image to evaluate the homogeneity of the pre-stress over the surface, the principal stress $\sigma_{1,\mathrm{MPi}}$ shall be measured at a minimum of three measurement points. Depending on the glass length and width, these points shall be distributed at the quarter points of both dimensions, as illustrated in Fig. 8.1b. To avoid interference from the compressive pre-stress zone along the edge, a minimum distance of 100 mm from the glass edge shall be maintained on all sides.

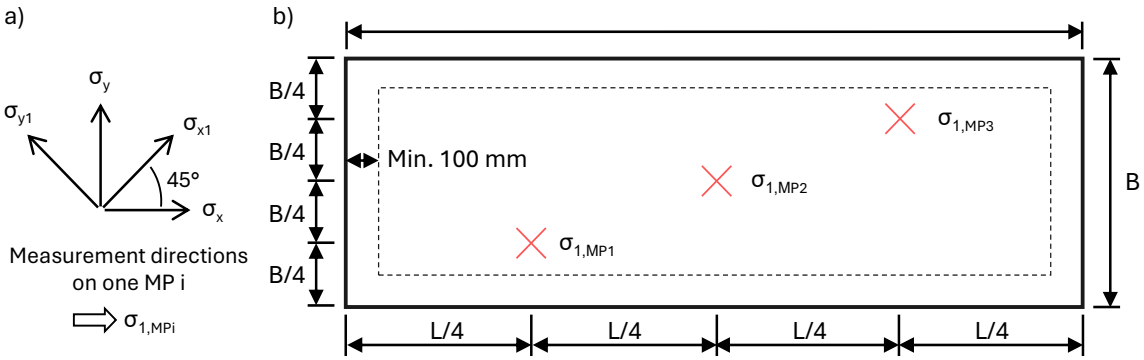

Figure 8.1: Recommended procedure for surface stress measurement: a) min. three measurement directions and b) specified measurement points, adapted from Efferz et al. (2025a)

For further evaluation of the pre-stress homogeneity, the principal stress difference $\sigma_{\mathrm{s,diff,MPi}}$ at each measurement point shall be checked. As defined in Equation (8.1), this value shall not exceed 15 MPa. In addition, the standard deviation of the principal stresses $\sigma_{\mathrm{1,MPi}}$, determined at the three measurement points, shall not exceed 10 MPa, as specified in Equation (8.2).

Finally, the mean value of the principal stress $\sigma_{\mathrm{1,MPi}}$, obtained from the three measurement points, shall be used as the decisive criterion to assess whether the respective specimen complies with the specified requirements, see Equation (8.3). The $\mathrm{limit}_{\mathrm{surface\ stress}}$ can be found in Table 8.1 and Fig. 8.4.

$$\sigma_{\mathrm{sdiff},MPi} = \sigma_{1,MPi} - \sigma_{2,MPi} \leq 15\,\mathrm{MPa} \tag{8.1}$$

$$\sigma_{s1,std} = \mathrm{std}(\sigma_{1,MPi}) \leq 10\,\mathrm{MPa} \tag{8.2}$$

$$\sigma_{s1,mean} = \mathrm{mean}(\sigma_{1,MPi}) \leq \mathrm{limit}_{\mathrm{surface\ stress}} \tag{8.3}$$

8.2 Measurement of edge stress

Edge stress is generated as a membrane stress during the cooling phase of the tempering process in the edge region of the glass pane. It is characterized by a continuous increase towards the glass edge, while the stress at a given position remains constant over the glass thickness. Due to the prevailing one-dimensional stress state in this region and the vanishing of one principal stress component, the edge stress can be calculated using Equation (8.4) as a function of glass thickness, the photoelastic constant, and the measured light retardation.

Light retardation in the edge region can in principle be measured using various photoelastic devices. However, most measuring instruments encounter difficulties in accurately capturing retardation values in the edge area due to the required edge processing for tempered glass in accordance with EN 12150-1 (2020) and EN 1863-1 (2012). The chamfered edge causes scattering of the incident light, which results in missing or highly inaccurate retardation

measurements in this region. This chamfered area is illustrated in Fig. 8.2a. Consequently, the retardation across the chamfer must be estimated using an extrapolation function.

The width of the chamfer typically ranges between 0.5 and 2 mm. As a result, the measurement procedure proposed in ASTM C1279 (2023) cannot be applied, since at least one of the two prescribed measurement points would be located within the chamfered region. As an alternative, retardation values shall be measured within the pre-stress zone at the edge, which extends from the 0th isochromatic order to the beginning of the chamfer. The zero-order isochromatic fringe represents the location at which the parabolic stress distribution across the glass thickness originates in the surface region of the pane. In general, the width of the edge pre-stress zone is larger for HSG than for TTG. As a general rule, the pre-stress zone at the edge of TTG is smaller than the corresponding glass thickness (≈ 0.6–1.0 t), whereas the compressive edge zone of HSG is slightly wider than the glass thickness (≈ 1.0–1.5 t).

Subsequently, the measured retardation values are interpolated using a polynomial function, which is then extrapolated across the chamfer to the glass edge. Within this research, a 3rd degree polynomial proved to be an appropriate compromise between flexibility, robust extrapolation behavior, and conservatively safe stress values for the quality control of tempered glass. In addition, the quality of the curve fitting is assessed using a coefficient of determination $R^2 \geq 0.95$ to exclude insufficiently fitted functions. The applied procedure is illustrated in Fig. 8.2b.

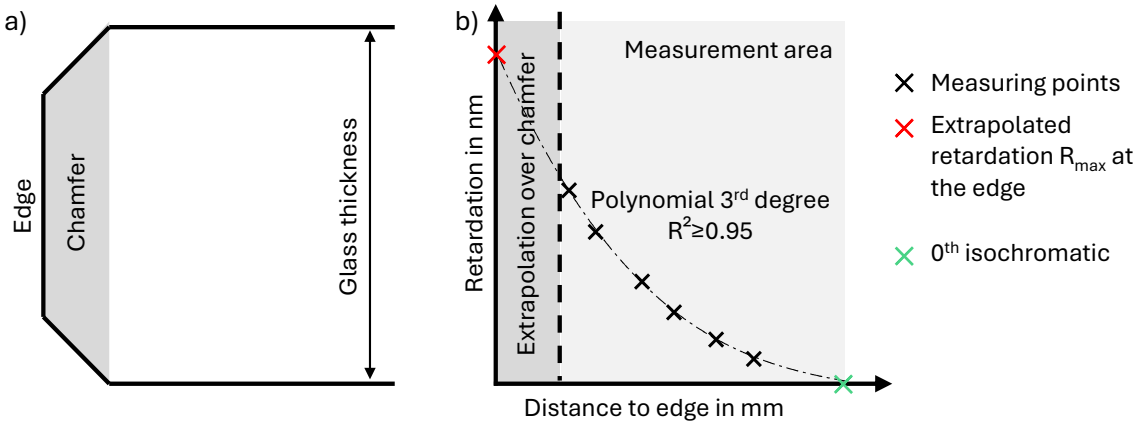

Figure 8.2: Recommended procedure for edge stress measurement: a) cross-section through glass edge with marking of the chamfer and b) diagram illustrating the measurement area with retardation measurement points and extrapolated value at the edge, from Efferz et al. (2025a)

Using the extrapolated retardation value R_{max}, the edge membrane stress $\sigma_{e,MPi}$ can be determined for each measurement point as a function of the actually measured glass thickness t and the photoelastic constant C, as given in Equation (8.4). In this work, the photoelastic constant was set to 2.72 TPa^{-1}.

$$\sigma_{e,MPi} = \frac{R_{max}}{t\,C} \tag{8.4}$$

This procedure shall be applied at a minimum of three measurement points on each of the two longitudinal edges of the glass pane. The measurement points shall be located at the

quarter points of the pane length, as illustrated in Fig. 8.3. This approach ensures that the conformity assessment of the glass product with respect to the glass type is independent of the pane format.

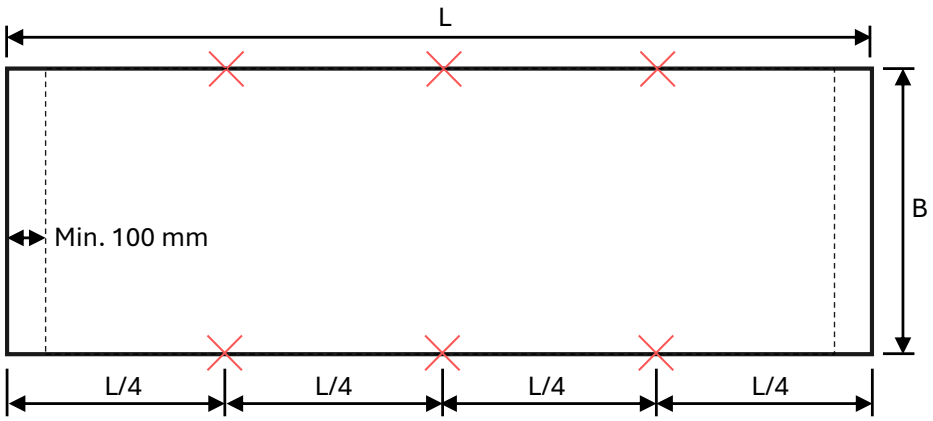

Figure 8.3: Recommended measurement points for edge stress from Efferz et al. (2025a)

The limit values for edge stress, defined in the following section, shall be evaluated based on the mean value of the individual measurements $\sigma_{\mathrm{e,MPi}}$, see Equation (8.6). To assess the homogeneity of the prestress along the edge, the variation among the measurement points shall be limited by a maximum standard deviation of 10 MPa, as specified in Equation (8.5)).

$$\sigma_{e,std} = \mathrm{std}(\sigma_{e,MPi}) \leq 10\,\mathrm{MPa} \tag{8.5}$$

$$\sigma_{e,mean} = \mathrm{mean}(\sigma_{e,MPi}) \leq \mathrm{limit}_{\text{edge stress}} \tag{8.6}$$

Currently, several measurement devices employing different methodologies for the determination of edge stress are available, including MWP, PST, carrier fringe method, and double-wedge compensators. In this work, the evaluations were performed using the MWP and the PST systems. The following paragraphs describe specific aspects that must be considered for these two measurement methods.

For measurement methods that do not provide a continuous retardation profile, such as the MWP system, several conditions must be satisfied. It was found that at least 5 supporting data points, representing integer and half-integer orders of the optical wavelength, are required to achieve a sufficiently robust interpolation function. Ideally, the MWP device should be equipped with three light sources in order to provide a larger number of supporting points for curve fitting. The assessment of edge stress determined by the MWP method is not feasible for a glass thickness of 4 mm and is only limitedly feasible for a thickness of 6 mm. For MWP, as the TTG limits indicated in Table 8.2 may not offer a definitive discrimination criterion for TTG, they nevertheless qualify as a quality characteristic for the purpose of evaluating the tempering degree of specimens that are specifically subjected to TTG parameters. For HSG with a thickness of 6 mm, an insufficient number of supporting points was observed in some cases. If the device is equipped with only two wavelengths, reliable measurements are considered possible only for glass thicknesses of 8 mm and above. To ascertain the efficacy of the limits in Table 8.2 as a quality control criterion for

HSG, a comprehensive evaluation must be conducted within the context of the production process.

For measurement methods such as PST, which allow the acquisition of a continuous retardation profile, no minimum requirement regarding the number of supporting points applies. However, the ratio of chamfer width to glass thickness shall be controlled, as an excessively large chamfer may lead to increased variability in the extrapolation behavior. For PST, the limits in Table 8.2 serve as reliable criteria for discrimination between the glass types and quality control of the tempering process.

It shall be noted that the limit values defined in this work are based on an extrapolation using a 3rd degree polynomial. Other measurement methodologies that were not investigated in this study but are intended for use in non-destructive quality control shall ensure that a manual evaluation of the edge stress is possible and that the extrapolation procedure is compatible with the approach described herein.

Furthermore, the integration of edge stress measurements into the quality control of tempered glass offers the advantage that certain measurement methods enable inline inspection. For example, devices based on the MWP methodology allow for 100% inspection of glass panes across all formats. In addition, an automated evaluation of edge stress measurements would reduce user-dependent inaccuracies and improve reproducibility.

8.3 Photoelastic limit values

TTG according to EN 12150-1 (2020) is characterized by a high characteristic bending tensile strength of 120 MPa and a fine, crumbly fracture pattern. The limit values defined in this work are intended to serve as minimum requirements, ensuring that both mechanical properties are fulfilled. At the same time, the approach aims to allow conformity assessment based on a single photoelastic measurement.

HSG according to EN 1863-1 (2012) is defined by a characteristic bending tensile strength of 70 MPa and a coarse fracture pattern. These two criteria are inherently conflicting: the strength requirement represents a minimum level of pre-stress, whereas the fracture pattern imposes an upper limit on the pre-stress. If a glass pane exhibits a characteristic bending strength of at least 70 MPa but shows an excessively fine fracture pattern with multiple islands, thereby compromising residual load-bearing capacity in laminated glass applications, it shall not be classified as conforming HSG. Consequently, the assessment of HSG requires two limit values for both edge stress and surface stress.

The limit values for edge stress of TTG and HSG are closer to each other than those defined for surface stress. For TTG, a simplified criterion applies in which the ratio of edge stress to surface stress is less than 1. In contrast, for HSG the ratio of edge stress to surface stress exceeds 1, particularly for larger glass thicknesses.

The limit values for surface stress measurements, which are intended for quality control of TTG according to EN 12150-1 (2020) and HSG according to EN 1863-1 (2012) and are applicable to glass panes of any format, are summarized in Table 8.1 as a function of glass thickness. The compressive surface stress has been shown to provide a reliable distinction between conforming and non-conforming HSG.

Table 8.1: Recommended limit values of surface stress [MPa] for thermally toughened and heat-strengthened glass made of clear float, varying by glass thickness but independent of glass format

Glass thickness [mm]	4	6	8	10	12
Thermally toughened glass EN 12150-1 (2020)	> 106	> 104	> 96	> 96	> 96
Heat-strengthened glass EN 1863-1 (2012)	23–66	23–66	23–60	23–53	23–50

The limit values for non-destructive quality control based on edge stress measurements are shown in Table 8.2 and apply to the fracture pattern and bending tensile strength requirements of glass products according to EN 12150-1 (2020) for TTG and EN 1863-1 (2012) for HSG. The limit values are independent of glass thickness and are valid for thicknesses ranging from 6 mm to 12 mm. The evaluations have demonstrated that the conformity assessment of TTG performs reliably with both edge stress measurement methods, whereas the conformity assessment of HSG based on edge stress measured using the MWP method is only of limited reliability. The actual limit value of 60 MPa, which is well suited when using the PST method, is associated with excessive uncertainty when applied to MWP measurements.

Table 8.2: Recommended limit values of edge stress [MPa] for thermally toughened and heat-strengthened glass made of clear float, varying by glass thickness but independent of glass format

Glass thickness [mm]	4	6	8	10	12
Thermally toughened glass EN 12150-1 (2020)	-	> 78	> 78	> 78	> 78
Heat-strengthened glass EN 1863-1 (2012)	-	44–60 *	44–60 *	44–60 *	44–60 *

*MWP: 56–60 MPa values require surface stress verification with limits in Table 8.1, else limit range = 44–56 MPa.

Therefore, a conservative limit of 56 MPa was defined for edge stress measurements, performed with the MWP system, to reliably detect non-conforming HSG specimens for safety reasons. However, this narrow validity range entails the risk that a considerable number of otherwise conforming HSG may be unnecessarily rejected. To remain on the safe side while avoiding excessive material waste, surface stress measurements can be used to validate the edge stress results. Accordingly, it is recommended that HSG specimens for which edge stress values measured by MWP fall within the range of 56 MPa to 60 MPa be subjected to additional surface stress measurements and assessed against the corresponding surface stress limit values.

The final photoelastic limits are also shown graphically in Fig. 8.4, where (a) shows the values for surface stress and (b) shows the values for edge stress for the glass products TTG and HSG, depending on glass thickness.

8.4 Limitations

The measurement values presented in Table 6.15 and Table 8.2 are valid exclusively for uncoated, tempered soda-lime-silicate glass. It remains to be verified whether the proposed

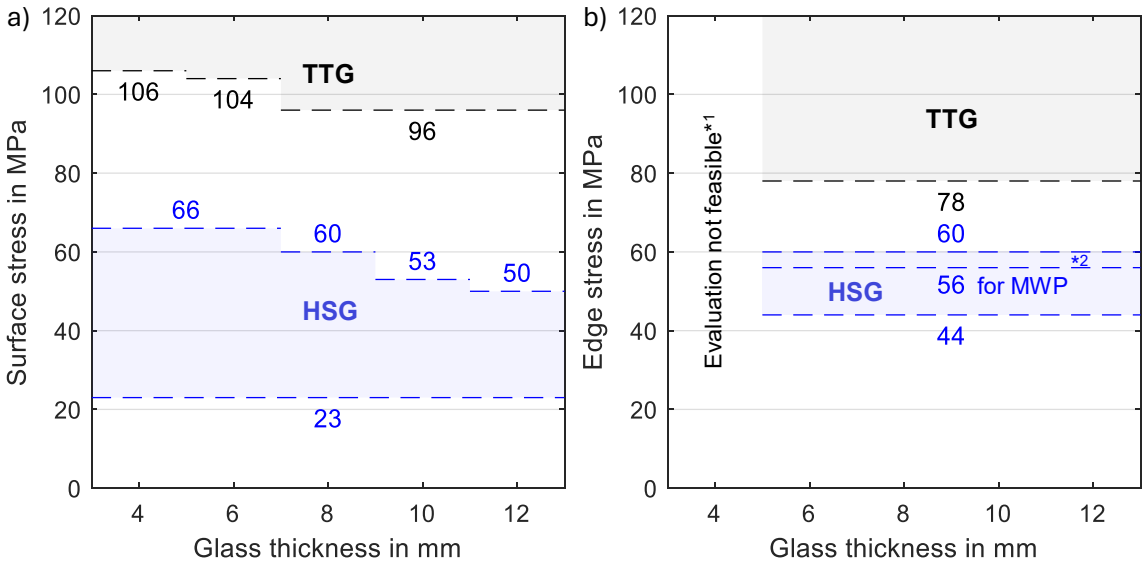

Figure 8.4: Final photoelastic limits for measurement of a) surface stress and b) edge stress depending on the glass thickness for thermally toughened glass and heat-strengthened glass; *1 Evaluation of 4 mm with edge stress is not feasible due to limited interpolation range and uncertain extrapolation with the available measurement devices; *2 Additional validating surface stress measurements for edge stress values in the range 56 to 60 MPa determined by MWP

limit values are also applicable to coated glass products. In this context, two main challenges must be addressed.

First, glass specimens with temperable coatings, applied prior to the tempering process, undergo a tempering process that differs from that of uncoated glass. Consequently, as furnace parameters are adjusted to accommodate the temperable coatings while still meeting the required mechanical properties, the resulting residual stress state may differ from that of uncoated glass. Consequently, the correlation between residual stresses obtained photoelastic measurements and mechanical properties determined by destructive tests may deviate from the relationships established in this work. Second, the photoelastic measurement techniques themselves are affected by coatings, as certain coatings alter the optical reflection and transmission properties of the glass. In particular, surface stress measurements may suffer from unreliable retardation detection, when measurements are performed on the coated side of the pane.

Limitations also apply to the measurement of edge stress. In this case, the de-coating process in the edge area represents a critical factor. For glass panes intended for use in insulating glass units, the coating is typically removed along the edge to facilitate bonding of the edge seal. This processing step may introduce mechanical damage in the de-coated region and result in locally varying optical transmission with different light intensities. As a consequence, isochromatics may not be correctly detected, which affects the positioning of data points in the fitting area and distorts the subsequent extrapolation behavior.

A reliable determination of edge stress is considerably more challenging for specimens with smaller glass thicknesses (4 mm and, in some cases, 6 mm), particularly, when using the MWP measurement method. The formation of edge isochromatics, which are

required for determining retardation at the glass edge, is strongly dependent on glass thickness. Isochromatics located within the chamfer region are not detectable due to edge processing. Consequently, thinner glass panes exhibit fewer edge isochromatics, resulting in an insufficient number of supporting data points for the interpolation and extrapolation procedure.

It should be noted that the strength values are correlated as direct measurements for individual specimens rather than as characteristic values derived from test series. It must be acknowledged, however, that the strength of glass is strongly influenced by micro-defects at the surface, which cannot be detected by photoelastic measurements. Furthermore, the lower limit value for HSG could not be validated, as no individual specimens were available that fell below the required bending tensile strength of 70 MPa. This limitation also applies to TTG in most cases: with the exception of one test series at a glass thickness of 4 mm, no specimens of the small-scale components exhibited a non-conforming fracture pattern. For the large-format specimens, only one test series at a glass thickness of 6 mm showed a fracture pattern that was too coarse.

9 Conclusion and Outlook

The European product standards EN 12150-1 (2020) for TTG and EN 1863-1 (2012) for HSG specify requirements for the bending tensile strength and fracture behavior. Presently, verification of these requirements is conducted through destructive testing within the factory's production control. Since these tests are time-consuming and generate material waste, this work investigated the potential of photoelastic measurements to reduce destructive testing while ensuring the mechanical properties of tempered glass. To accomplish this objective, it was first necessary to develop a reliable method for measuring edge stress. Secondly, limit values for surface and edge stress measurements had to be established for the purpose of controlling the conformity of the glass products TTG or HSG, thereby fulfilling the strength and fracture requirements.

Current manual methods for measuring edge stress are highly operator-dependent and exhibit limited measurement accuracy and reproducibility, which restricts their suitability for reliable quality control under production conditions. For tempered architectural glass, edge processing by beveling, grinding, or polishing is required. However, because the slope surface of the chamfer scatters the light emitted by the measurement device, retardation cannot be measured directly up to the glass edge. Therefore, the evaluation method suggested in ASTM C1279 (2023) could not be used as the retardation at the measurement points fall within the broad chamfer of the specimens.

Accordingly, a measurement method had to be developed that considers the effects of the chamfer and enables edge stress evaluation by suitable extrapolation. Therefore, Chapter 4 investigated standard-size glass specimens (360 mm x 1100 mm) in glass thicknesses of 4 mm to 12 mm using two photoelastic methods. The stationary PST device displays the measured retardation to the edge as a continuous curve on local points, allowing for good interpolation. Based on this dataset, the influence of polynomial interpolation functions 2nd, 3rd and 4th degree on the extrapolation behavior towards the edge was systematically analyzed. The evaluation of the goodness-of-fit parameters adjusted R^2 and SSE showed that the 2nd degree polynomial is not appropriate for the fitting function. The other two degrees both had a good similar fit within the measurement area, but they differed in the amount of the extrapolated values on the edge. As the safety properties of the tempered glass are to be guaranteed with the edge stress value, the polynomial of 3rd degree was selected for extrapolation of the subsequent analysis, which exhibited lower values and is therefore on the safe side. Finally, the coefficients of the cubic polynomial fitting function were analyzed, revealing a noticeable distinction between glass types and glass thicknesses.

The second photoelastic technique for edge stress, MWP, offers a method for obtaining retardations by using half and integer isochromatic orders from two or three photoelastic images acquired simultaneously in different wavelengths. To ensure a robust fitting function, the coefficients of the cubic polynomial fitting function determined by PST were applied to the retardation data points measured by MWP. Edge stress measurement using MWP

is well suited for implementation in the automated production process, as this technique is already employed in state-of-the-art inline measurement systems for quality control of anisotropy effects. To enable the use of MWP as an automated method for evaluating edge stresses in production control, it is recommended that the fitting parameters be defined as described in this work using an alternative measurement technique, such as the PST, which provides continuous retardation measurement points. Both methods are limited to the evaluation of edge stress in clear float glass specimens with thicknesses ranging from 6 mm to 12 mm.

Chapter 5 investigated the results of photoelastic measurements of surface stress using scattered light method and edge stress using MWP and PST on a total of 955 tempered glass specimens in thicknesses from 4–12 mm. Destructive tests, conducted in accordance with the European product standards EN 12150-1 (2020) for TTG and EN 1863-1 (2012) for HSG, enabled the classification of specimens based on their mechanical performance in bending strength and fracture pattern.

Furthermore, Pearson correlation analysis revealed strong, significant relationships between photoelastic and destructive test results. The comparison of the confidence intervals of r demonstrated a significantly stronger correlation between the number of fragments and surface stress than that between the number of fragments and edge stress. Additionally, no manufacturer-specific clustering was detected. Moderation analysis examined the influence of glass thickness. Specifically, for the relationship between the number of fragments and surface stress, significant differences in the slope of the regression line were observed for glass thicknesses of 4 mm and 6 mm. In models involving edge stress, the influence of glass thickness was less pronounced. Comparisons between edge stress and surface stress did not exhibit a one-to-one correspondence: TTG specimens generally showed higher surface stress values compared to edge stress, whereas HSG exhibited higher edge stress than surface stress.

The primary objective of this research was to establish limit values for surface stress and edge stress that are applicable across different glass formats and independent of the measurement method used in quality control, thereby reducing the need for destructive testing. In Chapter 6, quantile and logistic regression models were employed for this purpose. Using quantile regression applied to metric dependent variables, limit values for the photoelastic measurements were derived based on the intersection of the regression line with the required characteristic bending strength (120 MPa or 70 MPa) or the fracture pattern criterion (40 fragments). Selecting the quantile $\tau = 0.05$ ensured a conservative determination of limit values, accounting for the lower tail of the destructive variable distribution. By comparing the 95% confidence intervals of the regression coefficients for the thickness-specific models revealed that only the relationship between the number of fragments and surface stress demonstrated a statistically significant necessity for thickness-specific limit values for 4 mm, 6 mm and 8–12 mm TTG. However, no further distinction between the other limit values regarding glass thickness was necessary for TTG.

HSG requires two limit values to control both the bending strength and the fracture pattern. The lower limit values, determined by quantile regression, showed no thickness-specific behavior. Logistic regression was employed to define an upper criterion corresponding to the characteristic coarse fracture pattern required to ensure residual load-bearing capacity. In this context, different probability thresholds were investigated to identify a suitable limit value. Finally, for all regression models, the most appropriate limit values were selected

based on k-fold cross-validation. For edge stress, no thickness-specific limit values were detected for HSG, while the upper limit values for surface stress decreased with increasing glass thickness.

Since the statistical limit values were established on standard-size specimens, Chapter 7 aimed to validate these limits on large-format specimens. Photoelastic and destructive investigations were carried out on glass specimens with dimensions of 3000 mm x 1000 mm. Edge stress was measured using MWP, while surface stress was determined by the scattered light method. Subsequently, destructive fracture tests were conducted to assess conformity regarding the glass types of TTG and HSG. Finally, the effectiveness of photoelastic measurements for controlling product conformity was evaluated.

With respect to the research question of this dissertation, the results demonstrate that reliable limit values could be derived from the relationship between destructive tests and non-destructive measurements. Photoelastic methods demonstrate significant potential for sustainable and efficient quality control of large-format tempered glass. In particular, surface stress measurements and the associated limit values have proven to be highly suitable as a discriminating criterion for the classification of TTG and HSG. However, manual surface stress measurements are subject to operator dependence and are time-consuming, which limits their applicability for routine quality control.

In contrast, edge stress measurement using MWP offers clear advantages for automated production processes, as it enables rapid inspection of every individual pane without operator influence. For TTG, the derived edge stress limit values have proven to be well suited for conformity assessment of large-format TTG. Nevertheless, to increase reliability using MWP, it is recommended to apply the edge stress limit at specimens which are known pre-stressed with TTG parameters. For classifying HSG, the edge stress measurements using MWP was found to be suboptimal. A clear separation between conforming and non-conforming HSG proved to be particularly challenging. To, nevertheless, ensure the reliability of the load-bearing behavior related to the coarse fracture pattern, a very narrow limit range was selected, which consequently led to a considerable number of specimens being unnecessarily rejected. However, MWP measurements can be validated within a defined range by means of surface stress measurements and the corresponding limit values, thereby enhancing the overall reliability of the classification. In contrast, PST measurements of the edge stress showed a suitable discriminating criterion for the conformity of TTG and HSG.

It is generally recommended that manufacturers independently establish correlations between the photoelastic measurements surface and edge stress and the mechanical properties, such as fracture pattern and bending strength, within their factory production control. This would enable more reliable and tailored quality assurance adapted to specific production conditions of the manufacturer and glass types. For the measurement of edge stress using MWP, particularly in the quality control of HSG, further research into improved evaluation algorithms and data processing techniques is needed. Such advancements could enhance measurement accuracy and reliability, especially for thinner glass types where current methods show limitations.

Additionally, further investigations into large-format glass panes and their behavior during production are highly desirable. Inline edge stress scanning integrated into everyday manufacturing processes holds promise for 100% quality control but requires comprehensive studies to optimize the methodology and ensure robust implementation. Moreover, future

research should focus on coated glass products. Since coatings can significantly affect both the tempering process and photoelastic measurement results, adaptations of current measurement techniques and reassessment of existing limit values are essential to guarantee consistent and reliable quality control.

A further application in which this work provides an essential methodological foundation concerns the assessment of strength of point-fixed glass with edge-near holes. In such regions, stress concentration effects play a decisive role, and an accurate determination of the local edge stress is of particular importance for reliable strength evaluation. The approaches developed in this work establish the basis for measuring the edge stress at both the hole and the straight edge. However, further experimental and methodological research is required to validate and refine the applicability of edge stress measurements in the vicinity of holes.

Declaration on the use of Artificial Intelligence (AI)

During the preparation of this thesis, from August 2025 to February 2026, large language models (LLMs) were used to support various aspects of the research and writing process.

ChatGPT (OpenAI), and DeepL Write (DeepL) were used to improve the linguistic quality of the manuscript, including proofreading, grammar and spelling corrections, translation between German and English, and the refinement of academic formulations. ChatGPT was also used to assist with structuring and shortening text, developing alternative formulations, and brainstorming. Some passages were initially drafted in German and subsequently translated into English, while others were written directly in English. The scientific content, interpretation of results, and conclusions reflect the author's own work.

Perplexity (Perplexity AI) was used to support literature searches and identify potentially relevant scientific publications and sources. The relevance and suitability of the retrieved sources were assessed by the author.

ChatGPT was additionally used to assist with the development, modification, and troubleshooting of scripts in MATLAB and R for data analysis and figure generation. The generated or modified code was checked by the author, and the results were assessed for technical plausibility and consistency with the underlying data.

All AI-generated suggestions and outputs were critically reviewed by the author, who made the final decisions regarding their use. The author takes full responsibility for the content, scientific accuracy, and conclusions of this thesis.

Bibliography

Aben, H., Anton, J., and Errapart, A. (2008). "Modern Photoelasticity for Residual Stress Measurement in Glass". In: *Strain* 44.1, pp. 40–48. DOI: 10.1111/j.1475-1305.2008.00422.x.

Aben, H., Anton, J., Errapart, A., Hödemann, S., Kikas, J., Klaassen, H., and Lamp, M. (2010). "On non-destructive residual stress measurement in glass panels". In: *Estonian Journal of Engineering* 16.2, pp. 150–156. ISSN: 1736-6038. DOI: 10.3176/eng.2010.2.04.

Aben, H., Anton, J., Paemurru, M., and Õis, M. (2013). "A new method for tempering stress measurement in glass panels". In: *Estonian Journal of Engineering* 19.4. ISSN: 1736-6038. DOI: 10.3176/eng.2013.4.04.

Aben, H., Errapart, A., Ainola, L., and Anton, J. (2005). "Photoelastic tomography for residual stress measurement in glass". In: *Optical Engineering* 44.9.

Aben, H., Lochegnies, D., Chen, Y., Anton, J., Paemurru, M., and Õis, M. (2015). "A New Approach to Edge Stress Measurement in Tempered Glass Panels". In: *Experimental Mechanics* 55.2, pp. 483–486. ISSN: 00144851. DOI: 10.1007/s11340-014-9950-7.

Aben, H. and Guillemet, C. (1993). *Photoelasticity of Glass*. Berlin, Heidelberg: Springer Berlin Heidelberg. ISBN: 9783642500718. DOI: 10.1007/978-3-642-50071-8.

Achintha, M. (2021). "A validated modelling technique for incorporating residual stresses in glass structural design". In: *Structures* 29, pp. 446–457. ISSN: 23520124. DOI: 10.1016/j.istruc.2020.11.052.

Ajovalasit, A., Barone, S., and Petrucci, G. (1995). "Towards RGB photoelasticity: Full-field automated photoelasticity in white light". In: *Experimental Mechanics* 35.3, pp. 193–200.

Ajovalasit, A., Petrucci, G., and Scafidi, M. (2011). "Measurement of edge residual stresses in glass by the phase-shifting method". In: *Optics and Lasers in Engineering* 49.5, pp. 652–657. ISSN: 01438166. DOI: 10.1016/j.optlaseng.2011.01.004.

– (2012a). "Photoelastic Analysis of Edge Residual Stresses in Glass by Automated "Test Fringes" Methods". In: *Experimental Mechanics* 52.8, pp. 1057–1066. ISSN: 00144851. DOI: 10.1007/s11340-011-9558-0.

– (2012b). "RGB photoelasticity applied to the analysis of membrane residual stress in glass". In: *Measurement Science and Technology* 23.2. ISSN: 0957-0233. DOI: 10.1088/0957-0233/23/2/025601.

– (2015a). "Photoelastic Analysis of Edge Residual Stresses in Glass by the Automated Tint Plate Method". In: *Experimental Techniques* 39.3, pp. 11–18. ISSN: 07328818. DOI: 10.1111/ext.12017.

– (2015b). "Review of RGB photoelasticity". In: *Optics and Lasers in Engineering* 68, pp. 58–73. ISSN: 01438166. DOI: 10.1016/j.optlaseng.2014.12.008.

Ajovalasit, A., Petrucci, G., and Scafidi, M. (2014). "A critical assessment of automatic photoelastic methods for the analysis of edge residual stresses in glass". In: *The Journal of Strain Analysis for Engineering Design* 49.5, pp. 361–375. ISSN: 0309-3247. DOI: 10.1177/0309324713515466.

ANSI Z 97.1 (2015). *Standard for Safety Glazing Materials used in Buildings - Safety Performance Specifications and Methods of Test*. American National Standards Institute (ANSI).

Anton, J., Errapart, A., Paemurru, M., Lochegnies, D., Hödemann, S., and Aben, H. (2012). "On the inhomogeneity of residual stresses in tempered glass panels". In: *Estonian Journal of Engineering* 18.1. ISSN: 1736-6038. DOI: 10.3176/eng.2012.1.01.

Ascough, J. (1981). "A Review of the Scattered-Light Method in Photoelasticity". In: *Optics and Lasers in Engineering* 2, pp. 215–227. ISSN: 01438166.

ASTM C1048 (2025). *Standard Specification for Heat-Strengthened and Fully Tempered Flat Glass*. ASTM. West Conshohocken, PA: ASTM International.

ASTM C1279 (2023). *Standard Test Method for Non-Destructive Photoelastic Measurement of Edge and Surface Stresses in Annealed, Heat-Strengthened, and Fully Tempered Flat Glass*. West Conshohocken, PA: ASTM International.

Ayrox SRL. (2026). *NES-T Automatic Edge Stress Meter*. URL: https://www.ayrox.com/nes-t-automatic-edge-stress-meter (visited on 02/26/2026).

Azen, R. and Walker, C. M. (2011). *Categorical Data Analysis for the Behavioral and Social Sciences*. Routledge. ISBN: 9781136914249. DOI: 10.4324/9780203843611.

Backhaus, K., Erichson, B., Gensler, S., Weiber, R., and Weiber, T. (2021). *Multivariate Analysis*. Wiesbaden: Springer Fachmedien Wiesbaden. ISBN: 9783658325886. DOI: 10.1007/978-3-658-32589-3.

Backhaus, K., Erichson, B., Plinke, W., and Weiber, R. (2015). *Multivariate Analysemethoden. Eine anwendungsorientierte Einführung*. 14th ed. Berlin, Heidelberg: Springer Gabler Berlin, Heidelberg. ISBN: 9783662460764. DOI: 10.1007/978-3-662-46076-4.

Bateson, S., Hunt, J. W., Dalby, D. A., and Sinha, N. (1964). "Birefringence in Glass Measured by the Scattered-Light Technique with a Laser Source". In: *Applied Optics* 3.7. ISSN: 0003-6935. DOI: 10.1364/AO.3.000902.

Beason, W. L. and Morgan, J. R. (1984). "Glass Failure Prediction Model". In: *Journal of Structural Engineering* 110.2, pp. 197–212. ISSN: 0733-9445.

Brokmann, C. (2022). *A Model for the Stochastic Fracture Behavior of Glass and Its Application to the Head Impact on Automotive Windscreens*. Vol. 63. Wiesbaden: Springer Fachmedien Wiesbaden. ISBN: 978-3-658-36787-9. DOI: 10.1007/978-3-658-36788-6.

Buchinsky, M. (1998). "Recent advances in quantile regression models: a practical guideline for empirical research". In: *The Journal of Human Resources* Volume 33, Issue 1, pp. 88–126.

Datsiou, K. C. and Overend, M. (2018). "Weibull parameter estimation and goodness-of-fit for glass strength data". In: *Structural Safety* 73, pp. 29–41. ISSN: 01674730. DOI: 10.1016/j.strusafe.2018.02.002.

Deutsches Institut für Bautechnik, ed. (2016). *Z-70.3-55 Verglasungen aus teilvorgespanntem Glas "ipasafe TVG"*.

DIN 1249-11 (2023). *Glass in building - Part 11: Glass edges - Terms and definitions, characteristics of edge types and finishes*. Berlin: Deutsches Institut für Normung.

Dix, S. (2024). *A Concept for Measuring and Evaluating Optical Anisotropy Effects in Tempered Architectural Glass*. 1st. Vol. 70. Mechanik, Werkstoffe und Konstruktion im Bauwesen. Wiesbaden: Springer Fachmedien Wiesbaden and Imprint Springer Vieweg. ISBN: 9783658420291. DOI: 10.1007/978-3-658-42029-1.

Dix, S., Efferz, L., Sperger, L., Schuler, C., and Feirabend, S. (2021). "Analysis of residual stresses at holes near edges in tempered glass". In: *Engineered Transparency 2021. Glass*

in architecture and structural engineering. Ed. by Louter, C., Schneider, J., Tasche, S., and Weller, B. Berlin: Ernst & Sohn. ISBN: 9783433033203.

Dix, S., Schuler, C., Kolling, S., and Heil, J. (2022). "Digital full-field photoelasticity of tempered architectural glass: a review." In: *Optics and Lasers in Engineering* Volume 153. ISSN: 01438166. DOI: 10.1016/j.optlaseng.2022.106998.

Efferz, L. (2024). "Determining and evaluating edge stresses. Poster, Pecha Kucha". In: *glass melting pot*. Ed. by glasstec conference. Düsseldorf.

– (2025a). "Non-Destructive Quality Control in Thermally Toughened Glass". In: *Young Engineers Colloquium Munich 2025. Report*. Ed. by German Group of IABSE. Munich, pp. 86–87.

– (2025b). "Zerstörungsfreie Qualitätskontrolle von Einscheibensicherheitsglas mit spannungsoptischen Methoden". In: *Glas im konstruktiven Ingenieurbau 19*. Ed. by Labor für Stahl- und Leichtmetallbau an der Hochschule München. München.

Efferz, L. and Schuler, C. (2026). "Oberflächendruck- und Kantenmembranspannung in thermisch vorgespanntem Glas". In: *Stahlbau* 95.S2, pp. 134–140. DOI: https://doi.org/10.1002/stab.70160.

Efferz, L., Schuler, C., Schuster, M., Thiele, K., Riedel, H., Schneider, J., Strobel, A., Gammenthaler, B., Siegler, M., Frank, M., Groth, C., Schuller, T., and Pfannenstill, P. (2025a). *NEMA - Addition of photoelastic methods and analysis concepts to a standard for tempered safety glass to reduce destructive testing. Final report*. Hannover: Technische Informationsbibliothek. DOI: 10.34657/18731.

Efferz, L., Schuler, C., and Siebert, G. (2023). "Experimental determination of the strength of toughened glass in the area of near-edge holes". In: *Glass Structures & Engineering*. ISSN: 2363-5142. DOI: 10.1007/s40940-023-00245-w.

– (2024a). "Photoelastic Measurements and Evaluation Methods for Edge Stress in Architectural Tempered Glass". In: *Glass Structures & Engineering*. DOI: 10.1007/s40940-024-00270-3.

– (2025b). "Non-destructive, photoelastic quality control for large-format, thermally toughened glass". In: *Glass Structures & Engineering*. DOI: 10.1007/s40940-025-00302-6.

– (2026). "Statistical determination and evaluation of photoelastic limit for heat-strengthened glass. [accepted for publication]". In: *Glass Structures & Engineering*.

Efferz, L., Schuster, M., Kraus, M. A., Schuler, C., and Siebert, G. (2025c). "Key parameters for the non-destructive quality control of thermally toughened safety glass". In: *Journal of Building Engineering*. DOI: 10.1016/j.jobe.2025.112613.

Efferz, L., Thiele, K., Schuster, M., Schuler, C., Siebert, G., and Schneider, J. (2024b). "Relation between edge stress, bending strength, surface stress and fracture pattern of thermally toughened glass". In: *Glass Structures & Engineering*. DOI: 10.1007/s40940-024-00269-w.

Efron, B. and Tibshirani, R. J. (1994). *An Introduction to the Bootstrap*. Chapman and Hall/CRC. ISBN: 9780429246593. DOI: 10.1201/9780429246593.

EN 12150-1 (2020). *Glass in building – Thermally toughened soda lime silicate safety glass – Part 1: Definition and description*. European Committee for Standardization (CEN).

EN 1288-3 (2000). *Glass in building – Determination of the bending strength of glass - Part 3: Test with specimen supported at two points (four point bending)*. European Committee for Standardization (CEN).

EN 1863-1 (2012). *Glass in buildings - Heat strengthened soda lime silicate glass –Part 1: Definition and description*. European Committee for Standardization (CEN).

EN 1990 (2021). *Eurocode: Basis of structural design;* European Committee for Standardization (CEN).

EN 572-1 (2016). *Glass in building - Basic soda-lime silicate glass products - Part 1: Definitions and general physical and mechanical properties*. Berlin: European Committee for Standardization (CEN).

Fahrmeir, L., Künstler, R., Pigeot, I., and Tutz, G. (2007). *Statistik. Der Weg zur Datenanalyse*. 6th ed. Springer-Lehrbuch. Berlin and Heidelberg: Springer. ISBN: 3540697136.

Feingold, J. M. and Redner, A. S. (2003). "Stress relief - New PC Based Scanners Improve Quality and Productivity for Glass Fabricators". In: *International Glass Review* 2003.Issue 1, pp. 63–66.

Field, A. (2013). *Discovering Statistics Using IBM SPSS Statistics*. Introducing statistical methods. SAGE Publications. ISBN: 9781446249178. URL: https://books.google.de/books?id=srb0a9fmMEoC.

Genschel, U. and Meeker, W. Q. (2010). "A Comparison of Maximum Likelihood and Median-Rank Regression for Weibull Estimation". In: *Quality Engineering* 22.4, pp. 236–255. ISSN: 0898-2112. DOI: 10.1080/08982112.2010.503447.

Glantz, S. A., Slinker, B. K., and Neilands, T. B. (2016). *Primer of applied regression & analysis of variance*. Third edition. New York: McGraw-Hill Education. ISBN: 9780071824118.

GlasStress Ltd. (2013). *SCALP Instruction Manual*. Version Version 5.5. Tallinn, Estonia. URL: https://www.glasstress.com/web/scalp-05/ (visited on 02/26/2026).

– (2026). *AP-07 Automatic Transmission Polariscope*. URL: https://www.glasstress.com/web/ap-07/ (visited on 02/26/2026).

Griffith, A. A. (1921). "VI. The phenomena of rupture and flow in solids". In: *Philosophical Transactions of the Royal Society of London. Series A, Containing Papers of a Mathematical or Physical Character* 221.582-593, pp. 163–198. ISSN: 0264-3952. DOI: 10.1098/rsta.1921.0006.

Hair, J. F., Black, W. C., Babin, B. J., and Anderson, R. E. (2019). *Multivariate Data Analysis. A global perspective*. 8th ed. Cengage Learning, EMEA.

Hair, J. F., Hult, G. T. M., Ringle, C. M., Sarstedt, M., Danks, N. P., and Ray, S. (2021). *Partial least squares structural equation modeling (PLS-SEM) using R. A workbook*. Classroom companion Business. Cham, Switzerland: Springer. ISBN: 9783030805180.

Hayes, A. F. (2022). *Introduction to mediation, moderation, and conditional process analysis. A regression-based approach*. 3rd ed. New York: The Guilford Press. ISBN: 9781609182304.

Hedderich, J. and Sachs, L. (2016). *Angewandte Statistik*. Berlin, Heidelberg: Springer Berlin Heidelberg. ISBN: 978-3-662-45690-3. DOI: 10.1007/978-3-662-45691-0.

Hidalgo, L. M. and Elstner, M. (2018). "Anisotropic Effects in Architectural Glass". In: *FACADE TECTONICS. 2018 World Congress* (Los Angeles). Ed. by Noble, D., Kensek, K., Elder, and Matt. Vol. Volume 2. Facade Tectonics Institute. Los Angeles: Tectonic Press, pp. 3–22. ISBN: 978-1882352470.

Hosmer, D. W. and Lemeshow, S. (2000). *Applied Logistic Regression*. Wiley. ISBN: 9780471356325. DOI: 10.1002/0471722146.

Hox, J. J. (2018). *Multilevel analysis. Techniques and applications*. Quantitative methodology series. Mahwah N.J.: Lawrence Erlbaum Associates. ISBN: 0805832181.

Igartua, J.-J. and Hayes, A. F. (2021). "Mediation, Moderation, and Conditional Process Analysis: Concepts, Computations, and Some Common Confusions". In: *The Spanish journal of psychology* 24. DOI: 10.1017/SJP.2021.46.

ilis gmbh (2023). *StrainScope flex*. URL: https://ilis.de/de/produkte/strainscope-flex/ (visited on 02/26/2026).

ISO 12540 (2017). *Glass in building - Tempered soda lime silicate safety glass*. International Organization for Standardization.

ISO 22509 (2020). *Glass in building - Heat strengthened soda lime silicate glass*. International Organization for Standardization.

Jansen, S. (2020). *Machine learning for algorithmic trading. Predictive models to extract signals from market and alternative data for systematic trading strategies with Python*. Second edition. Birmingham, UK: Packt Publishing. URL: https://search.ebscohost.com/login.aspx?direct=true&scope=site&db=nlebk&db=nlabk&AN=2557666.

Jebsen-Marwedel, H. and Brückner, R. (2011). *Glastechnische Fabrikationsfehler*. Berlin, Heidelberg: Springer Berlin Heidelberg. ISBN: 978-3-642-16432-3. DOI: 10.1007/978-3-642-16433-0.

Kabacoff, R. I. (2022). *R in action. Data analysis and graphics with R and Tidyverse*. Third edition. Shelter Island, NY: Manning Publications Co. ISBN: 9781638357018. URL: https://search.ebscohost.com/login.aspx?direct=true&scope=site&db=nlebk&db=nlabk&AN=3224113.

Kirch, W., ed. (2008). *Encyclopedia of Public Health*. Dordrecht: Springer Netherlands. ISBN: 978-1-4020-5613-0. DOI: 10.1007/978-1-4020-5614-7.

Koenker, R. and Basset, G. W. (1978). "Regression Quantiles". In: *Ecometrica 46*, pp. 33–50.

Koenker, R. (2005). *Quantile Regression*. Cambridge University Press.

Kraus, A. M. (2019). "Machine Learning Techniques for the Material Identification of Laminated Glass in the Intact and Post-Fracture State". Dissertation. Munich: University of the Bundeswehr Munich.

Krzywinski, M. and Altman, N. (2014). "Visualizing samples with box plots". In: *Nature Methods* 11.2, pp. 119–120. ISSN: 1548-7105. DOI: 10.1038/nmeth.2813.

Laufs, W. (1998). *Systematische Untersuchungen der Eigenspannungsverteilung in thermisch vorgespannten Gläsern im Hinblick auf die Flächenfestigkeit, die Kantenfestigkeit und die Festigkeit im Bereich der Lochränder bei punktgestützten Glasscheiben. Forschungsbericht Lehrstuhl für Stahlbau der RWTH Aachen*. T 2772. Ed. by Fraunhofer IRB Verlag.

Laufs, W. (2000). *Ein Bemessungskonzept zur Festigkeit thermisch vorgespannter Gläser*. Vol. 45. Stahlbau. Aachen: Shaker. ISBN: 3826580443.

Lee, H. (2014). *Foundations of Applied Statistical Methods*. Cham: Springer International Publishing. ISBN: 978-3-319-02401-1. DOI: 10.1007/978-3-319-02402-8.

Lee, H., Cho, S., Yoon, K., and Lee, J. (2012). "Glass Thickness and Fragmentation Behavior in Stressed Glasses". In: *New Journal of Glass and Ceramics* 02.04, pp. 116–121. ISSN: 2161-7554. DOI: 10.4236/njgc.2012.24020.

Lohr, K. (2019). "Thermisch vorgespanntes Glas mit nachgeschliffenen Kanten". Institut für Baukonstruktion. Dissertation. Dresden: Technical University Dresden.

Lohr, K. and Weller, B. (2019). "Residual stress distribution in tempered glass with reground edges". In: *Glass Structures & Engineering* 4.1, pp. 99–115. ISSN: 2363-5142. DOI: 10.1007/s40940-018-0084-7.

Madjoubi, M. A., Bousbaa, C., Hamidouche, M., and Bouaouadja, N. (1999). "Weibull Statistical Analysis of the Mechanical Strength of a Glass Eroded by Sand Blasting". In: *Journal of the European Ceramic Society* 19, pp. 2957–2962.

Maxwell, J. C. (1873). *A Treatise on Electricity and Magnetism*. Clarendon Press.

Mognato, E., Barbieri, A., Schiavonato, M., and Pace, M. (2011). "Thermally toughened safety glass: correlation between flexural strength, fragmentation and surface compressive stress". In: *GPD Glass Performance Days 2011*, pp. 115–118.

Mognato, E., Bazzaco, P., Brocca, S., and Barbieri, A. (2019). "Surface Compression Comparative Measurements on Tempered Glass with Different Instruments". In: *GPD Glass Performance Days 2019*, pp. 381–384.

Mognato, E., Brocca, S., and Barbieri, A. (2017). "Thermally Processed Glass: Correlation Between Surface Compression, Mechanical and Fragmentation Test". In: *GPD Glass Performance Days 2017*, pp. 14–20. URL: https://api.semanticscholar.org/CorpusID:208303605.

Mognato, E., Brocca, S., and Comiati, F. (2018). "Which is the Right Reference Surface Compression Value for Heat Treated Glass?" In: *Challenging Glass Conference 6*, pp. 703–712.

Montgomery, D. C., Peck, E. A., and Vining, G. G. (2021). *Introduction to linear regression analysis*. Sixth edition. Wiley series in probability and statistics. Hoboken, New Jersey: Wiley. ISBN: 9781119578727.

Navarro, D. J. (2026). *Learning Statistics with R - A tutorial for Psychology Students and other Beginners*. LibreTexts. URL: https://learningstatisticswithr.com/ (visited on 02/17/2026).

Nehring, G. (2018). "Formfindung und Bemessung von kaltgebogenen Schalenstrukturen aus Dünnglas". Dissertation. Munich: University of the Bundeswehr.

Neumann, K. E. (1841). "Die Gesetze der Doppelbrechung des Lichts in comprimirten oder ungleichförmig erwärmten unkrystallinischen Körpern". In: *Annalen der Physik und Chemie* 130.12, pp. 449–476. ISSN: 00033804. DOI: 10.1002/andp.18411301203.

Nielsen, J. H. (2017). "Remaining stress-state and strain-energy in tempered glass fragments". In: *Glass Structures & Engineering* 2.1, pp. 45–56. ISSN: 2363-5142. DOI: 10.1007/s40940-016-0036-z.

Nielsen, J. H., Schneider, J., and Kraus, M. A. (2022). "The in-plane expansion of fractured thermally pre-stressed glass panes". In: *Construction and Building Materials* 327. ISSN: 09500618. DOI: 10.1016/j.conbuildmat.2022.126849.

Nielsen, J. H., Thiele, K., Schneider, J., and Meyland, M. J. (2021). "Compressive zone depth of thermally tempered glass". In: *Construction and Building Materials* 310. ISSN: 09500618. DOI: 10.1016/j.conbuildmat.2021.125238.

Nielsen, J. H. (2009). "Tempered glass - Bolted connections and related problems". Ph.D. Thesis. Lyngby: Technical University of Denmark.

Olvera Astivia, O. L. and Kroc, E. (2019). "Centering in Multiple Regression Does Not Always Reduce Multicollinearity: How to Tell When Your Estimates Will Not Benefit From Centering". In: *Educational and psychological measurement* 79.5, pp. 813–826. DOI: 10.1177/0013164418817801.

Paschotta, R. (2006). "Polarization of Light - an encyclopedia article". In: *RP Photonics Encyclopedia*. DOI: 10.61835/pl7.

Peatross, J. and Ware, M. (2015). *Physics of Light and Optics*. ISBN: 978-1-312-92927-2. DOI: 10.1364/FIO.2010.JWA64.

Peduzzi, P., Concato, J., Kemper, E., Holford, T. R., and Feinstein, A. R. (1996). "A simulation study of the number of events per variable in logistic regression analysis". In: *Journal of Clinical Epidemiology* 49.12, pp. 1373–1379. ISSN: 0895-4356. DOI: 10.1016/S0895-4356(96)00236-3.

Peters, T., Hof, P., Schuster, M., Schneider, J., and Seel, M. (2023). "Determination of the bending strength of glass via four point bending: correction of factor k_e in EN 1288-3". In: *Glass Structures & Engineering* 8, pp. 353–362. DOI: 10.1007/s40940-023-00232-1.

Porter, S. R. (2015). "Quantile Regression: Analyzing Changes in Distributions Instead of Means". In: *Higher Education: Handbook of Theory and Research*. Ed. by Paulsen, M. B. Vol. 30. Higher Education: Handbook of Theory and Research 30. Cham: Springer International Publishing, pp. 335–381. ISBN: 978-3-319-12834-4. DOI: 10.1007/978-3-319-12835-1_8.

Pour-Moghaddam, N. (2020). *On the Fracture Behaviour and the Fracture Pattern Morphology of Tempered Soda-Lime Glass*. Vol. 54. Wiesbaden: Springer Fachmedien Wiesbaden. ISBN: 978-3-658-28205-9. DOI: 10.1007/978-3-658-28206-6.

Pourmoghaddam, N., Kraus, M. A., Schneider, J., and Siebert, G. (2019). "Relationship between strain energy and fracture pattern morphology of thermally tempered glass for the prediction of the 2D macro-scale fragmentation of glass". In: *Glass Structures & Engineering* 4.2, pp. 257–275. ISSN: 2363-5142. DOI: 10.1007/s40940-018-00091-1.

Pourmoghaddam, N. and Schneider, J. (2018a). "Experimental investigation into the fragment size of tempered glass". In: *Glass Structures & Engineering* 3.2, pp. 167–181. ISSN: 2363-5142. DOI: 10.1007/s40940-018-0062-0.

– (2018b). "Finite-element analysis of the residual stresses in tempered glass plates with holes or cut-outs". In: *Glass Structures & Engineering* 3.1, pp. 17–37. ISSN: 2363-5142. DOI: 10.1007/s40940-018-0055-z.

R Core Team (2024). *R: A Language and Environment for Statistical Computing*. Vienna, Austria: R Foundation for Statistical Computing. URL: https://www.R-project.org/.

Ramakrishnan, V. and Ramesh, K. (2016). "A novel method for the evaluation of stress-optic coefficient of commercial float glass". In: *Measurement* 87, pp. 13–20. ISSN: 02632241. DOI: 10.1016/j.measurement.2016.03.014.

Ramesh, K. (2000). *Digital photoelasticity. Advanced techniques and applications*. Berlin: Springer. ISBN: 3540667954.

Ramesh, K. and Ramakrishnan, V. (2016). "Digital photoelasticity of glass: A comprehensive review". In: *Optics and Lasers in Engineering* 87, pp. 59–74. ISSN: 01438166. DOI: 10.1016/j.optlaseng.2016.03.017.

Ramesh, K. and Sasikumar, S. (2020). "Digital photoelasticity: Recent developments and diverse applications". In: *Optics and Lasers in Engineering* 135. ISSN: 01438166. DOI: 10.1016/j.optlaseng.2020.106186.

Redner, A. S. (1985). "Photoelastic measurements by means of computer-assisted spectral-contents analysis". In: *Experimental Mechanics* 25.2, pp. 148–153. DOI: 10.1007/BF02328805.

– (2003). "Automated Measurement of Edge Stress in Automotive Glass". In: URL: https://www.strainoptics.com/wp-content/uploads/2017/09/Automated-Measurement-of-Edge-Stress-in-Automotive-Glass.pdf.

Reichert, A. and Katte, H. (2005). *Grundlagen der Spannungsoptik*. Ed. by ilis gmbh.

Rinne, H. (2008). *The Weibull Distribution*. Chapman and Hall/CRC. ISBN: 9780429142574. DOI: 10.1201/9781420087444.

Scafidi, M., Pitarresi, G., Toscano, A., Petrucci, G., Alessi, S., and Ajovalasit, A. (2015). "Review of photoelastic image analysis applied to structural birefringent materials: glass and polymers". In: *Optical Engineering* 54.8. ISSN: 0091-3286. DOI: 10.1117/1.OE.54.8.081206.

Schaaf, B., Di Biase, P., Feldmann, M., Schuler, C., and Dix, S. (2017). "Full-surface and Non-destructive Quality Control and Evaluation by Using Photoelastic Methods". In: *Glass Processing Days*. Ed. by Tamglass Ltd Oy. Tampere.

Schneider, J., Kuntsche, J., Schula, S., Schneider, F., and Wörner, J.-D. (2016). *Glasbau*. Berlin, Heidelberg: Springer. ISBN: 978-3-540-28476-5. DOI: 10.1007/978-3-540-68927-0.

Schober, P., Boer, C., and Schwarte, L. A. (2018). "Correlation Coefficients: Appropriate Use and Interpretation". In: *Anesthesia and analgesia* 126.5, pp. 1763–1768. DOI: 10.1213/ANE.0000000000002864.

Schuler, C., Dix, S., Efferz, L., and Müller, P. (2022). *BeNAF - Bewertungskriterien zur Normung von Anisotropie-Effekten bei thermisch vorgespanntem Flachglas*. Ed. by BMWi. München: University of Applied Sciences Munich.

Sharples (2026). *Sharples S-67: Edge Stress Meter*. URL: https://www.sharplesstress.com/ (visited on 02/26/2026).

Siebert, G. and Maniatis, I. (2012). *Tragende Bauteile aus Glas. Grundlagen, Konstruktion, Bemessung, Beispiele*. ger. 2. vollst. überarb. Aufl. Bauingenieur-Praxis. Berlin: Wiley. ISBN: 9783433602782. DOI: 10.1002/9783433602782.

Softsolution GmbH (2023a). *CulletScanner*. URL: https://www.glassquality.com/de/produkte/culletscanner/ (visited on 02/26/2026).

– (2023b). *LineScanner*. URL: https://www.glassquality.com/de/products/linescanner/ (visited on 02/26/2026).

SPSS Analysis (2024). *Moderation Analysis in SPSS*. URL: https://spssanalysis.com/moderation-analysis-in-spss/ (visited on 02/23/2026).

Strainoptics Inc. (2012). *GES-100 Instruction Manual. Edge-Stress Meter with double wedge assembly*. URL: https://www.strainoptics.com/ges-100-edge-stress-meter/ (visited on 02/26/2026).

– (2026). *PES-100 Automated Edge-Stress Measurement System*. URL: https://www.strainoptics.com/pes-100-automated-edge-stress-measurement/ (visited on 02/26/2026).

– (2025). *GASP®*. URL: https://www.strainoptics.com/gasp-surface-polarimeter/ (visited on 02/26/2026).

Tabachnick, B. G. and Fidell, L. S. (2013). *Using Multivariate Statistics*. Pearson Education, Inc.

Teimouri, M., Hoseini, S. M., and Nadarajah, S. (2013). "Comparison of estimation methods for the Weibull distribution". In: *Statistics* 47.1, pp. 93–109. ISSN: 0233-1888. DOI: 10.1080/02331888.2011.559657.

The MathWorks, Inc. (2024a). *Evaluating Goodness of Fit*. Ed. by The MathWorks Inc. MATLAB & Simulink - MathWorks Deutschland. URL: https://de.mathworks.com/help/curvefit/evaluating-goodness-of-fit.html (visited on 04/17/2024).

– (2024b). *MATLAB*. Version R2024a. Natick, Massachusetts, USA: The MathWorks, Inc. URL: https://www.mathworks.com.

Thiele, K., Kraus, M., Schneider, J., and Nielsen, J. (2022a). "Statistische Charakterisierung der Druckzonentiefe vorgespannter Gläser". In: *ce/papers* 5.1, pp. 118–133. ISSN: 2509-7075. DOI: 10.1002/cepa.1663.

Thiele, K., Müller-Braun, S., and Schneider, J. (2022b). "Evaluation methods for surface compression stress measurements with unknown principle stress directions". In: *Glass Structures & Engineering* 7.2, pp. 121–137. ISSN: 2363-5142. DOI: 10.1007/s40940-022-00184-y.

Vajargah, K. F. and Masoomehnikbakht (2015). "Application REMLmodel and determining cut off of ICC bei Multi-Level Model based on Marcov Chains Simulation in health". In: *Indian Journal of Fundamental and Applied Life Sciences* Vol. 5 (S2).

Veer, F. A. and Rodichev, Y. M. (2016). "Improving the engineering strength of heat strengthened glass". In: *HERON* Vol. 61.2, pp. 121–140. URL: https://heronjournal.nl/61-2/3.pdf (visited on 02/23/2026).

Verma, V. K., Saxena, K., and Banodha, U. (2024). "Analysis Effect of K Values Used in K Fold Cross Validation for Enhancing Performance of Machine Learning Model with Decision Tree". In: *Advanced Computing*. Ed. by Garg, D., Rodrigues, J. J. P. C., Gupta, S. K., Cheng, X., Sarao, P., and Patel, G. S. Vol. 2053. Communications in Computer and Information Science 2053. Cham: Springer Nature Switzerland, pp. 374–396. ISBN: 978-3-031-56699-8. DOI: 10.1007/978-3-031-56700-1_30.

Vivek, R. and Ramesh, K. (2015). "Residual Stress Analysis of Commercial Float Glass Using Digital Photoelasticity". In: *International Journal of Applied Glass Science* 6.4, pp. 419–427. ISSN: 20411286. DOI: 10.1111/ijag.12106.

Voloshin, A. S. and Burger, C. P. (1983). "Half-fringe photoelasticity: A new approach to whole-field stress analysis". In: *Experimental Mechanics* 23.3, pp. 304–313. ISSN: 00144851.

Weibull, W. (1939). *A Statistical Theory of the Strength of Materials*. Ingeniörsvetenskapsakademien Handlingar Nr. 151. Stockholm: Generalstabens litografiska anstalts förlag.

Weller, R. (1941). "Three–Dimensional Photoelasticity Using Scattered Light". In: *Journal of Applied Physics* 12.8, pp. 610–616. ISSN: 0021-8979. DOI: 10.1063/1.1712947.

Xu, M. (2023). "Quantile Regression Model and Its Application Research". In: *Academic Journal of Science and Technology* 8.3, pp. 172–176. ISSN: 2771-3032. DOI: 10.54097/vt1qpm59.

Yoneyama, S., Morimoto, Y., Nomura, T., Fujigaki, M., and Matsui, R. (2003). "Real-time analysis of isochromatics and isoclinics using the phase-shifting method". In: *Experimental Mechanics* 43, pp. 83–89. DOI: 10.1007/BF02410488.

Zaccaria, M. and Overend, M. (2020). "Nondestructive Safety Evaluation of Thermally Tempered Glass". In: *Journal of Materials in Civil Engineering* 32.4. ISSN: 0899-1561. DOI: 10.1061/(ASCE)MT.1943-5533.0003086.

Zdaniuk, B. (2014). "Ordinary Least-Squares (OLS) Model". In: *Encyclopedia of Quality of Life and Well-Being Research*. Ed. by Michalos, A. C. Dordrecht: Springer Netherlands, pp. 4515–4517. ISBN: 978-94-007-0752-8. DOI: 10.1007/978-94-007-0753-5_2008.

A Appendix

A.1 Weibull

In Table A.1, the statistical details for evaluating the bending stress for each test series are presented, categorized by glass thickness t, manufacturer mfr, and pre-stress level. The Weibull parameters shape α and scale λ estimated using the maximum likelihood method, the location parameter x_0 was used as the mean of surface stress per test series. The characteristic bending strength f_k was defined as the one-sided 95% confidence bound of the 5% quantile, obtained through non-parametric bootstrap resampling.

Table A.1: Statistical details of Weibull evaluation of bending strength

t [mm]	mfr	Pre-stress level	n	mean [MPa]	std [MPa]	x_0 [MPa]	shape α	scale λ	f_k [MPa]
4	A	HSG low	10	139.19	21.47	52.35	4.18	95.10	94.16
4	A	HSG high	10	127.24	13.14	57.72	6.45	74.77	97.49
4	A	TTG low	10	174.79	17.93	124.56	3.35	55.31	132.62
4	A	TTG high	10	176.04	7.90	130.44	7.20	48.73	157.17
4	B	HSG low	10	123.26	18.27	44.72	4.51	85.68	83.95
4	B	HSG high	10	131.10	9.99	53.65	10.08	81.57	106.78
4	B	TTG low	8	151.03	14.61	97.39	4.52	58.99	121.33
4	B	TTG high	10	162.08	13.74	108.98	4.35	58.29	133.77
4	C	HSG low	10	116.57	10.86	47.53	8.70	73.32	90.64
4	C	HSG high	10	123.43	9.37	52.89	7.94	74.61	99.91
4	C	TTG low	10	156.59	9.36	112.14	5.72	48.14	136.41
4	C	TTG high	10	160.37	10.07	120.56	4.91	43.53	138.52
6	A	HSG low	10	127.51	13.41	55.59	6.55	77.23	96.84
6	A	HSG high	10	122.57	16.05	57.97	4.68	70.69	89.08
6	A	TTG low	10	163.06	10.45	109.30	6.10	57.84	138.53
6	A	TTG high	10	173.36	7.33	113.46	11.34	62.75	155.09
6	B	HSG low	10	133.18	13.48	51.72	9.40	86.41	101.09
6	B	HSG high	10	135.59	20.90	55.67	4.42	87.52	89.66
6	B	TTG low	10	192.49	19.21	116.33	5.04	83.23	150.77
6	B	TTG high	8	203.85	26.24	121.11	3.48	91.95	155.89
6	C	HSG low	10	115.75	18.65	48.35	4.77	73.81	73.72
6	C	HSG high	10	124.45	8.64	59.80	7.48	68.46	102.75
6	C	TTG low	10	161.61	9.36	103.49	6.84	62.04	139.55
6	C	TTG high	10	175.36	10.93	125.05	5.60	54.57	151.46
8	A	HSG low	10	130.62	16.31	59.06	5.03	77.96	96.61
8	A	HSG high	7	142.44	18.11	71.47	5.06	77.56	103.24
8	A	TTG low	10	170.66	16.58	109.75	5.16	66.26	130.18
8	A	TTG high	10	175.14	11.30	120.87	5.43	58.74	150.16
8	B	HSG low	10	111.10	17.96	41.99	4.35	75.87	74.35
8	B	HSG high	10	126.12	22.14	49.53	4.44	84.27	77.88
8	B	TTG low	10	200.35	32.20	112.46	3.20	98.53	140.90

t [mm]	mfr	Pre-stress level	n	mean [MPa]	std [MPa]	x_0 [MPa]	shape α	scale λ	f_k [MPa]
8	B	TTG high	10	249.29	22.73	160.73	4.64	97.11	202.31
8	C	HSG low	10	132.38	11.44	49.09	10.21	87.86	104.73
8	C	HSG high	10	154.60	6.44	81.97	13.18	75.47	137.83
8	C	TTG low	10	168.09	14.44	110.97	4.48	62.56	137.36
8	C	TTG high	10	173.19	9.43	124.15	5.52	52.92	152.48
10	A	HSG low	5	125.05	13.13	50.36	6.79	79.85	95.39
10	A	HSG high	5	147.93	5.70	72.31	17.22	77.97	133.16
10	A	TTG low	5	184.92	10.47	117.44	10.28	71.23	157.36
10	A	TTG high	5	177.48	14.20	121.10	5.70	61.37	145.96
10	B	HSG low	5	123.48	15.67	43.99	7.90	85.02	87.47
10	B	HSG high	5	123.89	8.90	48.82	11.53	78.60	100.93
10	B	TTG low	5	179.77	12.07	95.80	7.66	88.94	151.57
10	B	TTG high	5	205.26	17.40	131.12	6.20	80.26	164.16
10	C	HSG low	5	121.62	13.99	46.49	7.72	80.25	89.24
10	C	HSG high	5	153.69	12.57	71.68	7.56	87.11	125.08
10	C	TTG low	5	184.85	5.27	115.88	16.02	71.23	171.74
10	C	TTG high	5	190.71	4.51	122.01	17.47	70.69	179.27
12	A	HSG low	5	111.56	25.12	41.60	3.58	77.88	61.43
12	A	HSG high	5	158.32	6.63	73.96	14.86	87.20	141.77
12	A	TTG low	5	185.37	12.78	120.20	6.40	70.07	157.46
12	A	TTG high	5	189.95	13.19	128.40	6.41	66.40	160.85
12	B	HSG low	5	109.92	9.06	47.29	8.69	66.25	88.87
12	B	HSG high	5	119.36	20.44	49.61	4.60	76.66	75.91
12	B	TTG low	5	181.62	10.90	107.46	8.96	78.46	155.60
12	B	TTG high	5	220.43	21.08	150.21	5.50	76.64	168.19
12	C	HSG low	5	127.04	14.47	47.31	6.14	85.49	95.09
12	C	HSG high	5	135.34	15.69	62.50	6.85	78.45	97.51
12	C	TTG low	5	178.10	16.28	107.50	4.71	76.77	145.88
12	C	TTG high	5	192.32	9.04	116.97	10.57	78.98	170.55

A.2 Correlation analysis

The appendix for the correlation analysis is divided into small-format and large-format specimens. It includes histograms of the variables for the different models, and Q-Q plots to visually assess the assumption of normality. Finally, tables report Pearson's correlation coefficients r with 95% confidence intervals obtained by bootstrapping (2000 resamples), along with the corresponding sample sizes n. Significant correlations are indicated with *.

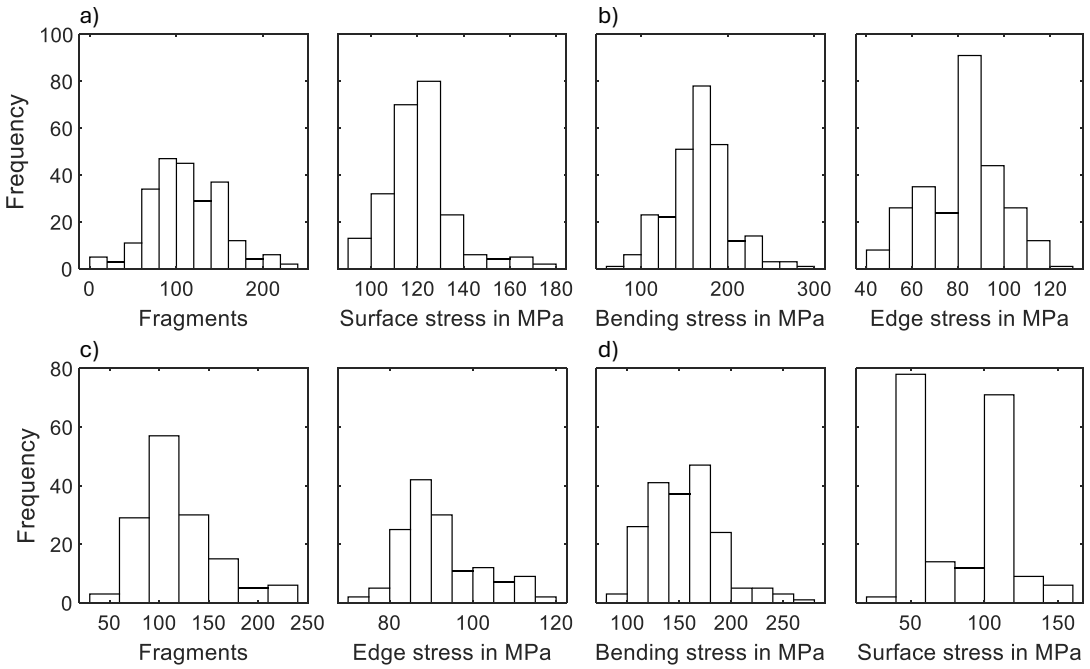

Figure A.1: Histograms for correlation models a) Fragments vs. Surface stress; b) Bending stress vs. Edge stress measured by multiple-wavelength photoelasticity; c) Fragments vs. Edge stress by MWP and d) Bending stress vs. Surface stress on small-format specimens

Table A.2: Pearson correlation analyses using bootstrapping with 2000 resamples for small-format specimens

Variable X	Variable Y	n	Pearson r	95% confidence intervals	p-value
Number of fragments	Surface stress	235	0.846	[0.806, 0.879]	0.000*
Number of fragments	Edge stress by MWP	145	0.571	[0.417, 0.676]	0.000*
Bending stress	Surface stress	192	0.856	[0.822, 0.888]	0.000*
Bending stress	Edge stress by MWP	267	0.800	[0.759, 0.840]	0.000*
Bending stress	Edge stress by PST	114	0.779	[0.725, 0.841]	0.000*
Edge stress by MWP	Surface stress	325	0.875	[0.854, 0.898]	0.000*
Edge stress by PST	Surface stress	46	0.941	[0.918, 0.966]	0.000*

* Correlation is statistically significant at $p < .001$

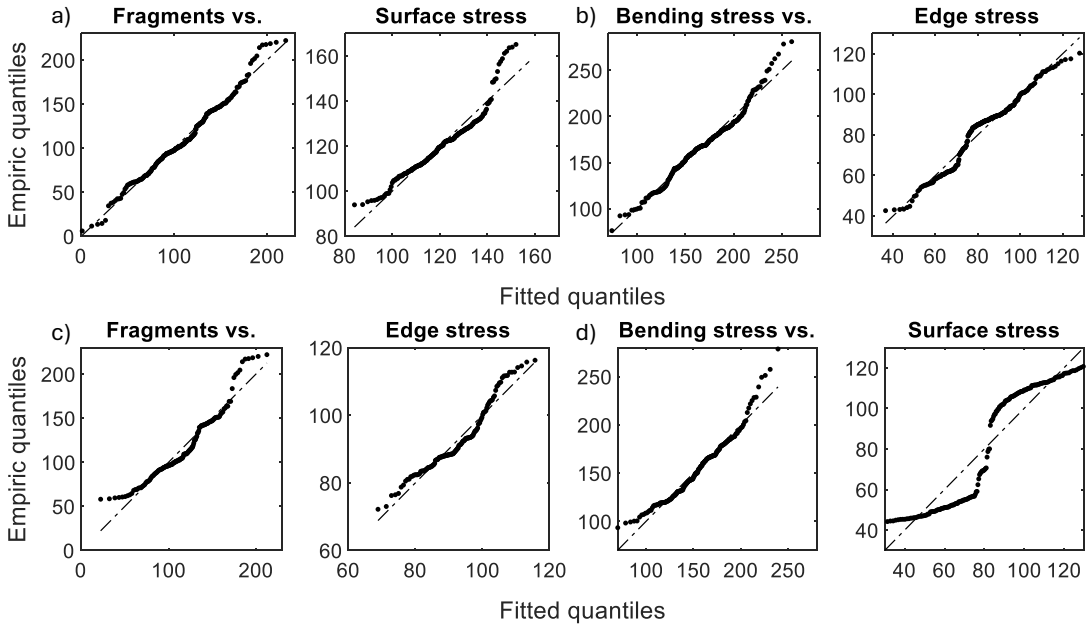

Figure A.2: Visual assessment of normal distribution using Q-Q plots for models a) Fragments vs. Surface stress; b) Bending stress vs. Edge stress measured by multiple-wavelength photoelasticity; c) Fragments vs. Edge stress measured by multiple-wavelength photoelasticity and d) Bending stress vs. Surface stress on small-format specimens

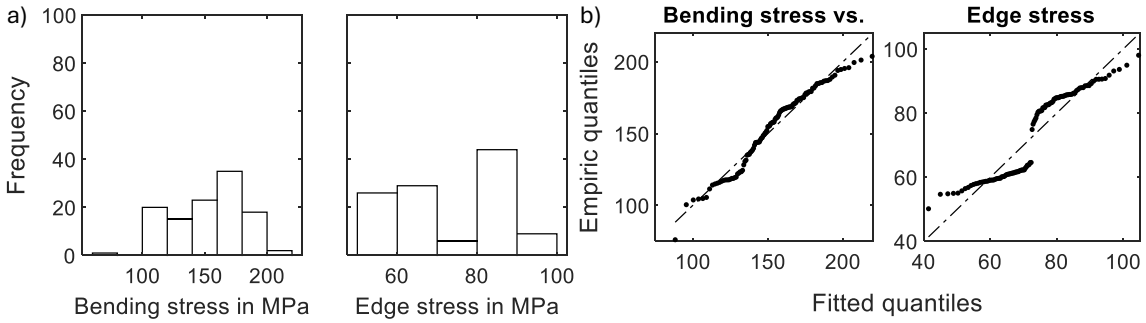

Figure A.3: a) Histograms and b) visual assessment of normal distribution using Q-Q plots for correlation model Bending stress vs. Edge stress measured by phase-shifting technique on small-format specimens

Table A.3: Pearson correlation analyses using bootstrapping with 2000 resamples for large-format specimens

Variable X	Variable Y	n	Pearson r	95% confidence intervals	p-value
Number of fragments	Surface stress	53	0.685	[0.548, 0.804]	0.000*
Number of fragments	Edge stress by MWP	53	0.545	[0.335, 0.711]	0.000*
Edge stress by MWP	Surface stress	98	0.877	[0.844, 0.915]	0.000*

* Correlation is statistically significant at $p < .001$

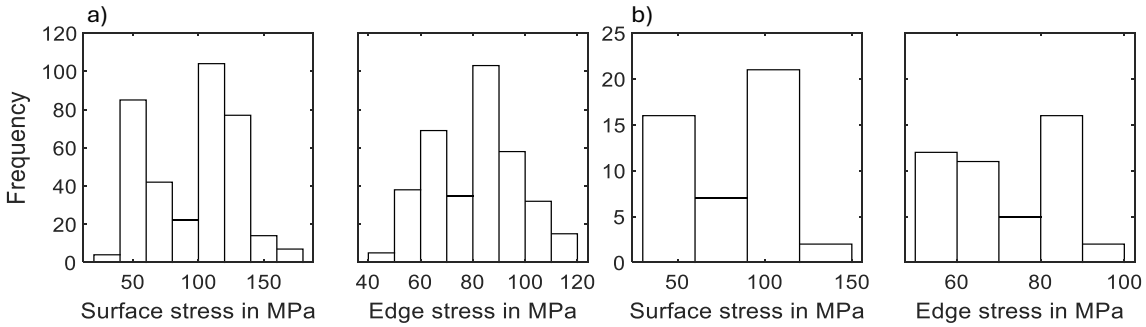

Figure A.4: Histograms for correlation models a) Surface vs. Edge stress by multiple-wavelength photoelasticity and b) Surface vs. Edge stress measured by phase-shifting technique on small-format specimens

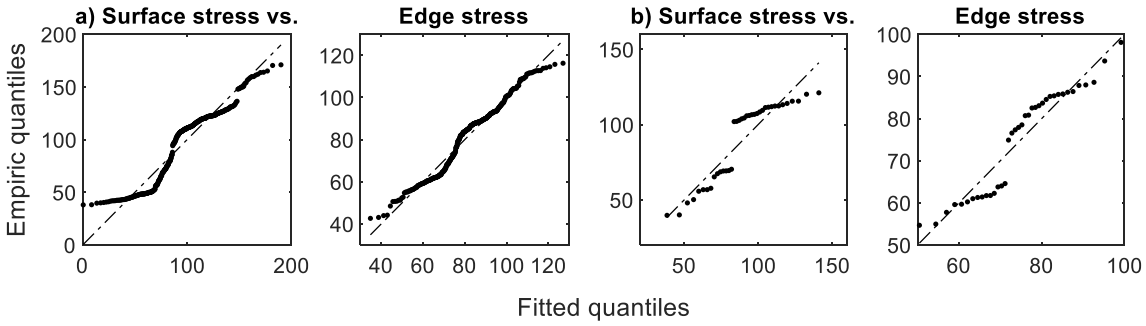

Figure A.5: Visual assessment of normal distribution using Q-Q plots for models a) Surface vs. Edge stress measured by multiple-wavelength photoelasticity and b) Surface vs. Edge stress by phase-shifting technique on small-format specimens

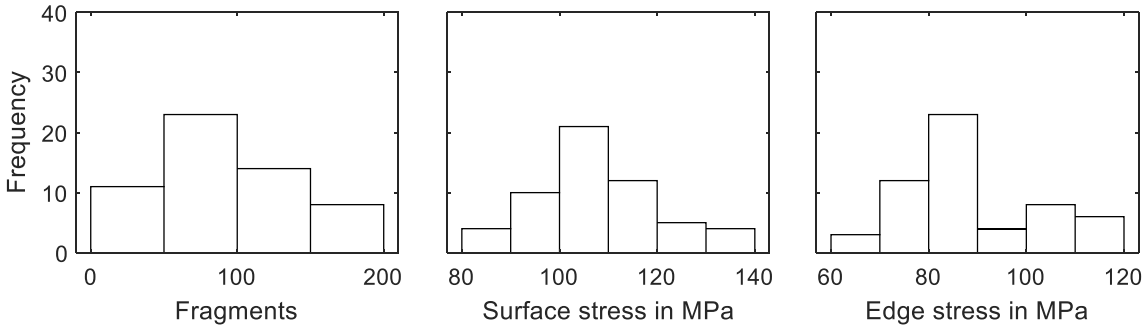

Figure A.6: Histograms for correlation models number of Fragments vs. Surface stress vs. Edge stress measured by multiple wavelength photoelasticity on large-format specimens

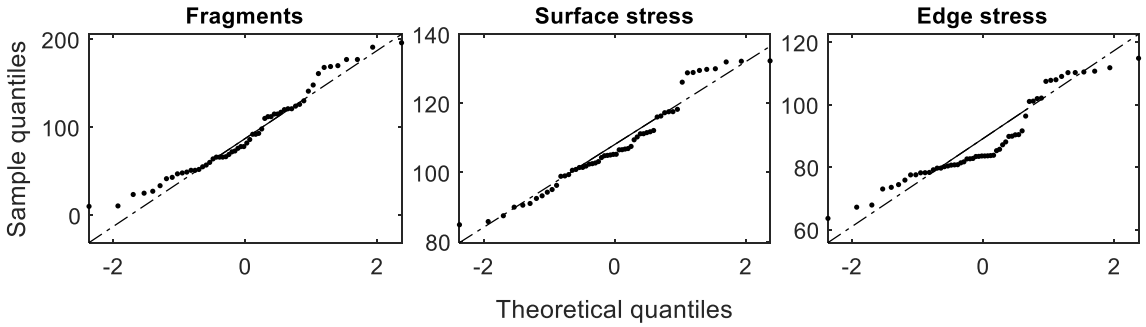

Figure A.7: Visual assessment of normal distribution using Q-Q plots for correlation models number of Fragments vs. Surface stress vs. Edge stress measured by multiple wavelength photoelasticity on large-format specimens

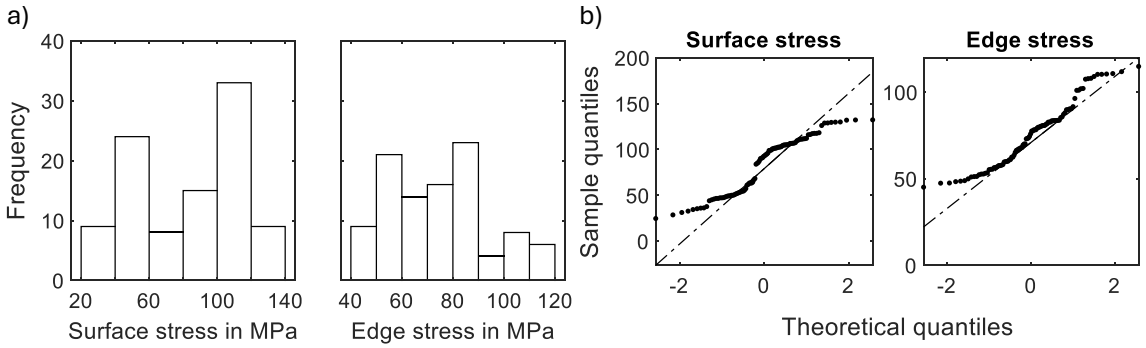

Figure A.8: a) Histograms and b) visual assessment of normal distribution using Q-Q plots for correlation model Surface stress vs. Edge stress measured by multiple wavelength photoelasticity on large-format specimens

A.3 Moderation analysis – contrast analysis

The following tables present the results of the pairwise contrast analysis obtained from the moderation model. The abbreviation t denotes the nominal glass thickness (in mm). Each row represents a unique pairwise comparison between the reference thickness and contrasting thickness. The reported estimate corresponds to the estimated difference in bending stress between the two thickness levels. A contrast is classified as statistically significant if the 95% confidence interval (determined by bootstrapping, 2000 resamples) does not include zero, indicating a statistically supported difference between the compared thickness levels. Redundant directional contrasts were removed to ensure a unique and non-redundant presentation of results.

Table A.4: Pairwise contrast analysis within the moderation analysis Bending stress ∼ Edge stress (measured by multiple-wavelength photoelasticity)

Reference t [mm]	Contrast t [mm]	Estimate	95% confidence interval	Statistical significance
6	8	0.3801	[-0.3189, 0.9015]	0
6	10	0.8534	[0.0453, 1.4222]	1
6	12	1.0341	[0.0719, 1.7643]	1
8	10	0.4732	[-0.0069, 0.9216]	0
8	12	0.6540	[-0.0662, 1.2772]	0
10	12	0.1807	[-0.6352, 0.8499]	0

Table A.5: Pairwise contrast analysis within the moderation analysis Fragments ∼ Edge stress (measured by multiple-wavelength photoelasticity)

Reference t [mm]	Contrast t [mm]	Estimate	95% confidence interval	Statistical significance
6	8	1.4675	[-0.3186, 3.1850]	0
6	10	1.5302	[-0.7450, 3.5916]	0
6	12	9.3608	[5.3516, 11.4242]	1
8	10	0.0627	[-2.1097, 1.9107]	0
8	12	7.8933	[4.2557, 10.0196]	1
10	12	7.8306	[4.2264, 10.3855]	1

Table A.6: Pairwise contrast analysis within the moderation analysis Bending stress ∼ Edge stress (measured by phase-shifting technique)

Reference t [mm]	Contrast t [mm]	Estimate	95% confidence interval	Statistical significance
6	8	0.1061	[-0.4053, 0.5674]	0
6	10	0.6962	[-0.0258, 1.3695]	0
6	12	0.8901	[0.1807, 1.8828]	1
8	10	0.5901	[-0.2025, 1.3083]	0
8	12	0.7840	[0.0327, 1.8446]	1
10	12	0.1939	[-0.6921, 1.3378]	0

Table A.7: Pairwise contrast analysis within the moderation analysis Bending stress ~ Surface stress

Reference t [mm]	Contrast t [mm]	Estimate	95% confidence interval	Statistical significance
4	6	0.2513	[0.0317, 0.5046]	1
4	8	0.3796	[0.1649, 0.6472]	1
4	10	0.1855	[-0.0184, 0.4095]	0
4	12	0.2583	[-0.0107, 0.4585]	0
6	8	0.1284	[-0.1453, 0.3980]	0
6	10	-0.0658	[-0.3555, 0.1728]	0
6	12	0.0070	[-0.3203, 0.2541]	0
8	10	-0.1942	[-0.4843, 0.0400]	0
8	12	-0.1214	[-0.4810, 0.1137]	0
10	12	0.0728	[-0.2200, 0.3214]	0

Table A.8: Pairwise contrast analysis within the moderation analysis Fragments ~ Surface stress

Reference t [mm]	Contrast t [mm]	Estimate	95% confidence interval	Statistical significance
4	6	1.5839	[1.0985, 2.0466]	1
4	8	-0.6953	[-1.0591, -0.2867]	1
4	10	-0.8970	[-1.4125, -0.4259]	1
4	12	-1.0519	[-1.4352, -0.5913]	1
6	8	-2.2792	[-2.6661, -1.9122]	1
6	10	-2.4809	[-2.9706, -1.9212]	1
6	12	-2.6358	[-3.0559, -2.2085]	1
8	10	-0.2017	[-0.5959, 0.2620]	0
8	12	-0.3566	[-0.6435, -0.0758]	1
10	12	-0.1549	[-0.5921, 0.3002]	0

A.4 Quantile regression models

The following tables present the statistical results of the quantile regression models, including intercept and predictor coefficients with 95% bootstrap confidence intervals based on 2,000 resamples. Here, t denotes the glass thickness and n the sample size of the regression model. Models are statistically significant if the bootstrap confidence interval does not crossing zero.

Table A.9: Statistical details of quantile regression model Surface stress vs. Number of fragments with 95% confidence intervals from bootstrapping with 2000 resamples for thermally toughened glass, statistical significance based on bootstrapp confidence intervals

t [mm]	n	Intercept coefficients	Predictor coefficients	Statistical significance
4	59	-403.21 [-518.83, -287.58]	3.89 [2.91, 4.86]	1
6	57	-479.67 [-540.74, -418.60]	5.00 [4.48, 5.52]	1
8	59	-187.54 [-208.82, -166.25]	2.35 [2.18, 2.52]	1
10	30	-79.52 [-185.71, 26.67]	1.42 [0.43, 2.40]	1
12	30	-84.33 [-187.01, 18.35]	1.37 [0.54, 2.19]	1
4–6	116	-336.72 [-462.77, -210.67]	3.35 [2.30, 4.40]	1
8–12	119	-135.74 [-196.50, -74.98]	1.83 [1.30, 2.35]	1
4–12	235	-259.03 [-297.52, -220.54]	2.74 [2.46, 3.02]	1

Table A.10: Statistical details of quantile regression model Surface stress vs. Bending stress with 95% confidence intervals from bootstrapping with 2000 resamples for thermally toughened glass, statistical significance based on bootstrapp confidence intervals

t [mm]	n	Intercept coefficients	Predictor coefficients	Statistical significance
4	49	76.52 [59.01, 94.03]	0.62 [0.42, 0.82]	1
6	48	76.31 [60.12, 90.49]	0.69 [0.55, 0.84]	1
8	46	52.75 [37.40, 68.09]	1.00 [0.84, 1.16]	1
10	25	59.52 [35.86, 83.19]	0.87 [0.64, 1.10]	1
12	24	61.71 [40.11, 83.32]	0.82 [0.55, 1.10]	1
6–12	143	60.95 [51.94, 69.97]	0.84 [0.75, 0.93]	1
4–12	192	62.44 [54.07, 70.82]	0.80 [0.71, 0.90]	1

Table A.11: Statistical details of quantile regression model edge stress measured by multiple-wavelength photoelasticity vs. bending stress with 95% confidence intervals from bootstrapping with 2000 resamples for thermally toughened glass and heat-strengthened glass; statistical significance based on bootstrap confidence intervals

t [mm]	n	Intercept coefficients	Predictor coefficients	Statistical significance
6	57	101.95 [42.73, 161.16]	0.59 [-0.12, 1.31]	0
8	105	38.04 [25.47, 50.61]	1.25 [1.03, 1.48]	1
10	53	-71.95 [-176.28, 32.38]	2.59 [1.44, 3.74]	1
12	52	-105.07 [-153.38, -56.76]	2.99 [2.44, 3.55]	1
6–12	267	21.21 [-4.02, 46.44]	1.33 [1.03, 1.64]	1

Table A.12: Statistical details of quantile regression model Edge stress measured by multiple-wavelength photoelasticity vs. Number of fragments with 95% confidence intervals from bootstrapping with 2000 resamples for thermally toughened glass, statistical significance based on bootstrapp confidence intervalss

t [mm]	n	Intercept coefficients	Predictor coefficients	Statistical significance
6	30	-58.16 [114.65, 1.68]	1.53 [0.91, 2.16]	1
8	57	-22.27 [104.99, 60.44]	1.09 [0.34, 1.84]	1
10	29	83.51 [408.58, 575.60]	-0.26 [-5.87, 5.36]	0
12	29	-1.95 [-728.49, 724.59]	0.80 [-7.47, 9.06]	0
6–12	145	-46.23 [-93.81, 1.35]	1.30 [0.78, 1.82]	1

Table A.13: Statistical details of quantile regression model Edge stress measured by phase-shifting technique vs. Bending stress with 95% confidence intervals from bootstrapping with 2000 resamples for thermally toughened glass and heat-strengthened glass, statistical significance based on bootstrapp confidence intervals

t [mm]	n	Intercept coefficients	Predictor coefficients	Statistical significance
6	39	10.29 [-12.56, 33.13]	1.54 [1.22, 1.85]	1
8	36	69.61 [6.05, 133.16]	0.74 [-0.27, 1.75]	0
10	19	13.58 [-34.29, 61.44]	1.70 [0.96, 2.43]	1
12	20	-107.93 [-190.72, -25.14]	3.26 [2.25, 4.27]	1
6–12	114	0.39 [-37.49, 38.28]	1.68 [1.20, 2.16]	1

Table A.14: Statistical details of quantile regression model Surface stress vs. Bending stress with 95% confidence intervals from bootstrapping with 2000 resamples for heat-strengthened glass, statistical significance based on bootstrapp confidence intervalss

t [mm]	n	Intercept coefficients	Predictor coefficients	Statistical significance
4	25	22.08 [-79.65, 123.81]	1.66 [-0.30, 3.61]	0
6	24	42.29 [-61.60, 146.19]	1.27 [-0.62, 3.16]	0
8	22	59.21 [24.42, 94.00]	0.84 [0.20, 1.48]	1
10	12	15.37 [-95.55, 126.29]	1.81[-0.44, 4.07]	0
12	12	-9.78 [-81.43, 61.86]	2.38 [1.04, 3.72]	1
4–12	95	45.26 [18.06, 72.47]	1.18 [0.64, 1.73]	1

A.5 Logistic regression models

In the following tables, th denotes the glass thickness in mm, n the sample size of the regression model, β the logistic regression coefficient, and OR the odds ratio. Linearity of the logit was assessed using the Box-Tidwell test. Potential outliers were evaluated based on standardized residuals, following the guidelines of Field (2013), and influential observations were assessed using Cook's distance. Model fit was evaluated using a likelihood ratio test (LRT) comparing the fitted model to an intercept-only model: the reported p-value corresponds to the χ^2 test of the reduction in deviance. Pseudo R^2 refers to Nagelkerke's R^2, and AUC denotes the area under the ROC curve. Extreme coefficient estimates indicate complete or quasi-complete separation between the conformity categories, which is also reflected by non-significant p-values of the χ^2 test at the 5% significance level. Significant models are indicated with *.

Table A.15: Statistical details of logistic regression model surface stress vs. conformity for thermally toughened glass

t [mm]	n	β	p-value	Odds ratio	LRT p-value	Influential outliers	Linearity of logit	Pseudo R^2	AUC
4 *	166	0.385	0.001	1.47	0.000	No	Yes	0.943	0.995
6	165	4.248	1.000	69.96	0.000	No	Yes	1.000	1.000
8	161	8.786	1.000	6542.13	0.000	No	Yes	1.000	1.000
10	85	5.438	1.000	229.90	0.000	No	Yes	1.000	1.000
12	84	5.152	1.000	172.74	0.000	No	Yes	1.000	1.000
8–12	330	17.187	1.000	29134312.33	0.000	No	Yes	1.000	1.000
4–12 *	661	0.334	0.000	1.40	0.000	No	Yes	0.971	0.998

* Model fit significant by likelihood-ratio χ^2 test

Table A.16: Statistical details of logistic regression model Edge stress measured by multiple-wavelength photoelasticity vs. Conformity for thermally toughened glass

t [mm]	n	β	p-value	Odds ratio	LRT p-value	Influential outliers	Linearity of logit	Pseudo R^2	AUC
8	210	16.566	1.000	15644495.56	0.000	No	Yes	1.000	1.000
10 *	111	1.114	0.006	3.05	0.000	No	Yes	0.922	0.994
12	108	12.712	1.000	331641.25	0.000	No	Yes	1.000	1.000
8–12 *	516	0.534	0.000	1.71	0.000	No	Yes	0.947	0.997

* Model fit significant by likelihood-ratio χ^2 test

Table A.17: Statistical details of logistic regression model Edge stress measured by phase-shifting technique vs. Conformity for thermally toughened glass

t [mm]	n	β	p-value	Odds ratio	LRT p-value	Influential outliers	Linearity of logit	Pseudo R^2	AUC
6	39	8.548	1.000	5155.89	0.000	No	Yes	1.000	1.000
8	36	11.596	1.000	108644.12	0.000	No	Yes	1.000	1.000
10	19	10.363	1.000	31678.86	0.000	No	Yes	1.000	1.000
12	20	8.807	1.000	6679.07	0.000	No	Yes	1.000	1.000
6–12	114	10.880	1.000	53115.52	0.000	No	Yes	1.000	1.000

* Model fit significant by likelihood-ratio χ^2 test

Table A.18: Statistical details of logistic regression model Surface stress vs. Conformity for heat-strengthened glass

t [mm]	n	β	p-value	Odds ratio	LRT p-value	Influential outliers	Linearity of logit	Pseudo R^2	AUC
4	166	-4.117	1.000	0.0163	0.000	No	Yes	1.000	1.000
6	165	-4.248	1.000	0.0143	0.000	No	Yes	1.000	1.000
8	161	-20.301	1.000	0.0000	0.000	No	Yes	1.000	1.000
10	85	-6.358	1.000	0.0017	0.000	No	Yes	1.000	1.000
12	84	-85.359	1.000	0.0000	0.000	No	Yes	1.000	1.000
4–8	492	-24.833	1.000	0.0000	0.000	No	Yes	1.000	1.000
4–12 *	661	-0.483	0.000	0.6168	0.000	No	Yes	0.968	0.998

* Model fit significant by likelihood-ratio χ^2 test

Table A.19: Statistical details of logistic regression model Edge stress measured by multiple-wavelength photoelasticity vs. Conformity for heat-strengthened glass

t [mm]	n	β	p-value	Odds ratio	LRT p-value	Influential outliers	Linearity of logit	Pseudo R^2	AUC
8 *	210	-0.259	0.000	0.772	0.000	No	Yes	0.797	0.966
10 *	111	-0.201	0.000	0.818	0.000	No	No	0.645	0.928
12 *	108	-0.143	0.000	0.867	0.000	No	No	0.525	0.873
8–12 *	429	-0.182	0.000	0.834	0.000	No	No	0.679	0.933

* Model fit significant by likelihood-ratio χ^2 test

Table A.20: Statistical details of logistic regression model Edge stress measured by phase-shifting technique vs. Conformity for heat-strengthened glass

t [mm]	n	β	p-value	Odds ratio	LRT p-value	Influential outliers	Linearity of logit	Pseudo R^2	AUC
6	39	-8.548	1.000	0.000	0.000	No	Yes	1.000	1.000
8	36	-2.226	0.098	0.108	0.000	No	No	0.848	0.985
10	19	-177.07	1.000	0.000	0.000	No	Yes	1.000	1.000
12	20	-52.695	1.000	0.000	0.000	No	Yes	1.000	1.000
6–12 *	114	-1.750	0.002	0.174	0.000	No	Yes	0.892	0.988

* Model fit significant by likelihood-ratio χ^2 test

A.6 k-fold validation

Table A.21: k-fold validation of the quantile regression model surface stress vs. bending stress for thermally toughened glass (t = 4 to 12 mm)

Iteration	$k = 1$	$k = 2$	$k = 3$	$k = 4$	$k = 5$
Limit [MPa]	72.22	71.39	72.22	67.47	71.41
Precision	88.00%	94.74%	95.45%	80.95%	93.75%
Recall	100.00%	100.00%	100.00%	100.00%	100.00%

Table A.22: k-fold validation quantile regression model Surface stress vs. Number of fragments for thermally toughened glass (t = 4 mm)

Iteration	$k = 1$	$k = 2$	$k = 3$	$k = 4$	$k = 5$
Limit [MPa]	112.75	113.89	113.89	112.75	114.07
Precision	100.00%	100.00%	100.00%	100.00%	100.00%
Recall	70.00%	70.00%	75.00%	77.78%	70.00%

Table A.23: k-fold validation quantile regression model Surface stress vs. Number of fragments for thermally toughened glass (t = 6 mm)

Iteration	$k = 1$	$k = 2$	$k = 3$	$k = 4$	$k = 5$
Limit [MPa]	103.51	103.74	103.74	103.69	103.89
Precision	100.00%	100.00%	100.00%	100.00%	100.00%
Recall	90.91%	100.00%	100.00%	100.00%	100.00%

Table A.24: k-fold validation quantile regression Surface stress vs. Number of fragments for thermally toughened glass (t = 8–12 mm)

Iteration	$k = 1$	$k = 2$	$k = 3$	$k = 4$	$k = 5$
Limit [MPa]	96.2	96.2	94	96.85	94.52
Precision	100.00%	100.00%	100.00%	100.00%	100.00%
Recall	95.65%	100.00%	100.00%	91.67%	100.00%

Table A.25: k-fold validation logistic regression model Surface stress for thermally toughened glass (t = 4 mm)

Iteration	$k = 1$	$k = 2$	$k = 3$	$k = 4$	$k = 5$
Limit [MPa]	104.98	109.18	110.17	109.12	108.91
Precision	92.31%	100.00%	100.00%	100.00%	100.00%
Recall	100.00%	64.29%	66.67%	76.47%	90.00%

Table A.26: k-fold validation logistic regression model Surface stress for thermally toughened glass (t = 6 mm)

Iteration	$k = 1$	$k = 2$	$k = 3$	$k = 4$	$k = 5$
Limit [MPa]	83.25	82.88	84.61	83.19	83.17
Precision	100.00%	100.00%	100.00%	100.00%	100.00%
Recall	100.00%	100.00%	100.00%	100.00%	100.00%

Table A.27: k-fold validation logistic regression model Surface stress for thermally toughened glass (t = 8–12 mm)

Iteration	$k = 1$	$k = 2$	$k = 3$	$k = 4$	$k = 5$
Limit [MPa]	92.31	92.31	91.18	93.27	92.31
Precision	100.00%	100.00%	100.00%	100.00%	100.00%
Recall	100.00%	100.00%	100.00%	100.00%	100.00%

Table A.28: k-fold validation quantile regression Edge stress measured by multiple-wavelength photoelasticity vs. Number of fragments for thermally toughened glass (t = 8–12 mm)

Iteration	$k = 1$	$k = 2$	$k = 3$	$k = 4$	$k = 5$
Limit [MPa]	67.52	66.26	69.05	60.25	67.22
Precision	100.00%	100.00%	100.00%	100.00%	100.00%
Recall	100.00%	100.00%	100.00%	100.00%	100.00%

Table A.29: k-fold validation quantile regression Edge stress measured by multiple-wavelength photoelasticity vs. Bending stress for thermally toughened glass (t = 6–12 mm)

Iteration	$k = 1$	$k = 2$	$k = 3$	$k = 4$	$k = 5$
Limit [MPa]	73.83	73.06	72.18	74.97	74.84
Precision	90.91%	97.14%	91.30%	97.14%	97.06%
Recall	100.00%	100.00%	100.00%	100.00%	100.00%

Table A.30: k-fold validation quantile regression Edge stress measured by phase-shifting technique vs. Bending stress for thermally toughened glass (t = 6–12 mm)

Iteration	$k = 1$	$k = 2$	$k = 3$	$k = 4$	$k = 5$
Limit [MPa]	71.21	70.73	69.8	69.64	69.8
Precision	100.00%	100.00%	100.00%	100.00%	100.00%
Recall	100.00%	100.00%	100.00%	100.00%	100.00%

Table A.31: k-fold validation logistic regression model Edge stress measured by multiple-wavelength photoelasticity for thermally toughened glass (t = 6–12 mm), probability threshold 0.95

Iteration	$k = 1$	$k = 2$	$k = 3$	$k = 4$	$k = 5$
Limit [MPa]	83.44	82.87	83.27	83.67	83.56
Precision	100.00%	100.00%	100.00%	100.00%	100.00%
Recall	92.54%	87.27%	92.75%	89.09%	88.89%

Table A.32: k-fold validation logistic regression model Edge stress measured by multiple-wavelength photoelasticity for thermally toughened glass (t = 6–12 mm), probability threshold 0.5

Iteration	$k = 1$	$k = 2$	$k = 3$	$k = 4$	$k = 5$
Limit [MPa]	77.84	77.23	77.72	78.05	78.64
Precision	97.06%	93.22%	95.77%	98.11%	100.00%
Recall	98.51%	100.00%	98.55%	94.55%	97.22%

Table A.33: k-fold validation logistic regression model Edge stress measured by phase-shifting technique for thermally toughened glass (t = 6–12 mm), probability threshold 0.95

Iteration	$k = 1$	$k = 2$	$k = 3$	$k = 4$	$k = 5$
Limit [MPa]	77.84	77.23	77.72	78.05	78.64
Precision	97.06%	93.22%	95.77%	98.11%	100.00%
Recall	98.51%	100.00%	98.55%	94.55%	97.22%

Table A.34: k-fold validation quantile regression model Surface stress vs. Bending stress for heat-strengthened glass (t = 4–12 mm)

Iteration	$k = 1$	$k = 2$	$k = 3$	$k = 4$	$k = 5$
Limit [MPa]	21.19	21.19	19.12	20.88	22.62
Precision	78.95%	73.68%	84.21%	84.21%	84.21%
Recall	100.00%	100.00%	100.00%	100.00%	100.00%

Table A.35: k-fold validation logistic regression Surface stress for heat-strengthened glass (t = 4–8 mm)

Iteration	$k = 1$	$k = 2$	$k = 3$	$k = 4$	$k = 5$
Limit [MPa]	65.76	65.76	65.76	65.60	65.76
Precision	100.00%	100.00%	100.00%	100.00%	100.00%
Recall	100.00%	100.00%	100.00%	98.00%	100.00%

Table A.36: k-fold validation logistic regression Surface stress for heat-strengthened glass (t = 10 mm)

Iteration	$k = 1$	$k = 2$	$k = 3$	$k = 4$	$k = 5$
Limit [MPa]	54.37	54.24	53.43	54.34	55.58
Precision	100.00%	100.00%	100.00%	100.00%	100.00%
Recall	100.00%	100.00%	100.00%	100.00%	100.00%

Table A.37: k-fold validation logistic regression Surface stress for heat-strengthened glass (t = 12 mm)

Iteration	$k = 1$	$k = 2$	$k = 3$	$k = 4$	$k = 5$
Limit [MPa]	54.37	54.24	53.43	54.34	55.58
Precision	100.00%	100.00%	100.00%	100.00%	100.00%
Recall	100.00%	100.00%	100.00%	100.00%	100.00%

Table A.38: k-fold validation quantile regression model Edge stress measured by multiple-wavelength photoelasticity vs. Bending stress for heat-strengthened glass (t = 6–12 mm)

Iteration	$k = 1$	$k = 2$	$k = 3$	$k = 4$	$k = 5$
Limit [MPa]	41.58	39.77	32.19	38.28	40.82
Precision	22.64%	25.93%	16.67%	22.64%	18.87%
Recall	100.00%	100.00%	100.00%	100.00%	100.00%

Table A.39: k-fold validation quantile regression model Edge stress measured by phase-shifting technique vs. Bending stress for heat-strengthened glass (t = 6–12 mm)

Iteration	$k = 1$	$k = 2$	$k = 3$	$k = 4$	$k = 5$
Limit [MPa]	41.44	40.15	43.63	37.18	43.63
Precision	27.27%	43.48%	43.48%	30.43%	26.09%
Recall	100.00%	100.00%	100.00%	100.00%	100.00%

Table A.40: k-fold validation logistic regression Edge stress measured by multiple-wavelength photoelasticity for heat-strengthened glass (t = 8–12 mm), probability threshold FPR <0.1

Iteration	$k = 1$	$k = 2$	$k = 3$	$k = 4$	$k = 5$
Limit [MPa]	64.75	65.24	62.50	64.75	63.21
Precision	79.31%	68.57%	92.31%	66.67%	86.96%
Recall	92.00%	72.73%	70.59%	63.64%	64.52%

Table A.41: k-fold validation logistic regression Edge stress measured by multiple-wavelength photoelasticity for heat-strengthened glass (t = 8–12 mm), probability threshold Prec > 0.9

Iteration	$k = 1$	$k = 2$	$k = 3$	$k = 4$	$k = 5$
Limit [MPa]	55.62	56.21	55.64	55.93	55.64
Precision	100.00%	77.78%	100.00%	80.00%	100.00%
Recall	24.00%	21.21%	23.53%	18.18%	19.35%

Table A.42: k-fold validation logistic regression Edge stress measured by phase-shifting technique for heat-strengthened glass (t = 8–12 mm), probability threshold 0.95

Iteration	$k = 1$	$k = 2$	$k = 3$	$k = 4$	$k = 5$
Limit [MPa]	60.34	60.15	60.70	59.74	60.17
Precision	100.00%	100.00%	100.00%	100.00%	100.00%
Recall	83.33%	83.33%	90.00%	36.36%	66.67%